

SYNAPTIC PLASTICITY AND HEBBIAN CELL ASSEMBLIES

by

Richard Christopher Gerkin

B.S., Stanford University, 2001

Submitted to the Graduate Faculty of
The School of Medicine in partial fulfillment
of the requirements for the degree of
Doctor of Philosophy

University of Pittsburgh

2008

UNIVERSITY OF PITTSBURGH
SCHOOL OF MEDICINE

This dissertation was presented

by

Richard Christopher Gerkin

It was defended on

January 15th, 2008

and approved by

Chairman: Daniel J. Simons, Professor, Department of Neurobiology

Andrew B. Schwartz, Professor, Department of Neurobiology

Robert E. Kass, Professor, Adjunct Professor, Department of Neuroscience

Jonathan E. Rubin, Associate Professor, Department of Mathematics

Alison L. Barth, Adjunct Professor, Department of Neuroscience

Kevin J. Staley, Professor, Dept. of Neurology, Harvard Medical School

Dissertation Advisor: Guo-Oiang Bi, Associate Professor, Dept. of Neurobiology

Copyright © by Richard Christopher Gerkin

2008

SYNAPTIC PLASTICITY AND HEBBIAN CELL ASSEMBLIES

Synaptic dynamics are critical to the function of neuronal circuits on multiple timescales. In the first part of this dissertation, I tested the roles of action potential timing and NMDA receptor composition in long-term modifications to synaptic efficacy. In a computational model I showed that the dynamics of the postsynaptic $[Ca^{2+}]$ time course can be used to map the timing of pre- and postsynaptic action potentials onto experimentally observed changes in synaptic strength. Using dual patch-clamp recordings from cultured hippocampal neurons, I found that NMDAR subtypes can map combinations of pre- and postsynaptic action potentials onto either long-term potentiation (LTP) or depression (LTD). LTP and LTD could even be evoked by the same stimuli, and in such cases the plasticity outcome was determined by the availability of NMDAR subtypes. The expression of LTD was increasingly presynaptic as synaptic connections became more developed. Finally, I found that spike-timing-dependent potentiability is history-dependent, with a non-linear relationship to the number of pre- and postsynaptic action potentials. After LTP induction, subsequent potentiability recovered on a timescale of minutes, and was dependent on the duration of the previous induction.

While activity-dependent plasticity is putatively involved in circuit development, I found that it was not required to produce small networks capable of exhibiting rhythmic persistent activity patterns called reverberations. However, positive synaptic scaling produced by network inactivity yielded increased quantal synaptic amplitudes, connectivity, and potentiability, all favoring reverberation. These data suggest that chronic inactivity upregulates synaptic efficacy by both quantal amplification and by the addition of silent synapses, the latter of which are

rapidly activated by reverberation. Reverberation in previously inactivated networks also resulted in activity-dependent outbreaks of spontaneous network activity. Applying a model of short-term synaptic dynamics to the network level, I argue that these experimental observations can be explained by the interaction between presynaptic calcium dynamics and short-term synaptic depression on multiple timescales. Together, the experiments and modeling indicate that ongoing activity, synaptic scaling and metaplasticity are required to endow networks with a level of synaptic connectivity and potentiability that supports stimulus-evoked persistent activity patterns but avoids spontaneous activity.

TABLE OF CONTENTS

ACKNOWLEDGEMENTS	XVII
PREFACE	XVIII
1. GENERAL INTRODUCTION	1
1.1. MULTIPLE TIMESCALES OF SYNAPTIC DYNAMICS	2
1.1.1. Short-term synaptic dynamics.....	2
1.1.2. Long-Term Synaptic Plasticity	7
1.1.3. Calcium and synaptic plasticity	8
1.1.4. Spike-Timing Dependent Plasticity	10
1.1.5. Metaplasticity.....	13
1.1.6. Synaptic scaling and homeostasis.....	13
1.1.7. Unanswered questions	14
1.2. NETWORK ACTIVITY IN HIPPOCAMPAL NEURONS	15
1.2.1. Recurrent excitatory hippocampal networks	15
1.2.2. Hippocampal networks <i>in vitro</i> and <i>in silico</i>	19
1.2.3. Mechanisms determining the timing of synchronous activity in recurrent neuronal networks	22
1.2.4. Cultured Hippocampal Neurons as a Model System	23
1.2.5. Network Activity in Cultured Hippocampal Neurons	24

1.2.6.	Reverberation in Small Cultured Networks.....	25
1.2.7.	Unanswered Questions.....	29
2.	POSTSYNAPTIC CALCIUM TIME COURSE AS A SIGNAL FOR SPIKE-TIMING-DEPENDENT PLASTICITY	30
2.1.	INTRODUCTION	30
2.1.1.	STDP and the Integration of Complex Stimuli.....	30
2.1.2.	Defects in the traditional calcium hypothesis of bidirectional long-term synaptic plasticity.....	31
2.2.	METHODS	33
2.2.1.	Neuronal and Synaptic Dynamics.....	33
2.2.2.	Calcium Detectors.....	37
2.3.	RESULTS	40
2.3.1.	Results for doublets.....	41
2.3.2.	Results for triplets	42
2.4.	DISCUSSION.....	45
2.4.1.	Applicability to other experimental preparations	45
2.4.2.	Alternative models to explain the data.....	46
2.4.3.	Correspondence to biological signaling pathways.....	47
2.4.4.	Calcium sources	48
2.4.5.	Accumulation of plasticity across stimuli.....	50
3.	MODULAR COMPETITION IN SPIKE-TIMING-DEPENDENT PLASTICITY MEDIATED BY NMDA RECEPTOR SUBTYPES	51
3.1.	INTRODUCTION	51

3.2.	METHODS	53
3.2.1.	Electrophysiology	53
3.2.2.	Pharmacology	54
3.2.3.	Quantification of NMDAR subtype specificity of NVP-AAM077	55
3.2.4.	1/CV ² Analysis.....	57
3.2.5.	Model of NMDAR Subtype Selectivity in STDP	59
3.3.	RESULTS	62
3.3.1.	NMDAR subtypes in cultured hippocampal neurons	62
3.3.2.	Roles of NMDAR subtypes in the induction of bi-directional STDP	67
3.3.3.	Roles of endocannabinoids and the locus of presynaptic depression	71
3.3.4.	Integration of NMDAR subtype-mediated STDP.....	76
3.3.5.	Dynamic competition of signaling modules	80
3.4.	DISCUSSION.....	86
3.4.1.	Evidence for a veto module	86
3.4.2.	Specificity of NR2A-NR antagonism	88
3.4.3.	Alternative techniques for the study of NMDAR subtype selectivity in synaptic plasticity.....	89
3.4.4.	Presynaptic mechanisms of STDP.....	90
3.4.5.	Mechanisms of subtype selectivity	92
4.	INTEGRATION OF SPIKE-TIMING-DEPENDENT POTENTIATION ACROSS MULTIPLE TIME SCALES	95
4.1.	INTRODUCTION	95
4.2.	METHODS	96

4.2.1.	Experimental methods	96
4.2.2.	Statistical Model for the Contribution of Spike Pairings to STDP	96
4.3.	RESULTS	98
4.3.1.	Integration of potentiation across pairings.....	98
4.3.2.	Integration of potentiation across inductions.....	100
4.4.	DISCUSSION.....	105
4.4.1.	Possible sources of inter-pairing cooperativity.....	105
4.4.2.	Possible sources of dependence on induction history.....	106
4.4.3.	Independence of individual synapses.....	108
4.4.4.	Implications of the observed metaplasticity	108
5.	RECIPROCAL REGULATION OF PERSISTENT ACTIVITY AND SYNAPTIC EFFICACY IN A SMALL NEURONAL CIRCUIT.....	110
5.1.	INTRODUCTION	110
5.2.	METHODS	112
5.2.1.	Cell Culture	112
5.2.2.	Electrophysiology	114
5.2.3.	Pharmacology	115
5.2.4.	Analysis and Statistics	116
5.3.	RESULTS	118
5.3.1.	Reverberation is enhanced in chronically inactivated cultured networks...	118
5.3.2.	Functional synaptic connectivity is shifted towards excitation by chronic inactivation.....	122

5.3.3.	Role of reduced inhibition in increased reverberation after chronic inactivation.....	126
5.3.4.	Reverberation-driven synaptic potentiation.....	129
5.3.5.	Reverberation and functional connectivity are rapidly enhanced.....	133
5.3.6.	Critical threshold behavior in reverberatory networks	137
5.3.7.	Emergence of spontaneous activity in chronically inactivated networks ...	141
5.3.8.	Requirements for the emergence of spontaneous activity	145
5.3.9.	History-dependence in the transition between regimes of activity	149
5.4.	DISCUSSION.....	153
5.4.1.	Quantal scaling vs. Functional scaling.....	154
5.4.2.	Reduction of inhibition by inactivity favors reverberation.....	155
5.4.3.	Role of nonsynaptic changes	155
5.4.4.	Synaptic potentiation driven by reverberation.....	156
5.4.5.	Stable reverberation as a homeostatic target.....	157
5.4.6.	Function of a “critical” level of persistent activity	159
5.4.7.	The origin of spontaneous activity.....	159
5.4.8.	Relevance to the brain.....	160
6.	ASYNCHRONOUS RELEASE DETERMINES NETWORK DYNAMICS IN CULTURED HIPPOCAMPAL NEURONS	163
6.1.	INTRODUCTION	163
6.2.	METHODS	164
6.2.1.	The dynamics of presynaptic Ca^{2+}	164
6.2.2.	Residual Ca^{2+} and asynchronous release	166

6.2.3.	Short-term synaptic dynamics.....	167
6.2.4.	Neuronal model and network connectivity	170
6.2.5.	Identification and analysis of network activity	174
6.2.6.	Calculation of the probability of a polysynaptic current cluster (PSCC) ...	174
6.3.	RESULTS	176
6.3.1.	Dependence of reverberatory output on synaptic parameters in a model with short-term synaptic dynamics	176
6.3.2.	Critical threshold behavior in reverberatory networks	180
6.3.3.	Intracellular calcium drives the regime of spontaneous activity.....	182
6.3.4.	Presynaptic calcium dynamics can explain the activity-dependent emergence of spontaneous activity.....	186
6.3.5.	Synaptic states and the emergence of spontaneous activity.....	191
6.4.	DISCUSSION.....	197
6.4.1.	A critical level of synaptic connectivity supports stable reverberation	197
6.4.2.	Linearity of the mapping between synaptic parameters and network responses	198
6.4.3.	Online long-term synaptic plasticity	198
6.4.4.	Alternative implementations of synaptic transmission	199
6.4.5.	Role of asynchronous release.....	200
6.4.6.	Future experimental investigation of presynaptic $[Ca^{2+}]$ as a determinant of network activity.....	202
6.4.7.	Asynchronous release interacts with synaptic depression on two timescales to determine network output	203

7.	GENERAL DISCUSSION	204
7.1.	GENERALIZATION OF STDP AS A UNIVERSAL RULE OF SYNAPTIC MODIFICATION.....	204
7.2.	SEPARATION OF THE STRUCTURAL AND SIGNALING ROLES OF A SINGLE MOLECULE	205
7.3.	INTEGRATION OF NMDAR SUBTYPE SELECTIVITY INTO A REALISTIC DYNAMIC MODEL OF STDP	206
7.4.	COOPERATIVITY ACROSS SPIKE PAIRINGS CAN INFORM THE PARAMETER CHOICES IN THE DYNAMIC MODEL	206
7.5.	RECIPROCAL IMPACT OF STDP AND NETWORK ACTIVITY	207
7.6.	LIMITATIONS OF USING TTX TO STUDY NETWORK HOMEOSTASIS	209
7.7.	RELEVANCE TO EPILEPSY <i>IN VIVO</i>	210
7.8.	EPILOGUE.....	211
8.	GENERAL METHODS	212
8.1.	CELL CULTURE.....	212
8.2.	ELECTROPHYSIOLOGY.....	213
8.3.	PHARMACOLOGY.....	213
8.4.	ANALYSIS AND STATISTICS.....	213
	BIBLIOGRAPHY	215

LIST OF TABLES

Table 2.1: Conductance values for the postsynaptic Ca ²⁺ detector model of STDP	34
Table 2.2: Parameters governing postsynaptic calcium dynamics.....	35
Table 2.3: Parameters governing postsynaptic glutamate receptors	37
Table 2.4: Parameters governing postsynaptic calcium detectors.....	39
Table 3.1: Parameters governing the simplified model of NMDAR-dependent STDP integration.	61
Table 3.2: NR2A-NR abundance predicts change in synaptic strength even when initial strength is taken into account.....	82
Table 4.1: Parameters used in the spike-pairing integration model.	98
Table 5.1: Comparison of control and TTX-treated cultures.	127
Table 5.2: TTX-treatment predicts the development of spontaneous activity even when reverberation duration is taken into account.....	146
Table 6.1: Parameters for the reverberation model.	172

LIST OF FIGURES

Figure 1.1: Presynaptic Ca ₂₊ controls asynchronous neurotransmitter release at glutamatergic synapses	6
Figure 1.2: Spike-timing-dependent plasticity (STDP) in cultured hippocampal neurons	12
Figure 1.3: Strong recurrent connectivity exists in hippocampal circuitry	18
Figure 1.4: Network activity in the disinhibited hippocampal slice	21
Figure 1.5: The small network “island” culture model	27
Figure 1.6: Reverberation in small cultured networks	28
Figure 2.1: The postsynaptic [Ca ₂₊] detector model recapitulates results from STDP experiments	44
Figure 3.1: NMDAR current amplitudes and kinetics in the presence of subtype-selective antagonists.....	66
Figure 3.2: Spike-timing-dependent potentiation specifically requires non-NR2B-NRs (putative NR2A-NRs), while spike-timing-dependent depression specifically requires NR2B-NRs	70
Figure 3.3: Spike-timing-dependent depression favors a presynaptic expression locus but does not depend on CB1 antagonism	75
Figure 3.4: Triplet experiments show that potentiation is unmasked by antagonizing NR2B-NRs, while either depression is unmasked or potentiation is abolished by antagonizing NR2A-NRs	79

Figure 3.5: A simplified dynamic model of modular competition captures the subunit and stimulus specificity of STDP	85
Figure 4.1: Dependence of spike-timing-dependent potentiation on individual spike pairings and potentiation history	104
Figure 5.1: Reverberation is enhanced in TTX-treated cultures.....	121
Figure 5.2: Synaptic scaling is reflected differently in the amplitude of miniature and evoked currents.....	125
Figure 5.3: Reduced synaptic inhibition mediates the extended duration of reverberation in in TTX-treated cultures.....	128
Figure 5.4: TTX-treated cultures exhibit enhanced reverberation-driven synaptic potentiation	132
Figure 5.5: Synaptic scaling alone without subsequent activity is not sufficient to augment reverberation in TTX-treated cultures	136
Figure 5.6: Control networks operate near a critical synaptic threshold for reverberation	140
Figure 5.7: TTX-treated networks exhibit an activity-dependent transition to a regime of spontaneous activity.....	144
Figure 5.8: Enhancement of spontaneous activity in TTX-treated networks is facilitated but not dependent upon NMDA receptors	148
Figure 5.9: The transition to spontaneous activity can be reversed by temporary suspension of AMPAergic synaptic transmission.	151
Figure 5.10: Pharmacological enhancement of synaptic efficacy results in the activity-dependent emergence of spontaneous activity	152
Figure 6.1: Short-term synaptic dynamics at synaptic connections in the reverberation model	169

Figure 6.2: Effects of altered synaptic parameters on reverberation	179
Figure 6.3: Critical threshold behavior in control networks	181
Figure 6.4: Intracellular [Ca ₂₊] drives spontaneous activity, asynchronous release, and a component of reverberation-driven synaptic potentiation	185
Figure 6.5: The probability of a subsequent, spontaneous synchronous network event increases with reverberation duration.....	190
Figure 6.6: The activity-dependent emergence of spontaneous activity is dependent on synaptic connectivity, and leaves a limited connectivity regime for stable reverberation.....	195

ACKNOWLEDGEMENTS

Cheryl, for giving me love and emotional support during my time in graduate school; Mom and Dad, for refusing to let me accept less than the best from myself; Guoqiang, for always listening to my wild ideas, and for never letting me concede an argument on the grounds of mental fatigue; My collaborators (Jon Rubin and Carson Chow, chapter 2; Pakming Lau, chapters 3 and 5; David Nauen, chapter 2; Jichuan Zhang, chapter 4, Vladislav Volman and Eshel Ben-Jacob, chapter 6); Pakming, Huaxing, Xi, David, and the rats for giving me so many great cells to work with, and to the whole lab for a friendly, engaging scientific environment; Pakming, for being a leader and an expert in my field and in the lab; CNUP students, faculty, and staff for always making sure that my own hard work and creativity was the only limiting factor in my graduate progress; Committee members, for taking the time to help me refine my graduate mission and improve this document; CNUP, CNBC, NSF, and NIH for a Predoctoral Training Award (T32 NS007433-06), an IGERT Award (DGE-9987588), and a National Research Service Award (F31 MH077430)

PREFACE

What happens when you hook one neuron to another, and how do the properties of the neurons (and the hook) influence the result? I came to graduate school with a question of this breadth, and decided to start with the seemingly simple preparation of cells in a dish to figure out the answers. To my delight, I learned that answers to these kinds of questions cannot be found with a handful of bar graphs, box and arrow diagrams (Lazebnik, 2002), and ideas from an undergraduate neuroscience textbook. Understanding the brain will continue to require new, irreducibly complex concepts concerning the dynamics of neural function. It is my sincerest hope that, with enough of these concepts, we can produce an intelligible description of the brain and all of its processes.

1. GENERAL INTRODUCTION

Donald Hebb conceived of behavior as emerging from the coordinated activity of so-called "cell assemblies", groups of neurons that activate one another in sequences (Hebb, 1949). To consolidate behaviors during learning, Hebb imagined:

"Let us assume then that the persistence or repetition of a reverberatory activity (or 'trace') tends to induce lasting cellular changes that add to its stability. The assumption can be precisely stated as follows: When an axon of cell A is near enough to excite a cell B and repeatedly or persistently takes part in firing it, some growth process or metabolic change takes place in one or both cells such that A's efficiency, as one of the cells firing B, is increased."

I have organized my graduate research around the predictions of these two statements. The second of these is a prediction of the phenomenon of spike-timing-dependent plasticity, which I address in chapters 2, 3, and 4. The first posits a mutual relationship between plasticity and the formation of cell assemblies, which I treat in chapters 5 and 6. The remainder of this introduction covers background in synaptic and network dynamics needed to attack these issues theoretically and experimentally.

1.1. MULTIPLE TIMESCALES OF SYNAPTIC DYNAMICS

The earliest observations of the dynamic synapse (Eccles and O'Connor W, 1941) showed that its activity was both time and history-dependent. Yet the cavalier use of terms like “synaptic efficacy” – insofar as it implies a single number – has obfuscated neurophysiology. In fact, synaptic transmission is a dynamical process; its components operate on many interacting timescales (Abraham and Bear, 1996). This feature of synaptic transmission deserves attention, as this temporal hierarchy may endow synapses with the capacity needed to transmit information (Abbott et al., 1997) and store memory (Fusi et al., 2005).

1.1.1. Short-term synaptic dynamics

At the fastest timescale are short-term synaptic dynamics; the impact of the synapse on the post-synaptic neuron depends heavily on the timing and number of recent action potentials (Fatt and Katz, 1951; Zucker and Regehr, 2002), and the brain may be able to exploit these properties to facilitate communication between neurons (Abbott et al., 1997; Tsodyks and Markram, 1997; Fuhrmann et al., 2002). Two principle forces are at work: first, while the number and nature of the various vesicle pools is still disputed (Brody and Yue, 2000; Schneggenburger et al., 2002; Sullivan, 2007), it is generally accepted that the release of vesicles may leave a synaptic bouton less release-competent for a limited time. Exactly how strong the effect of this "short-term depression", and how long it lasts, depend upon the number of vesicles immediately available, and the rapidity with which new vesicles are placed into the so-called "readily releasable pool" (Rosenmund and Stevens, 1996; Zucker and Regehr, 2002).

The second principal force regulating short-term dynamics is presynaptic, intraterminal free Ca^{2+} concentration ($[\text{Ca}^{2+}]$) (Zucker, 1993; Burnashev and Rozov, 2005). $[\text{Ca}^{2+}]$ is highly regulated (Zucker, 1999), with a > 10000-fold concentration difference across the plasma membrane. Each action potential opens voltage-gated Ca^{2+} channels, permitting $[\text{Ca}^{2+}]$ elevation in the presynaptic terminal (Xu et al., 2007), and calcium-sensitive machinery couples this elevation to vesicular exocytosis (Sudhof, 2004; Schneggenburger and Neher, 2005).

Since $[\text{Ca}^{2+}]$ elevation alone is at least partly sufficient to cause exocytosis (Schneggenburger and Neher, 2000; Bollmann and Sakmann, 2005), mechanisms to restore baseline $[\text{Ca}^{2+}]$ levels are required to temporally restrict synaptic transmission. These mechanisms include endogenous $[\text{Ca}^{2+}]$ buffers and extrusion mechanisms (Helmchen et al., 1997; Sinha et al., 1997; Sabatini and Regehr, 1998; Lin et al., 2005). However, according to the "residual calcium hypothesis" (Katz and Miledi, 1968; Miledi and Thies, 1971), the efficacy of these mechanisms is limited; lingering, elevated $[\text{Ca}^{2+}]$ from one action potential combines with that from a second action potential to increase the probability of vesicle fusion in response to the second, a phenomenon known as "short-term facilitation" (Zucker and Regehr, 2002) but see (Cohen and Van der Kloot, 1986; Blundon et al., 1993). Residual calcium can also enable "asynchronous" neurotransmitter release (Del Castillo and Katz, 1954; Barrett and Stevens, 1972; Goda and Stevens, 1994), or random synaptic vesicle exocytosis at long latency (>20 ms) from an action potential (Fig. 1.1a). Asynchronous release is made possible by distinct calcium-sensing release machinery (Nishiki and Augustine, 2004; Sun et al., 2007) more sensitive to lower $[\text{Ca}^{2+}]$, and possibly by the slower rate of calcium clearance mechanisms in this $[\text{Ca}^{2+}]$ regime. The $[\text{Ca}^{2+}]$ affinity of asynchronous release varies considerably across preparations (Augustine and Neher, 1992; Heidelberger et al., 1994; Schneggenburger and Neher, 2005), and

low $[Ca^{2+}]$ affinity of the release apparatus may be associated with an abundance of asynchronous release, especially in developing neurons (Hagler and Goda, 2001). In cultured hippocampal neurons, asynchronous release is responsible for ~10% of the total neurotransmitter release attributable to a single action potential (Goda and Stevens, 1994). However, as the number of presynaptic action potentials increases, this percentage increases sharply as short-term depression reduces the synchronous component and further $[Ca^{2+}]$ elevation increases the asynchronous component of synaptic transmission (Rosenmund and Stevens, 1996; Hagler and Goda, 2001)(Fig. 1.1b,c,d). Asynchronous release can be abolished with minimal interruption to the synchronous (<20 ms) phase of transmission by enhancing the $[Ca^{2+}]$ buffering capacity of the intracellular milieu with slow exogenous buffers (Cummings et al., 1996a) (Hagler and Goda, 2001), indicating that residual $[Ca^{2+}]$ is indeed responsible for this phenomenon (Fig. 1.1e).

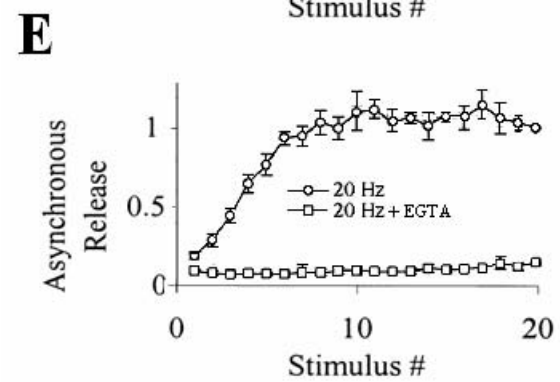
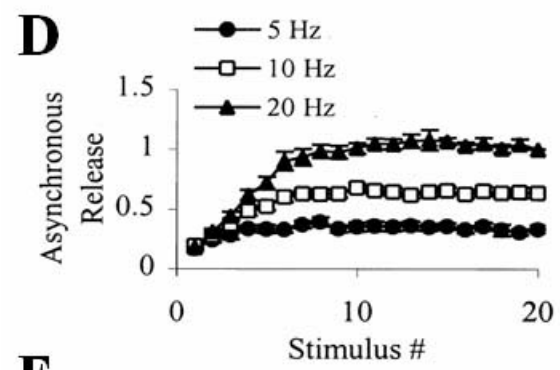
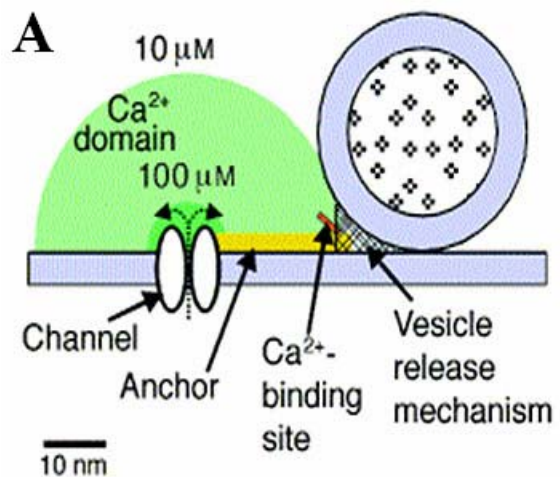


Figure 1.1: Presynaptic Ca^{2+} controls asynchronous neurotransmitter release at glutamatergic synapses. **A**, Presynaptic Ca^{2+} channels directly control evoked neurotransmitter release, but diffusion causes free $[\text{Ca}^{2+}]$ elevation throughout the terminal. **B**, Somatic membrane current recorded under voltage clamp in response to a single presynaptic action potential, reflecting mostly synaptic input. Mostly synchronous release (large peak) occurs when Ca^{2+} is the major extracellular divalent ion. **C**, When Sr^{2+} is the major extracellular divalent ion, asynchronous events become dominant, illustrating the capacity of the release machinery to support asynchronous release. The traces in **C** and **D** are individual voltage clamp recordings from single neurons, in which one action potential was evoked in a presynaptic partner immediately before the onset of the large inward current. **D**, In normal extracellular calcium, the asynchronous component of transmission is enhanced as a function of stimulus frequency and number. **E**, In the presence of the cell-permeable Ca^{2+} buffer EGTA-AM, asynchronous release develops much more slowly with each stimulus. In **D** and **E**, the measured value is charge transfer and the ordinate is normalized to the final value for the condition generating the most asynchronous release in each panel. All data from cultured hippocampal neurons; adapted from (Goda and Stevens, 1994; Hagler and Goda, 2001).

1.1.2. Long-Term Synaptic Plasticity

The size of neurotransmitter quanta and the probability of their release in response to presynaptic action potentials can be increased or decreased for hours *in vitro* by particular transient stimulation patterns (Malenka and Bear, 2004). Extracellularly recorded field potentials, which reflect the summation of many synaptic currents, can be increased for weeks *in vivo* by such patterns (Bliss and Lømo, 1973; Douglas and Goddard, 1975; Abraham, 2003). Such changes in synaptic strength alter mnemonic representations (Dragoi et al., 2003), are caused by experience *in vivo* (Clem and Barth, 2006; Whitlock et al., 2006) and manipulations that interfere with these long-term changes commonly disrupt learning ability (Ekstrom et al., 2001; Nakazawa et al., 2004).

These long lasting increases in synaptic efficacy, dubbed “long-term potentiation” (LTP), and analogous decreases (“long-term depression” or “LTD”), have become the dominant model of learning, memory, and representational plasticity (Stevens, 1996; Buzsaki and Chrobak, 2005). A variety of protocols have been used to induce LTP and LTD. Typically, these involve the use of stimulation frequencies not commonly observed *in vivo* (Albensi et al., 2007) or forced, extended excursions to specific membrane potentials (Gustafsson et al., 1987; Dudek and Bear, 1992; Mulkey and Malenka, 1992; Chen et al., 1999a). Such experiments also lack precise identification and control of both pre- and postsynaptic neurons, precluding knowledge of precisely what activity is occurring, and in which neurons. Furthermore, spiking activity in cortical structures is sparse under physiological conditions (Kerr et al., 2005). Thus, if classical plasticity-induction protocols inform us about long-term synaptic dynamics *in vivo*, it may be

due to hyper-activation of signaling pathways that normally respond to more modest membrane potential trajectories. These concerns suggest that an understanding of physiologically relevant long-term plasticity requires additional tools.

1.1.3. Calcium and synaptic plasticity

An integral part of the machinery responsible for long-term synaptic plasticity is postsynaptic free calcium, $[Ca^{2+}]$, whose concentration is tightly regulated (Cornelisse et al., 2007).

Postsynaptic $[Ca^{2+}]$ is necessary and sufficient for long-term synaptic plasticity: LTP and LTD are abolished by loading postsynaptic neurons with $[Ca^{2+}]$ buffers (Lynch et al., 1983; Mulkey and Malenka, 1992), and elevating postsynaptic $[Ca^{2+}]$ directly recapitulates LTP (Malenka et al., 1988) and LTD (Yang et al., 1999). More modest suppression of $[Ca^{2+}]$ accumulation causes protocols that normally potentiate synaptic efficacy to instead depress it (Cummings et al., 1996b; Nishiyama et al., 2000). These data have inspired a model of long-term synaptic plasticity that depends only on the peak $[Ca^{2+}]$ level: high plateaus of $[Ca^{2+}]$ accumulation result in potentiation, while lower levels result in depression (Bear et al., 1987; Lisman, 1989; Artola and Singer, 1993), and intermediate levels result in no net change in synaptic strength (Lisman, 2001).

Long-term synaptic plasticity has largely been studied at glutamatergic synapses. At these synapses, two critical mediators of a rise in $[Ca^{2+}]$ are N-Methyl-D-Aspartate Receptors (NMDARs), a family of ionotropic glutamate receptors (Cull-Candy et al., 2001; Cull-Candy et al., 2006; Isaac et al., 2007); and release of Ca^{2+} from intracellular stores (Fitzjohn and Collingridge, 2002), linked to metabotropic glutamate receptors (mGluRs, (Fagni et al., 2000;

Hermans and Challiss, 2001). At the Schaeffer collateral CA3-CA1 synapse of the hippocampus, the activation of the NMDAR, with its calcium-permeable pore, is essential for both LTP (Collingridge et al., 1983) and LTD (Dudek and Bear, 1992; Mulkey and Malenka, 1992). How one type of receptor could mediate both the strong, LTP-inducing calcium signal and the weak, LTD-inducing $[Ca^{2+}]$ signal attracted early attention (Bear and Malenka, 1994). The simplest hypothesis stated that differential levels of activation of the NMDAR in response to different stimuli were responsible for $[Ca^{2+}]$ signals unique to LTP or to LTD (Lisman, 1989). In contrast to NMDARs, the role of mGluRs in NMDAR-dependent LTP is disputed (Bortolotto et al., 1999), but their involvement in LTD has been firmly established (Christie et al., 1996; Bashir, 2003).

The NMDAR has a unique property which allows for coincidence detection. Mg^{2+} ions largely block the NMDAR channel pore at resting membrane potentials, precluding calcium influx when glutamate is bound (Mayer et al., 1984; Nowak et al., 1984; McBain and Traynelis, 2006). However, at depolarized membrane potentials, such as those associated with postsynaptic spiking, Mg^{2+} block is relieved and the channel exhibits an ohmic current-voltage relationship (Dingledine et al., 1986; Hablitz and Langmoen, 1986). Because this change in conductance more than offsets the reduction in driving force for calcium ions experienced at elevated membrane potentials (Jahr and Stevens, 1993), NMDAR-mediated calcium currents are enhanced when the presynaptic stimulus is strong enough to evoke postsynaptic spiking. This is consistent with the observation that larger $[Ca^{2+}]$ signals are better at producing LTP, which is often associated with such spiking; likewise, partial blockade of NMDARs during LTP-inducing protocols (Cummings et al., 1996b), or during spontaneous activity (Bains et al., 1999), resulting in reduced $[Ca^{2+}]$ signals, can result in LTD.

1.1.4. Spike-Timing Dependent Plasticity

Hebb conceived of synaptic plasticity as a phenomenon designed to reinforce causal relationships in the activity of neurons. Traditional plasticity protocols, in addition to being non-physiological, ignore this context for synaptic plasticity as outlined by Hebb: synaptic strengthening should be a consequence of a causal relationship between the firing patterns of two neurons, thus ensuring that those firing patterns are consolidated (Seung, 2000).

The existence of temporal requirements for synaptic plasticity (Levy and Steward, 1983) can be directly tested in the context of the Hebbian postulate: what would result when the spikes of an identified neuron A followed or preceded in time the spikes of an identified neuron B ? As Hebb predicted, when A fires before B , the strength of the synaptic connection between A and B is potentiated; the converse of Hebb's rule also holds: the synaptic connection from B to A is depressed (Magee and Johnston, 1997; Markram et al., 1997; Debanne et al., 1998). In hippocampal culture, among other preparations, these rules are only observed for pairs of glutamatergic neurons, and both directions of synaptic modification require NMDAR activation (Bi and Poo, 1998).

Most importantly, the change in synaptic efficacy is critically determined by not only the sign of the timing between spikes, but its magnitude. The demonstration of a quantitative "STDP curve" (Bi and Poo, 1998), in which the relative timing of pre- and postsynaptic action potentials is precisely mapped to a degree of synaptic modification, remains the seminal contribution to this field (Fig. 1.2). The canonical STDP relationship has been duplicated in a number of preparations (Feldman, 2000; Froemke and Dan, 2002), including *in vivo* (Zhang et al., 1998; Meliza and Dan, 2006), and its application to the computation of plasticity outcomes in response to arbitrary pre- and postsynaptic spike trains has been generalized as the "first-order STDP

rule".

Using this rule, modeling studies have invoked STDP as a mechanistic explanation for a range of phenomena including synchronization (Nowotny et al., 2003), phase precession (Sato and Yamaguchi, 2003), receptive field expansion and contraction (Mehta et al., 1997; Mehta et al., 2000; Yao et al., 2004; Meliza and Dan, 2006), auto-associative memory (Lengyel et al., 2005), reinforcement learning (Rao and Sejnowski, 2001; Florian, 2007), homeostasis (Song et al., 2000; Kempter et al., 2001; Rubin, 2001; Izhikevich and Desai, 2003), efferent copy cancellation (Roberts, 2005), and others (Letzkus et al., 2007). While the first-order rule is reversed or otherwise modified in some brain areas (Dan and Poo, 1992; Chen and Thompson, 1995; Bell et al., 1997; Egger et al., 1999; Tzounopoulos et al., 2004), and in interneuron populations (Lu et al., 2007; Tzounopoulos et al., 2007), it remains a popular approximation of the complexity of STDP.

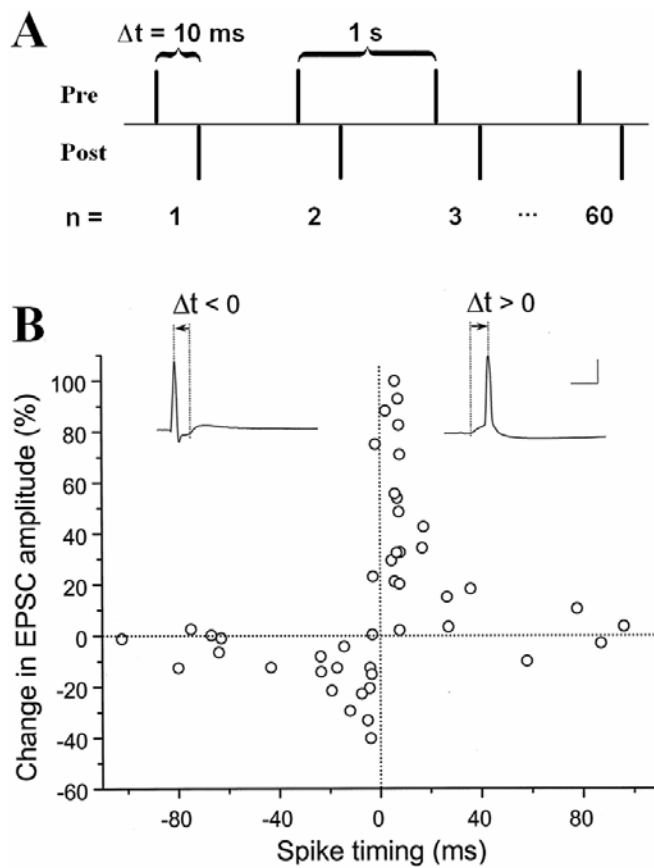


Figure 1.2: Spike-timing-dependent plasticity (STDP) in cultured hippocampal neurons. **A**, STDP is induced by repetitive pairing of pre- and postsynaptic action potentials at a fixed timing interval. **B**, STDP is a function of the timing interval, with potentiation for $\Delta t > 0$, and depression for $\Delta t < 0$. Each data point is one experiment. Insets are recordings from the postsynaptic neuron showing the membrane potential trajectory during each pairing. Adapted from (Bi and Poo, 1998).

1.1.5. Metaplasticity

The rules of synaptic plasticity are themselves subject to regulation, a phenomenon known as “metaplasticity” (Abraham and Bear, 1996). Metaplasticity is commonly revealed by pre-conditioning treatments which modify the induction threshold or expression magnitude of LTP (Le Ray et al., 2004; Zhang et al., 2005) or LTD (Philpot et al., 2003) in response to plasticity induction protocols.

Activity (or lack thereof) is one such conditioning treatment. For example, depriving juvenile animals of normal cortical input decreases the threshold for LTP induction and increases the threshold for LTD induction (Kirkwood et al., 1996). This potentially homeostatic compensation (Bienenstock et al., 1982) results in a circuit biased in favor of potentiation.

Plasticity itself is another conditioning treatment. Ceiling and floor effects can result in decreasing returns to successive LTP and LTD inductions, but the recent history of synaptic plasticity can influence subsequent plasticity through less trivial mechanisms as well, including reducing modification thresholds or “locking out” subsequent modifications (Montgomery and Madison, 2002; Hellier et al., 2007). Synaptic plasticity that occurs *in vivo* can also occlude or prime subsequent synaptic modification (Rioult-Pedotti et al., 2000; Tsvetkov et al., 2002; Clem and Barth, 2008).

1.1.6. Synaptic scaling and homeostasis

The direction of synaptic modification can also oppose ongoing activity, an anti-Hebbian phenomenon. In response to challenges that either increase or decrease neuronal activity from

baseline levels, quantal synaptic amplitudes can be bidirectionally regulated to counteract the challenge (O'Brien et al., 1998; Turrigiano et al., 1998). When the challenge is modest, the statistical structure of network activity can be gradually restored to pre-challenge levels (Beggs and Plenz, 2003). Synaptic scaling thus may act homeostatically to constrain the activity of neurons and circuits to a restricted operating range; however, the precise nature of the quantity being homeostatically regulated by synaptic scaling, is unknown.

When the scaling is positive, it is reflected in increases in the density of postsynaptic AMPARs (Wierenga et al., 2005), and/or increases in the size of presynaptic boutons and the probability of neurotransmitter release (Murthy et al., 2001). Synaptic scaling is typically studied *in vitro* in developing networks, but also occurs in the developing hippocampus (Echegoyen et al., 2007), the developing cortex (Desai et al., 2002), and the mature cortex *in vivo* (Goel and Lee, 2007).

1.1.7. Unanswered questions

Calcium- and NMDAR-dependent plasticity on multiple time-scales is well-established, however several questions remain unanswered. First, how can a calcium signal, driven by the millisecond-timing of single action potentials mediate potentiation, depression, or both simultaneously (chapter 2)? How can NMDAR activation, activated by such precisely timed stimuli, mediate these same outcomes; in which proteins and in what physiological changes might this capacity be localized (chapter 3)? How can plasticity mediated by the timing of spikes be integrated over timescales ranging from milliseconds to minutes, and how does the plasticity response change as a function of history and time (chapter 4)?

1.2. NETWORK ACTIVITY IN HIPPOCAMPAL NEURONS

The idea that a recurrent excitatory network could generate reproducible patterns of activation, corresponding to a memory trace (Lorente De No, 1933), is straightforward. Considering the implications of a property of the brain that reinforced causal relationships between pairs of neurons, Hebb proposed that self-organizing "cell assemblies" would become strong attractors (Hebb, 1931). This was the first clear prediction of synaptic plasticity, and was made in the proper context: the function of synaptic plasticity is correctly understood in the context of the behavior of a network.

1.2.1. Recurrent excitatory hippocampal networks

The hippocampus is critical for declarative memory in humans (Milner and Penfield, 1955; Eichenbaum, 2001) and spatial navigation in rodents (Morris et al., 1982; Burgess et al., 2002; Nakazawa et al., 2004; Leutgeb et al., 2005). However, the role of the hippocampus in memory was discovered incidentally because it is a common generator of another network phenomenon -- seizures (Penfield and Milner, 1958). This highlights the dual interest in the hippocampus in neurobiology. While the normal initiation, propagation, and termination of hippocampal activity patterns may be of interest to models of memory, abnormalities in any of these stages of activity can pique the interest of researchers investigating models of hippocampally-focused seizures, a symptom of mesial temporal lobe epilepsy (Sano, 1997). This highlights the difficult role that the hippocampus is asked to perform -- utilize a dense interconnectivity (Traub and Miles, 1991) that makes the storage and recall of tremendous numbers of patterns possible, while avoiding

pathological hyper-activation that can compromise memory (Giovagnoli and Avanzini, 1999; Leritz et al., 2006) and other cognitive functions.

Area CA3 of the hippocampus is one of the most highly recurrently connected areas of the brain (Fig. 1.3), with each CA3 pyramidal neuron synapsing onto 1-5% of other ipsilateral CA3 pyramidal neurons (Lorente De No, 1934; Miles and Wong, 1986; Miles et al., 1988; Amaral et al., 1990; Traub et al., 1991). This anatomical feature has led to the hypothesis that patterned input, containing a subset of the features of an engram, is completed as the pattern of activity in CA3 evolves towards one of many energetically favored states (attractors) made possible by this recurrent network (Marr, 1971; McNaughton and Morris, 1987; Nakazawa et al., 2002; Leutgeb and Leutgeb, 2007).

Because of the high density of recurrent connectivity in CA3, it has long been investigated as an initiation site for spontaneous activity (Buzsaki et al., 1990). Experimentally, it is the initiation site for both paroxysmal depolarizing shifts (PDS, a large spontaneous depolarization of a neuronal population) (Prince, 1968; Schwartzkroin and Prince, 1978) and sharp waves (Buzsaki, 1986), and may be a generator for the hippocampal theta rhythm (Strata, 1998; Buzsaki, 2002).

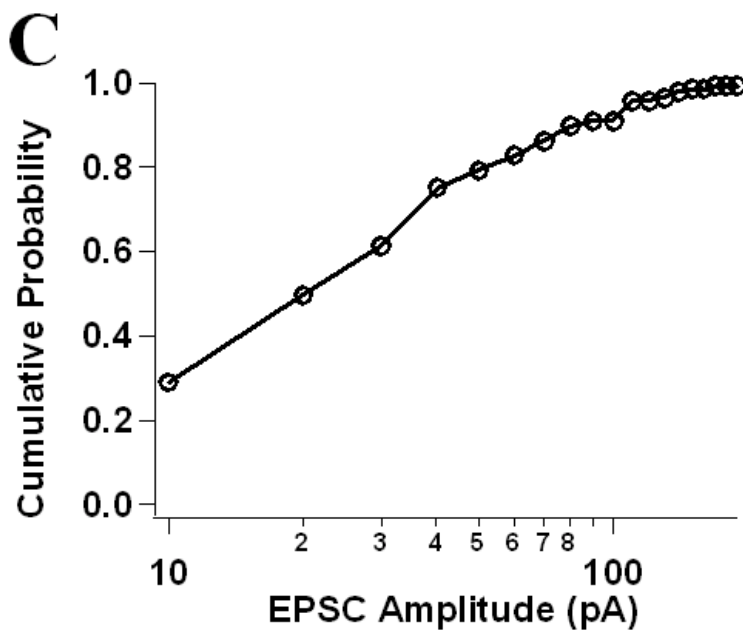
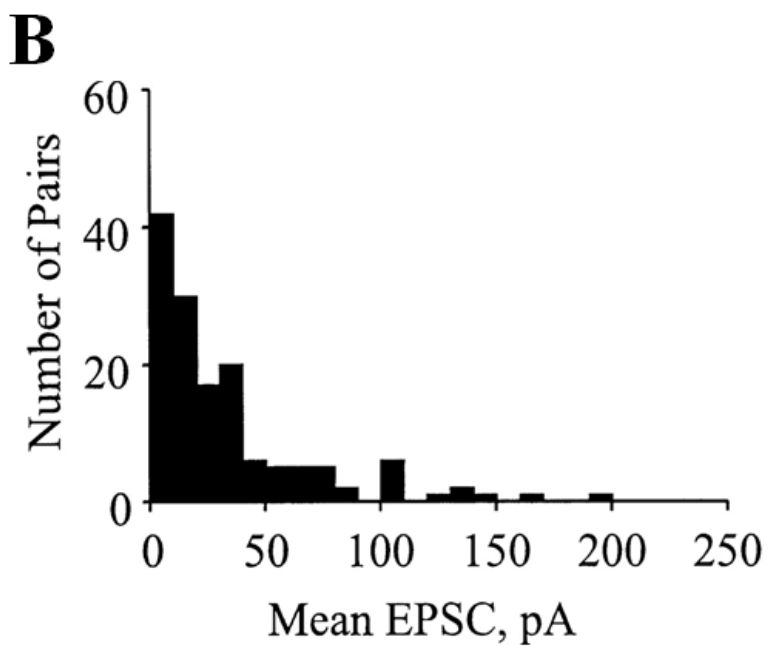
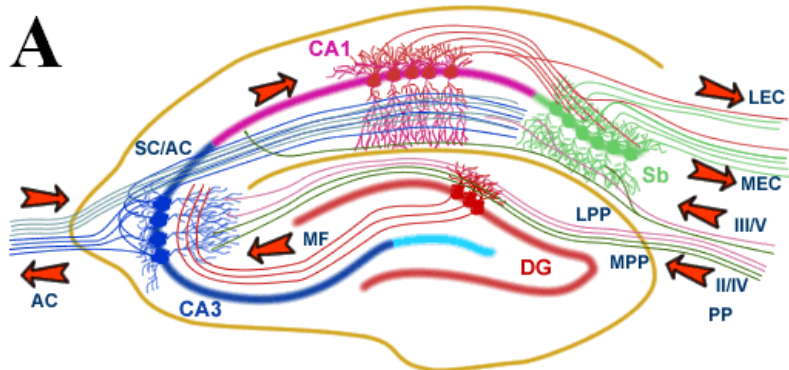


Figure 1.3: Strong recurrent connectivity exists in hippocampal circuitry. **A**, Schematic of the fundamental “trisynaptic” hippocampal circuit. Input arriving from cortical layers II and IV via the perforant path (PP) arrives at the granule cell of the dentate gyrus (DG). Mossy fibers (MF) from this area makes synapses onto the neurons of area CA3, which exhibits substantial recurrent connectivity. The output of area CA3 reaches area CA1, whose pyramidal cells project to the subiculum (Sb) and out to the entorhinal cortex (EC). **B**, Histogram of evoked postsynaptic currents in response to presynaptic stimulation for pairs of connected neurons in area CA3 of a cultured hippocampal slice, illustrating the skewed distribution of these connection strengths. In this preparation, ~1/3 of recorded pairs exhibit monosynaptic connections. **C**, Same data as *B*, plotted as a cumulative histogram on a logarithmic scale to illustrate the functional form of the amplitude distribution. Adapted from (Pavlidis and Madison, 1999).

1.2.2. Hippocampal networks *in vitro* and *in silico*

Because the canonical circuitry of the hippocampus (Fig. 1.3a) is repeated throughout its dorso-ventral axis, the transverse hippocampal slice is an accessible and relevant model system for exploring these dynamics further (Schwartzkroin and Prince, 1977). Patch clamp recordings and histochemical analyses have enabled the kinetics, conductances, and distribution of various ion channels to be reliably estimated experimentally. These data have been incorporated into successively more realistic models of CA3 (Traub and Wong, 1982; Traub et al., 1989; Traub et al., 1991; Traub et al., 1994b; Poirazi et al., 2003b) and the hippocampus at large (Traub and Miles, 1991; Bennett et al., 1994). However, a major limitation of these early models, which may have resulted from limited data from paired patch clamp recordings, was insufficient attention to the features of short-term synaptic dynamics.

Nonetheless, sufficiently detailed neuronal models have reproduced certain phenomena observed in intracellularly recorded neurons *in vitro*, especially in tissue taken from developing hippocampi (Swann et al., 1991) (Fig. 1.4a). These models have emphasized the consequences of positive feedback in a massively recurrent excitatory network modeled after CA3. In simulation, spontaneous uncorrelated spiking at low frequencies can give rise to a network-wide increase in firing rates, either stochastically, or due to stimulation of an axonal population (Traub and Wong, 1982; Haas and Jefferys, 1984; Miles et al., 1988), a result consistent with observations made in hippocampal slices (Schwartzkroin and Prince, 1978; Traub and Wong, 1982; Miles et al., 1988; Traub et al., 1993; Traub et al., 1996). These firing-rate increases last for ~100 ms, and typically span most or all of the CA3 network. In model networks their

termination has generally been attributed to hyperpolarizing conductances mediated by $[Ca^{2+}]$ elevations during the burst (Schwartzkroin and Stafstrom, 1980).

In some cases, secondary bursts are observed (Traub et al., 1996)(Fig. 1.4b), whose generation has been attributed to time- or activity-dependent inactivation of these hyperpolarizing conductances (MacVicar and Tse, 1989; Charpak et al., 1990), and/or the accumulation of an activity-dependent intrinsic inward conductance (Caeser et al., 1993), combined with elevated excitability due to extracellular K^+ accumulation (Haas and Jefferys, 1984; Louvel et al., 1994). Slow desensitization of NMDARs has been suggested to be responsible for the eventual cessation of these secondary bursts (Traub et al., 1994a), although whether this is in fact a dominant mechanism has been unclear (Traub et al., 1996).

In contrast to other types of synchronous network activity (Bartos et al., 2007, inhibition does not appear to be important for the generation or these events, although it can help to shape their timing {Cobb, 1995 #1593; Mann and Paulsen, 2007}). In general, inhibition reduces the probability and duration of these events, and abolishing inhibition pharmacologically shows that excitatory synaptic events are responsible for synchronizing and sustaining such network activity (Schwartzkroin and Prince, 1977; Mueller and Dunwiddie, 1983; Korn et al., 1987; Miles and Wong, 1987; Chamberlin and Dingledine, 1989). Thus, many researchers choose to study CA3 activity in partially or completely disinhibited slices, in order to eliminate one potential source of variance, to increase the number of recorded events for statistical purposes, or to study epileptogenic tissue, which is associated with reduced synaptic inhibition (Obenaus et al., 1993; Morin et al., 1998; McCormick and Contreras, 2001; El-Hassar et al., 2007).

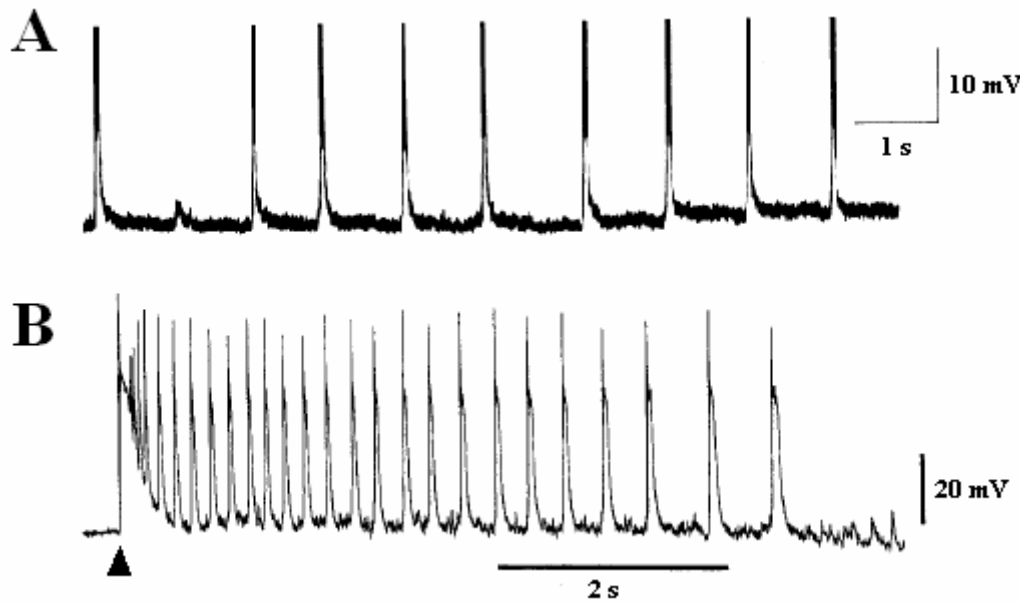


Figure 1.4: Network activity in the disinhibited hippocampal slice. **A**, In a slice that exhibits spontaneous synchronization, due to an increase in extracellular K^+ concentration, synchronous network events recur continuously at 1 Hz. Adapted from (Korn et al., 1987). **B**, In a slice that does not exhibit spontaneous synchronization of the neuronal population, a single stimulation of collaterals (arrowhead) can evoke a rhythmic oscillation, lasting for seconds, composed of synchronous population events. Adapted from (Traub et al., 1996). In both *A* and *B*, the data are single traces recorded in current clamp from pyramidal neurons in area CA3 of the hippocampus.

1.2.3. Mechanisms determining the timing of synchronous activity in recurrent neuronal networks

In many real and model networks, including the disinhibited hippocampal slice, rhythms exist which alternate between periods of high excitation and periods of relative quiescence (Fig. 1.4a). In principle, these rhythms can be explained by positing a form of inhibitory feedback to terminate recurrent excitation, and by assuming that the decay time of the inhibitory feedback regulates the interval between cycles (Whittington et al., 2000). In practice, uniquely identifying the inhibitory process(es) actually responsible for the generation of oscillatory behavior is a nontrivial problem, due in part to the fact that several processes may share similar decay time constants. Compounding the problem, some rhythms have variable inter-peak intervals, challenging the deterministic assumptions typically involved in discovering a mechanism.

In the disinhibited hippocampal slice, the occurrence of synchronous events is associated with an increase in the rate of excitatory postsynaptic potentials (EPSPs) prior to onset (Chamberlin et al., 1990). The frequency of these rhythmic events can be modulated by manipulations that change the excitability of individual neurons, amplifying the effect of these EPSPs on spike generation. For example, raising extracellular K⁺ concentration reduces both the mean and the variance of the inter-event interval (Rutecki et al., 1985; Staley et al., 2001). This suggests that increasing cellular excitability permits the network to more rapidly resynchronize as it recovers from “inhibition” imposed by its most recent discharge. The “inhibition” itself could have a wide range of forms, all with recovery times on the order of seconds. However, in this preparation synaptic depression has been shown to be the essential mediator of this inhibition (Staley et al., 1998). While synaptic depression recovers on multiple timescales, depending on the history of presynaptic activity, its longest timescale, ~3-11 s (Liu and Tsien,

1995; Stevens and Wesseling, 1998), determines the statistical properties of rhythmic discharges in hippocampal slices (Staley et al., 2001).

1.2.4. Cultured Hippocampal Neurons as a Model System

The hippocampal slice retains some of the anatomical features of a hippocampus *in vivo*; however, the slicing procedure severs a substantial fraction of neuronal processes, activates stress-related proteins, and alters phosphorylation states (Aitken et al., 1995), leaving the experimenter with a network whose properties may be tuned for the brain in which it was recently embodied, rather than the context in which it is examined. An alternative approach is to use primary hippocampal cultures (Banker and Cowan, 1977; Banker and Goslin, 1998). In this technique, neurons are completely dissociated from the hippocampus and the laminar structure is destroyed. However, processes regrow to form functional synaptic connections between neurons (Kaech and Banker, 2006). Thus, hippocampal cultures offer a network at equilibrium -- its structure is not radically altered prior to recording, and its neurons are tuned to the dynamic context of the circuit studied in the experiment.

Cultures facilitate perforated-patch clamp recordings, which make it possible to obtain stable intracellular recordings for many hours from single neurons (Rae et al., 1991; Akaike and Harata, 1994). They also lend themselves to pharmacological challenges or genetic manipulations over a wide range of timescales (hours to months)(Potter and DeMarse, 2001), while requiring very small quantities of drugs or viral vectors. Lastly, diffusion in cultures is significantly faster than in slices or *in vivo*, allowing rapid solution exchange, which permits dose-response curves to be rapidly constructed, and enables the modulation of network

properties within seconds.

While a hybrid protocol, organotypic culture (Gahwiler et al., 1997) better preserves the *in vivo* anatomical circuitry (Bolz, 1994), unlike primary culture it cannot be used to create networks of arbitrary size (Lau and Bi, 2005), shape (Feinerman et al., 2005), and large-scale connectivity. Because primary cultured neurons and glia are pipetted onto glass coverslips, modifications can be made to these coverslips to ensure that cells only "stick" to certain locations (Kaech and Bunker, 2006). Chemo-attractants and -repellants can be used to further dictate where each group of neurons can send its processes.

1.2.5. Network Activity in Cultured Hippocampal Neurons

By default, cultured cells can be grown across an entire coverslip, a condition called "confluence". These confluent networks are the basis for the overwhelming majority of research into the network properties of cultured neurons. Confluent cultured hippocampal neurons can exhibit behaviors resembling those observed in the disinhibited hippocampal slice, such as low frequency, spontaneous, synchronous network activity (Furshpan, 1991). This makes this system an intriguing seizure model (Sombati and Delorenzo, 1995), based upon the assumption that recurrent excitation is the principal source of seizures *in vivo*, and that epileptogenesis is a process by which positive feedback recurrent excitation is enhanced (McCormick and Contreras, 2001).

When cultures are made from embryonic rats (E19), nearly all of the principal cells of the network are likely to be from area CA3 and CA1, as the granular layer of the dentate gyrus does not form until E21 (Altman and Bayer, 1990). The high rate of recurrent connectivity in these

areas makes it unsurprising that patterns of spontaneous, synchronous network activity should exist in cultured networks. However, spontaneous action potential discharge can be minimized if cultures are sufficiently sparse (Wilcox et al., 1994). Nonetheless, when acutely challenged with excitatory media, non-synchronous networks exhibit spontaneous synchronous discharges that can persist after withdrawal of the excitatory challenge (Sombati et al., 1991; Sombati and Delorenzo, 1995). Compounds that are shown to either block the acute effect, or reverse the effect at some later time, may be considered anti-epileptogenic and of possible therapeutic value. However, it is not trivial to find anti-epileptogenic compounds that reduce the duration or probability of network synchrony without otherwise modulating “normal” spontaneous network activity that may be essential to its proper function.

1.2.6. Reverberation in Small Cultured Networks

On a 12 mm coverslip, treatment with a uniform pattern of poly-L-lysine prior to the plating of neurons and glia produces a confluent network with the dynamics described above. However, alternative dynamics are revealed by studying smaller networks, where cells and synapses are more narrowly localized. Our lab has developed expertise in producing hexagonal arrays of 1 mm poly-L-lysine spots (Lau and Bi, 2005). When these spots are generated with care, neurons and glia will be restricted to the spots, forming several independent networks. While it is possible that diffusible signals could cross from one island to another, the possibility of axons or dendrites crossing bare glass to reach another island is remote (Wyart et al., 2002). Each of these independent networks can be studied simultaneously, or in sequence, using patch clamp or imaging techniques. Because the entire network can be visualized under a microscope at 10x

magnification (Fig. 1.5a), complete neuron counts and morphological examinations can be made, and the activity of every neuron can be monitored using, for example, Ca^{2+} imaging.

We have used these island networks as a model system for the Hebbian cell assembly. In contrast to large networks, confluent across the coverslip, spontaneous synchronous activity in these island networks is rare. Spontaneous uncorrelated action potentials are also infrequent. However, if a single neuron is stimulated with a suprathreshold depolarization for ~ 1 ms, a polysynaptic current cluster (PSCC) can be observed under voltage clamp recording, lasting ~ 150 ms (Fig. 1.6a, blue trace (Lau and Bi, 2005)). Current clamp records show that this PSCC causes depolarizations resulting in 0-2 action potentials. Dual recordings and Ca^{2+} imaging indicate that a PSCC reflects superthreshold activation of most neurons in the island network (Lau and Bi, 2008).

In contrast to confluent networks, island networks frequently exhibit subsequent PSCCs, beginning ~ 100 ms after the first, and continuing at 4-10 Hz for seconds. These chains of PSCCs are termed "reverberations", after the terminology Hebb used for sequences of cell activation in his theoretical cell assembly (Hebb, 1949), and are reminiscent of events seen in disinhibited hippocampal slices under elevated extracellular K^+ (Traub et al., 1996).

Reverberations are critically dependent on asynchronous neurotransmitter release (Lau and Bi, 2005), which dominates the recorded membrane current in the interval between PSCCs. The intervals between PSCCs within a reverberation tends to increase monotonically (Fig. 1.6a, red trace), analogous to so-called tertiary events in the disinhibited hippocampal slice model of reverberation (Hablitz, 1984; Miles et al., 1984; Traub et al., 1996). Analysis of voltage clamp recordings and Ca^{2+} imaging shows serial correlation across PSCCs in the sequence of neuronal activation within a PSCC (Lau and Bi, 2008).

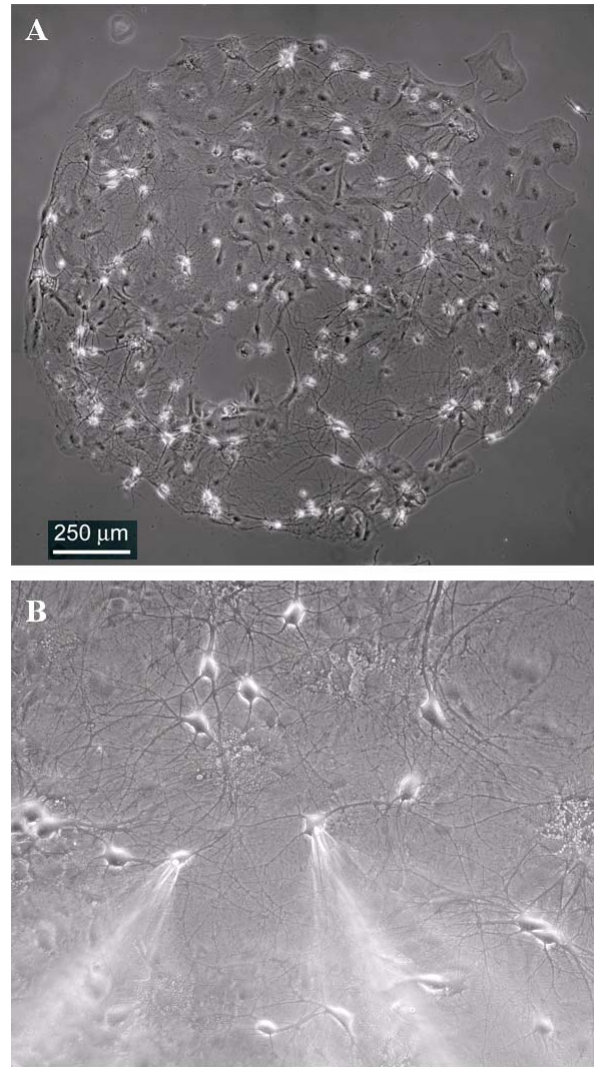


Figure 1.5: The small network “island” culture model. **A**, A restricted island of neurons and glia can be identified and targeted for recording. 50-100 neurons can be found on a typical island. Adapted from (Lau and Bi, 2005). **B**, Two neurons from an island recorded using the perforated patch clamp configuration.

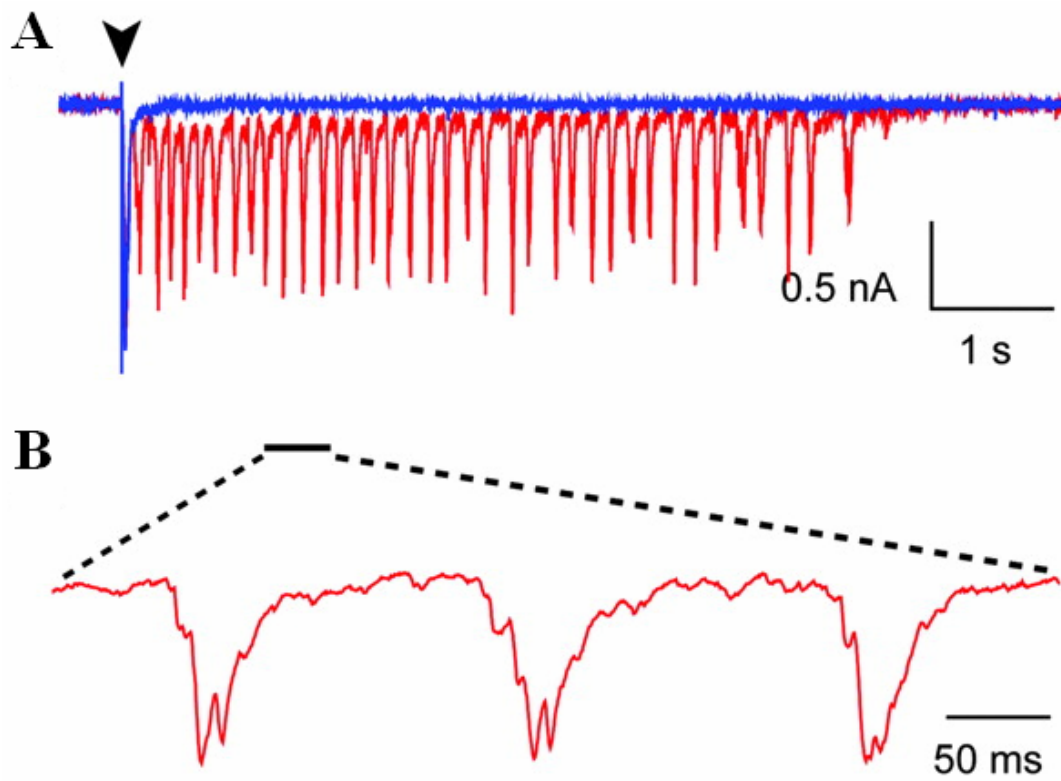


Figure 1.6: Reverberation in small cultured networks. **A**, A transient (1 ms) suprathreshold stimulus (arrowhead) delivered to a single neuron evokes either a single synchronous network event (blue), or a reverberation consisting of many such events, lasting for seconds (red), as visualized in voltage clamp. **B**, Expansion of the red trace in **A**, illustrating the similarity between synchronous network events, reflecting cell assembly organization. Adapted from (Lau and Bi, 2005).

1.2.7. Unanswered Questions

Persistent network activity patterns are ubiquitous in many preparations *in vitro* and *in vivo*, however the relationship between the plasticity of synaptic transmission and the evolution of these activity patterns is unknown, and will be addressed here. First, how do Hebbian plasticity and synaptic scaling contribute to the development of network architectures that support reverberations; what quantity or neuronal function is regulated by synaptic homeostasis (chapter 5)? Second, how do the timescales of presynaptic calcium regulation and synaptic dynamics determine the existence, persistence and stability of a reverberatory regime (chapter 6)?

2. POSTSYNAPTIC CALCIUM TIME COURSE AS A SIGNAL FOR SPIKE-TIMING-DEPENDENT PLASTICITY

2.1. INTRODUCTION

2.1.1. STDP and the Integration of Complex Stimuli

Hippocampal neurons involved in memory tasks often fire in bursts containing multiple action potentials (O'Keefe and Recce, 1993); thus, the first-order STDP rule (Chapter 1Aiv) may have limited applicability in predicting changes in synaptic efficacy in response to naturalistic activity patterns. However, by combining multiple spike-timing "motifs" -- pairs of one pre- and one postsynaptic spike -- into a complex stimulus, "second-order" rules can be discovered (Bi and Rubin, 2005). A typical null hypothesis for these experiments states that the plasticity outcome of complex spike pairings will be the linear sum of the first-order rule applied to all temporal interactions of pre- and postsynaptic spikes.

However, because the signaling mechanisms for plasticity are likely to be nonlinear, it is unsurprising that second-order rules that do not, in fact, match this hypothesis. Indeed, in contrast to the first-order rules, which are consistent across a wide range of preparations (Markram et al., 1997; Bi and Poo, 1998; Zhang et al., 1998; Feldman, 2000; Nishiyama et al., 2000; Sjostrom et al., 2001; Froemke and Dan, 2002; Zhou et al., 2005; Letzkus et al., 2006),

these second-order rules are highly variable, and not produced by a simple summation of first order rules (Sjostrom et al., 2001; Froemke and Dan, 2002; Wang et al., 2005).

To describe these complex stimuli, one can refer to the order of presynaptic spikes ("A") and postsynaptic spikes ("B"). Under the null hypothesis, the triplet stimulus "ABA", in which two presynaptic spikes flank a postsynaptic spike in time, and the triplet stimulus "BAB", in which two postsynaptic spikes flank the presynaptic spike, should result in the same plasticity outcome, which the first-order rule predicts is a combination of strengthening due to the "AB" motif, and weakening due to "BA" motif.

In hippocampal culture, ABA (or ABBA) stimuli result in neither LTP nor LTD, but rather no change in synaptic strength. BAB (or BAAB) stimuli, by contrast, result in LTP of a magnitude similar to that seen with the first-order AB stimulus (Wang et al., 2005). In connections between layer 5 neurons of visual cortex, LTP dominates the response to these mixed stimuli, regardless of the order of motifs (Sjostrom et al., 2001). At horizontal connections within layer 2/3, yet another set of rules is observed (Froemke and Dan, 2002), in which earlier spikes have more influence than later spikes in determining the sign and magnitude of synaptic plasticity. These diverse results have rendered difficult the search for a general second-order rule applying to all experimental preparations (Bi and Rubin, 2005).

2.1.2. Defects in the traditional calcium hypothesis of bidirectional long-term synaptic plasticity

Calcium is an essential second messenger in signaling cascades for LTP and LTD (Lynch et al., 1983; Yang et al., 1999). According to the conventional wisdom, high postsynaptic $[Ca^{2+}]$

produces LTP and low $[Ca^{2+}]$ produces LTD, the so-called calcium level hypothesis (Lisman, 1989). On the surface, such a simple requirement would seem sufficient to explain STDP. An EPSP arriving just before a postsynaptic back-propagating action potential would benefit from voltage-dependent Mg^{2+} unblock and enhanced NMDAR currents (high $[Ca^{2+}]$, LTP), while one arriving after the action potential would be too late to exploit this condition (low $[Ca^{2+}]$, LTD). Indeed, this basic schema has been used to model STDP (Karmarkar and Buonomano, 2002; Shouval et al., 2002)

However, this approach fails to explain several aspects of the data. First, low postsynaptic $[Ca^{2+}]$ should also occur when a presynaptic spike precedes a postsynaptic spike by a sufficient temporal interval. For some large, positive interval, the EPSP should have decayed to the point where amplification of NMDAR conductance by the backpropagating action potential produces $[Ca^{2+}]$ equal to that associated with LTD (Shouval et al., 2002). However, experimentally there is typically no LTD observed for large, positive spike-timing (Bi and Poo, 1998; Froemke and Dan, 2002; Froemke et al., 2005). Second, whereas a presynaptic spike followed by a postsynaptic spike results in LTP, adding a second presynaptic spike after the postsynaptic spike results in no LTP (Wang et al., 2005). Since it is unclear how this second presynaptic spike could actually lower postsynaptic $[Ca^{2+}]$, the calcium level hypothesis appears deficient. In this chapter, I present an alternative model for the transduction of spike times into STDP outcomes. This model exploits the entire postsynaptic $[Ca^{2+}]$ time course, rather than just the level, and in so doing recapitulates experimental results for spike doublets and triplets.

2.2. METHODS

2.2.1. Neuronal and Synaptic Dynamics

The model was implemented with two compartments. In each compartment, the membrane potential evolved according to:

$$v' = I \frac{I_L + I_{Na} + I_{Ca} + I_K + I_{coup} + I_{in}}{C_m} \quad \text{eq. 2.1}$$

where I_L is a leak current; I_{Na} is a sodium current; I_{Ca} is a high-threshold calcium current; I_K is the sum of a potassium A current, a delayed rectifier potassium current, and a calcium-activated potassium afterhyperpolarization current, all based on experimental data (Poirazi et al., 2003a). I_{coup} is the electrical coupling between the compartments, and I_{in} corresponds to current injections (in the soma) or to synaptic currents, I_{AMPA} and I_{NMDA} (in the spine), as described in equations 2.3-2.8. Membrane capacitance C_m was normalized to $1 \mu\text{F}/\text{cm}^2$ and all conductances were scaled accordingly to maintain appropriate membrane potential dynamics in our compartmental reduction. Equations governing the evolution of state variables for non-synaptic currents are derived from (Traub et al., 1991; Traub et al., 1994b) and are available in (Rubin et al., 2005). All dynamic variables were updated in 0.1 ms time-steps.

Table 2.1: Conductance values for the postsynaptic Ca²⁺ detector model of STDP

Parameter (mS/cm ²)	Value (Soma)	Value (Spine)	Description	Source and Comments
g_L	0.1	0.1	Leak conductance	All values are peak conductances for maximal activation; (Poirazi et al., 2003a)
g_{Na}	30	7	Sodium conductance	
$g_{K(A)}$	7.5	12	A-type potassium conductance	
$g_{K(dr)}$	14	0.867	Delayed rectifier potassium	
$g_{K(mAHP)}$	25	0	Afterhyperpolarization conductance	
$g_{Ca(L)}$	7	25	L-type calcium conductance	
g_{coup}	1.125	1.125	Conductance between compartments	

We implemented calcium dynamics similar to (Traub et al., 1994b) in each compartment, which take the form:

$$\chi' = \Phi I_{Ca} - \beta_1(\chi - \chi_0) - \beta_2(\chi - \chi_0)^2 - \frac{\Delta\chi}{d} \quad \text{eq. 2.2}$$

where χ is the calcium concentration in μM , χ_0 denotes the resting calcium concentration, d is a diffusion time constant between compartments, $\Delta\chi$ is the concentration difference between compartments, and $\beta_{1,2}$ control the strength of linear and nonlinear calcium buffering, respectively. The current I_{Ca} denotes calcium influx through voltage gated channels, with Φ representing the change in calcium concentration per unit of calcium influx. Parameters were selected to match experimental data on dendritic calcium dynamics (Koester and Sakmann, 1998; Yuste et al., 1999; Murthy et al., 2000; Sabatini et al., 2002), with resting calcium levels constrained by specific experimental results (Pozzo-Miller et al., 1999; Yuste et al., 1999; Maravall et al., 2000).

Table 2.2: Parameters governing postsynaptic calcium dynamics.

Parameter	Value (Soma)	Value (Spine)	Description	Source and Comments
Φ ($M^* cm^2 A^{-1}$)	0.01	0.01	Increase in $[Ca^{2+}]$ per unit calcium current	(Sabatini et al., 2002)
β_1 (ms^{-1})	0.083	0.083	First-order calcium decay time constant	
β_2 ($ms^{-1} \mu M^{-1}$)	0.0138	0.0138	Second-order calcium decay time constant	
d (ms)	1000	1000	$[Ca^{2+}]$ coupling between compartments	
x_0 (μM)	0.05	0.07	Baseline $[Ca^{2+}]$	(Yuste et al., 1999; Maravall et al., 2000)

Current flowing through NMDARs is composed of a diversity of ions, each with different driving forces and conductance sensitivities to postsynaptic membrane potential. Thus, I distinguished between the calcium current through these channels (used to compute changes in calcium concentration), and the total current (used to compute changes in membrane potential). I implemented each of these with equations of the form:

$$I = -g^* s^* m^*(v - v_{rev}) \quad \text{eq. 2.3}$$

where g is a constant maximal channel conductance density, s is the time and glutamate-dependent activation level of the channels, m measures the voltage-dependence (which for NMDARs is determined by the degree of Mg^{2+} block), and v_{rev} is the reversal potential of the current. I chose parameters for NMDAR based on the data from (Jahr and Stevens, 1990b, 1993), using:

$$m_{NMDA} = \frac{1}{1 + 0.3[Mg^{2+}]e^{-\nu}} \quad \text{eq. 2.4}$$

with the extracellular magnesium concentration $[Mg^{2+}] = 2 \text{ mM}$, according to the concentration used in STDP experiments in hippocampal culture (Wang et al., 2005). γ reflects the voltage-dependence of this Mg block (Jahr and Stevens, 1990a). For current flowing through AMPARs, which are largely calcium impermeable, I considered only its contribution to membrane potential, and assumed that the channel was non-rectifying ($m=1$). For both types of synaptic currents, I used activation equations that yield simulated, stimulus-induced time courses that resemble those observed in experiments conducted at room temperature (Perouansky and Yaari, 1993; Andrasfalvy and Magee, 2001). These take the form:

$$s = s_{\text{rise}} + s_{\text{fast}} + s_{\text{slow}} \quad \text{eq. 2.5}$$

$$s_{\text{rise}}' = -\Phi(1 - s_{\text{fast}} - s_{\text{slow}})f_{\text{pre}}(t) - s_{\text{rise}}/\tau_{\text{rise}} \quad \text{eq. 2.6}$$

$$s_{\text{fast}}' = \Phi(a_{\text{fast}} - s_{\text{fast}})f_{\text{pre}}(t) - s_{\text{fast}}/\tau_{\text{fast}} \quad \text{eq. 2.7}$$

$$s_{\text{slow}}' = \Phi(1 - a_{\text{fast}} - s_{\text{slow}})f_{\text{pre}}(t) - s_{\text{slow}}/\tau_{\text{slow}} \quad \text{eq. 2.8}$$

where $f_{\text{pre}}(t)$ represents a step pulse corresponding to the timing of the presynaptic action potential.

Table 2.3: Parameters governing postsynaptic glutamate receptors

Parameter	Value			Description	Comments and Source		
	AMPAR	NMDAR					
		Current	Ca ²⁺				
v_{rev} (mV)	0	0	140	Reversal potential for synaptic current	(Poirazi et al., 2003a)		
γ (mV ⁻¹)	∞	0.062	0.124	V _m -dependence of synaptic currents	(Jahr and Stevens, 1990a, 1993)		
g (mS/cm ²)	0.05	0.3	25	Synaptic conductance	(Perouansky and Yaari, 1993; Andrasfalvy and Magee, 2001)		
τ_{rise} (ms)	0.58	2	2	Time constants for the synaptic current			
τ_{fast} (ms)	7.6	10	10				
τ_{slow} (ms)	25.69	45	45				
a_{fast}	0.903	0.527	0.527	Relative weight given to τ_{fast}	Used to scale the rising phase to the duration of the simulation time step		
Φ (ms ⁻¹)	20	20	20				

2.2.2. Calcium Detectors

Plasticity outcomes our computed in this model by a biophysically plausible detection system that responds to [Ca²⁺] and produces output of the appropriate sign and magnitude. Five detector agents respond to the instantaneous [Ca²⁺] in a dendritic compartment, which could reflect a spine or simply a dendritic segment. Different calcium time courses lead to different time courses of the detectors P , V and A , which compete to influence a plasticity variable W , which is initialized to zero to favor neither potentiation nor depression. W serves as a measure of the sign and magnitude of synaptic strength changes from baseline. B and D act as filters (e.g. extra steps in a signaling pathway) to map [Ca²⁺] time courses onto the correct final values of W . I have since found that the data shown in Figure 2.1 can be reproduced by collapsing the A,B,D depression pathway into two ODEs instead of three, with simplification to the equations below,

further increasing the plausibility of the model, but for consistency with published data I show the original form here. The detector equations are:

$$P' = \frac{p_\sigma(\chi) - c_p AP}{\tau_w} \quad \text{eq. 2.9}$$

$$V' = \frac{v_\sigma(\chi) - V}{\tau_v} \quad \text{eq. 2.10}$$

$$A' = \frac{a_\sigma(\chi) - A}{\tau_a} \quad \text{eq. 2.11}$$

$$B' = \frac{b_\sigma(A) - B - c_d BV}{\tau_b} \quad \text{eq. 2.12}$$

$$D' = \frac{d_\sigma(B) - D}{\tau_d} \quad \text{eq. 2.13}$$

$$W' = \frac{\alpha_w}{1 + e^{(p-P)/k_p}} - \frac{\beta_w}{1 + e^{(d-D)/k_d}} - \frac{W}{\tau_w} \quad \text{eq. 2.14}$$

where χ in all cases represents $[\text{Ca}^{2+}]$ in the “spine” compartment. I chose the calcium sensitivity for P and A to match the Hill equation:

$$f_\sigma(x) = \frac{1}{1 + (\theta_f/x)^{n_f}} \quad \text{eq. 2.15}$$

with parameters taken from previous modeling work on the activation, autophosphorylation, and dephosphorylation of CaMKII (Holmes, 2000; Lisman and Zhabotinsky, 2001). The other detector (B, D, V) steady states have the form:

$$f_\sigma(x) = \frac{\alpha_f}{1 + e^{(\theta_f - x)/\sigma_f}}$$
eq. 2.16

Table 2.4: Parameters governing postsynaptic calcium detectors.

Parameter	Value	Description	Comments and Source
θ_p (μM)	4	$[\text{Ca}^{2+}]$ Activation threshold for P (potentiation)	$(\text{Zhabotinsky}, 2000;$ $\text{Lisman and Zhabotinsky},$ $2001)$
θ_a (μM)	0.6	$[\text{Ca}^{2+}]$ Activation threshold for A (depression)	
θ_v (μM)	2	$[\text{Ca}^{2+}]$ Activation threshold for V (veto)	
θ_d	2.6	B Activation threshold for D (depression)	
θ_b	0.55	A Activation threshold for B (depression)	
τ_p (ms)	50	Decay time constant for P	
τ_a (ms)	5	Decay time constant for A	
τ_v (ms)	10	Decay time constant for V	
τ_d (ms)	250	Decay time constant for D	
τ_b (ms)	40	Decay time constant for B	
c_p	0.5	Inhibition of P by A	These are free parameters chosen to recapitulate the experimental results.
τ_w (ms)	500	Decay time constant of W	
α_w	0.0016	Relative contribution of potentiation to W	
β_w	0.0012	Relative contribution of depression to W	
n_p	4	Hill exponent for P	
n_a	3	Hill exponent for A	
σ_v (μM)	0.05	Activation width for V	
σ_d	0.01	Activation width (by B) for D	
σ_b	0.02	Activation width (by A) for B	
k_p	0.1	Activation width (by P) for W	
k_d	0.002	Activation width (by D) for W	These are free parameters chosen to recapitulate the experimental results.
α_v	1.0	Growth rate of V	
α_d	1.0	Growth rate of D	
α_b	5.0	Growth rate of B	
c_d	4	Inhibition of B by the veto (V)	
p	0.3	Activation threshold (by P) for W	
d	0.01	Activation threshold (by D) for W	

It is critical that $\theta_p > \theta_a$ and $\theta_v > \theta_a$ ensuring that there is a regime of $[Ca^{2+}]$ in which depression can be activated without being inhibited (“vetoed”) and without activating potentiation.

2.3. RESULTS

We propose that it is not simply a postsynaptic $[Ca^{2+}]$ level that determines plasticity outcomes, but the dynamic postsynaptic $[Ca^{2+}]$ timecourse (Sabatini et al., 2002; Ismailov et al., 2004). To demonstrate how this could occur, we constructed a two-compartment model of a CA3 pyramidal neuron (Methods, 2.2.1; Tables 2.1-2.3) incorporating realistic somatodendritic conductances (Traub et al., 1991; Traub et al., 1994b), as well as $[Ca^{2+}]$ dynamics in a postsynaptic compartment (Jahr and Stevens, 1990b, 1993; Yuste et al., 1999). To use the $[Ca^{2+}]$ timecourse to discriminate between plasticity outcomes, we constructed a set of coupled ordinary differential equations (ODEs) (Fig. 2.1a; Methods, 2.2.2; Table 2.4).

The model functions as follows: high $[Ca^{2+}]$ rapidly activates a potentiating process **P**, medium $[Ca^{2+}]$ rapidly activates a process **V**, and low $[Ca^{2+}]$ slowly activates a process **A**. **A** in turn activates a depressing process **D** through an intermediate process **B**. However, **B** can be inhibited (“vetoed”) by **V**, allowing **V** to indirectly inhibit **D**. The consequence of this arrangement is that only long-lasting excursions of $[Ca^{2+}]$ to low values can successfully activate **D**.

2.3.1. Results for doublets

To illustrate the function of the model, we show the postsynaptic $[Ca^{2+}]$ time course for 4 kinds of spike pairings. First, pairings in which postsynaptic spikes precede presynaptic spikes, or so-called AB spike pairings: $\Delta t=10$ and $\Delta t=40$ (Fig. 2.1b); and second, pairings in which the order of spikes is reversed, so-called BA spike pairings: $\Delta t=-10$ and $\Delta t=-60$ (Fig. 2.1d).

The major source of postsynaptic calcium influx is NMDARs, whose conductance is a product of postsynaptic membrane depolarization and glutamate concentration in the synaptic cleft. Thus, large calcium influx will only occur when the postsynaptic spike follows the presynaptic spike at a short latency. Consequently, a large peak $[Ca^{2+}]$ concentration results for spike interval $\Delta t = 10$, activating **P** (Figure 2.1b), whereas a shorter peak $[Ca^{2+}]$ concentration occurs for $\Delta t = 40$, failing to do so.

Why is **D** not activated by the $\Delta t = 40$ $[Ca^{2+}]$ profile? For both $\Delta t = 10$ and $\Delta t = 40$, there is sufficient $[Ca^{2+}]$ elevation to activate a process **V** (Fig. 2.1c), which inhibits the ability of **A** to activate **B** to the threshold level needed to activate **D**. Combined with the failure of $\Delta t = 40$ to activate **P**, neither potentiation nor depression results for this spike-timing. Thus, the inclusion of the process **V** explains the lack of LTD for large, positive spike-timing.

For negative spike-timing, there is no NMDAR conductance during the time of postsynaptic action potential backpropagation. Consequently, the interval $\Delta t = -10$ results in a much shorter peak $[Ca^{2+}]$ which also fails to activate **P**. However, the width of the $[Ca^{2+}]$ time course (Fig. 2.1d) is sufficient to activate **A** (Fig. 2.1a), which in turn activates **D**. By contrast, the $[Ca^{2+}]$ profile for $\Delta t = -60$ is not sufficiently wide, due to large timing gap between pre- and postsynaptic activation, and fails to activate **A** (or **D**).

Using this detector scheme, the resultant plasticity was computed for a wide range of values of Δt . Figure 2.1e shows the correspondence between the model results and data from hippocampal cultures (Bi and Poo, 1998). This model also reproduces data from non-STDP plasticity protocols; among them are presynaptic stimulation at various frequencies, and the pairing protocol for a range of postsynaptic holding potentials (data not shown).

2.3.2. Results for triplets

For spike triplets, the same processes can explain the resulting plasticity. Let $\Delta t=\{a,b\}$ reflect a triplet stimulus with an interval a equal to the difference between the first two spikes (as with doublets, where a positive number represents presynaptic activation first), and an interval b between the second and third spike, according to the same sign convention. For the $\Delta t=\{10,-10\}$ stimulus, an example of an ABA pairing (Fig. 2.1f), **P** and **V** are both activated due to the large $[Ca^{2+}]$ peak. However, postsynaptic $[Ca^{2+}]$ remains modestly elevated for a greater time compared to the AB stimulus, permitting **A** to continue its buildup after **V** has decayed, leading to the activation of **D**. Because both potentiation and depression are activated, no net plasticity results for the ABA case.

In the case of the $\Delta t=\{-10,10\}$ stimulus, an example of a BAB pairing (Fig. 2.1g), **V** is activated by calcium influx associated with the second postsynaptic action potential as **A** is accumulating. It is thus able to “veto” the effect of **A** on **B** and prevent the activation of **D**, resulting in only potentiation. The results for triplets thus match experimental results from hippocampal cultures (Wang et al., 2005).

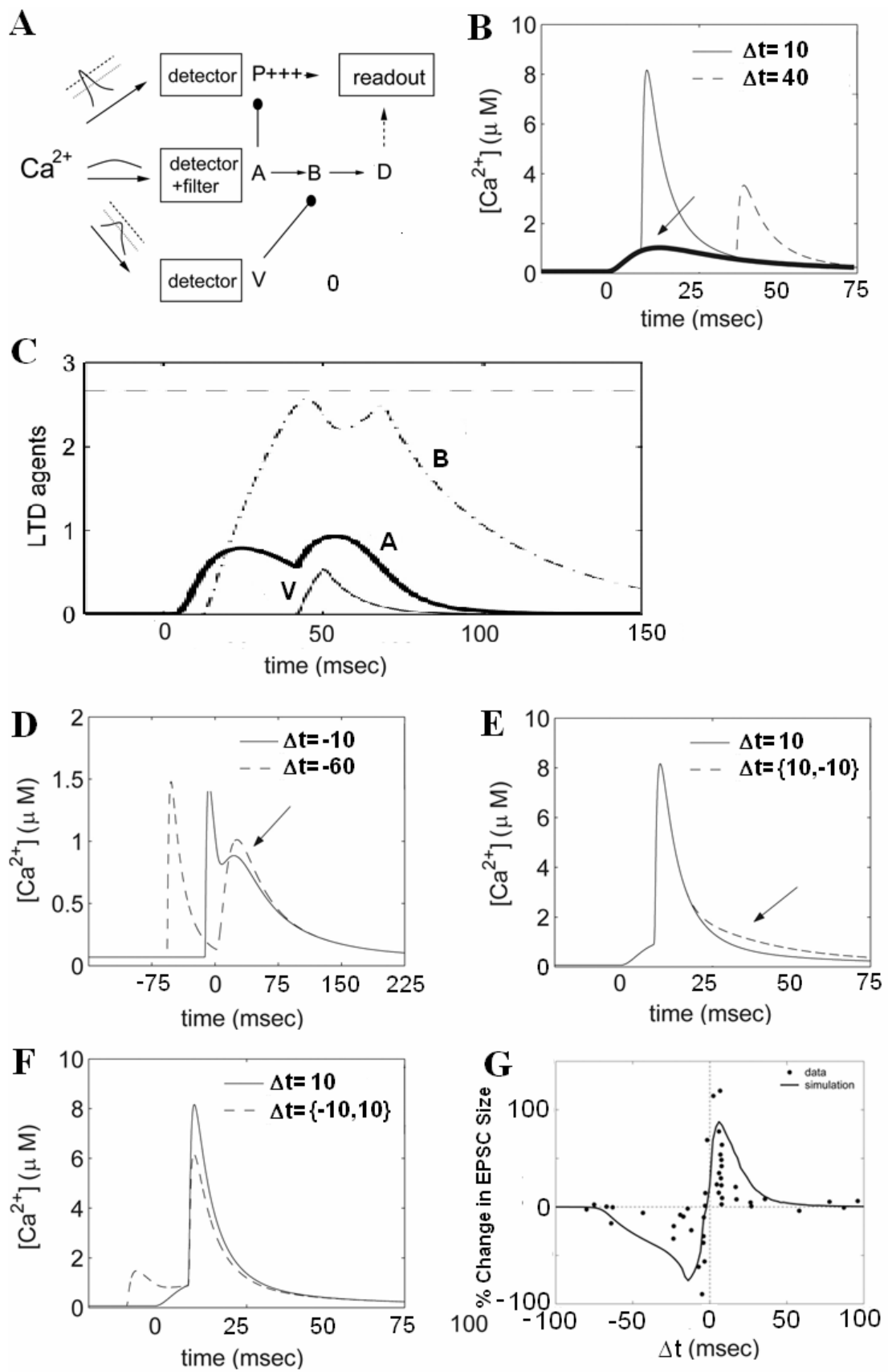


Figure 2.1: The postsynaptic $[Ca^{2+}]$ detector model recapitulates results from STDP experiments. **A**, The detector uses a set of coupled ODEs to determine the magnitude and sign of the change in synaptic strength from the $[Ca^{2+}]$ time course (Methods, 2.2.2). **B**, Postsynaptic $[Ca^{2+}]$ is substantially magnified by backpropagating action potentials that occur 10 ms after the onset of the EPSP, and less magnified when the interval is 40 ms. The dark, solid line reflects the contribution of an EPSP alone. In figures B-F, the first presynaptic spike occurs at $t = 0$ ms. **C**, Time course of three of the $[Ca^{2+}]$ detectors activated by the stimulus containing a 40 ms interval. Activation of V inhibits B , preventing it from reaching a threshold need to activate depression. **D**, $[Ca^{2+}]$ remains near the μM range for an extended period when the backpropagating action potential precedes the EPSP by 10 ms, but this regime is narrower when the interval is 60 ms. **E**, The period of modest $[Ca^{2+}]$ elevation is broadened when a second EPSP follows the backpropagating action potential, permitting the activation of depression. **F**, Addition of a second backpropagating action potential before the EPSP extends the duration of modest $[Ca^{2+}]$ elevation, but this is followed by a large $[Ca^{2+}]$ elevation capable of activating module V in panel A. V can then inhibit the $[Ca^{2+}]$ growth of the depression process and prevent it from reaching a threshold level for activation. **G**, Simulation using the detector scheme in A produces an STDP curve quantitatively similar to the data (superimposed) shown in Fig. 1.2B. In figure panels B,D,E, and F, “A” and “B” refer to pre- and postsynaptic neuron spike times, respectively.

2.4. DISCUSSION

This model reproduces the results of spike-timing-dependent plasticity experiments in hippocampal cultured neurons. In contrast to previous models (Shouval et al., 2002), it does not produce a second “LTD window” for $\Delta t > 0$, consistent with several experimental reports ((Bi and Poo, 1998; Feldman, 2000; Froemke et al., 2005), but see (Nishiyama et al., 2000)). Because the amplitude of $[Ca^{2+}]$ transients decays monotonically with increasing $\Delta t > 0$, and the threshold level of $[Ca^{2+}]$ required to produce LTD is believed to be less than that required to produce LTP ((Lisman, 1989; Artola and Singer, 1993)), this second LTD window is an inevitable consequence of a detector scheme that only considers peak or average $[Ca^{2+}]$. By using information from the dynamic time-course of this $[Ca^{2+}]$ signal, this limitation can be overcome. Thus, it is plausible that neurons actually do use this information to generate their plasticity responses to experimental STDP protocols.

2.4.1. Applicability to other experimental preparations

Using the same set of detectors, we also explained the results from triplet experiments, in which two action potentials occur one neuron and one occurs in the other. However, the results of triplet experiments are far more system-dependent than are doublet experiments. For example, for horizontal connections in layer II/III of the rodent cortex, the efficacy of individual spike pairings is a function of the number and timing of prior presynaptic spikes; earlier presynaptic spikes have a greater effect than later ones. In layer V, LTP always trumps LTD when they are coactivated. Therefore, the parameters used in our model cannot describe the STDP signal

transduction machinery in all neurons. However, the model can still explain these results through a change in parameters, which could correspond to diversity in the activity levels of particular kinases or phosphatases across brain areas or neuronal phenotypes. For example, reducing the decay time constant of V would result in a “veto” of depression in response to any protocol in which P was activated. Thus, potentiation would trump depression in response to most arbitrary spike trains.

2.4.2. Alternative models to explain the data

There are alternative schemes to avoid the second LTD window and explain the triplet results. Because there are a finite number of postsynaptic NMDARs, and glutamate concentration begins to decay shortly after the presynaptic action potential, the CV of the number of activated NMDARs increases with increasing $\Delta t > 0$. Because of this variability, in some cases, e.g. $\Delta t = 40$, there could either be a large $[Ca^{2+}]$ signal or a negligible $[Ca^{2+}]$ signal. With each spike pairing, the $[Ca^{2+}]$ signal could reach LTP-, LTD-, or no change-associated levels, even in a classical model that does not take into account the $[Ca^{2+}]$ time course. The mean resultant plasticity over many individual spike pairings could thus be ~ 0 , resulting in no second LTD window (Shouval and Kalantzis, 2005).

Because neurotransmitter release is stochastic, combinations of pre- and postsynaptic action potentials will result in some pairings in which a presynaptic vesicle is not released, and the postsynaptic compartment only experiences a back-propagating action potential. Thus, at individual synapses ABA triplets will sometimes manifest as “only” AB or BA pairings. Meanwhile, BAB pairings will often have no presynaptic release at all. In a model where

potentiation always trumps depression, not requiring a veto, ABA triplets would yield a linear sum of the resultant plasticity from an effective sequence of potentiating AB pairings and depressing BA pairings, resulting in no net change in synaptic strength. Meanwhile, BAB pairings would only influence synaptic modification in the event of presynaptic release, in which case potentiation would trump depression. Thus, stochastic synaptic transmission could in principle explain the triplet results (Cai et al., 2007). This model would predict that the result of ABA pairings would depend upon the relative probabilities of the first and the second presynaptic action potential in evoking neurotransmitter release. However, experimentally no dependence on paired pulse ratio was found for the plasticity resulting from ABA pairings (Wang et al., 2005).

2.4.3. Correspondence to biological signaling pathways

The schematic shown in Figure 2.1a has similarity to an early calcium-dependent kinase/phosphatase postsynaptic signaling system (Lisman and Zhabotinsky, 2001); by analogy, **P** represents CaMKII; **A**, **B**, and **D** represent CaN and PP1; and **V** could represent PKA. In the biological system, CaMKII is inhibited by PP1, which is in turn activated by CaN and inhibited by PKA. As proof of principle, I reconfigured the model along these lines, eliminating one ODE (reducing the depressing **A,B,D** pathway from three equations into two; data not shown). The results were qualitatively similar to the full model, explaining the same experimental results. This lends additional plausibility to the dynamic model proposed here, and motivates future experiments to determine if the **V** module, with its potential to “veto” depression, exists. If it does, I predict that it may be based on the activity of a kinase, such as PKA, associated with inhibiting the effect of postsynaptic protein phosphatases.

This model was implemented using only the postsynaptic $[Ca^{2+}]$ time course, a function of postsynaptic receptor activation and the membrane potential. The membrane potential is itself determined by a variety of somatic and dendritic ion channels which have been described in detail (Traub et al., 1991; Traub et al., 1994b; Poirazi et al., 2003a). In particular, the A-type potassium conductance has been proposed as a critical mediator of spike-timing-dependent potentiation. However, we found no significant contribution of this conductance to the results of our model (data not shown). In general, the model is sensitive to specific values of intrinsic membrane conductances. This results from the requirement that potentiation and depression balance each other correctly in plasticity neutral stimuli such as the ABA triplet. A change in, for example, the conductance of afterhyperpolarizing currents could substantially alter the relief from Mg^{2+} -block experienced by NMDARs during the second presynaptic spike, thus increasing or decreasing the magnitude of depression and disrupting its cancellation with potentiation. Indeed, experimental manipulations of AHP magnitude also cause disruptions in the timing rules regulating STDP (Fuenzalida et al., 2007). Given the diversity of STDP integration rules observed across brain areas (Sjostrom et al., 2001; Froemke and Dan, 2002; Wang et al., 2005), it is doubtful that a model robust to changes in physiologically constrained parameters would capture a “general phenomenon” of STDP.

2.4.4. Calcium sources

Does calcium represent a homogeneous signal in the postsynaptic department? Despite our treatment as such, it is unlikely that calcium from independent sources, e.g. NMDARs and L-type calcium channels, are treated identically by effectors in the postsynaptic neuron. For

example, important calcium-sensing signaling molecules such as CaMKII are known to associate with NMDARs. Furthermore, NMDAR subtypes are now known to have differential contributions to LTP and LTD in certain preparations (Liu et al., 2004; Massey et al., 2004; Gerkin et al., 2007) (see Chapter 3). Thus, a further step in the construction of models that explain the transduction of stimuli into synaptic plasticity might involve spatial localization of receptors and calcium sensors in a postsynaptic compartment. Further experiments will be required to constrain such a model.

Calcium from non-NMDAR sources, such as L-type calcium channels, has a role in STDP (Bi and Poo, 1998). The L-type conductance is included explicitly in the model (Table 2.1, eq. 2.1), and with the existing parameter set it is required to obtain LTD, but not LTP, as in experiments. Because the back-propagating action potential activates this conductance, associated calcium influx begins shortly after the the postsynaptic spike time. The duration of this modest $[Ca^{2+}]$ elevation is sufficient to activate the LTD detectors only if it is followed within a critical time window by presynaptic activation. Were the L-type conductance blocked, spike pairings with negative timing would produce similar $[Ca^{2+}]$ profiles as presynaptic spikes alone, which do not modify synaptic strengths here (see (Rubin et al., 2005)) or in experiment (Bi and Poo, 1998). For positive spike-timing, the magnitude of calcium influx through NMDARs in the model is sufficiently large to obviate the need for calcium from L-type channels, and thus these channels are not required for spike-timing-dependent LTP.

We tested the roles of T- and R-type calcium channels, using the published conductance values (Poirazi et al., 2003a), but found that these had little if any effect on the model, and thus excluded them. Their lack of effect may have stemmed from the low firing rate in the modeled protocol; because both pre- and postsynaptic neurons fired only one spike per second, the

duration of both depolarization and of post-spike afterhyperpolarization may have been insufficient to substantially activate these voltage-dependent conductances.

In more mature hippocampal neurons, bursts of postsynaptic action potentials are required to observe spike-timing-dependent potentiation (Pike et al., 1999; Meredith et al., 2003). In light of the model, this result could be explained by changes in dendritic conductances during development ultimately restrict the back-propagation of action potentials, such that larger numbers of sequential action potentials are required to achieve the same quantity of postsynaptic calcium influx. Indeed, in some preparations backpropagating Na^+ spikes alone may not be sufficient to generate the required postsynaptic depolarization and calcium influx, and calcium spikes may be required (Kampa et al., 2007). In this case, R- and T-type calcium channels have an essential role (Kampa et al., 2006).

2.4.5. Accumulation of plasticity across stimuli

Our model also assumes that signaling modules rapidly interact on a timescale faster than the interval between successive spike pairings. However, the decay time of W , the final term integrating potentiation and depression, is slow, allowing individual spike pairings to interact with one another. While changes in W do affect the magnitude of plasticity produced by each combination of pre- and postsynaptic action potentials, they do not qualitatively affect the results of the various stimuli relative to one another. Further experiments will be required to determine the degree to which spike pairings or triplets interact with one another to generate long-term synaptic modifications (Chapter 4).

3. MODULAR COMPETITION IN SPIKE-TIMING-DEPENDENT PLASTICITY MEDIATED BY NMDA RECEPTOR SUBTYPES

3.1. INTRODUCTION

As in conventional synaptic plasticity protocols (Malenka and Nicoll, 1999), spike-timing-dependent plasticity (STDP) signaling relies on Ca^{2+} influx through NMDARs (Sjostrom and Nelson, 2002; Bi and Rubin, 2005). However, it is unclear how NMDARs reliably map the temporal pattern of spikes onto the activation of appropriate downstream targets leading to opposing directions of synaptic modification. NMDARs containing NR2A and/or NR2B subunits predominate in the mammalian forebrain (Cull-Candy et al., 2001), but the potential of these subunits to determine the polarity of synaptic modification remains controversial (Tang et al., 1999; Liu et al., 2004; Massey et al., 2004; Barria and Malinow, 2005; Berberich et al., 2005; Weitlauf et al., 2005; Morishita et al., 2006).

The NMDAR itself is believed to be a tetrameric structure with four subunits (Cull-Candy et al., 2001). Two of these subunits are the NR1 protein, an obligatory component of all NMDARs, in all brain areas, at all stages of development (Monyer et al., 1994). The other two subunits can be any combination of so-called NR2 subunits: NR2A, NR2B, NR2C, and NR2D (Paoletti and Neyton, 2007). These subunits confer each NMDAR with distinct properties (Monyer et al., 1992; Cull-Candy and Leszkiewicz, 2004), and are highly

developmentally regulated (Monyer et al., 1994; Sheng et al., 1994). NR2C and NR2D are not found in the hippocampus except in interneurons (Miyashiro et al., 1994; Janssens and Lesage, 2001), while NR2A is scarce in early development and is gradually upregulated with development and activity (Monyer et al., 1994; Sheng et al., 1994; Law et al., 2003; Neyton and Paoletti, 2006).

LTP and LTD are also developmentally regulated (Feldman et al., 1999; Rosenzweig and Barnes, 2003; Jiang et al., 2007). Both decline in magnitude (and increase in induction threshold) during development (Harris and Teyler, 1984; Dudek and Bear, 1993), which when combined with the developmental profile of NMDAR subunits, suggests the hypothesis that NR2B facilitates and NR2A suppresses plasticity. Superficially, this hypothesis is supported by the kinetics conferred by the various NMDAR subunits. NR1-NR2B NMDARs exhibit more slowly decaying synaptic currents than do NR1-NR2A NMDARs (Vicini et al., 1998; Cull-Candy et al., 2001). It has been argued that this slower decay permits a wider range of postsynaptic spike times to relieve Mg²⁺ block and permit Ca²⁺ influx, thus enhancing LTP; preliminary evidence for this hypothesis was provided by an NR2B overexpressing mouse (Tang et al., 1999), which showed both enhanced LTP and enhanced learning and memory, believed to be a behavioral correlate of LTP (Stevens, 1998; Whitlock et al., 2006).

However a kinetic interpretation of this result is questionable. Overexpressing the even slower NR2D subunit (Cull-Candy et al., 2001) leads to a decrement in LTP (Okabe et al., 1998), and developmental changes in the magnitude of LTP are not necessarily cotemporal with kinetic changes in NMDAR currents (Barth and Malenka, 2001). Furthermore, subunit overexpression can also lead to an increase in total NMDAR number (Tang et al., 1999) and thus enhanced plasticity through a generic mechanism not specifically related to the properties of the NR2B

subunit. Second, because LTD is developmentally downregulated (Dudek and Bear, 1993) a rescue of juvenile LTD could also explain gain of function behavioral data. Pharmacological blockers of NR2B-NMDARs, such as ifenprodil (Carter et al., 1988; Williams, 1993), are typically unable to abolish LTP (Liu et al., 2004; Massey et al., 2004). This indicates that even if NR2B is critical for LTP, it may have a structural, rather than ionotropic, role in the signal transduction pathway (Lisman and McIntyre, 2001; Sanhueza et al., 2007).

Previous attempts to determine the role of NMDAR subtypes in bidirectional synaptic plasticity have utilized conventional protocols in which the presynaptic neuron is not precisely identified and postsynaptic activity is either unknown or suppressed. Thus, it is unknown whether NMDAR subunit specificity, if it exists, can extend to physiological forms of plasticity that involve temporally precise activity patterns (Bliss and Schoepfer, 2004). In this chapter I examine the existence and implications of such specificity.

3.2. METHODS

3.2.1. Electrophysiology

Only monosynaptic connections between glutamatergic neurons were studied. Polysynaptic currents, identified based on the latency of EPSC onset (>5 ms), were excluded because their timing could not be precisely controlled. As in previous studies (Wang et al., 2005), only connections with strengths >50 pA and <500 pA were selected for these experiments to reduce both heterogeneity in STDP induction and voltage clamping artifacts. During STDP induction,

the postsynaptic cell (constant current injected to hold at -65 to -70 mV) was in current clamp, and stimulation was 1-2 nA current injection for 2 ms, sufficient to elicit a spike). Presynaptic stimulation was given by step depolarization (100 mV, 1-2 ms). The neurons were not spontaneously active under recording conditions. Changes in synaptic strength were calculated from the averaged EPSC amplitude 0-10 min before and 15-30 min after the stimulation paradigm. Recordings showing significant changes (>10%) in series (20-40 M Ω) or input resistance (500-1500 M Ω) were excluded from further analysis.

3.2.2. Pharmacology

NVP-AAM077, to preferentially block NR2A-NRs, or Ro25-6981, to selectively block NR2B-NRs, was perfused into the bath >10 minutes prior to the induction of STDP. Addition of either reagent caused no detectable change in the (primarily AMPAR mediated) postsynaptic response, or in the paired pulse ratio (50 ms inter-pulse-interval). NMDAR currents were obtained in 10 μ M glycine, 0 Mg²⁺, and 10 μ M CNQX. Under these conditions, rapid rundown of the NMDAR current to a steady state was observed (Rosenmund and Westbrook, 1993), at which point NMDAR current amplitudes and decay time constants were measured. NMDAR decay time constants were obtained by fitting single exponentials to the region 40-340 ms after the stimulus. NMDAR current amplitude was defined as the mean current 5-55 ms after presynaptic stimulus onset. Due to the lesser affinity of glycine for NR2A-NRs vs. NR2B-NRs (Kutsuwada et al., 1992), adding a saturating concentration of glycine may enhance NR2A-NR current more than NR2B-NR current, thus overestimating synaptic NR2A-NR currents; furthermore, CNQX can compete with glycine for the glycine binding site on the NMDAR (Lester et al., 1989).

However, the effective concentration of glycine is probably irrelevant, since the results reported here do not rely on any specific ratio of NMDAR subtypes. NMDAR currents were also present, although substantially reduced in magnitude, in the absence of added glycine (data not shown), confirming that glycine site agonists (glycine or D-serine) persist among neurons co-cultured with glial cells, as seen previously (Yang et al., 2003). Because the effects of steady-state Mg²⁺ block in NR2A-NRs and NR2B-NRs are indistinguishable (Monyer et al., 1994; Kuner and Schoepfer, 1996; Yang et al., 2003), I make the assumption that recording NMDAR currents in Mg²⁺-free solution does not bias measurements towards either of these two subtypes.

3.2.3. Quantification of NMDAR subtype specificity of NVP-AAM077

In order to estimate the specificity of the competitive antagonist NVP-AAM077 at the concentration I used for our experiments, I recorded synaptic NMDAR currents in pairs of hippocampal neurons as described above. For each experiment, I measured these NMDAR currents (a) in the absence of NMDAR antagonists (I_{NMDAR}), (b) in the presence of 0.4 μM NVP-AAM077 (I_{NVP}), (c) in the presence of 0.3 μM Ro25-6981 (I_{Ro25}), and (d) in the presence of both 0.4 μM NVP-AAM077 and 0.3 μM Ro25-6981 (I_{Both}), with each step followed by a washout period.

The fraction of Ro25-sensitive current that is blocked by NVP-AAM077 is:

$$x = \frac{(I_{NMDAR} - I_{NVP}) - (I_{Ro25} - I_{Both})}{(I_{NMDAR} - I_{Ro25})} \quad \text{eq. 3.1}$$

Using equation 3.1 on each of 8 different synaptic connections gave a result of $x = 35.5 \pm 7.6\%$ (median 34.6%), implying that 0.4 μM NVP-AAM077 blocks about 1/3 of the Ro25-sensitive (NR2B-containing) NMDAR current.

The synaptic NMDAR population is likely to contain receptors that possess either NR2A, NR2B, or both NR2 subunits. To analyze this, the fraction of the current carried by NMDARs possessing only NR2A subunits will be denoted A , by those possessing only NR2B subunits as B , and by those possessing both as AB . The fractional contribution from any other source (NMDAR or otherwise) providing synaptic current under these conditions will be denoted Z . By definition, $A + B + AB + Z = 1$. Let us denote the fraction of A blocked by NVP-AAM077 as N_A , the fraction of B blocked by NVP-AAM077 as N_B , the fraction of AB blocked by NVP-AAM077 as N_{AB} , and the fraction of Z blocked by NVP-AAM077 as N_Z , with corresponding variables for the current blocked by Ro25-6981 (R_A , R_B , R_{AB} and R_Z). Thus, equation B1 can also be written as:

$$x = \frac{(N_A * A + N_{AB} * AB + N_B * B + N_Z * Z) - (N_A * A * (1 - R_A) + N_{AB} * AB * (1 - R_{AB}) + N_B * B * (1 - R_B) + N_Z * Z * (1 - R_Z))}{R_A * A + R_{AB} * AB + R_B * B + R_Z * Z} \quad \text{eq. 3.2}$$

Because of the high selectivity of Ro25-6981, $R_A \sim 0$, and because each of N_Z , R_Z , and Z is likely to be very small, I can approximate:

$$x \approx \frac{N_{AB} * AB * R_{AB} + N_B * B * R_B}{AB * R_{AB} + B * R_B} \quad \text{eq. 3.3}$$

For the extreme cases of $AB = 0$ or $B = 0$, $x = N_B$ or $x = N_{AB}$, respectively. Even without assuming these extremes, equation 3.3 shows that the empirically calculated x corresponds to an average of the block by NVP-AAM077 of NR2B-NR2B and NR2A-NR2B subtypes, weighted according to their relative abundance at the synapse and sensitivities to Ro25-6981. Because Ro25-6981 is a more efficacious and selective derivative of ifenprodil, 0.3 μM is likely adequate to antagonize the NR2A-NR2B subtype with sufficient efficacy that $R_{AB} \sim R_B$ (Tovar and Westbrook, 1999; Hatton and Paoletti, 2005), implying that x is simply weighted according to the abundance of these subtypes in the synaptic NMDAR population.

We observed that I_{Both} had a slow decay; when fit to a double exponential with the time constants of the Ro25-6981 sensitive (putative NR2B-NR) and insensitive (putative NR2A-NR) current components, it had a negligible (< 1%) contribution from the faster of these two components; thus, the block by Ro25-6981 and NVP-AAM077 together effectively abolishes all of the NR2A-NR components. Since the IC_{50} for Ro25-6981 at NR2A-NRs is 52 μM (Fischer et al., 1997), 0.3 μM Ro25-6981 cannot significantly antagonize NR2A-NRs. Therefore, 0.4 μM NVP-AAM077 must be sufficient to abolish nearly the entire NR2A-NR component.

3.2.4. 1/CV² Analysis

Under the assumptions of 1/CV² analysis, the coefficient of variation (CV) for a series of observations of macroscopic postsynaptic current is given by $\text{CV} = \sigma/\mu = (np(1-p)q^2)^{1/2}/npq = (1-p)^{1/2}/(np)^{1/2}$, where n is the number of neurotransmitter release sites, p is the probability of release, and q is the quantal size. Thus, $1/\text{CV}^2 = np/(1-p)$. Under the ideal assumptions, p and q are identical at every release site; even for the more realistic case where p and q assume unique

values at every site, plasticity corresponding to linear scalings of n , p , q , or any combination of the three, will still secure the conventional interpretation of $1/CV^2$ analysis; in this interpretation, multiplicative changes in $1/CV^2$ greater than the change in synaptic efficacy correspond to changes primarily in release probability, while the reverse corresponds to changes primarily in quantal amplitude (Faber and Korn, 1991).

Coefficient of variation (CV) was computed by analyzing a segment 0 to 10 minutes ($n=30$ EPSCs) before the STDP induction protocol (*before*), and a segment 15 to 30 minutes ($n=45$ EPSCs) after the STDP induction protocol (*after*). It is assumed that a stationary binomial process governs synaptic transmission at each bouton during each segment. Because synaptic efficacy could be evolving during the *after* time period, the slope during this period is not necessarily zero, and so measuring the conventional variance, $\Sigma(\mu-x_i)^2/(n-1)$ would overestimate the intrinsic trial-to-trial variance of the synaptic response, and thus give fictive decreases in $(1/CV^2)$ as a result of STDP induction. To address this problem, I subtracted the best linear fit (minimizing the sum of the squared error) from the “before” and “after” segments before measuring the variance. Similar results were obtained by computing the non-stationary variance, (Noceti et al., 1996).

Under the same assumptions as those for CV analysis, I define a new measure, the LTD index, that is calculated from the change in synaptic strength divided by the change in $1/CV^2$, and is equal to:

$$\frac{(n_1 p_1 q_1)/(n_0 p_0 q_0)}{\frac{n_1 p_1}{1-p_1} / \frac{n_0 p_0}{1-p_0}} = \frac{q_1}{q_0} * \frac{1-p_1}{1-p_0} \quad \text{eq. 3.4}$$

The subscripts 0 and 1 indicate values before and after STDP induction, respectively.

Compared with the unity line in a CV analysis plot (Fig. 3.3c), values of the LTD index above 1 represent points below the unity line (putative increases in $(1-p)$, i.e. likely presynaptic changes) and values below 1 represent points above the line (putative decreases in q , i.e. likely postsynaptic changes).

The LTD index has the advantage of condensing the changes in pre- and/or postsynaptic efficacy into a single number, such that decreases in p , n , and q lead to LTD indices greater than, equal to, and less than 1, respectively. As a single number, the LTD index lends itself to univariate statistical tests not possible with the two-dimensional coordinate derived from a $1/\text{CV}^2$ analysis (Fig. 3.3c); alternatively, abandoning the synaptic strength change dimension and considering the value $1/\text{CV}^2$ itself does not provide useful information. Interpretation of the LTD index involves the same assumptions made in conventional $1/\text{CV}^2$ analysis as discussed above. Because both the $1/\text{CV}^2$ and the LTD index are quotients of numbers with identical units, a value of x is as likely as a value of $1/x$ under the null hypothesis of no consistent difference between the numerator and the denominator (quotient of 1). Thus, logarithmic axes and transformations are used in Figures 3.3c and 3.3d to normalize the representation of the data.

3.2.5. Model of NMDAR Subtype Selectivity in STDP

This model is a simple reduction of the model presented in chapter 2 and uses only four ODEs. As in that model, the variables P , D , and V represent the activation level of signaling modules (enzymatic pathways) activated by $[\text{Ca}^{2+}]$ signals. However, instead of tracking the spatio-temporal details of calcium dynamics, the equations are simplified such that each variable

increases when a particular spike doublet (combination of pre- and postsynaptic spikes) occurs. In choosing the doublets that would drive the integration of each variable, I observed that 1) The $[Ca^{2+}]$ threshold required to achieve potentiation is higher than that required to achieve depression (Lisman, 1989; Stemmer and Klee, 1994; Yang et al., 1999; Shouval et al., 2002; Bradshaw et al., 2003) and 2) the *ab* (pre-before-post) doublet provides more calcium influx than the *ba* doublet (Nevian and Sakmann, 2004, 2006). These observations motivate the following equations to describe the plasticity response:

$$P' = ab(t) \cdot p_{off} * P \quad \text{eq. 3.5}$$

$$D' = ba(t) + ab(t) - d_{off} * (D + \lambda * V * D) \quad \text{eq. 3.6}$$

$$V = ab(t) - v_{off} * V \quad \text{eq. 3.7}$$

$$W' = \frac{1}{1 + e^{(1-P)/p_{steep}}} - \frac{1}{1 + e^{(1-D)/d_{steep}}} - w_{off} W \quad \text{eq. 3.8}$$

In these equations, P (the potentiation pathway) only responds to the *ab* doublet in order to reflect a high $[Ca^{2+}]$ threshold, while D (the depression pathway) responds to both the *ab* and *ba* doublets. I chose V to account for the experimental observation that, even when potentiation is pharmacologically blocked, potentiating stimuli are often able to “veto” depressing stimuli, resulting in an absence of depression. Therefore, V directly inhibits D . Lastly, I assume a simple scheme of modular specificity as illustrated in Fig. 2.6a (solid lines only): P can respond only when NR2A-NRs are not inhibited, whereas D and V can respond only when NR2B-NRs are not inhibited. $ab(t)$ and $ba(t)$ are transient signals representing the timing of the aforementioned spike doublets. To accord with the experimental protocol, these signals are activated (set equal to 1 for a period of 5 ms) whenever the corresponding spike doublet is present in the STDP

induction protocol (once per second). They are equal to zero otherwise. If both the ab and ba doublets are present (e.g. the ABA triplet protocol), they are activated 10 ms apart from one another. W reflects a final integration of P and D , and its sign and magnitude reflect the final outcome of an STDP induction.

Table 3.1: Parameters governing the simplified model of NMDAR-dependent STDP integration.

Parameter	Description	Value
p_{off}	The rate at which the activation of the potentiation	1/30
d_{off}	The rate at which the activation of the depression	1/30
v_{off}	The rate at which the activation of the “veto” pathway V	1
w_{off}	The rate at which the final readout W decays.	1/100
λ	The effect of the “veto” pathway V on the depression	1000
p_{steep}	The sensitivity of W to the activation of P .	1/5
d_{steep}	The sensitivity of W to the activation of D .	1/5

The parameter choices do not require fine-tuning, although large changes in the parameters can lead to different outcomes for triplet experiments (in control conditions), such as those observed in other preparations (Sjostrom et al., 2001; Froemke and Dan, 2002). However, our model does require that the kinetics of V (represented by v_{off}) must be faster than those of the other modules in order to reflect the rapid deactivation of the veto module and ensure that simulations match experiment results for triplet stimuli.

3.3. RESULTS

3.3.1. NMDAR subtypes in cultured hippocampal neurons

Previous studies on the roles of NMDAR subtypes in synaptic plasticity have used ifenprodil or its structural analogue Ro25-6981, which specifically block NR2B-NRs (Williams, 1993; Fischer et al., 1997), and NVP-AAM077, which preferentially inhibits NR2A-NRs (Feng et al., 2004; Liu et al., 2004; Berberich et al., 2005; Weitlauf et al., 2005). However, the use of pharmacological agents to dissect NMDAR subtype contributions has been criticized, especially because of the disputed selectivity of NVP-AAM077 (Neyton and Paoletti, 2006). Because NVP-AAM077 is a competitive antagonist, the effective receptor block will be a function of the magnitude and dynamics of glutamate concentration in the cleft, which are not accurately replicated using iontophoresis. Therefore, direct application of glutamate, the most common means for testing compound specificity, cannot be used as a proxy to determine the effect of NVP-AAM077 on responses induced by synaptic activity.

In order to examine the existence of distinct NMDAR subtypes in our system, I tested NVP-AAM077 directly on synaptic transmission, ensuring that the relevant temporal profile of glutamate was used to make this measurement. To evaluate the effect of antagonists on synaptic NMDAR currents, I identified pairs of glutamatergic neurons by intracellular stimulation, and recorded evoked synaptic currents in one neuron in response to stimulation of its presynaptic partner in the presence of 10 μM CNQX, 0 Mg^{2+} , and 10 μM glycine. Either 0.3 μM Ro25-6981, 0.4 μM NVP-AAM077 or a combination of these was then added to the bath to assess the effect of these reagents on the NMDAR current (Fig. 3.1a,b). Ro25-6981 caused a $37.9 \pm 5.1\%$

decrease in the magnitude of the NMDAR current (Fig. 3.1f) and a decrease in the average decay time of the current (Methods, 3.2.2) from 122.3 ± 15.7 ms to 88.5 ± 9.7 ms (mean \pm SEM, $p < 0.05$ by a paired t-test, Fig. 3.1e), suggesting the predominance of a rapidly decaying NR2A-NR component in the remaining current. In contrast, application of NVP-AAM077 caused a decrease in the magnitude of the NMDAR current of $65.6 \pm 4.3\%$ (Fig. 3.1f), but an increase in the decay time from 136.3 ± 14.3 ms to 179.7 ± 20.0 ms ($p < 0.05$ by a paired t-test, Fig. 3.1e), indicating the predominance of a slow NR2B-NR component in the remaining current.

Because NVP-AAM077 has also been shown to block a fraction of NR2B-NR current in heterologous expression systems and in NR2A-NR knockout animals (Berberich et al., 2005; Weitlauf et al., 2005), I determined its specificity in our preparation. Based on synaptic NMDAR currents in the presence of either, neither, or both $0.4 \mu\text{M}$ NVP-AAM077 and $0.3 \mu\text{M}$ Ro25-6981, I estimated (Methods, 3.2.3) that $0.4 \mu\text{M}$ NVP-AAM077 blocked nearly all of the Ro25-6981 insensitive current (non-NR2B-NR current), as well as $\sim 1/3$ ($35.5 \pm 7.6\%$) of the Ro25-6981 sensitive current (NR2B-NR current, Fig. 3.1f).

Thus, the apparent specificity of NVP-AAM077 in response to synaptically released glutamate our system is less than that previously observed for oocyte-expressed human NMDARs and wild-type rat hippocampal slices (Liu et al., 2004), but greater than that observed for rodent NMDARs expressed in HEK cells, or in hippocampal neurons from NR2A knock-out mice (Berberich et al., 2005; Weitlauf et al., 2005). Differences in the expression of triheteromeric NMDARs as well as variations in glutamate concentration across these preparations, and thus in the ability of NVP-AAM077 to out-compete glutamate at each NMDAR subtype, may be partly responsible for the inconsistency of the literature. However, because NVP-AAM077 and Ro25-6981 reveal NMDAR subpopulations with vastly different

kinetics, and because NR1-NR2A-NR2B triheteromers have similar kinetic and pharmacological properties to NR1-NR2B-NR2B-NRs (Vicini et al., 1998; Hatton and Paoletti, 2005), I will refer for simplicity to the Ro25-6981 sensitive subpopulation with slow kinetics as NR2B-NRs, and the NVP-AAM077 sensitive subpopulation with fast kinetics as NR2A-NRs.

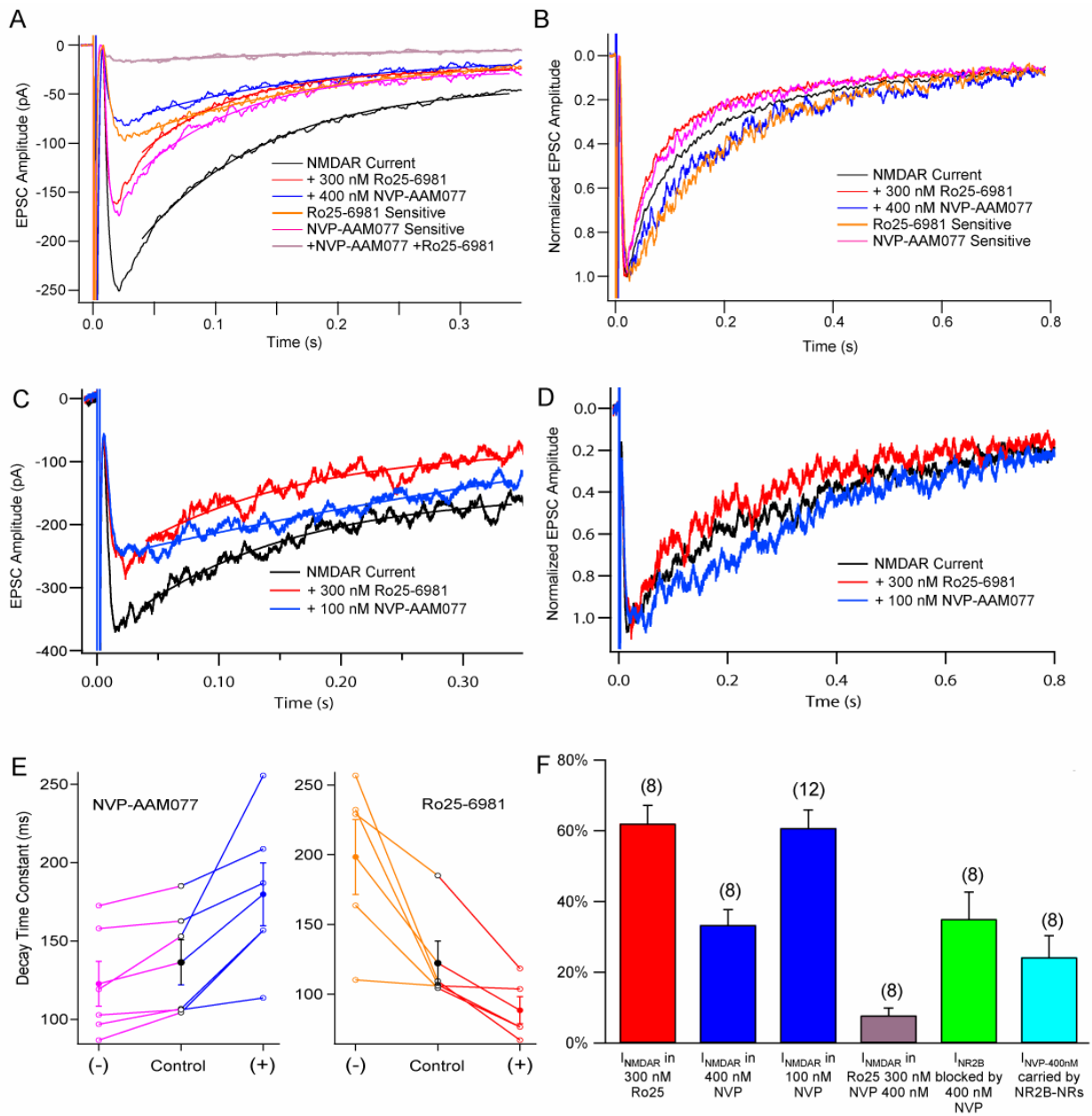


Figure 3.1: NMDAR current amplitudes and kinetics in the presence of subtype-selective antagonists. **A**, Example synaptic currents in the presence of 10 μM CNQX, 10 μM glycine, and 0 Mg^{2+} . Single-exponential fits are superimposed as solid lines. **B**, The traces from **A** normalized and peak-aligned. The trace corresponding to simultaneous presence of both drugs is omitted for clarity. **C,D** Same as **A,B** but for a smaller concentration of NVP-AAM077. **E1**, NMDAR current decay times in the absence of drugs (center), in the presence of 0.4 μM NVP-AAM077 (right, +), and the NVP-AAM077 sensitive component (left, -), ($n=5$; $p<0.05$ for each, paired t-test). Filled circles are mean values. **E2**, Same as **E1**, except 0.3 μM Ro25-6981 is used ($n=6$, $p<0.05$ for each, paired t-test) **F**, The fraction of NMDAR current remaining in 0.3 μM Ro25-6981; remaining in 0.4 μM NVP-AAM077; remaining in 0.1 μM NVP-AAM077; remaining in both Ro25-6981 and NVP-AAM077; the fraction of NR2B-NR current (Ro25-6981-sensitive) blocked by NVP-AAM077; the NR2B-NR contribution to the current blocked by NVP-AAM077; the number of unitary synaptic connections tested for each condition is indicated in parentheses throughout. Error bars are SEM.

3.3.2. Roles of NMDAR subtypes in the induction of bi-directional STDP

To study the roles of NMDAR subtypes in STDP, dual perforated voltage-clamp recordings were performed in the presence of either 0.3 μ M Ro25-6981 or 0.4 μ M NVP-AAM077. After obtaining a 10-15 minute baseline of synaptic responses, a spike-timing-dependent pairing protocol was delivered (1 Hz stimulation for 60 seconds with the postsynaptic cell in current clamp; spike timing Δt was between 8 and 10 ms for “pre-post” and between -8 and -10 ms for “post-pre” spike pairs) to induce spike-timing-dependent LTP or LTD. I confirmed that under control conditions, as in previous studies using this system (Bi and Poo, 1998; Wang et al., 2005), pre-post (AB) spike-pairing resulted in synaptic potentiation (Fig. 3.2a,g,h; $120.6 \pm 3.8\%$, n=8 , p<0.001 vs. unity), while post-pre (BA) spike-pairing resulted in synaptic depression (Fig. 3.2b,g,h; $85.1 \pm 2.9\%$, n=18, p<0.001 vs. unity). Blockade of NR2B-NRs with Ro25-6981 had no significant effect on spike-timing-dependent potentiation (Fig. 3.2c,g,h; $115.5 \pm 4.3\%$, n=6 , p<0.05 vs. unity, p>0.3 vs. control), but abolished spike-timing-dependent depression (Fig. 3.2d,g,h; $101.2 \pm 2.0\%$, n=7, p>0.5 vs. unity, p<0.01 vs. control), indicating that NR2B-NRs are required for spike-timing-dependent depression but not for potentiation.

In contrast, addition of the NR2A-preferring antagonist NVP-AAM077 (0.4 μ M) prevented the synaptic potentiation typically induced by pre-post spike pairs (Fig. 3.2e,g,h; $101.4 \pm 3.5\%$, n=7, p>0.5 vs. unity, p<0.01 vs. control) without significantly altering the synaptic depression induced by post-pre spike pairs (Fig. 3.2f,g,h; $86.5 \pm 2.4\%$, n=6 , p<0.005 vs. unity, p>0.5 vs. control), arguing for a requirement of NR2A-NR activation in spike-timing-dependent potentiation but not depression. Because 0.4 μ M NVP-AAM077 blocks more NMDAR current

than does 0.3 μ M Ro25-6981, the possibility existed that the magnitude of the remaining NMDAR current, rather than the subtype mediating it, had led to abolition of LTP in NVP-AAM077 but not Ro25-6981. To test this possibility, I repeated the LTP experiments in 0.1 μ M NVP-AAM077, a concentration that blocks a similar amount of NMDAR current as 0.3 μ M Ro25-6981 ($37.9 \pm 5.1\%$ for 0.3 μ M Ro25-6981, n=8; $39.2 \pm 5.1\%$ for 0.1 μ M NVP-AAM077, n=12; p>0.4, Fig. 3.1c,d,f). LTP was still absent under this condition (Fig. 3.2g,h; $100.8 \pm 4.8\%$, n=14, p<0.01 vs. control, p<0.05 vs. LTP in 0.3 μ M Ro25-6981, p>0.5 vs. unity).

Therefore, in response to pairs of pre- and postsynaptic spikes, a unitary synaptic connection (the sum of all synapses made by one cell onto another) is capable of generating either NR2B-independent (and likely NR2A-dependent) potentiation or NR2B-dependent depression in a manner determined only by the timing of individual action potentials. This evidence suggests that the induction of STDP is mediated by distinct functional modules, with an NMDAR subpopulation containing the NR2A subunit preferentially driving the potentiation module and NR2B-NRs driving the depression module.

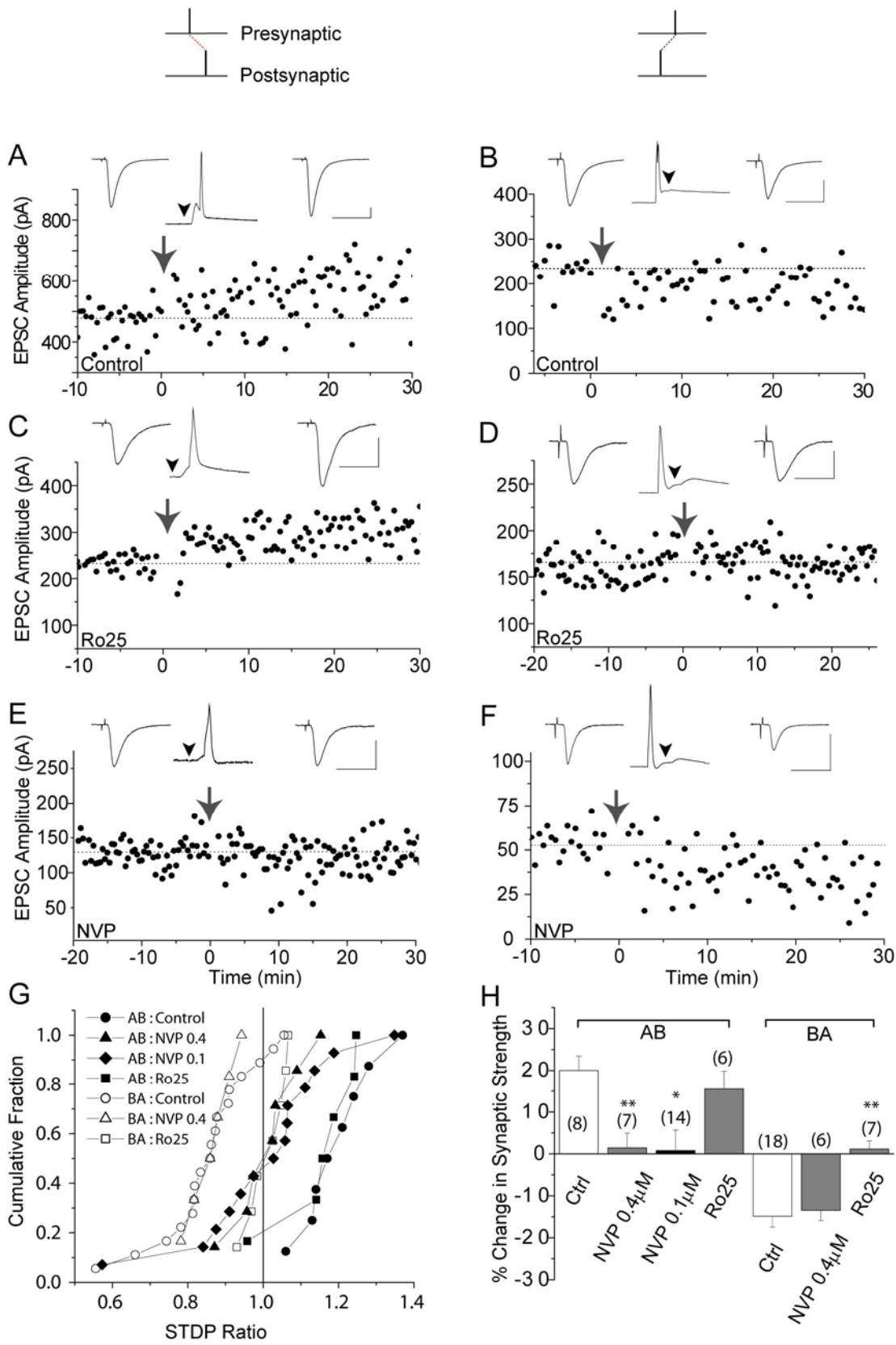


Figure 3.2: Spike-timing-dependent potentiation specifically requires non-NR2B-NRs (putative NR2A-NRs), while spike-timing-dependent depression specifically requires NR2B-NRs.

A, Potentiation is induced by positive spike-timing ($\Delta t=+8\text{ms}$). **B**, Depression is induced by negative spike-timing ($\Delta t=-8\text{ms}$). **C**, Potentiation induced by positive spike-timing persists in the presence of $0.3 \mu\text{M}$ Ro25-6981. **D**, Negative spike-timing fails to induce depression in the presence of Ro25-6981. **E**, Positive spike-timing fails to induce potentiation in the presence of $0.4 \mu\text{M}$ NVP-AAM077. **F**, Depression induced by negative spike-timing remains intact in the presence of $0.4 \mu\text{M}$ NVP-AAM077. **G**, Cumulative histogram of experiments with spike pairs. AB, pre-post spike pairs; BA, post-pre spike pairs. **H**, Change in synaptic strength for all experiments with spike pairs (mean \pm SEM). * indicates $p<0.05$ vs. corresponding controls; ** indicates $p<0.01$ (Student's t-test). AB control vs. AB Ro25-6981: $p=0.56$; BA control vs. BA $0.4 \mu\text{M}$ NVP-AAM077: $p=0.80$. Insets are example traces from the postsynaptic cell before (left), during (middle) and after (right) STDP induction; arrowheads indicate presynaptic cell stimulation. Scale bars: 20 ms, 100 pA (voltage clamp). Autaptic EPSPs in the postsynaptic cell are visible in some insets.

3.3.3. Roles of endocannabinoids and the locus of presynaptic depression

The cannabinoid receptor CB1 has been implicated in spike-timing-dependent depression, but not potentiation, in cortical neurons (Sjostrom et al., 2003; Bender et al., 2006). It has been proposed that CB1 receptors located on presynaptic terminals receive a timing-dependent retrograde signal from activated postsynaptic neurons, which coordinates with the activation of presynaptic NR2B-NRs to produce depression (Sjostrom et al., 2003). Because spike-timing-dependent depression in our system also required activation of NR2B-NRs (though the locus of these NR2B-NRs is unidentified), it was of interest to examine the role of CB1 signaling. In the presence of the CB1 antagonist AM-251 (1-2 μ M), I attempted to induce LTD using “post-pre” spike pairs ($\Delta t = -8$ to -10 ms)(Fig. 3.3a). LTD resulted (Fig. 3.3a,b; $90.0\% \pm 3.1\%$, $n=15$, $p<0.005$ vs. unity), and while it appeared to be less pronounced than under control conditions, this difference was not significant (control: $85.2\% \pm 2.9\%$, $n=18$, $p<0.0001$ vs. unity, $p>0.25$ for AM-251 vs. control). Thus, I found no evidence that CB1 signaling contributes significantly to spike-timing-dependent depression in hippocampal neurons.

Although this LTD did not require the putative retrograde messenger pharmacology observed in cortical timing-dependent LTD, I wondered whether the locus of spike-timing dependent LTD could still be presynaptic (Sjostrom et al., 2003; Bender et al., 2006). Indeed, I found a modest increase in paired-pulse ratio following post-pre spike pairs in both AM-251 and in control conditions (PPR, after vs. before: $112.8 \pm 6.3\%$ in control, $n=9$, $p<0.1$ vs. unity; $109.8 \pm 3.6\%$ in AM-251, $n= 15$, $p<0.01$ vs. unity), suggesting possible involvement of presynaptic mechanisms.

Because recent studies have suggested that paired-pulse facilitation can have postsynaptic

origins (Bagal et al., 2005), I also performed a $1/CV^2$ analysis (Methods, 3.2.4). This analysis compares the change in the coefficient of variation (CV) to the change in the mean synaptic response as a result of plasticity induction (Faber and Korn, 1991). Changes in release probability (p) are reflected by greater changes in $1/CV^2$ than in mean strength, whereas the reverse is true for changes in quantal size (q). This analysis showed great variability in the relationship between changes in $1/CV^2$ and changes in mean synaptic strength (Fig. 3.3c). According to the logic of this analysis, this suggested a non-uniform LTD expression locus. I then reasoned that the locus of LTD might change with synaptic development, as has been observed for LTP (Palmer et al., 2004). Thus, I subdivided the experiments into those with high initial unitary connection strengths (the largest dozen connections, 416.9 ± 31.6 pA, $n = 12$, HIGH) and those with low unitary connection strengths (the remaining connections, 122.3 ± 15 pA, $n = 20$, LOW). While the LOW group still showed no consistent locus of LTD (Fig. 3.3c, open symbols, 8/20 points below the unity line, $p > 0.25$), the HIGH group showed a consistent presynaptic locus (Fig. 3.3c, closed symbols, 12/12 points below the unity line, $p < 0.001$). These data indicate that the expression of spike-timing-dependent LTD has a more consistent presynaptic locus in strong unitary connections. Because mean unitary connection strength increases with development, this may reflect a shift towards a presynaptic locus for LTD during synaptic maturation.

CV analysis can be cumbersome because the data are compared to a unity line in a two-dimensional space, and the relationship between this space and fundamental parameters of quantal analysis is not intuitive. To collapse the information provided by this analysis into a single dimension with intuitive meaning, we considered the quantal assumptions of $1/CV^2$ analysis and used algebraic rearrangement (Methods, 3.2.4) to show that the fractional change in

mean synaptic strength divided by the fractional change in $1/CV^2$ is equal to the fractional change in quantal size, q_{after}/q_{before} , times the fractional change in the failure rate, $(1-p_{after})/(1-p_{before})$. This product, referred to here as the *LTD index*, should be less than 1 when LTD is mostly postsynaptic, and greater than 1 when LTD is mostly presynaptic. This index is thus a simplified representation of the information provided by a $1/CV^2$ analysis of the data, permitting it to be easily plotted against other experimental variables without recourse to higher dimensional spaces.

As shown in Fig. 3.3d, I found that the LTD index is strongly positively correlated with initial synaptic strength ($r=0.70$, $p<0.05$ for control; $r=0.50$, $p<0.05$ for AM-251; $r=0.54$, $p<0.005$ for pooled data; the log of the product was used for correlation, due to the *a priori* distribution for this measure; see Methods, 3.2.4), highlighting a tendency towards presynaptic LTD in stronger connections. The data could not be explained by enhanced LTD in stronger synaptic connections, because we did not observe a significant correlation between the magnitude of LTD and initial synaptic strength ($r=0.13$; $p=0.48$), consistent with previous results (Bi and Poo, 1998; Wang et al., 2005). These data suggest that, at least in strong synapses, retrograde signaling mechanisms other than the endocannabinoid/CB1 system are responsible for spike-timing-dependent LTD in hippocampal neurons.

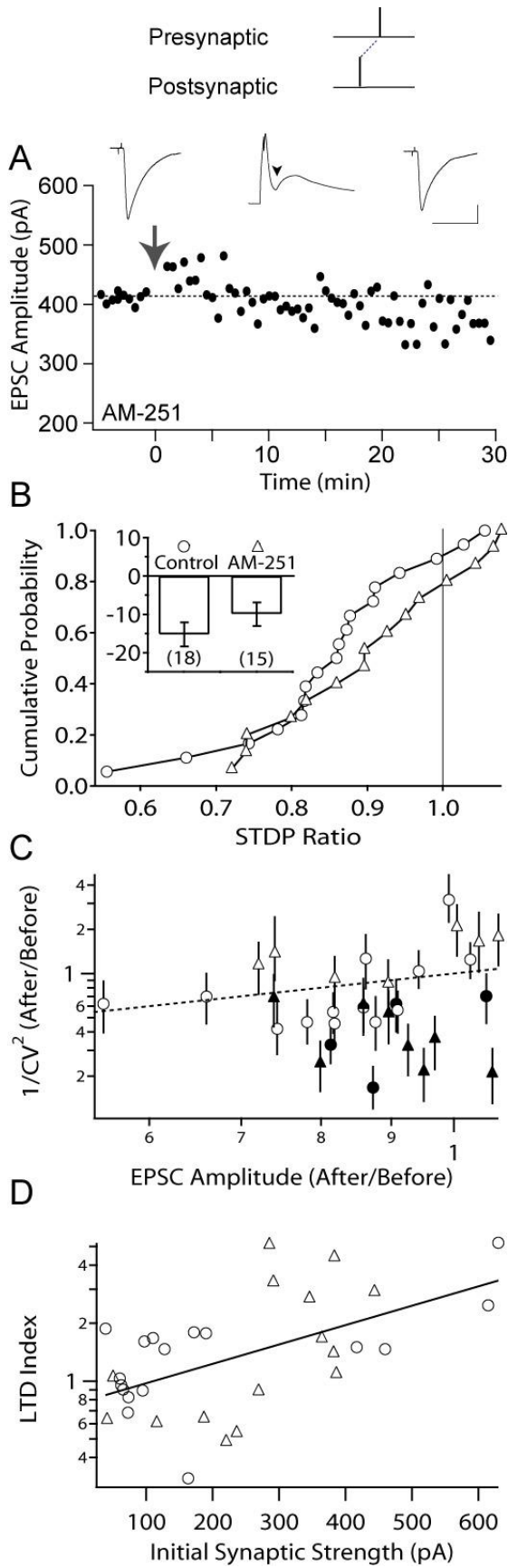


Figure 3.3: Spike-timing-dependent depression favors a presynaptic expression locus but does not depend on CB1 antagonism. **A**, Example showing spike-timing-dependent LTD in the presence of AM-251. **B**, Cumulative histogram of experiments using 1-2 μ M AM-251 compared with controls. Inset is % change in synaptic strength for each condition. **C**, CV analysis shows that only strong synaptic connections have a consistently presynaptic locus. Open symbols are weak connections; Closed symbols are strong connections (see text). Error bars indicate standard error of the $1/CV^2$ measurement. **D**, Correlation between the LTD index (ratio between the multiplicative changes in synaptic strength and $1/CV^2$, see Methods) and the initial synaptic strength ($r=0.54$, $p<0.005$ for the null hypothesis of no correlation). This correlation suggests that strong unitary connections are more likely than weak connections to show increased failure rate ($1-p$), rather than decreased quantal size (q), after LTD induction. In *B-D*, Circles are control experiments; Triangles are experiments done in AM-251. Insets, arrowheads, and scale bars are as in Figure 3.2.

3.3.4. Integration of NMDAR subtype-mediated STDP

Neuronal activity *in vivo* involves ongoing complex spike patterns that contain both positive and negative spike timings, with the final plasticity outcome following second-order rules of STDP integration (Froemke and Dan, 2002; Sjostrom and Nelson, 2002; Wang et al., 2005). The simplest paradigm for such integration involves spike triplets, with two spikes in one neuron temporally bisected by one spike in the other neuron. Thus, each triplet consists of both pre-post and post-pre spike-pairing doublets. The spike-timing interval for each doublet was chosen to be 8-10 ms, for consistency with spike pair experiments.

As in previous studies using cultured hippocampal neurons (Wang et al., 2005), the pre-post-pre (ABA) triplet led to apparent cancellation of potentiation and depression with no net change in synaptic strength (Fig. 3.4a,g,h; $100.2 \pm 2.7\%$, n=5, p>0.4 vs. unity), while the post-pre-post (BAB) triplet yielded potentiation (Fig. 3.4b,g,h; $121.0 \pm 2.5\%$, n=5, p<0.005 vs. unity). These results are also seen in spike quadruplets and are independent of the paired-pulse ratio of the synaptic connection (Wang et al., 2005). However, in the presence of Ro25-6981, the ABA triplet induced potentiation of synaptic strength (Fig. 3.4c,g,h; $115.6 \pm 1.7\%$, n=5, p<0.001 vs. unity, p<0.005 vs. control), suggesting that blocking NR2B-NRs unmasks potentiation. On the other hand, Ro25-6981 had no significant effect on the synaptic potentiation produced by the BAB triplet (Fig. 3.4d,g,h; $119.6 \pm 3.5\%$, n=6, p<0.005 vs. unity, p>0.5 vs. control).

In the presence of NVP-AAM077, the ABA triplet produced synaptic depression (Fig. 3.4e,g,h; $87.5 \pm 2.3\%$, n=10, p<0.001 vs. unity, p<0.05 vs. control), highlighting that preferentially blocking NR2A-NRs unmasks depression in this condition. These results are

consistent with the idea that the timing of spikes in the ABA triplet normally leads to the concomitant activation and subsequent cancellation of both the NVP-AAM077 sensitive potentiation and Ro25-6981 sensitive depression modules. However, for the BAB triplet stimulation protocol, I found that NVP-AAM077 did not unmask depression, but rather resulted in no net change in synaptic strength (Fig. 3.4f,g,h; $100.1 \pm 5.0\%$, n=9, p>0.5 vs. unity, p<0.05 vs. control), suggesting that the depression module failed to activate in response to this spike-timing pattern. Because an additional postsynaptic spike (BAB vs. BA) is apparently sufficient to eliminate depression even in the absence of the expression of potentiation, these results may be explained by an unidentified “veto” module, as suggested by the postsynaptic calcium detector modeling in chapter 2. Such a veto would involve the specific suppression of the depression pathway in response to potentiating stimuli. Overall, the results from triplet experiments show that a single protocol can yield potentiation or depression (or no change), depending only on the availability of NMDAR subtypes.

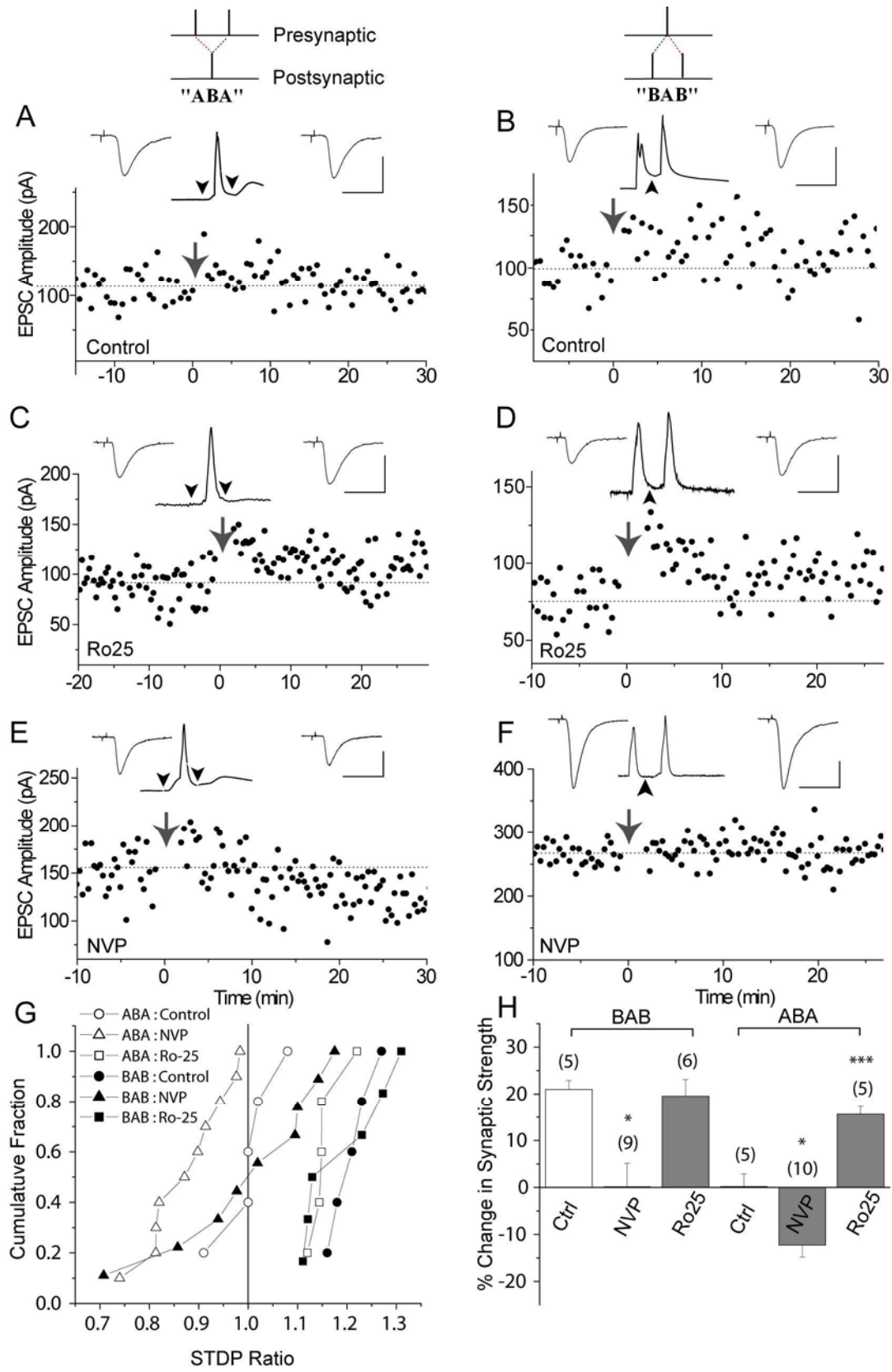


Figure 3.4: Triplet experiments show that potentiation is unmasked by antagonizing NR2B-NRs, while either depression is unmasked or potentiation is abolished by antagonizing NR2A-NRs. **A**, The ABA triplet causes no net change in synaptic strength. ($\Delta t=+8\text{ms}, -8\text{ms}$). **B**, The BAB triplet causes synaptic potentiation ($\Delta t=-8\text{ms}, +8\text{ms}$). **C**, Potentiation is unmasked in the ABA triplet in the presence of $0.3 \mu\text{M}$ Ro25-6981. **D**, Potentiation persists in the BAB triplet in the presence of Ro25-6981. **E**, Depression is unmasked in the ABA triplet in the presence of $0.4 \mu\text{M}$ NVP-AAM077. **F**, The BAB triplet yields no net change in synaptic strength in the presence of $0.4 \mu\text{M}$ NVP-AAM077. **G**, Cumulative histogram of all experiments with spike triplets. **H**, Change in synaptic strength for all experiments with spike triplets (mean \pm SEM). * $p<0.05$ vs. corresponding controls; *** $p<0.005$ (Student's t-test). Insets, arrowheads, and scale bars are as in Figure 2.

3.3.5. Dynamic competition of signaling modules

These findings demonstrate that NMDAR subtypes differentially activate competitive signaling modules in the induction and integration of STDP, and complement our previous observations supporting modularity through the activation of the kinase CaMKII and the phosphatase calcineurin (CaN) (Wang et al., 2005). Together, these results indicate that the activity of specific NMDARs is closely tied to the activation of specific enzymes. In particular, they suggest that a subpopulation of NMDARs, whose fast kinetics and NVP-AAM077 sensitivity implicate the NR2A subunit, may drive the activation of CaMKII, leading to synaptic potentiation. They also suggest that the activation of an NR2B-containing NMDAR subpopulation coordinates with L-type Ca^{2+} channels (Bi and Poo, 1998) and CaN to produce depression (Fig. 3.5a).

To investigate the possibility of a veto module, I extended (Methods, 3.2.5) a simplified version of the postsynaptic calcium detector model in chapter 2 (Rubin et al., 2005) to reflect NR2 subunit specificity. Since AB spike pairings yield higher levels of Ca^{2+} influx than BA spike-pairings (Nevian and Sakmann, 2004), these two spike doublets should be readily distinguishable by Ca^{2+} sensitive machinery (e.g. CaMKII, CaN) in the postsynaptic density. Thus, I provided the timing of these doublets directly as inputs to our model. The model consists of three dynamic elements: a potentiation module **P** (by analogy to CaMKII), activated by Ca^{2+} influx through Ro25-insensitive (putative NR2A-containing) NMDARs, as well as a depression module **D** (by analogy to the calcineurin/PP1 system) and a rapidly inactivating veto module **V** (corresponding to an unidentified kinase or other signaling enzyme), both of which are activated

by Ca^{2+} influx through NR2B-NRs. \mathbf{P} and \mathbf{D} are integrated to give \mathbf{W} , which relates to the consequent change in synaptic strength. Consistent with the Ca^{2+} threshold being greater for synaptic potentiation than depression (Lisman, 1989; Yang et al., 1999; Shouval et al., 2002) and the affinity of CaMKII for Ca^{2+} /Calmodulin being lower than that of CaN/PP1 (Stemmer and Klee, 1994; Bradshaw et al., 2003), \mathbf{P} and \mathbf{V} respond only to pre-post spike doublets, while \mathbf{D} responds to both pre-post and post-pre spike doublets.

In this model, perfect antagonism of the putative NR2A-NR pathway corresponds to a silencing of \mathbf{P} . However, the pre-post doublet can still activate \mathbf{V} through NR2B-NRs; if this occurs immediately after \mathbf{D} has been activated (e.g. post-pre-post triplet), \mathbf{D} will be silenced by the transient \mathbf{V} . In contrast, perfect antagonism of NR2B-NRs allows only \mathbf{P} to be activated. \mathbf{P} responds only to the pre-post doublet, yielding potentiation. This model makes predictions about the sign of changes in synaptic strength resulting from each of 12 stimulus conditions (Figs. 3.5b) that agree with our experimental findings (Figs. 3.2 and 3.4). Furthermore, it is in agreement with the results of our previous work on the integration of STDP (Wang et al., 2005). The veto also helps explain more generally why LTP stimuli often do not yield LTD when LTP pathways are blocked, despite putatively sufficient Ca^{2+} influx; for example, LTD is not observed in the presence of NVP-AAM077 in response to high-frequency stimulation (HFS) (Liu et al., 2004). Since NVP-AAM077 is not perfectly selective for NR2A-NRs, I also simulated the model using the levels of antagonism of the NR2A-NR and NR2B-NR components found experimentally (Fig. 3.1f) for NVP-AAM077 (Fig. 3.5c). Because of the modular competition inherent in the model, it proved robust to this imperfect selectivity, and LTD was preserved as in the experimental data.

Because these results suggest that potentiation may be driven by the activation of a module tied to NR2A-NRs, I hypothesized that LTP might be correlated with the abundance of these receptors. To test this, I measured the magnitude (Methods, 3.2.3) of NMDAR currents 30 minutes after STDP induction. In accordance with a role for NR2A-NRs in spike-timing-dependent LTP, the potentiation observed in the presence of Ro25-6981 was proportional (least-squares linear regression, $r=0.84$, $p<0.01$) to the relative abundance of the putative NR2A-NR current (NMDAR current in the presence of Ro25-6981 normalized to AMPAR current amplitude in the absence of drugs and in normal Mg^{2+} at the same synaptic connection; Fig. 3.5d, red). Using a multiple linear regression model (Table 2.2), I found that this correlation was not explained by the dependence of STDP on the initial strength of the unitary connection (Bi and Poo, 1998).

Table 3.2: NR2A-NR abundance predicts change in synaptic strength even when initial strength is taken into account.

Results of a multiple linear regression with covariates NR2A-NR abundance (defined in the main text) and initial synaptic strength used to explain the value of the % change in synaptic strength.

Parameter	Value	Error	t-value	p-value
Intercept (%)	-4.49	6.77	-0.66	0.54
NR2A-Abundance	134.4	30.3	4.43	0.007
Initial Strength (pA)	0.035	0.017	2.07	0.09

Thus, potentiation depends quantitatively on the relative level of functional NR2A-NR expression in the synaptic population. No statistically significant correlation was observed ($r=-0.43$, $p=0.19$) between the relative abundance of NR2B-NRs (as measured by the fraction of

NMDAR current blocked by Ro25-6981, normalized to AMPAR current) and synaptic depression (Fig. 3.5d, blue). While potentiation of NMDAR currents themselves during LTP could confound this analysis by shuffling data points along the abscissa, such potentiation is reported to be proportional to the potentiation of AMPAR currents (Watt et al., 2004). Thus, the shift of these data points along the abscissa should be proportional to their value along the ordinate, leaving correlation magnitudes unchanged.

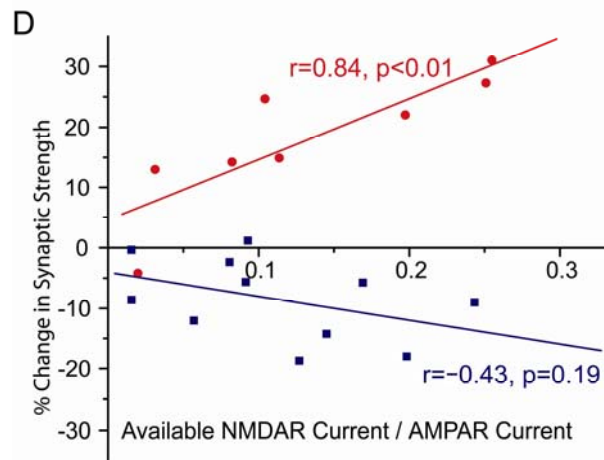
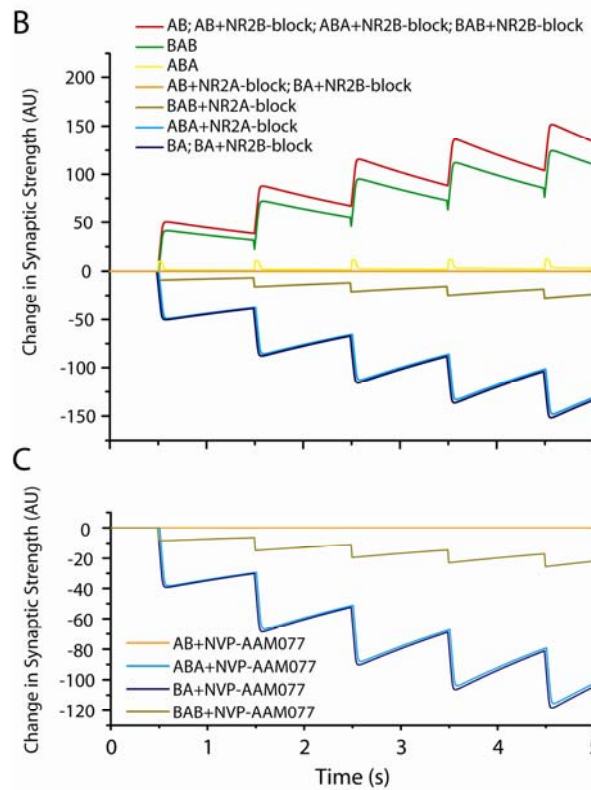
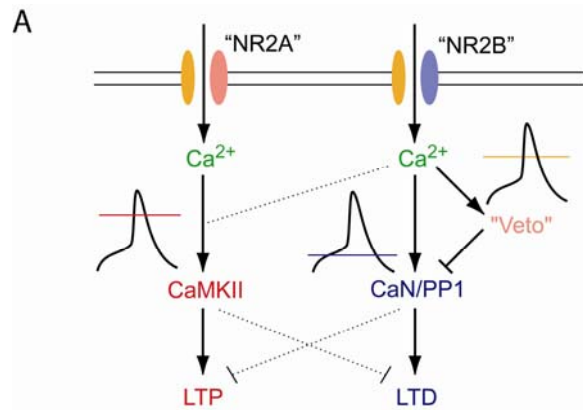


Figure 3.5: A simplified dynamic model of modular competition captures the subunit and stimulus specificity of STDP. **A**, A schematic representation of the proposed pathways for the transduction of STDP. In this model, putative NR2A and NR2B-containing NMDARs are proposed to lie on the postsynaptic membrane, although presynaptic NMDARs have not been definitively excluded. Solid black curves depict Ca^{2+} transients. Horizontal lines depict thresholds of Ca^{2+} influx necessary to activate each module. Dotted lines indicate potential competitive relationships between the potentiation and depression modules. **B**, Results from a simple simulation (Methods, 3.2.5) corresponding to the schematic representation, where AB refers to pre-post spike pairs, BA refers to post-pre spike pairs, ABA refers to pre-post-pre spike triplets, and BAB refers to post-pre-post spike triplets. In the simulation, correlated spiking is repeated 5 times at 1 Hz. “Plasticity readout” corresponds to the variable W in the model, an indicator related to the magnitude of final synaptic modification. The results from correlated spiking repeated 60 times continue the same trend and are omitted for clarity. **C**, Results obtained for block by 0.4 μM NVP-AAM077, assuming that in addition to blocking NR2A-NRs, it blocks 1/3 of the current from NR2B-NRs, as reported in Figure 1. **D**, LTP observed in the presence of Ro25-6981 induced by protocols with “pre-post” spike doublets is plotted (red) against putative NR2A-NR abundance (NMDAR current in the presence of Ro25-6981 normalized by AMPAR current). LTD observed in the presence of NVP-AAM077 induced by protocols with “post-pre” doublets is plotted (blue) against the relative abundance of NR2B-NRs (NMDAR current blocked by Ro25-6981 normalized by AMPAR current.)

3.4. DISCUSSION

In this study, I show that for spike-timing-dependent plasticity, two subpopulations of NMDARs preferentially mediate the activation of distinct functional modules. Together with other recent findings (Wang et al., 2005; Zhou et al., 2005), these results suggest that STDP cannot be explained by the classical picture wherein the overall level of postsynaptic $[Ca^{2+}]$ alone determines the plasticity outcome (Artola and Singer, 1993). Superficially, the basic results of STDP appear to be consistent with this classical “calcium hypothesis” because the Ca^{2+} influx through NMDARs is greater for AB stimuli than for BA stimuli (Nevian and Sakmann, 2004). However, reducing Ca^{2+} influx with Ro25-6981 in the otherwise plasticity-neutral ABA condition actually unmasked LTP (Fig. 3.4a,e,f). Furthermore, while partial reduction of Ca^{2+} influx with Ro25-6981 abolished depression in the post-pre spike pairing (BA) (Fig. 3.2b,e,f), a greater reduction by NVP-AAM077 (Fig. 3.1f), did not compromise depression (3.2d,e,f). These nonlinearities are explained by the existence of NMDAR subtype-specific potentiation and depression modules, the dynamic competition of which determines the outcome of STDP.

3.4.1. Evidence for a veto module

Interestingly, the AB and BAB stimuli failed to produce depression in the presence of NVP-AAM077, despite Ca^{2+} influx putatively sufficient, as indicated by the success of BA under the same conditions, to activate the depression module. One possibility is that the NR2B-NR-mediated, CaN-dependent depression module is actively suppressed (“vetoed”) in a spike timing-dependent fashion by a module which is not of itself potentiation. This veto would be activated

by moderately strong $[Ca^{2+}]$ transients but be NVP-AAM077 insensitive (i.e. Ca^{2+} influx through NR2B-NRs would be sufficient). While this concept is similar to the calcium detector scheme explored earlier, by separating NMDAR-mediated Ca^{2+} influx into distinct pools the current model (Fig. 3.5b,c) can match experimental outcomes with fewer detectors. Additionally, the recruitment of synaptic depression may have other timing requirements that render large but brief $[Ca^{2+}]$ transients insufficient for this task (Chapter 2, (Mizuno et al., 2001)).

In both this and the previous model, it is critically important that the value of v_{off} , the inverse time constant for the veto variable, be high (i.e. for the veto to decay rapidly). Without such a rapid decay, the veto would suppress the buildup of depression that occurs immediately after the buildup of potentiation, as in the ABA triplet. This would result in the ABA triplet yielding potentiation instead of the observed cancellation of potentiation and depression. Indeed, a slowly decaying veto would yield results similar to those observed in paired recordings from layer 5 pyramidal neurons in visual cortex, in which positively-timed spike pairs consistently trump negatively-timed pairs, regardless of order, and yield potentiation (Sjostrom et al., 2001). Lowering the value of λ , the “force” of the veto on the depression pathway, would permit depression to cancel potentiation regardless of the relative order of potentiation and depressing spike pairs. In this instance, the plasticity outcome would be simply determined by the relative frequency of potentiating ($\Delta t > 0$) and depressing ($\Delta t < 0$) spike pairs in the overall stimulus, a common assumption in early STDP models (Song et al., 2000). Other parameter choices are chosen simply to reflect the accumulation of resultant plasticity over the course of a 1 Hz stimulation paradigm and do not qualitatively affect the competition observed in the model.

3.4.2. Specificity of NR2A-NR antagonism

A crucial issue in this and related studies has been the specificity of antagonists (Neyton and Paoletti, 2006). I showed that 0.4 μ M NVP-AAM077 blocked ~1/3 of the synaptic NR2B-NR currents in our preparation. This analysis, based on measurements using 0.033 Hz stimuli, may overestimate the “nonspecific” blockade of NR2B-NRs by NVP-AAM077 during STDP paradigms (≥ 1 Hz presynaptic stimulation), because the NR2B-NR inhibition by NVP-AAM077 is weaker for more sustained agonist application (Weitlauf et al., 2005). It also makes the assumption that the pharmacological profile of the “running-down” component of the NMDAR current (Rosenmund and Westbrook, 1993), which was not measured, is not substantially different from the steady-state component.

Whatever the precise fraction of NR2B-NR block caused by 0.4 μ M NVP-AAM077, it cannot itself have abolished potentiation, because full NR2B-NR block with Ro25-6981 fails to do so. Ultimately, the final plasticity outcome for STDP (and perhaps classical LTP/LTD) may be determined by the competition among NMDAR subtype-dependent signaling modules rather than by the absolute activation of a particular module (or related receptor subtype). Therefore, although pharmacological separation of NMDAR subtypes is imperfect, differential inhibition of subtypes could have a decisive effect by biasing this competition (Mallon et al., 2004; Li et al., 2006).

Some NMDARs may be NR1-NR2A-NR2B triheteromers with the kinetic properties of NR2B, and a sensitivity to ifenprodil-like compounds more reminiscent of NR2B than NR2A (Brimecombe et al., 1997; Kew et al., 1998; Hatton and Paoletti, 2005; Neyton and Paoletti, 2006). There are no direct studies concerning the ability of NVP-AAM077 to block such receptors. To account for this, the calculation of the empirical specificity of NVP-AAM077 for

each NMDAR subtype uses a weighted average of the block of NR2B-NRs and the block of NR2A-NR2B-NRs by NVP-AAM077 (Methods, 3.2.3; Equation 3.3). However, because NR2A-NR2B-NRs are believed to have slow kinetics similar to those of NR2B-NRs (Vicini et al., 1998), and the current blocked by NVP-AAM077 has much more rapid kinetics (Fig. 3.1b,d,e), the majority of this NVP-AAM077 sensitive current is likely to be mediated by NMDARs containing only the NR2A subunit. NVP-AAM077 can also block NR2C-containing NMDARs (Feng et al., 2004); however, these are believed to be mostly absent in hippocampal principal neurons *in vivo* (Monyer et al., 1994), and in culture (Miyashiro et al., 1994; Janssens and Lesage, 2001; Okada and Corfas, 2004). The rapid kinetics of the NVP-AAM077 sensitive NMDAR current also argue against the presence of these kinetically slow NMDAR subtypes.

3.4.3. Alternative techniques for the study of NMDAR subtype selectivity in synaptic plasticity

Because of controversy concerning the specificity of NVP-AAM077 in the antagonism NR2A-NMDARs (Neyton and Paoletti, 2006), substantial experimental justification for its use was required (Fig. 3.1). For future pharmacological exploration of NMDAR subtypes in plasticity, it is worth considering the use of Zn^{2+} . Zn^{2+} not only exhibits selectivity for NR2A- over NR2B-NMDARs, but it is a non-competitive antagonist. This latter property validates the use of existing pharmacological data in the study of real synapses, and permits the use of an elegant residue substitution technique (Hatton and Paoletti, 2005), which allows the impact of Zn^{2+} on triheteromeric NMDARs to be assessed. This will be essential knowledge if research on NMDAR subtype selectivity in synaptic plasticity is to continue to bear fruit.

3.4.4. Presynaptic mechanisms of STDP

Our $1/CV^2$ analyses indicate that for a subpopulation of synapses, spike-timing-dependent LTD is presynaptically expressed, in consonance with the findings at cortical synapses (Sjostrom et al., 2003; Bender et al., 2006). However, this LTD apparently did not require a CB1 receptor signaling pathway, in contrast to what has been observed in the neocortex (Sjostrom et al., 2003; Bender et al., 2006). One possibility is that other cannabinoid receptors such as the AM-251 insensitive CBsc receptor (Hajos et al., 2001) play an important role in the control of glutamatergic transmission in the hippocampus (Hoffman et al., 2005). Despite this evidence for the presynaptic expression of LTD, our model contains an implicit assumption that the signaling modules P , D , and V all reside in the postsynaptic compartment where they interact with one another as well as upstream and downstream signaling factors. This assumption is favorable because these modules must be able to discriminate between stimuli with millisecond precision to achieve the correct plasticity outcome. In such a picture, presynaptic expression of LTD would occur only after the completion of an upstream computation occurring entirely in the postsynaptic compartment. Under certain conditions (e.g. BA), the completion of this computation through dynamic interaction among postsynaptic signaling modules could result in the production of a retrograde messenger, which in turn would induce the expression of LTD at a presynaptic locus.

However, recent studies have revealed possibilities for presynaptic coincidence detection in the induction of certain types of synaptic plasticity, including spike-timing-dependent depression in the neocortex involving retrograde endocannabinoid signaling and activation of putatively presynaptic NR2B-NRs (Duguid and Sjostrom, 2006). If similar mechanisms exist in hippocampal neurons, an attractive alternative to purely postsynaptic modules would be a

framework in which postsynaptic NR2A-NRs linked to a postsynaptic P worked in concert with presynaptic NR2B-NRs linked to a presynaptic D . In fact, the general features of our model of modular competition are also compatible with this picture, as long as V resides in the same compartment with D , due to kinetic considerations. Unfortunately I was unable to directly test this idea because manipulations such as selective blockade of presynaptic NR2B-NRs are difficult to attain under perforated patch-clamp conditions.

It should be noted that as with classical $1/CV^2$ analysis, interpretation of the LTD index relies on the assumption that the individual synapses comprising a unitary synaptic connection act independently, and have stationary statistical properties within each region of time that is analyzed. Furthermore, changes in statistical properties are assumed to be homogenous across these synapses, although the equations can be rederived without this assumption (Silver, 2003; Saviane and Silver, 2006). Lastly, it should be noted that variability in baseline values of release probability across experiments, even if homogeneous across the individual synapses with one experiment, can cause artifactual variability in the LTD index, even when the relative contribution of pre- and postsynaptic changes during LTD is uniform. This results because the quantity $(1-a*p_0)/(1-p_0)$, which represents the LTD index for an observed LTD magnitude a expressed entirely presynaptically, is a non-flat function of the initial release probability p_0 . Consequently, it is possible that the increase in the apparent presynaptic contribution of LTD in strong unitary connections is an artifact of comparatively large initial values of p in these connections. However, for this artifact to be significant, p_0 would have to be quite large at individual synapses; meanwhile, most synapses in hippocampal cultures have release probability < 0.3 (Murthy et al., 1997).

3.4.5. Mechanisms of subtype selectivity

There are several potential mechanisms by which NMDAR subtypes could selectively activate different modules. One possibility is the differential localization of the two subtypes on pre- and postsynaptic compartments, as discussed above. For the alternative hypothesis of all-postsynaptic modules, it has been suggested that the subcellular localization (e.g. synaptic vs. extrasynaptic) of NR2A- and NR2B-NRs could confer upon them differential sensitivity to contrasting stimulus patterns (Bliss and Schoepfer, 2004). Differential subcellular localization could also lead to different spatiotemporal patterns of calcium influx and intrasynaptic diffusion, thus preferentially activating different modules. At a finer scale, specific macromolecular assemblies (Kennedy et al., 2005) responsible for activating potentiation or depression could be directly coupled to synaptic NR2A- and NR2B-NRs, respectively (Kim et al., 2005; Li et al., 2006; Tigaret et al., 2006). In such cases, Ca^{2+} transients at “micro-domains” (Blackstone and Sheng, 2002) may directly activate such molecular modules, including those involving CaMKII or CaN, leading to structural and functional changes at synapses.

Because activated CaMKII localizes to NR2B-NRs, their interaction is likely to be important for LTP expression (Bayer et al., 2001; Barria and Malinow, 2005). Yet the role of NMDAR subtypes in scaffolding and in signaling may be quite distinct. Because NR2A-NRs experience more rapid relief of Mg^{2+} block by back-propagating action potentials (Clarke and Johnson, 2005), and have a 4x higher peak open probability than NR2B-NRs (Chen et al., 1999b; Erreger et al., 2005), NR2A-NRs may permit significantly greater Ca^{2+} influx during STDP-associated EPSP-Spike interactions than do NR2B-NRs (Kampa et al., 2004). Thus, NR2A-NRs may be necessary to activate a (soluble) pool of inactive CaMKII. The activated CaMKII could then bind to NR2B-NRs (Barria and Malinow, 2005) and recruit AMPARs for the expression of

LTP (Lisman et al., 2002). The signal/scaffold model also puts NR2B-NRs in a prime position to mediate LTD, since phosphatases activated by Ca^{2+} influx through NR2B-NRs would be optimally located to disrupt this assembly. Nonetheless, in some brain areas, during early development, or under certain genetic manipulations, LTP may in part be signaled by non-NR2A NMDAR subtypes (Barth and Malenka, 2001; Lu et al., 2001; Barria and Malinow, 2005; Berberich et al., 2005; Weitlauf et al., 2005; Zhao et al., 2005). Consistent with this variability, our preliminary data suggests that a different kind of NMDAR subtype specificity for STDP may exist earlier in synaptic development: for neurons of age 8-9 DIV, the AB spike pairing protocol ($\Delta t=8$ ms) results in significant potentiation ($146.5 \pm 14.2\%$, $n=6$, $p<0.05$) in the presence of 0.1 μM NVP-AAM077, despite the capacity of this drug to block NR2A-NR currents.

Another possibility lies in the capacity of calcineurin to inhibit NMDAR currents that immediately follow backpropagating action potentials. Inclusion of blockers of calcineurin, or of the NR2A-NR n-terminus, which binds to calcineurin, into the postsynaptic recording pipette abolishes this effect (Froemke et al., 2005), suggesting that interaction of calcineurin with NR2A-NRs mediates this NMDAR current inhibition. This indicates that the calcium contribution of postsynaptic NR2A-NRs may be reduced in response to BA spike pairings, and thus may not contribute significantly to downstream signaling in response to such stimuli. This might explain the failure of NR2A-NR blockade to reduce LTD resulting from BA spike pairings; however, it might be difficult for such an inhibitory mechanism to preserve LTP in response to BAB spike triplets under control conditions.

Finally, because of the striking difference in the decay time constants of NR2A- and NR2B-NR-mediated currents, it is also possible that kinetics are responsible for subtype specific activation of STDP modules. Previous attempts to explain differential roles for NMDAR

subtypes based on kinetics (Erreger et al., 2005) have relied on differences in the stimulation frequency used to evoke LTP compared with LTD. However, in STDP potentiation and depression are achieved at the same stimulus frequency. Thus, a different mechanism is needed for a kinetic model to explain STDP. Indeed, a postsynaptic $[Ca^{2+}]$ time-course model (chapter 2) recapitulates the results from previous spike multiplet experiments, as well as conventional protocols for the induction of synaptic plasticity (Rubin et al., 2005). The difference in NMDAR-mediated current kinetics between those observed in the presence of NVP-AAM077 and those in the presence of Ro25-6981 (Fig. 3.1b,d,e) may provide further evidence that slow Ca^{2+} transients are better for depression, and fast Ca^{2+} transients are better for potentiation (Zhou et al., 2005).

In summary, NR2A-NRs have fast decay kinetics, are more synaptically localized, and interact preferentially with downstream signaling pathways involved in LTP, whereas NR2B-NRs have slower kinetics, are frequently found extrasynaptically, and interact with LTD pathways. Thus, kinetics, localization, and signaling interactions may all favor the same discrimination and work in parallel to ensure reliable modular competition in NMDAR-dependent synaptic plasticity.

4. INTEGRATION OF SPIKE-TIMING-DEPENDENT POTENTIATION ACROSS MULTIPLE TIME SCALES

4.1. INTRODUCTION

The repetition of spike-timing between neurons is observed during a variety of behaviors (Sutherland and McNaughton, 2000) and may be a generic feature of neuronal circuits (Izhikevich, 2006). Spike-timing-dependent plasticity (STDP) can be induced by repetitive stimulation of a postsynaptic neuron and a presynaptic neuron, fiber bundle, or sensory input, with a fixed timing between pre- and postsynaptic activation. However, the contribution of individual spike pairings to plasticity has been rarely explored (Froemke et al., 2006; Wittenberg and Wang, 2006). A minimum number of stimuli may be required to induce measurable LTP (Huerta and Lisman, 1995; Remy and Spruston, 2007), and the saturability of LTP may provide a practical maximum (O'Connor et al., 2005b).

Furthermore, the potentiability of synapses is likely to be a function of their history, a phenomenon known as “metaplasticity” (Abraham and Bear, 1996). In a common model of metaplasticity, the firing frequencies associated with LTP and LTD are modified by recent activity (Bienenstock et al., 1982). However, in the context of STDP, metaplasticity could regulate the efficacy of individual spike pairings, at a fixed frequency, within a sequence, or the efficacy of entire sequences separated by minutes. To investigate these possibilities, I recorded

from pairs of monosynaptically connected cultured hippocampal neurons and evoked spike-timing-dependent potentiation using different numbers of spike pairings (a presynaptic spike followed by a postsynaptic spike, $\Delta t = 10$ ms). After measuring the resultant LTP, I delivered a second set of spike pairings after an interval of minutes to evoke further LTP. I then used these experimental results to evaluate a model of spike-timing dependent metaplasticity.

4.2. METHODS

4.2.1. Experimental methods

All experiments were carried out in the manner described in chapter 3.

4.2.2. Statistical Model for the Contribution of Spike Pairings to STDP

I assumed that each unitary synaptic connection between two neurons was composed of n independent, binary synapses, of which a fraction f were already in the potentiated state. For each of s spike pairings, the probability p of potentiating those synapses in the depressed state was set equal to $p_0(1-\exp(-s/s_0))$, with a ratio w between the strengths of the potentiated and non-potentiated states for individual synapses. $s_0 > 0$ reflects the hypothesis that an individual spike pairing is more effective in producing potentiation when it has been preceded by earlier spike pairings, perhaps due to a priming of some enzymatic pathway. In this model, once a synapse potentiates, it becomes frozen in the potentiated state. The probability that a previously

unpotentiated single synapse will be potentiated after s stimuli is:

$$y(s) = 1 - [1 - p_0(1 - e^{-1/s_0})][1 - p_0(1 - e^{-2/s_0})] \dots [1 - p_0(1 - e^{-s/s_0})] = 1 - g(s) \quad \text{eq. 4.1}$$

The observed potentiation (total efficacy of all synapses after / total efficacy of all synapses before) as a function of the number of spike pairings is given by:

$$\begin{aligned} Q(s) &= \frac{nf'w + n(1-f')}{nfw + n(1-f)} \\ &= \frac{f'w + (1-f')}{fw + (1-f)} \end{aligned} \quad \text{eq. 4.2}$$

where f' is the fraction of potentiated synapses after induction. $Q(s)$ generates the curves plotted in Fig. 4.1a and 4.1f, and is the prediction against which the experimental measurements are compared. The expectation value of f' after s spike pairings is given by:

$$E(f') = \sum f' \cdot p(f') = f + \frac{1}{n} [y(1-y)^{m-1} C_1^m + 2y^2(1-y)^{m-2} C_2^m + \dots + my^m C_m^m] \quad \text{eq. 4.3}$$

Where $m = n*(1-f)$, the number of previously unpotentiated synapses, $y=y(s)$ as in equation 4.1, and C_j^i represents the number of combinations of j selections from i choices = $i!/(j!*(i-j)!)$.

Thus, the expected value for observed potentiation $Q(s)$ can be obtained by substituting equation 4.1 into 4.3 and 4.3 into 4.2. By seeding with a wide variety of initial guesses for p_0 , s_0 , and f , I fit this function to the data by globally minimizing the least squared error, resulting in the values reported in the main text. Varying n has little effect for sufficiently large n , i.e. $n>10$, and

the efficacy of single hippocampal synapses in cultured hippocampal neurons (Nauen and Bi, 2008) suggests that n exceeds this value for the unitary connections studied in this analysis.

Table 4.1: Parameters used in the spike-pairing integration model.

Parameter	Description	Source/Comments
p_0	Maximal probability of potentiation by a single spike pairing	Free parameter
s_0	Characteristic number of spike pairings to get e-fold closer to $p=p_0$	Free parameter
f	Fraction of synapses in the unpotentiated state prior to induction.	(O'Connor et al., 2005a); Free parameter
w	Ratio of EPSC amplitude from the potentiated to the unpotentiated state.	(O'Connor et al., 2005a)
n	Number of synapses per paired connection	Nauen and Bi, 2008; results are independent of n for large n .

4.3. RESULTS

4.3.1. Integration of potentiation across pairings

To investigate the contribution of individual spike pairings to LTP, I delivered either 4, 10, 16, 20, 60, 64, or 120 potentiating spike pairings to pairs of hippocampal neurons. The resultant LTP is shown in Figure 4.1a. The non-linear relationship between LTP and spike pairings argues against a simple additive model for the contribution of individual spike pairings (Song et al., 2000). A more plausible model might involve multiplicative scaling, in which the potentiation induced by a single spike pairing is proportional to the difference between the initial

value and an upper bound of synaptic strength (Kistler and van Hemmen, 2000; Rubin, 2001), which results in decreasing returns to each spike pairing. However, the data show increasing returns to each spike pairing in the range <20 pairings.

The total synaptic connection between a pair of neurons, known as the unitary connection, consists of many individual synapses ($n = 10\text{-}100$ individual synapses per unitary connection for these experiments, (Nauen and Bi, 2008)). By assuming independence between the individual synapses that compose a unitary (total) synaptic connection between a pair of neurons, one can model the data by assuming that with each spike pairing, each individual synapse has a probability p of potentiating its strength by a multiplicative factor w . The value w may be fixed across individual synapses, reflecting a binary option for synaptic strength and all-or-none potentiation (Petersen et al., 1998; O'Connor et al., 2005a).

The supralinearity apparent for small numbers of spike pairings could reflect a resistance of synapses to potentiation from random spike pairings appearing in noisy stimuli. This resistance was modeled by assuming that p grows asymptotically towards p_0 with each pairing (with time constant s_0) up to a maximum value p_0 . Reflecting the fact that “naïve” synapses are distributed between two levels of strength (O'Connor et al., 2005a), I initialized a fraction f of the synapses to have strength w , and a fraction $(1-f)$ to have strength 1. Thusly, potentiation of a single synapse from the weaker state to the stronger state corresponds to a multiplicative increase to its strength of factor w . For s spike pairings over n individual synapses, observed LTP under this model is given above (Methods, 4.2.2).

In this statistical model, the mean predicted LTP is invariant to n . Also, w has been measured at ~ 2.23 at the juvenile (P14-P21) rat CA3-CA1 synapse (O'Connor et al., 2005a), constraining the family of functional relationships between LTP and s . The value f has been

measured at 0.29 in the hippocampal slice (O'Connor et al., 2005a), but the activity (and potentiation) history between acute slice and culture is likely to be sufficiently different to justifying freeing this parameter.

With p_0 , s_0 , and f free, a best functional fit to the data was obtained, shown in Figure 4.1a. The sum of the squared error was minimized using $f = 0.706$, $p_0 = 0.079$, $s_0 = 13.8$. The size of s_0 indicates that some cooperativity among spike pairings is required to produce appreciable potentiation. The large value of f suggests that the spontaneous activity prevalent in cultured neurons may contribute to the ongoing conversion of synapses to a potentiated state. However, LTP may be associated with either the potentiation of existing synapses or the addition of new, unpotentiated synapses (Zhao et al., 2006), clouding speculation on LTP-associated changes in f .

4.3.2. Integration of potentiation across inductions

Next, I investigated the potentiation exhibited by a second set of spike pairings several minutes after the first. Both sets used 60-64 spike pairings. Because potentiation caused by STDP protocols appears to stabilize between 15-20 minutes after pairing (see Fig. 3.2 and 3.4 for examples), I divided the data into two halves: experiments in which the second induction was delivered shortly after the first (RECENT, time after first induction = 14.8 ± 0.5 minutes), and experiments in which the second induction was delivered at a greater latency from the first (DISTANT, time after first induction = 24.6 ± 2.1 minutes). I found that the potentiation caused by the second set was dependent on the time since the first set (Potentiation vs. Time since first induction: $r=0.38$, $p<0.01$ by Spearman's rank correlation test); insufficient time between sets resulted in decreased potentiability. The RECENT group showed no additional potentiation (Fig.

4.1b; $99.9 \pm 6.9\%$, n=9; p<0.01 vs. first induction, p>0.4 vs. unity), whereas the DISTANT group showed potentiation that was similar to the first induction (Fig. 4.1b; $123.6 \pm 5.5\%$, n=9; p>0.3 vs. first induction, p<0.005 vs. RECENT).

Finally, I combined these approaches to study the integration of two kinds of STDP inductions with differing temporal orders. In one set of experiments (“16:64”, Fig. 4.1c), I delivered 16 spike pairings, followed 20-30 minutes later by 64 spike pairings. In the second set (“64:16”, Fig. 4.1d), I delivered 64 spike pairings, followed at the same interval by 16 spike pairings. In both sets of experiments, the total number of spike pairings was equal to 80, but I hypothesized that metaplasticity might influence the relative efficacy of the second induction in both groups, affecting the final outcome.

64 spike pairings, whether delivered first, or after 16 spike pairings, caused a similar level of potentiation ($119.7 \pm 5.6\%$ vs. $120.7 \pm 7.5\%$, respectively). However, while 16 spike pairings potentiated synaptic connections when delivered first ($110.2 \pm 3.7\%$), it had no net effect when delivered after 64 spike pairings ($95.6 \pm 4.0\%$, p<0.02 vs. first inductions, p>0.2 vs. unity). In total, the “16:64” group showed significantly more total potentiation than the “64:16” group ($132.7 \pm 8.6\%$, n=7 vs. $114.1 \pm 6.9\%$, n=14; p<0.05) (Fig. 4.1e).

To understand the possible source of this effect, I used the same model as above. The decrease in synaptic potentiation resulting from 16 pairings, when it follows 64 pairings, could, intuitively, be explained by a decrease in p_o , an increase in f , a decrease in s_0 , or a decrease in w . However, there is no significant difference between the first and second induction for potentiation induced by 64 pairings, so I constrained f , which determines the maximum possible potentiation to the value obtained above (Fig. 4.1a). For similar reasons, a decrease in w or p_o cannot simultaneously explain both results. A decrease in s_0 , however, could dramatically

reduce the potentiation observed for small numbers of pairings without affecting that seen for large numbers of pairings, consistent with the data (Fig. 4.1f, green line is best fit given by $f = 0.706$, $p_0 = 0.37$, $s_0 = 291$). This would substantially increase in the inter-pairing cooperativity requirement for spike-timing-dependent potentiation.

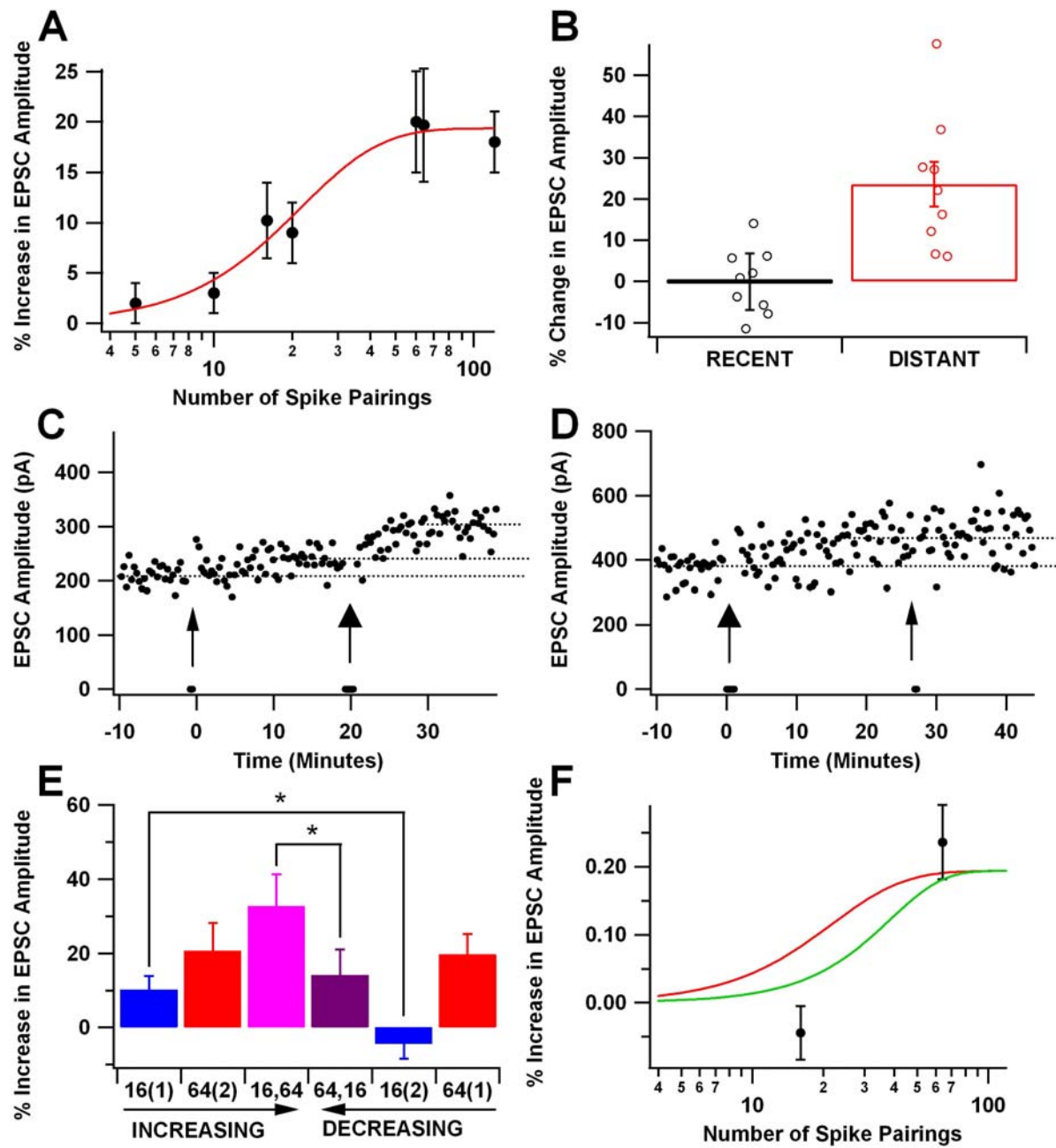


Figure 4.1: Dependence of spike-timing-dependent potentiation on individual spike pairings and potentiation history. **A**, Potentiation is a non-linear function of the number of spike pairings ($\Delta t=10\text{ms}$). The red line is a fit using least squares regression to equation 4.2 (Methods, 4.2.2) **B**, A second set of 60 spike pairings yields synaptic potentiation when delivered >17.5 minutes after the first set (DISTANT), but delivers no potentiation if delivered <17.5 minutes after the first set (RECENT; $p<0.005$ vs. DISTANT). **C**, Potentiation by 16 spike pairings (small arrow) can be followed by potentiation by 64 spike-timing (large arrow). **D**, Potentiation by 64 spike pairings (large arrow) is followed by no potentiation in response to 16 spike pairings (small arrow). **E**, Total potentiation across multiple inductions is not commutative. More potentiation results when the number of spike pairings is increasing from the first to the second induction than when it is decreasing. **F**, Similar to **A**, except using only data from a second induction following 60-64 spike pairings by a DISTANT interval. The blue line is a least squares regression of equation 4.2 to the data, and the red line is duplicated from **A** for comparison. * indicates $p<0.05$.

4.4. DISCUSSION

These data show that individual spike pairings cannot be treated independently, but rather exhibit cooperativity that becomes maximal within approximately a dozen pairings. I have implemented this cooperativity in the model according to eq. 4.1, assuming that the resistance to potentiation by individual spike pairings decays exponentially with spike pairing number; while alternative forms may be equally plausible, the phenomenon itself is qualitatively evidenced by the supralinearity in Fig. 4.1a for low numbers of spike pairings.

4.4.1. Possible sources of inter-pairing cooperativity

The source of this cooperativity is unknown; however any dynamic model in which signaling pathways include both forward and reverse processes could potentially explain the results. For example, a model in which the concentration of some factor X, represented as $[X]$, both accumulates with each spike pairing and decays with time will have a mean value between pairings of $[X]$, which increases with each pairing until reaching a steady state. Intuitively, this steady state will be exponentially approached with a time constant τ_{decay} , the decay time constant of $[X]$. In the model, this would yield $s_0 = \tau_{\text{pairing}}/\tau_{\text{decay}}$, where τ_{pairing} is the interval between spike pairings. Thus, the value of $s_0=13.8$ derived from the experiments, combined with an inter-pairing-interval of 1 second, corresponds to a τ_{decay} of 72 ms, and could point to an enzymatic

pathway with a time constant on this order. This heuristic analysis assumes that the probability of potentiation with each spike pairing is proportional to the concentration of [X], when in fact many intervening nonlinearities are likely to determine this probability.

Could [X] be the postsynaptic calcium concentration, $[Ca^{2+}]$? If so, the decay time constant for postsynaptic $[Ca^{2+}]$ would have to decrease substantially after the first induction to explain the dramatic increase in s_0 (13.8 to 291) seen for the second induction. This could be implemented by, for example, a recruitment of additional postsynaptic calcium buffers after the first induction. Because buffer capacity is finite, sharp non-linearities associated with free calcium clearance could in principle effect a large change in s_0 with a small change in buffer concentration.

Alternatively, [X] could be the concentration of a second effector associated with synaptic potentiation such as CaMKII. Because activated CaMKII can autocatalyze its own phosphorylation, large changes in s_0 could be effected by small changes in, for example, the activity of phosphatases which oppose CaMKII phosphorylation. It is plausible that a series of modifications at different points along the synaptic potentiation signaling pathway could account for the change in s_0 .

4.4.2. Possible sources of dependence on induction history

These data cannot be explained by changes in synaptic strength resulting from the first induction that are not yet completed by the time of second induction in the RECENT group. In contrast to non-physiological plasticity protocols, synaptic efficacy after spike pairing is generally stable or slightly increasing during the period 15-40 minutes after induction (for

examples, see (Wang et al., 2005; Gerkin et al., 2007). Thus, declining synaptic efficacy prior to the second induction cannot explain the difference between the two groups. Rather, the data suggest that some process occurs on a timescale of tens of minutes in which potentiability, initially reduced by the first induction, returns to synapses. This process could include insertion of new, unphosphorylated AMPARs (Hayashi et al., 2000), the insertion of new “slots” capable of recruiting receptors (Shi et al., 2001), or the growth of spines (Harris et al., 2003; Chen et al., 2007).

Can the reduced efficacy of 16 pairings, when preceded by 64 pairings, be explained by a ceiling effect? First, 64 pairings elicited at a similar interval after 64 pairings shows no decrement in LTP (4.1b). Second, 80 total pairings, delivered with the 16 preceding rather than following the 64, yields significantly more potentiation than when the temporal order is reversed (4.1e). These non-trivial changes to the response function, described in Fig. 4.1f, cannot be explained by a simple saturation of potentiation.

I have assumed in this model that f , p_0 , and w do not change between inductions. This decision was motivated by the failure of such changes to explain the data, but they cannot be ruled out. In particular, it would seem that f must change as a result of the first induction, since some fraction of unpotentiated synapses have become potentiated. However, because the large s limit of the potentiation magnitude is similar for the first and second induction (for 64 spike pairings), it would seem that some unpotentiated synapses must come online to allow for further synaptic potentiation. This could correspond to the unsilencing of existing synapses (Isaac et al., 1995; Liao et al., 1995) or the formation of new synapses (Bozdagi et al., 2000).

4.4.3. Independence of individual synapses

I have also assumed that the individual synapses composing a unitary synaptic connection behave independently. Within a single induction, this assumption may be plausible, since vesicle release sites may act independently (Oertner et al., 2002), but see (Abenavoli et al., 2002). Furthermore, elevations in postsynaptic $[Ca^{2+}]$ can be restricted to single postsynaptic compartments, limiting the capacity of signals to diffuse to other synaptic sites, even in the absence of dendritic spines (Murthy et al., 2000), although the spatial isolation of downstream effectors is unclear. Glutamate uncaging at single synaptic sites shows that synaptic potentiation can be restricted to a range of $<10 \mu M$ (Harvey and Svoboda, 2007), providing a spatial lower limit to the assumption of independence. Across inductions, the phenomenon of “synaptic tagging” (Martin and Kosik, 2002), in which locally active plasticity machinery captures proteins produced in response to plasticity-inducing stimuli at another site, renders the independence assumption more suspect. For STDP in CA1 pyramidal neuron dendrites, prior synaptic modification due to induction at a single site can indeed influence the modifiability of other synaptic sites in response to subsequent inductions, albeit with inter-induction-intervals more than an order of magnitude lower than those reported here (Harvey and Svoboda, 2007).

4.4.4. Implications of the observed metaplasticity

One interpretation for the change in the cooperativity threshold for spike-timing-dependent potentiation is that experiencing 64 spike pairings “desensitizes” these synapses to the subsequent 16 spike pairings. Having experienced a particular duration of correlated spiking,

these synapses may become resistant to lesser durations. Such a metaplasticity rule would permit synapses to tune themselves to the recent statistics of their environment, allowing them to ignore transient correlations that fail to represent meaningful stimuli. Interestingly, this sensitivity may be externally regulated. Activation of D1 receptors increases the potentiation induced by 10 spike pairings, but not by 60 spike pairings (Zhang and Bi, 2007). Therefore, in accordance with the statistical model, s_0 may be decreased by neuromodulation, reducing the duration of temporal correlation required for spike-timing-dependent potentiation.

5. RECIPROCAL REGULATION OF PERSISTENT ACTIVITY AND SYNAPTIC EFFICACY IN A SMALL NEURONAL CIRCUIT

5.1. INTRODUCTION

Persistent activity is a hallmark of neurons both *in vivo* and *in vitro* (Major and Tank, 2004).

Positive feedback through excitatory synaptic activation can enable neuronal networks to encode information that corresponds to, but outlasts, transient stimuli (Wang, 2001), and permit working

memory (Constantinidis and Wang, 2004). Intuitively, networks with weak synaptic connectivity might fail to recruit sufficient recurrent circuitry to support persistent activity.

Conversely, highly connected networks with strong synapses could over-activate recurrent circuits, producing spontaneous, interminable persistent activity. Stimulus-evoked but temporally restricted persistent activity patterns are observed in a variety of systems (Fuster and Alexander, 1971; Miyashita, 1988; Goldman-Rakic, 1995; Miller et al., 1996) and suggest that synaptic efficacy may be tuned to support these patterns. We hypothesized that ongoing activity during development might act as a control signal to mediate this tuning.

There are two candidate mechanisms: as Donald Hebb predicted, causal relationships in the firing of pairs of neurons could consolidate persistent activity patterns (Hebb, 1949). Thus, activity-dependent Hebbian synaptic plasticity (Dan and Poo, 2004) could sculpt the network topology. However, Hebbian plasticity alone may be unstable, and thus require adaptive changes

in synaptic potentiability to avoid runaway positive feedback (Turrigiano and Nelson, 2000).

Second, a non-Hebbian scaling mechanism (Marder and Goaillard, 2006) could be used to achieve an overall target level of synaptic strength. Since synaptic efficacy can be bidirectionally regulated to counteract changes in neuronal activity (O'Brien et al., 1998; Turrigiano et al., 1998), synaptic scaling could act homeostatically to constrain circuit configurations to a restricted operating range; however, the precise nature of the quantity being homeostatically regulated by synaptic scaling is unknown. Furthermore, the impact of such scaling on self-sustaining activity patterns has received little experimental attention.

To test the potential roles of these two forms of synaptic plasticity in shaping networks that support persistent activity patterns, we used small, spontaneously organizing networks of cultured hippocampal neurons. These networks exhibit stimulus evoked “reverberations” (Lau and Bi, 2005), patterns of oscillatory, persistent network activity lasting for seconds and evoked by the transient stimulation of a single neuron (Fig. 5.1b).

To specifically test the dual hypotheses that Hebbian plasticity and synaptic scaling are involved in shaping a network to support persistent activity, we raised cultured hippocampal networks in the presence of the voltage-gated Na^+ channel blocker tetrodotoxin (TTX) prior to the development of polysynaptic circuitry (Methods, 5.2.1). Despite the absence of action potentials, and thus Hebbian plasticity, during this period of chronic inactivation, reverberations of greater duration and frequency were observed after washout compared with control networks. However, this increase developed over time after the complete withdrawal of TTX, suggesting that reverberatory activity was self-consolidating in the previously silenced networks.

Excitatory synaptic connectivity in control and TTX-treated networks was also similar just after TTX withdrawal, but this connectivity was increased within minutes by reverberatory

activity. While the total excitatory synaptic connectivity was just great enough to support reverberation in control networks, it exceeded this threshold considerably in TTX-treated networks, and spontaneous, chaotic activity often emerged in an activity-dependent fashion in these latter networks. Furthermore, excitatory synapses were more potentiable in TTX-treated networks, driving synapses even further above the level of efficacy required for persistent activity. Both inhibitory connectivity and pairwise strength was reduced by TTX treatment, and blocking inhibition reduced the disparity between control and TTX-treated networks.

These data support a model in which ongoing activity drives synaptic efficacy in each network to a critical level that just permits reverberatory activity, while suppressing positive feedback synaptic potentiation that could drive the network beyond this point. In this model, chronically interrupting ongoing activity shifts networks away from this critical state, and subjects them to runaway positive feedback when activity is restored.

5.2. METHODS

5.2.1. Cell Culture

Low-density cultures of dissociated embryonic rat hippocampal neurons were prepared as previously described (Wilcox et al., 1994; Wang et al., 2005). Hippocampi were removed from embryonic day 18–20 (E18–20) rats and treated with trypsin for 15 min at 37°C, followed by washing and gentle trituration. The dissociated cells were plated at densities of 60,000-80,000 cells/ml onto poly-L-lysine-coated glass coverslips in 35 mm Petri dishes, and placed in an

incubator at 37°C. The poly-L-lysine on the coverslips was applied in a hexagonal pattern of ~1 mm diameter circular spots using a custom made stamp, with ~1.5 mm between the centers of adjacent spots. The culture medium was DMEM (BioWhittaker, Walkersville, MD) supplemented with 10% heat-inactivated fetal bovine serum (Hyclone, Logan, UT), 10% Ham's F12 with glutamine (BioWhittaker), and 50 U/ml penicillin–streptomycin (Sigma, St. Louis, MO). Twenty-four hours after plating, 1/3 of the culture medium was replaced with fresh medium, supplemented with 20 mM KCl. Both glial and neuronal cell types are present under these culture conditions.

At 8–10 days *in vitro* (DIV), before the developmental onset of reverberation, 1 μM tetrodotoxin (TTX) was added to half of the dishes, and a sham addition was made to the other dishes, before returning dishes to the incubator. Cytosine arabinoside (Sigma) was also added to each culture dish (final concentration, 5 μM) to prevent overgrowth of glial cells and preserve the isolation of networks. Cultures were then used for recording 24–120 hours afterwards, between 10–15 DIV, when reverberatory activity was commonly observed. The mean DIV for control and TTX data points did not significantly differ. A typical network selected for the present study consisted of 50–100 neurons on a confluent patch of glial cell monolayer on a poly-L-lysine island (Fig. 1.5a), similar to those used previously (Lau and Bi, 2005). When such a network was confined to one island, isolated from contact with other islands by visible neuronal processes or a confluent glial layer, it was used in the present study. Larger networks consisting of overlapping islands often exhibited spontaneous activity and were avoided in the present study.

5.2.2. Electrophysiology

Pairs of synaptically connected glutamatergic neurons were recorded using the perforated whole-cell patch-clamp technique at room temperature. The pipette solution contained (in mM): K-gluconate 136.5, KCl 17.5, NaCl 9, MgCl₂ 1, HEPES 10, EGTA 0.2, and 200 µg/ml amphotericin B (pH 7.2). The external bath solution contained (in mM): NaCl 150, KCl 3, CaCl₂ 3, MgCl₂ 2, HEPES 10, and glucose 5 (pH 7.4). Presynaptic stimulation was given by step depolarization (100 mV, 1-2 ms), delivered to a single neuron. In network experiments, during the recording period, each stimulus (a single suprathreshold pulse lasting 1.5 ms) was delivered to a single neuron at an interval of 30 s. Network activity was monitored via intracellular recordings in one or two neurons, typically in voltage clamp, to measure the recurrent synaptic activity evoked by stimulation. If reverberation was not observed in response to stimulation of at least 3 neurons, the network was considered to be reverberation incompetent (Fig. 5.2d).

Spontaneous mEPSCs were recorded in 1 µM TTX and 5 µM bicuculline methiodide (BMI). When BMI was absent, event rates were largely unchanged, reflecting an extremely low rate of mIPSCs. Recordings showing significant changes (>10%) in series (20-40 MΩ) or input resistance (500-1500 MΩ) were excluded from further analysis.

Neurons used in paired recordings were typically 50-150 microns apart, which is less than the median distance between two random neurons on a 1 mm island. The only criteria for choosing which pairs to record were: sharing the same field of view, and confidence that a long-lasting gigaohm seal could be obtained. Only monosynaptic connections were considered evidence of a connection between neurons, and this was defined as an EPSC with a rising phase beginning less than 5 ms after the onset of the presynaptic stimulus (Gerkin et al., 2007), as in chapter 3. Only neurons in which the peak of a monosynaptic EPSC could be quantitatively

resolved, or in which this component was visibly absent, were used for determining the distribution of connection strengths. Evoked EPSC amplitude was computed by averaging over all trials in which a monosynaptic component could be identified, 10-20 minutes after a seal was obtained on the postsynaptic neuron, to allow for perforation of the membrane by amphotericin B. Only synaptic connections in which a PSC could be identified (i.e. non-zero responses) were included in the analysis of amplitude. Analysis of evoked IPSCs was done similarly to EPSCs, and were distinguished from EPSCs by their much slower decay kinetics. For determining the fraction of recorded neurons of each phenotype, production of any glutamatergic current in a postsynaptic partner was considered evidence of glutamatergicity, since GABAergic neurons cannot evoke a polysynaptic response at this time in development.

5.2.3. Pharmacology

Throughout the recordings, cultures were perfused with fresh HBS at a constant rate of ~1 ml/min. In recordings from TTX-treated cultures, TTX was either washed out prior to recording (Figs. 5.1-2) or neurons were maintained in TTX continuously until after recordings had begun (Figs. 5.3-9). Stock solutions of all drugs were first prepared in water or DMSO and diluted (1:1000) in HBS when being used.

Reverberation duration, as described below, was calculated as the mean over at least 5 stimuli. In the presence of CNQX, only stimuli beginning at least 5 minutes after wash-in of each dosage were used. Addition of APV, MPEP, LY367385, Wortmannin, or TNP-ATP was done concurrently with washout of TTX (for TTX-treated cultures). The period between TTX washout and the first stimulus was 15-20 minutes. The time course of TTX washout could be

confirmed by examining the sodium current in the stimulus artifact of the presynaptic neuron, which reached steady state ~ 5 minutes after TTX washout.

5.2.4. Analysis and Statistics

Reverberations were identified by searching a smoothed copy (Gaussian smoothing kernel; width 25 ms) of the continuously recorded current for maxima (largest inward current). For each maximum, the current was scanned forward and backward in time away from the maximum to identify crossings of a threshold set at 10% of that maximum. The threshold crossings farthest from the original maximum with no additional crossings for 500 ms were defined to be the start-point and end-point of the reverberation. For stimulus-evoked reverberations, this start-point invariably occurred just after the onset of the stimulus. Only a trace with reverberation duration > 500 ms was considered a successful reverberation. Traces with shorter durations usually contained only one polysynaptic current cluster (PSCC) and were considered failures. The 500 ms criterion is motivated by the observation that reverberatory activity, as assessed subjectively, exhibits PSCCs at a typical frequency of 4-10 Hz, with 2 Hz, $(500 \text{ ms})^{-1}$, being an absolute lower bound. For each experiment, at least ten stimuli were delivered at 0.033 Hz under a given pharmacological condition to compute the features of reverberations under that condition.

To identify spontaneous network events, we used an identical technique, except that a median filter (width 50 ms) was incorporated to avoid the detection of isolated spontaneous EPSCs not reflecting a PSCC. As above, a 500 ms criterion was used to separate events, such that two PSCCs occurring within 500 ms were considered “linked” and counted only once.

Thusly, a sequence of PSCCs containing no >500 ms inter-PSC cluster intervals was detected as a single event. If it was immediately preceded by an external stimulus (<50 ms before onset), then it was not considered spontaneous. The emergence of spontaneous activity was defined as a peak spontaneous event rate exceeding 0.1 Hz, the maximal spontaneous event rate observed in recordings of control cultures.

Candidate spontaneous EPSCs were identified using an established method (Kudoh and Taguchi, 2002), with a threshold of 5 pA (~3 times the standard deviation of the noise) Candidates were then manually visualized and accepted or rejected based on appearance. For calculation of mEPSC potentiation, the median amplitude of the population was used due to the skewed distribution of event amplitudes.

Events recorded in TTX and BMI are by definition mEPSCs, while events detected in between reverberations (see densely populated area in Figure 3.7b,c), may also contain EPSCs evoked by spontaneous presynaptic action potentials. To minimize the contribution of action potential driven events during this period, only EPSCs recorded > 5 seconds after the end of a reverberation were included in the analysis. The similarity in mean amplitude between these EPSCs and the mEPSCs recorded minutes later in TTX (Fig. 3.7b,c), suggests that the overwhelming majority of these events were not mediated by action potentials. The potentiation of sEPSC frequency varied greatly across recordings, in part due to variability in the initial frequency. In order to normalize comparison, we computed the logarithm of the fractional change in frequency before computing statistics.

A bootstrap comparison of means was used for all statistical comparisons except those involving more heavily skewed distributions, in which a Wilcoxon rank test was used (as noted in the text). A Bonferroni correction for multiple comparisons to the same control was made

where applicable. Comparisons to unity (100%, no change in synaptic strength) remain uncorrected. Values are reported as mean \pm SEM, and all error bars in graphs are SEM, unless indicated otherwise.

5.3. RESULTS

To determine whether activity-dependent Hebbian plasticity was required to promote the development of reverberatory circuits, we chronically blocked neuronal activity in developing networks with TTX (1 μ M) before the appearance of suprathreshold synaptic potentials, and we recorded from these networks after activity was restored. Reverberation requires recurrent synaptic excitation (Lau and Bi, 2005); thus, if activity blockade with TTX prevented the emergence of reverberation when activity was restored, this would suggest a role for action-potential-mediated activity in instructing the formation of a reverberatory network, possibly by promoting the development of the required synaptic connectivity. However, if this circuitry arose in the absence of activity, then scaling mechanisms acting to facilitate network activity would be implicated.

5.3.1. Reverberation is enhanced in chronically inactivated cultured networks

1-5 days after TTX treatment, we replaced the culture medium with a control ACSF (Methods, 5.2.2) and transferred neurons to the recording chamber. There we obtained perforated whole cell patch clamp recordings from pairs of neurons in both TTX-treated ($n=55$) and control sister

cultures (n=22). We waited ~20 minutes to allow equilibration of the perforating agent (amphotericin B) with the membrane, permitting steady-state access resistance for the duration of the recording, and to ensure complete washout of residual TTX. We then applied suprathreshold voltage pulses (100 mV, 1.5 ms) to one neuron and measured the resultant recurrent, network activity in the membrane current records (Methods, 5.2.2,4). If activity-dependent synaptic development were a requirement for the developmental onset of reverberations, these reverberations should be observed less frequently in recordings from cultures chronically inactivated with TTX. In fact, we saw a significant increase in the fraction of networks (Methods, 5.2.4) competent to exhibit reverberation (Fig. 5.1d; CTL: $38.1 \pm 10.9\%$; TTX: $72.7 \pm 6.1\%$; p<0.005), and in the maximum duration of reverberations (Fig. 5.1e; CTL: 2.92 ± 0.92 s; TTX: 5.35 ± 0.60 s; p<0.005) in the chronically inactivated networks.

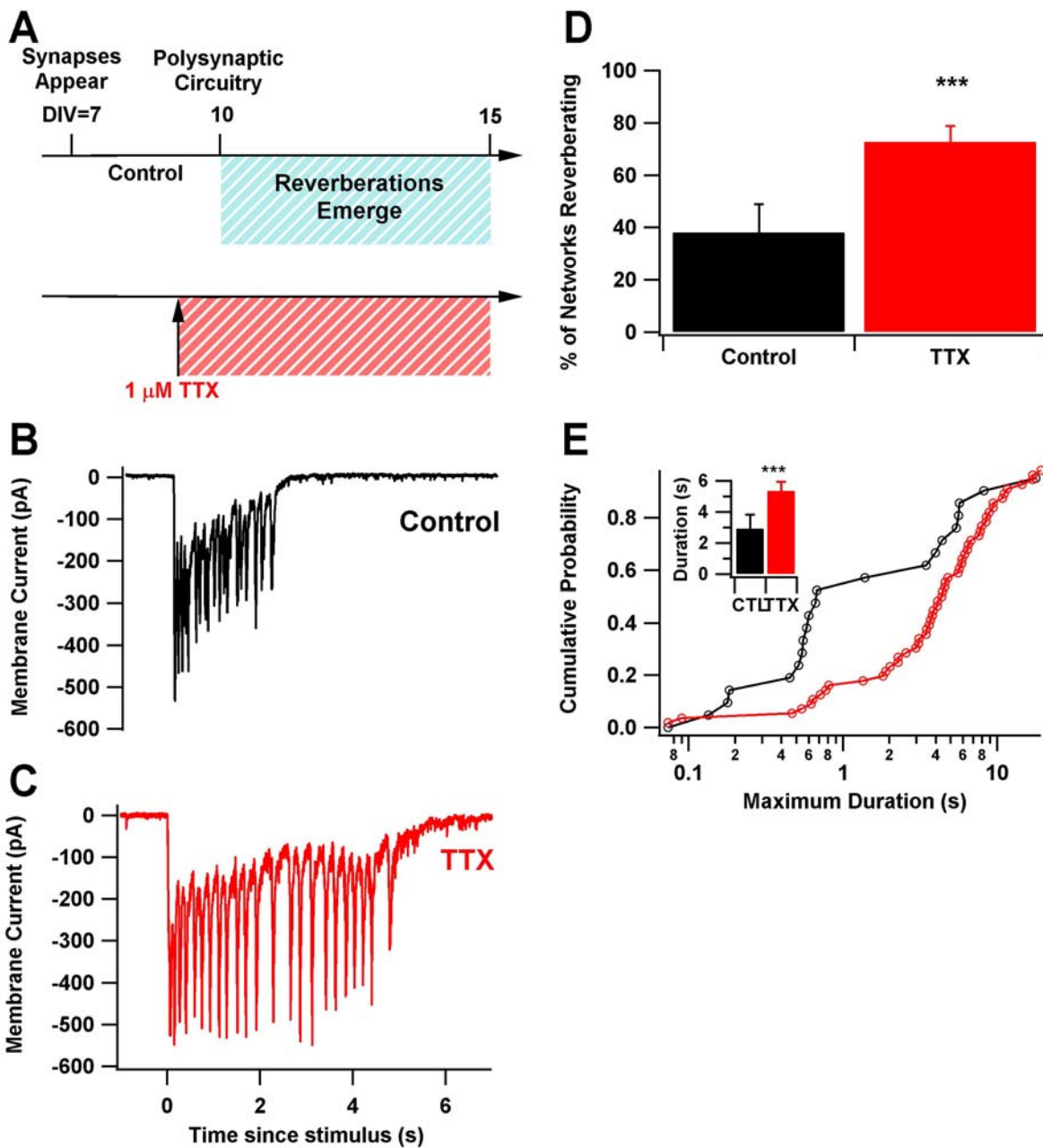


Figure 5.1: Reverberation is enhanced in TTX-treated cultures. **A**, Schematic of the experimental protocol, showing the relevant developmental time points. DIV refers to days *in vitro*, the number of days that the neurons have been in culture. **B**, Example of a reverberation in a control network. **C**, Example of a reverberation in a TTX-treated network. **D**, The fraction of networks exhibiting reverberation is enhanced in TTX-treated cultures. **E**, The duration of reverberations is enhanced in TTX-treated cultures. Inset shows the mean duration. *** indicates p<0.005 vs. corresponding controls.

5.3.2. Functional synaptic connectivity is shifted towards excitation by chronic inactivation

Chronically inactivated cultured neurons undergo synaptic scaling (O'Brien et al., 1998; Turrigiano et al., 1998; Thiagarajan et al., 2005; Shepherd et al., 2006), in which the quantal amplitude of miniature excitatory postsynaptic currents (mEPSCs) is increased, putatively as a homeostatic response to decreased activity levels (Turrigiano and Nelson, 2004). We hypothesized that positive synaptic scaling might endow networks with a greater probability and duration of reverberation. To test this hypothesis, we first recorded miniature EPSCs (mEPSCs) from both control and TTX-treated networks (prior to TTX withdrawal). We observed an increase in the amplitude of mEPSCs in TTX-treated cultures compared with control sister cultures (Fig. 5.2a; CTL: 11.6 ± 0.2 pA; TTX 15.6 ± 0.5 pA; $p < 0.0001$). By contrast, this was not accompanied by a significant change in the frequency of mEPSCs in TTX-treated cultures (Fig. 5.2b; CTL: 0.74 ± 0.17 Hz, n=12; TTX: 0.68 ± 0.19 Hz, n=12; $p > 0.3$).

Since recurrent synaptic activity is presumably mediated by action potential driven transmission, we examined whether the increase in the amplitude of miniature synaptic currents was also reflected in an increase in evoked synaptic currents. To test this, we measured evoked synaptic transmission between pairs of simultaneously recorded nearby neurons, according to the protocol of Figure 5.1. After stimulating one neuron, the unitary connection (the current amplitude of the monosynaptic component (Methods, 5.2.2) of the synaptic response) was measured in a simultaneously recorded postsynaptic partner. Because miniature synaptic inhibitory currents are also reduced by chronic inactivation (Kilman et al., 2002) (Hartman et al.,

2006), we examined both glutamatergic and GABAergic unitary synaptic connections. In hippocampal cultures, morphology is not a reliable predictor of neuronal phenotypes, and thus the evoked synaptic currents themselves were used to distinguish between glutamatergic and GABAergic neurons. In TTX-treated cultures, a larger fraction of neurons (CTL: n=109; TTX: n=70) were identifiable as glutamatergic on the basis of these evoked currents (CTL: $55.0 \pm 4.7\%$; TTX: $78.5 \pm 4.9\%$; p<0.001), whereas a substantially smaller fraction of neurons were identifiable as GABAergic (CTL: $31.3 \pm 4.4\%$; TTX: $11.4 \pm 3.8\%$; p<0.005). The remainder made no observable postsynaptic responses and could not be characterized. Similarly, the probability that a potential response (CTL: n=121; TTX: n=79) was glutamatergic was enhanced (Fig. 5.2c; CTL: $27.3 \pm 4.0\%$; TTX: $45.6 \pm 5.6\%$; p<0.005), while the probability of such a response being GABAergic was decreased (Fig. 5.2c; CTL: $14.1 \pm 3.2\%$; TTX: $6.3 \pm 2.7\%$; p<0.05). Consistent with a homeostatic hypothesis, this suggested a net shift in functional synaptic connectivity towards excitation in response to chronic inactivation. Along with the apparent reduction in the number of GABAergic synaptic connections, the mean strength of evoked GABAergic responses was substantially reduced by inactivation (Fig. 5.2d: CTL: 180.1 ± 48.5 pA, n=25; TTX: 53.0 ± 23.7 pA, n=10; p<0.005 by Wilcoxon Rank Test). However, both the mean strength and the overall distribution of glutamatergic responses were very similar (Fig. 5.2e: CTL: 140.5 ± 33.5 pA, n=33; TTX: 143.1 ± 31.9 pA, n=35; p>0.63 by Kolmogorov-Smirnov test). These data suggested that synaptic scaling, evident at the level of mPSCs, had mixed effects at the level of evoked synaptic transmission.

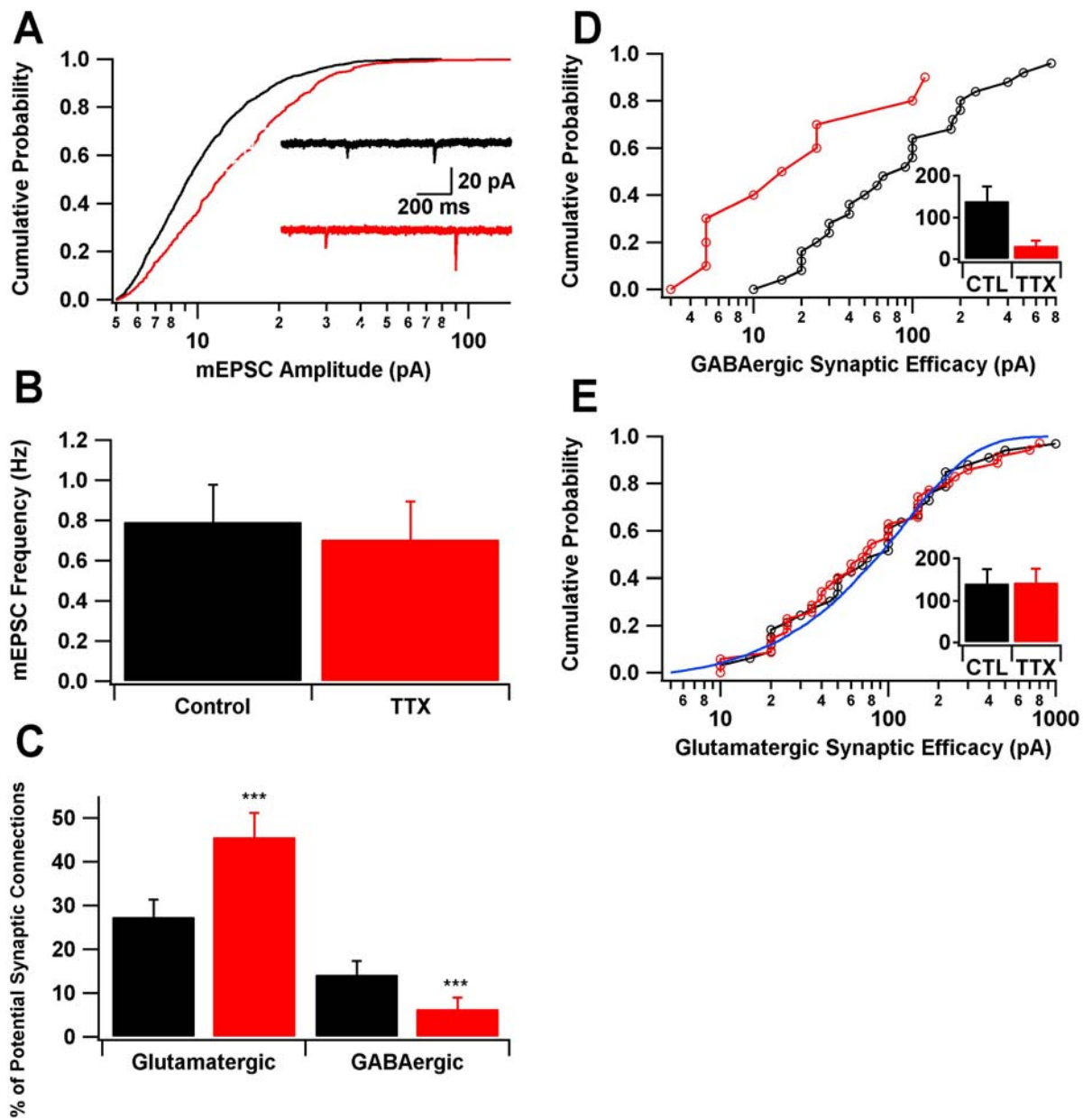


Figure 5.2: Synaptic scaling is reflected differently in the amplitude of miniature and evoked currents. **A**, The amplitude of mEPSCs recorded in TTX is enhanced in TTX-treated culture; $p<0.0001$ (Kolmogorov-Smirnov test). Experiments using control cultures are shown in black, and TTX-treated cultures are shown in red. **B**, The frequency of mEPSCs is not significantly different between control and TTX-treated cultures ($p>0.4$). In **A** and **B**, recordings are made prior to the withdrawal of TTX. **C**, In paired recordings between random nearby neurons, a larger fraction of postsynaptic neurons showed an evoked response from identified and stimulated presynaptic neurons of the glutamatergic phenotype, and a smaller fraction showed a GABAergic response, in TTX-treated cultures. **D**, The amplitude of evoked GABAergic currents is smaller in TTX-treated cultures than in control cultures. **E**, The amplitude of evoked glutamatergic currents is similar in TTX-treated cultures and in control cultures. The blue line is an exponential fit to the entire dataset. *** indicates $p<0.005$ vs. corresponding controls.

5.3.3. Role of reduced inhibition in increased reverberation after chronic inactivation

Inhibition is involved in terminating recurrent excitatory network phenomena in a variety of systems (Morimoto et al., 2004; Mann and Paulsen, 2007). In small cultured hippocampal networks, inhibition can abort the onset or hasten the termination of reverberations, but is not essential to the phenomenon of reverberation itself (Lau and Bi, 2005). Because the increases in reverberation competence and duration after TTX treatment were accompanied by a decrease in functional synaptic inhibition, we hypothesized that reduced inhibition could mediate the observed increase in reverberatory behavior.

To test this hypothesis, we repeated the network experiments in the presence of the GABA_A antagonist bicuculline methiodide (BMI, 5 μM) to block phasic synaptic inhibition (Fig. 5.3a,b). This increased both the probability (Fig. 5.3c; CTL: $78.6 \pm 11.4\%$, , n=14, p<0.05; TTX: $93.8 \pm 4.3\%$, n=32, p<0.05; p-values vs. the conditions in Fig. 1) and maximal duration (Fig. 5.3d, CTL: 5.26 ± 1.00 s, n=14, p<0.05; TTX: 6.36 ± 0.69 s, n=32, p=0.08) of reverberation. However, in the presence of BMI the differences in reverberation between control and TTX-treated networks were not significant (probability: 1.19x, p>0.2, duration: 1.21x, p=0.06) than in networks recorded with inhibition left intact (probability: 1.91x, p<0.005, duration: 1.83x, p<0.005). For a variety of measures, in the presence of BMI, the TTX-treated networks were no longer significantly different from the control networks (Table 5.1). The lesser effects of BMI in TTX-treated networks were consistent with a reduced role for inhibition in shaping the reverberatory dynamics, and with a reduction in the availability of inhibitory synaptic transmission, in these networks in the absence of BMI.

Table 5.1: Comparison of control and TTX-treated cultures.

Competence is the percentage of networks displaying at least one reverberation. Probability is the fraction of stimuli for which reverberation was observed. Reverberation defined as duration > 0.5 s. Polysynaptic defined as duration > 0.025 s.

Property	No BMI			BMI		
	Control	TTX	p	Control	TTX	p
n	22	56				
DIV	13.7 ± 0.7	13.5 ± 0.2	>0.35	13.0 ± 0.5	13.4 ± 0.2	>0.35
Maximum Reverberation	2.92 ± 0.92	5.35 ± 0.60	<0.005	5.26 ± 0.99	6.36 ± 0.69	>0.2
Reverberation Competence	$38.1 \pm 10.9\%$	$74.5 \pm 5.9\%$	<0.005	$78.6 \pm 11.4\%$	$93.8 \pm 4.3\%$	0.07
Reverberation Probability	$41.2 \pm 7.3\%$	$56.4 \pm 4.7\%$	>0.15	$62.4 \pm 8.8\%$	$63.1 \pm 5.1\%$	>0.45
Polysynaptic Probability	$65 \pm 4.9\%$	$83.4 \pm 3.0\%$	<0.05	$80.2 \pm 6.9\%$	$89.0 \pm 3.0\%$	>0.2
Median Reverberation	1.90 ± 0.44	2.63 ± 0.24	<0.05	$3.08 \pm 0.62\%$	$2.57 \pm 0.24\%$	>0.2
Median Polysynaptic Event	0.75 ± 0.27	1.7 ± 0.21	<0.005	$1.62 \pm 0.45\%$	$1.78 \pm 0.28\%$	>0.4
Reverberations per Stimulus	0.25 ± 0.08	0.96 ± 0.17	<0.005	0.85 ± 0.25	1.34 ± 0.21	<0.1
Rheobase Current (pA)	104.1 ± 12.0	67.7 ± 12.1	<0.005			

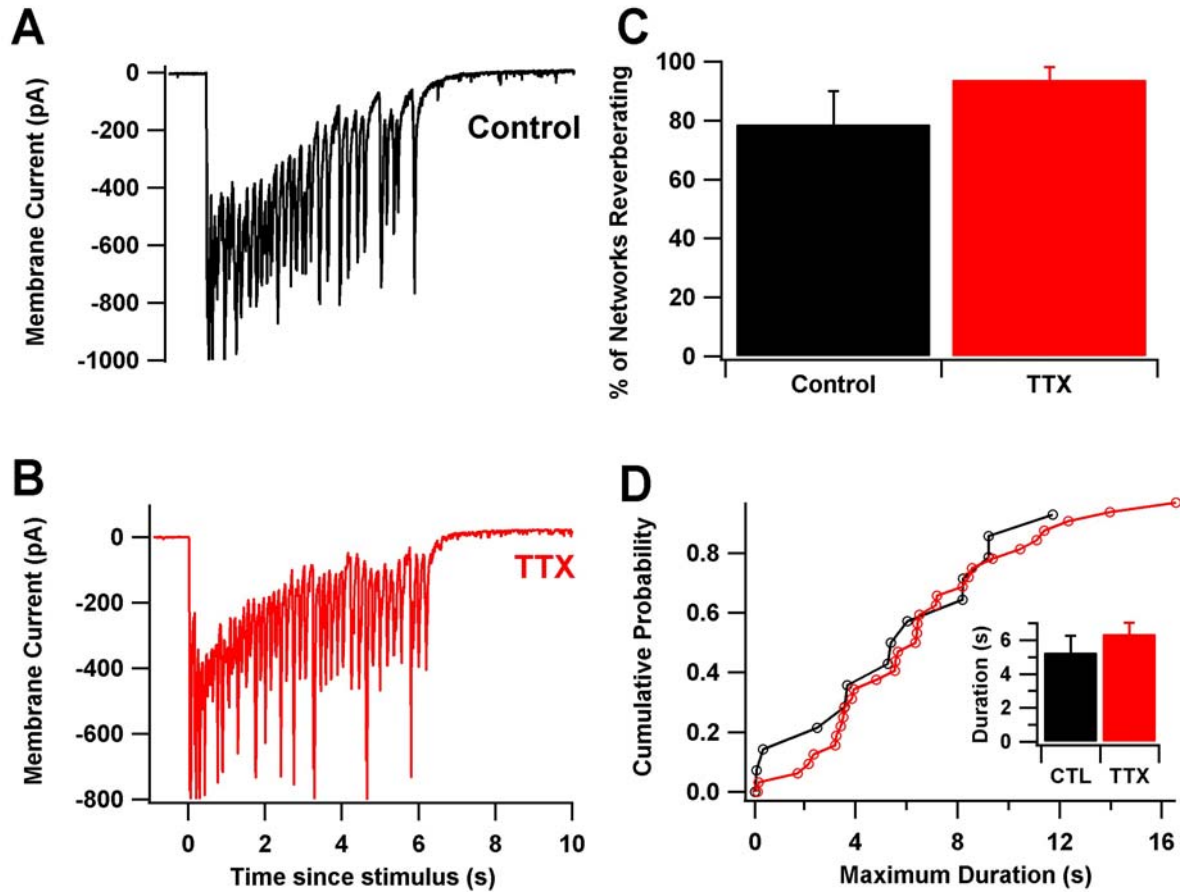


Figure 5.3: Reduced synaptic inhibition mediates the extended duration of reverberation in TTX-treated cultures. **A**, Example of a reverberation in a control network in the presence of 5 μ M BMI. **B**, Same as A, but for a TTX-treated network. **C**, Reverberation competence, the fraction of networks exhibiting reverberation, is nearly unity in the presence of BMI ($p>0.2$ for control vs. TTX). **D**, The maximal duration of reverberations is similar for control and TTX-treated cultures in the presence of BMI ($p>0.05$). Inset shows the mean duration.

5.3.4. Reverberation-driven synaptic potentiation

Synchronous network activity can produce synaptic potentiation (Bains et al., 1999; Abegg et al., 2004; Debanne et al., 2006). To confirm that synaptic potentiation could be induced by reverberation, we measured mEPSCs in TTX both before the first stimulus, and after a period of reverberation. BMI was used in these and subsequent experiments (unless noted otherwise) to control for differences in inhibition between control and TTX-treated networks. In contrast to the experiments described in Fig. 1, TTX was present continuously from the initial chronic application until washout several minutes after recordings had begun. For control experiments TTX was added immediately before recording had begun. Washout of TTX during recordings caused no change in the amplitude or frequency of spontaneous EPSCs, indicating that nearly all events recorded after TTX washout but before stimulation corresponded to mEPSCs. These events could thus be directly compared to events recorded after reverberation, in the presence of TTX. We found that both mEPSC amplitude and frequency could be rapidly increased by reverberation (Fig. 5.4a), and that this potentiation could last for at least 30 minutes (Fig. 5.4b,c). In control cases, it was typical for potentiation to saturate after 1-3 reverberations (Fig. 5.4b, 1-2 minutes, red line). In TTX-treated networks, however, potentiation could accumulate over many reverberations (Fig. 5.4c), suggesting that it was less rapidly saturable.

Furthermore, we found that the degree of synaptic potentiation 25-30 minutes after reverberatory activity was greater in TTX-treated cultures than in controls (Fig. 5.4d,e; mEPSC amplitude: CTL: $115.8 \pm 3.5\%$, n=15 neurons; TTX: $136.8 \pm 6.7\%$, n=7 neurons; p<0.01; mEPSC frequency (log): CTL: $116.5 \pm 6.5\%$; TTX: $140.0 \pm 10.8\%$; p<0.05). To determine whether the increased potentiability of mEPSCs in TTX-treated cultures was an artifact of differential levels of activity during the reverberatory period, we compared the degree of

potentiation in mEPSC size and frequency to either the total charge recorded during that period, the number of reverberations observed, or the number of spontaneous events observed. In no case did we find a correlation ($r = -0.08$ to 0.06 for these potential correlates), suggesting that differential levels of activity could not explain the enhancement of potentiability in TTX-treated cultures and that potentiation may have been saturated in both cases.

To determine the mechanism of this synaptic potentiation, and whether it was similar to conventional long-term potentiation (LTP), we repeated the experiments on TTX-treated cultures acutely subjected to putative blockers of synaptic potentiation during the reverberatory period. Amino-phosphovaleric acid (APV, $25 \mu\text{M}$) was used to block NMDAR currents, and a cocktail of 6-methyl-2-(phenylethynyl)-pyridine (MPEP) and (+)-2-methyl-4-carboxyphenylglycine (LY367385) were used to block class I metabotropic glutamate receptors. Significant reductions in the amplitude component of potentiation were observed (Fig. 5.4d,e; mEPSC amplitude: TTX+APV: $120.4 \pm 3.7\%$, $n=7$ $p<0.05$ vs. TTX-treated alone; TTX+LY+MPEP: $111.3 \pm 6.3\%$, $n=7$, $p<0.05$; mEPSC frequency (log): TTX+APV: $134.6 \pm 8.4\%$, $p>0.3$; TTX+LY+MPEP: $137.1 \pm 7.9\%$, $p>0.35$), suggesting both NMDAR- and mGluRI-dependent components of potentiation in TTX-treated cultures.

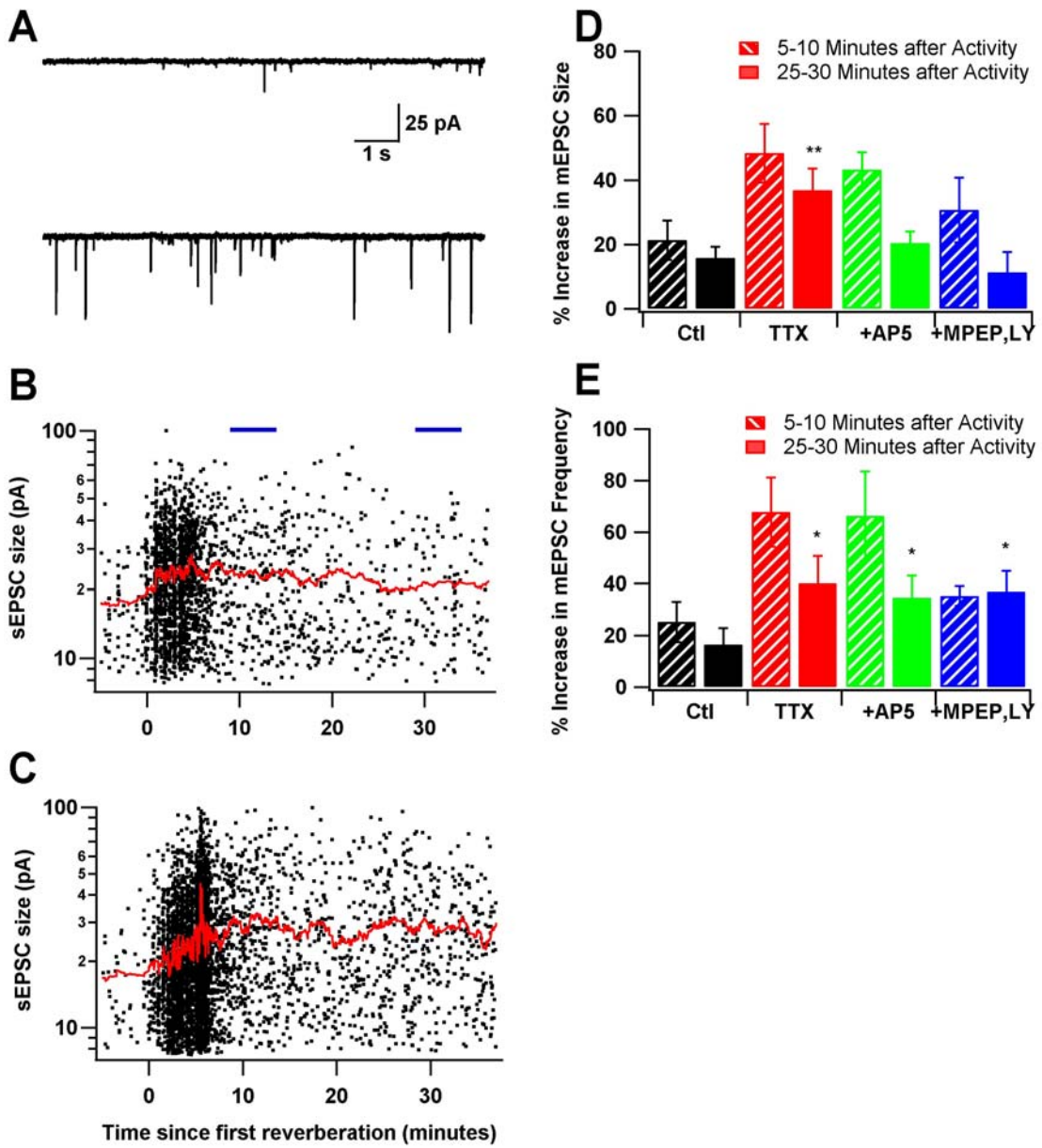


Figure 5.4: TTX-treated cultures exhibit enhanced reverberation-driven synaptic potentiation.

A, Two traces illustrating the amplitude and frequency of mEPSCs recorded in TTX before (top) and after (bottom) reverberations. **B**, The time course of EPSC potentiation in a representative control experiment. Black dots are individual EPSCs, the red line is a moving average. **C**, Same as **B**, but for a TTX-treated network. Note that the potentiation takes longer to saturate, and the steady-state value is larger than in **B**. **D**, Summary data for the increase in mEPSC amplitude after reverberation. Each bar corresponds to one of the two temporal regions (analogous to short- and long-term potentiation) illustrated with blue lines in **B** (same regions in **C**). + sign in category label indicates that these networks were also chronically inactivated with TTX. **E**, Similar to **D**, except for the increase in mEPSC frequency, illustrating that the potentiation is reflected as an increase in both the amplitude and frequency of mEPSCs. * indicates $p < 0.05$ vs. control; ** indicates $p < 0.01$.

5.3.5. Reverberation and functional connectivity are rapidly enhanced

The capacity of reverberations to rapidly potentiate the amplitude and frequency of spontaneous synaptic currents led us to wonder if this potentiation might have occurred after the withdrawal of TTX but before recording in the cultures recorded previously (Fig. 5.1). Thus, we replicated these experiments, with the change that TTX was not withdrawn until after recording had begun to prevent the induction of any Hebbian plasticity prior to recording. In these experiments, control (Fig. 5.5a, n=16) and TTX-treated (Fig. 5.5b, n=28), we assessed the response of the network to the first single neuron stimulus, with no synchronous network activity observed prior to that stimulus. Compared to the earlier experiments, we saw no significant increase in the fraction of networks exhibiting reverberation as a result of TTX treatment (Fig. 5.5c; CTL: $18.8 \pm 10.1\%$; TTX: $21.4 \pm 7.9\%$; p>0.35). The duration of the first successful reverberation was also not significantly different between control and TTX-treated networks (Fig. 5.5d; CTL: 3.06 ± 0.44 s; TTX: 4.24 ± 1.09 s; p>0.45 by Wilcoxon Rank Test).

Because the reverberatory capacity of networks immediately after withdrawal of TTX (Fig. 5.5) was less than that after extended withdrawal (Fig. 5.1), we hypothesized that rapid changes in synaptic connectivity may have been responsible for this difference. To test this, we assessed monosynaptic responses between pairs of neurons in response to the first presynaptic stimulus in experiments where withdrawal of TTX did not occur until after recording had begun. In these experiments, we found that monosynaptic connection probability between pairs was not significantly altered by chronic inactivity (Fig. 5.5e; CTL: $28.5 \pm 8.5\%$; TTX: $24.7 \pm 4.7\%$; p>0.3), and the evoked currents were also similar to those seen in controls (Fig. 5.5f; CTL: 129.4

± 18.6 pA, n=46; TTX: 151.2 ± 22.0 pA, n=40; p>0.15). Consistent with a rapid enhancement of the connection probability in TTX-treated cultures by activity after TTX withdrawal (compare Fig. 5.5e to Fig. 5.2b), in some cases we observed the appearance of new monosynaptic connections some time after the first reverberation (3/20 cases). Consistent with this increase in synaptic connectivity, the probability of observing a reverberation after several minutes of recording from these networks approached the levels seen in earlier experiments (CTL: $37.5 \pm 12.5\%$; TTX: $64.3 \pm 9.2\%$; p<0.05).

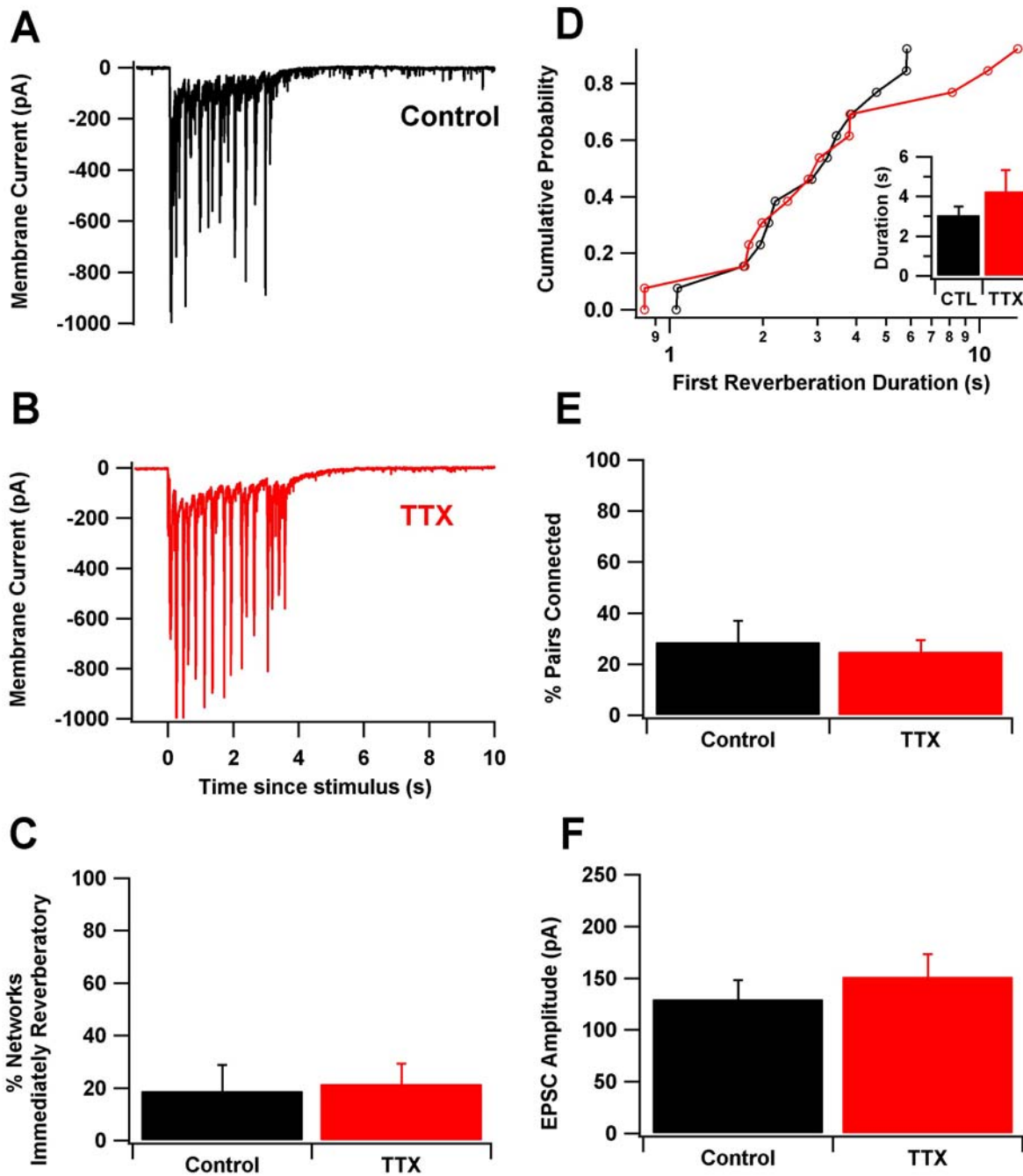


Figure 5.5: Synaptic scaling alone without subsequent activity is not sufficient to augment reverberation in TTX-treated cultures. **A**, Example of the first reverberation in a control network. **B**, Same as A, but for a TTX-treated network, in which TTX was not withdrawn until continuous recording had begun. **C**, The fraction of networks which elicit a reverberation in response to the first intracellular stimulus is not affected by TTX treatment. **D**, The duration of the first reverberation is not enhanced by TTX treatment. Inset shows the mean duration ($p>0.35$). **E**, The fraction of recorded pairs exhibiting excitatory synaptic connections does not differ from controls immediately after the withdrawal of TTX. **F**, The mean amplitude of evoked excitatory synaptic currents is also similar immediately after withdrawal of TTX.

5.3.6. Critical threshold behavior in reverberatory networks

Computational models support the hypothesis that reverberation becomes possible after excitatory synapses are sufficiently strong (Volman et al., 2007). We reasoned that because most control networks do not exhibit reverberation (Fig. 5.1d), those that do may have synapses just strong enough to support this activity pattern. Meanwhile, since most TTX-treated networks do exhibit reverberation, some of these networks are likely to have synaptic efficacies or connection probabilities that are well above the values necessary to observe reverberation. Thus, we predicted that reverberatory activity in control networks should be highly sensitive to small decrements in excitatory synaptic efficacy, while TTX-treated networks should be less sensitive to such decrements.

In order to test this prediction experimentally, we made perforated patch clamp recordings in the presence of small doses of the AMPAR antagonist CNQX. In these cultures, the entire measured EPSC is blocked by saturating doses of CNQX, indicating that AMPARs mediate the postsynaptic current. To convert the dose of this drug to a fractional change in synaptic efficacy, we first measured the effect of CNQX on monosynaptic AMPAR-mediated currents (Fig. 5.6a). Using this information, we found that control networks were indeed highly sensitive to CNQX application. In control networks that exhibited reverberation, and in the absence of BMI, 50-100 nM CNQX (Fig. 5.6b, 5.2%-11.6% block of AMPARs, n=17) was sufficient to completely abolish reverberation in half of the experiments. In TTX-treated networks, by contrast, a much larger concentration of CNQX (Fig. 5.6b, 200-250 nM, 23.8-29.2% block of AMPARs, n=15) was required to abolish reverberations in half of the

experiments. Furthermore, among control networks in which reverberation was not abolished, a steep drop in reverberation duration was exhibited upon application of small doses of CNQX; in TTX-treated networks this drop was much shallower (Fig. 5.6c). These dose-response relationships support the idea that reverberating control networks dwell in a steep segment of the reverberation duration/competence vs. unitary synaptic conductance functions, indicating threshold behavior. These networks appear to have synaptic conductances just strong enough to support reverberation. By contrast, TTX-treated networks are somewhat more densely connected and occupy a shallower segment of this function, implying that they lie farther to the right of such a threshold.

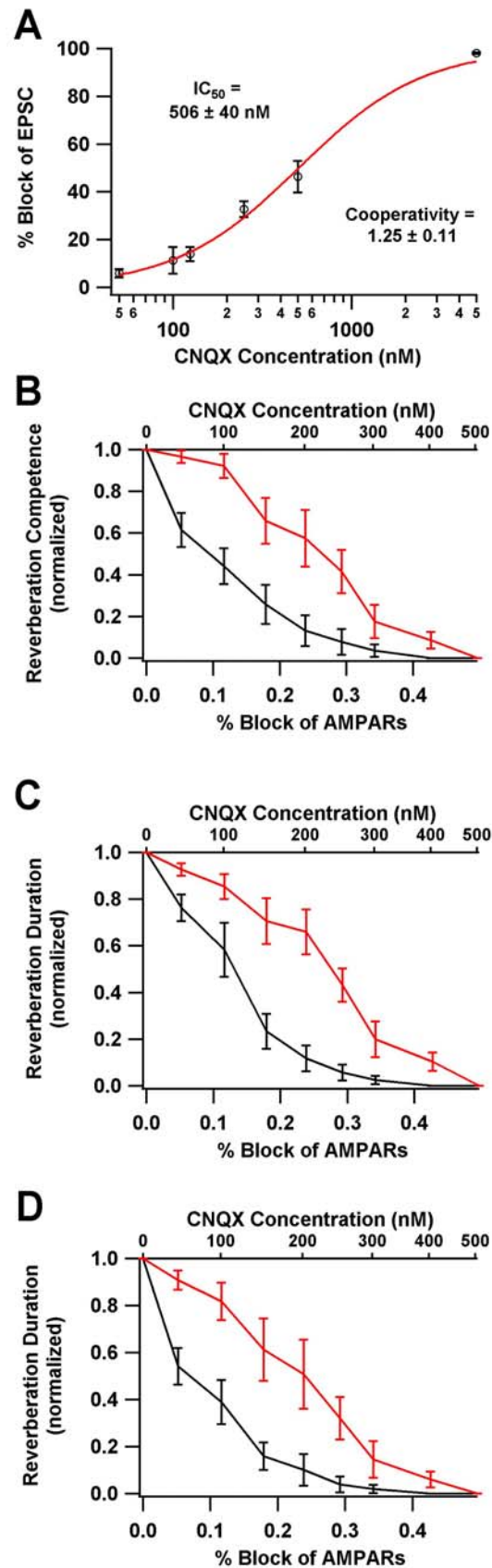


Figure 5.6: Control networks operate near a critical synaptic threshold for reverberation.

A, Monosynaptic EPSCs from connected pairs were subject to various concentrations of CNQX to create a dose-response curve. **B**, The capacity of networks to exhibit at least one reverberation was measured in different concentrations of CNQX (Black: Control; Red: TTX-treated). % block of AMPARs is calculated from the CNQX concentration using the data in A. **C**, Same as B, but for the duration of reverberations in reverberation-competent networks. **D**, Same as C, but the durations of polysynaptic activity in non-competent networks are included.

5.3.7. Emergence of spontaneous activity in chronically inactivated networks

In order for neurons involved in a persistent activity pattern to be available for future computations, that activity pattern must eventually abate. Continuous, spontaneous activation of the same circuit may comprise a seizure, and may itself be epileptogenic (Morimoto et al., 2004; Sutula, 2004). Intuitively, for persistent activity to be both reliably evoked and terminated the statistics of neuronal excitability and synaptic connectivity should strongly favor recurrent activity at the onset, but eventually shift in favor of termination.

To determine how synaptic scaling and reverberation-driven potentiation might affect the reproducibility of reverberation across a recording session, we recorded from both control and TTX-treated networks for ~ 1 hour, delivering a stimulus to one neuron (one “trial”) at 30 second intervals. In control networks, after a rapid growth phase that lasted for 1-3 trials (consistent with the time course of synaptic potentiation, Fig. 5.4b), reverberation duration was quite stable over time (Fig. 5.7a,b), as seen previously (Lau and Bi, 2005). However, in TTX-treated networks we frequently observed a state transition from stimulus-evoked reverberation to stimulus-independent spontaneous activity (Fig. 5.7c,d). This transition occurred both in the presence and in the absence of the GABA_A-receptor antagonist BMI (data not shown), indicating that it was not dependent upon synaptic inhibition. While a reverberation was composed of several consecutive polysynaptic current clusters (PSC clusters) of monotonically increasing interval (Fig 5.7e, 100-300 ms), each spontaneous event typically consisted of one or two PSC clusters, and the interval between spontaneous events was typically random, and > 1 s (Fig. 5.7f). It was well fit by an inverse Gaussian distribution, typically used to describe threshold crossing

times in a random walk (Chhikara and Folks, 1989), arguing against the involvement of a cell-autonomous intrinsic oscillation in driving these events. This interval was predictive of the duration of the ensuing spontaneous event (Fig. 5.7g), but event duration was not predictive of the subsequent interval (data not shown), suggesting that the accumulation of and recovery from synaptic depression could be a mechanism for the timing of their initiation and termination, and that they could be analogous to spontaneous interictal events seen in disinhibited hippocampal slices (Staley et al., 1998; Staley et al., 2001).

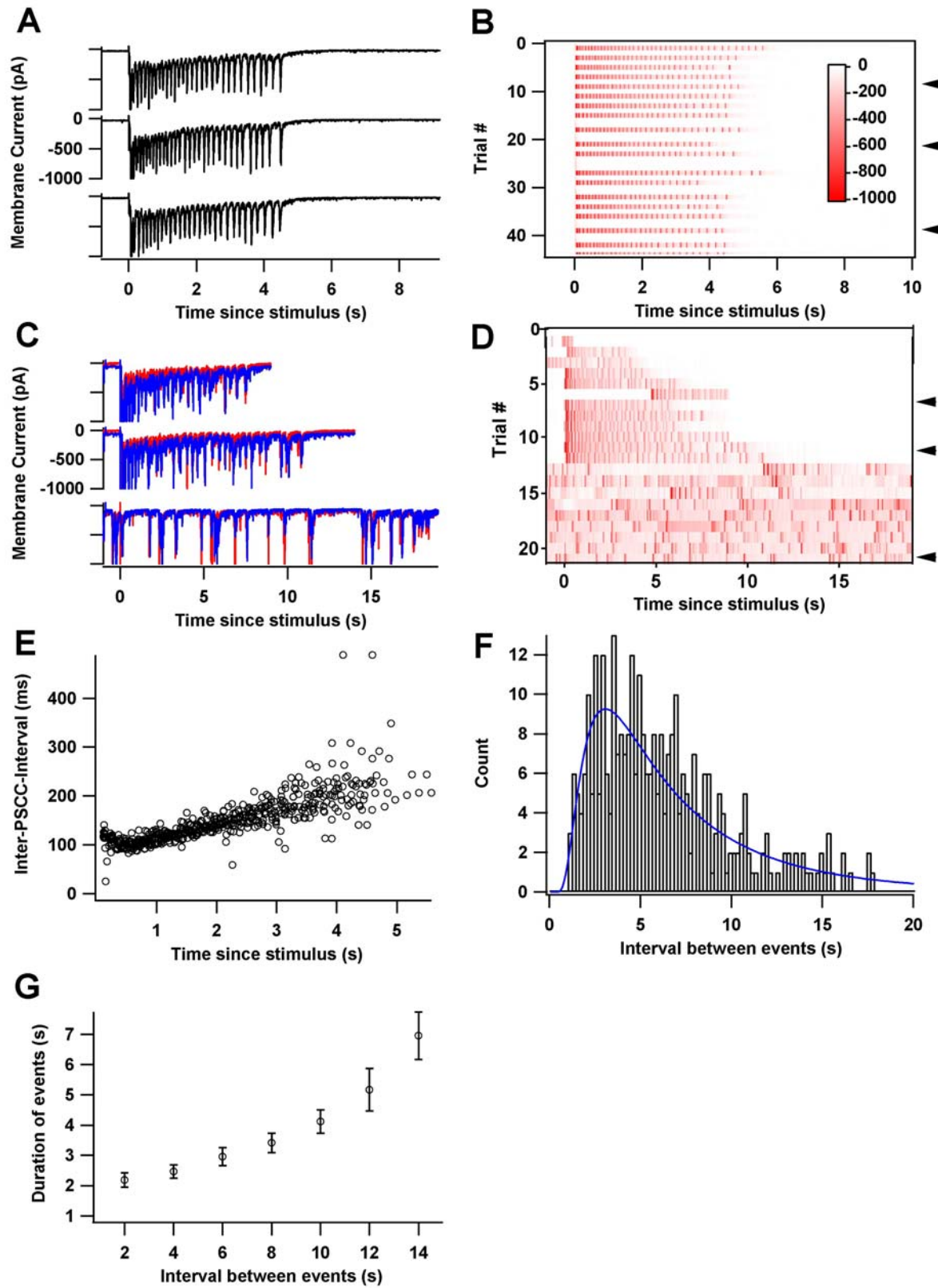


Figure 5.7: TTX-treated networks exhibit an activity-dependent transition to a regime of spontaneous activity. **A**, Three stimulus-evoked reverberations in a control network. **B**, Membrane current over several trials, illustrating that reverberation duration achieves a steady state, and that activity can be unambiguously associated with the stimulus. **C**, Three stimulus-evoked reverberations in a TTX-treated network. Red and blue traces represent two simultaneously recorded neurons, indicating that spontaneous activity is a network phenomenon. **D**, Similar to **B**, but for the TTX-treated network. The reverberation duration shows a trial-dependent increase, and spontaneous activity emerges which is unassociated with the timing of the stimulus. **E**, Timing of PSCCs over 40 trials of stimulus-evoked reverberation from a control network. **F**, Histogram of intervals between events in a representative TTX-treated network, after spontaneous activity has emerged. The blue line is a fit to an inverse gaussian distribution, modeling the onset of events as the result of threshold crossings in a random walk process. **G**, The duration of spontaneous network events is correlated with the interval since the previous event (figure is binned in 2s intervals; raw data: $r=0.45$, $p<10^{-16}$), indicating a long time-scale recovery process consistent with synaptic depression.

5.3.8. Requirements for the emergence of spontaneous activity

To quantify the degree to which a state transition had occurred in a given network, we measured the rate of spontaneously occurring events (Methods, 5.2.4). If the only activity in the network were stimulus-induced reverberations, this rate would be equal to zero. By visual inspection, TTX-treated networks showed a much greater intensity of spontaneous activity >20 minutes after the first stimulus. To quantify this in a more objective fashion, we computed the rate of spontaneous network events during this same period (Fig. 5.8a: CTL: 0.013 ± 0.009 Hz, n=12 networks; TTX: 0.130 ± 0.026 Hz, n=45 networks; $p<0.005$ by Wilcoxon rank test). Once spontaneous activity emerged, it did not disappear for the duration of recording, although in some cases, the rate exhibited a slight decline. It was common for this transition to spontaneous activity to occur after the longest reverberation of the experiment, suggesting the involvement of an activity-dependent process in its genesis. Furthermore, the extent of emergent spontaneous activity was correlated to the typical length of reverberations (Fig. 5.8b: CTL: $r=0.52$, $p<0.05$; TTX: $r=0.56$; $p<0.0001$); however, control networks with particularly long reverberations did not exhibit this transition. Multiple regression analysis indicated that TTX-treatment promoted the emergence of spontaneous activity even when reverberation duration was taken into account (Table 5.2).

We wondered what mechanism could be responsible for the emergence of spontaneous activity in TTX-treated networks. One candidate was synaptic potentiation, driven by reverberations (Fig. 5.4). Perhaps synaptic potentiation in a network with a high degree of recurrent activity could result in instability in the quiescent state. To test this possibility, we

added either the NMDAR-antagonist APV (n=10) or the mGluRI antagonists MPEP and LY367385 (n=6) to the bath prior to the first stimulus. Although APV delayed the onset of spontaneous activity (Fig. 5.8c, TTX: 8.7 ± 1.8 minutes; TTX+APV: 18.5 ± 2.6 minutes, $p < 0.05$; TTX+LY+MPEP: 7.5 ± 1.5 minutes, $p > 0.4$), neither drug was able to prevent it from ultimately emerging in TTX-treated networks (Fig. 5.8d; Methods, 5.2.4). We next speculated that the glial factor TNF- α , acting through the neuronal kinase PI3K, a pathway required for synaptic scaling (Stellwagen and Malenka, 2006), could be contributing an additional increase in synaptic strength upon the restoration of activity. However, the PI3K inhibitor Wortmannin, added prior to recording (n=3), was also unable to block the emergence of spontaneous activity (Fig. 5.8d).

Table 5.2: TTX-treatment predicts the development of spontaneous activity even when reverberation duration is taken into account.

Results of a multiple linear regression using the covariates median reverberation duration (in seconds) and 'TTX-treated' (control = 0 or TTX-treated = 1) to explain the rate of spontaneous events (see text) that eventually emerge.

Parameter	Value	Error	t-value	p-value
Intercept (%)	-0.211	0.112	-1.88	0.07
Reverberation Duration	0.094	0.021	4.52	<0.0001
TTX-treated	0.388	0.102	3.80	0.0004

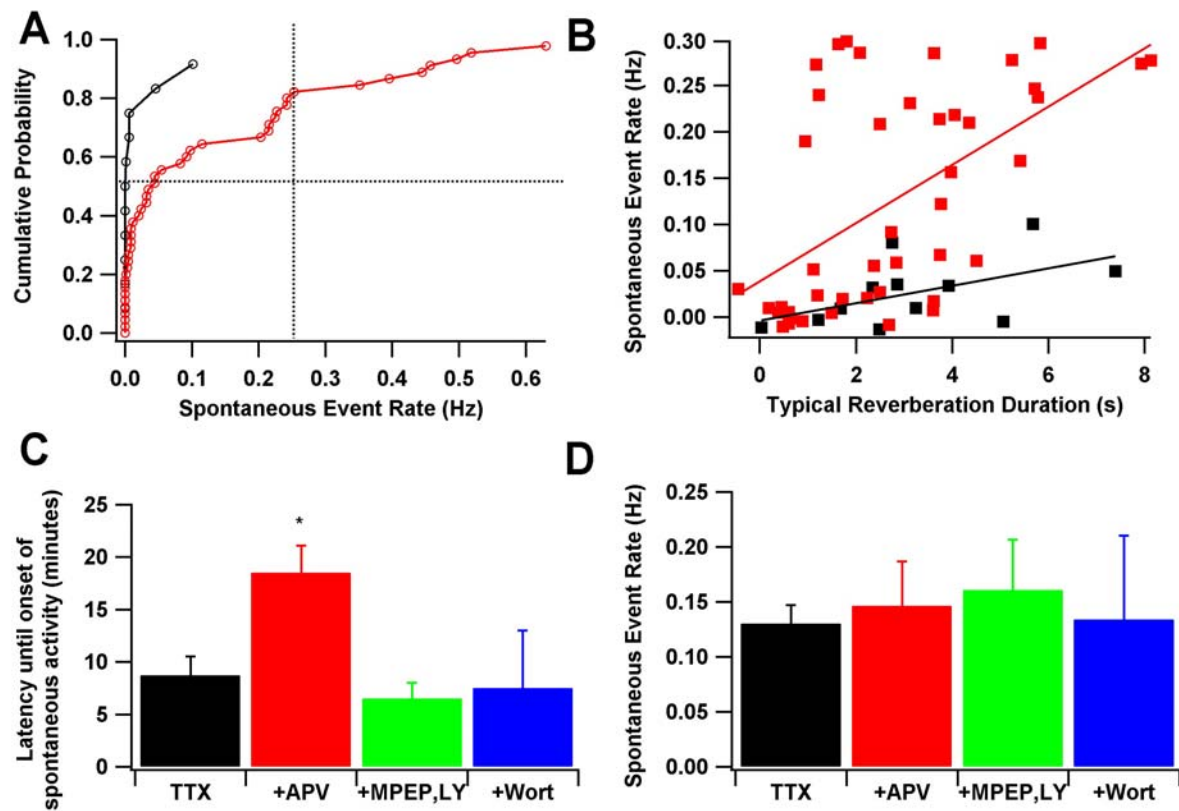


Figure 5.8: Enhancement of spontaneous activity in TTX-treated networks is facilitated but not dependent upon NMDA receptors. **A**, The rate of spontaneous network events observed ≥ 20 minutes after the first stimulus. Each data point represents one experiment (one network). Experiments using control cultures are shown in black, and TTX-treated cultures are shown in red ($p < 0.001$ by Wilcoxon Rank Test). **B**, The emergence of spontaneous activity is correlated with the duration of reverberation, but this is insufficient to explain the difference in emergence between control and TTX-treated cultures. Data points were randomly, slightly perturbed around their actual values to avoid overlap for illustration purposes. **C**, NMDAR activation accelerates the onset of spontaneous activity ($p < 0.05$ by two-tailed ANOVA). **D**, Blockers of synaptic potentiation pathways fail to abolish the eventual emergence of spontaneous activity ($p > 0.3$ by two-tailed ANOVA). For **D** and **E**, + sign in category label indicates that these networks were also chronically inactivated with TTX.

5.3.9. History-dependence in the transition between regimes of activity

To test the possibility that some non-specific activity-dependent synaptic potentiation that we had not blocked pharmacologically had caused spontaneous activity to emerge, we added small doses of CNQX to networks after they began to exhibit spontaneous activity. We predicted that if synaptic potentiation acted by producing an increase in AMPAR number or function, and thus in unitary synaptic conductance, some dose of CNQX might be able to reverse this change and restore normal stimulus-evoked reverberatory behavior. However, we found no dose that could abolish spontaneous activity while preserving the duration of stimulus-evoked reverberation present earlier in each experiment ($n=5$ networks). Similar results were obtained by antagonizing synaptic efficacy at a presynaptic locus using the A1 receptor agonist 2-chloro-adenosine (2-CAD, $n=2$ networks). However, if synapses were sufficiently antagonized (~500 nm CNQX, Fig. 5.9d) to block spontaneous activity for a period of minutes, spontaneous activity did not reappear after washout. Instead, normal stimulus-evoked reverberation was restored (Fig. 5.9e). And, after several minutes of reverberation, the transition to spontaneous activity recurred (Fig. 5.9f, 5/5 networks exhibited the overall pattern of responses shown in Fig. 5.9), although the latency until the emergence of spontaneous activity was occasionally decreased, perhaps as a result of residual synaptic potentiation. This result implied hysteresis in the relationship between synaptic efficacy and patterns of persistent activity. Specifically, the data suggested that stimulus-evoked reverberation and stimulus-independent spontaneous activity were two quasi-stable network regimes. Only with sufficient activity, or inactivity, could transitions between these regimes be made.

To test the idea that increased synaptic efficacy was sufficient to increase reverberation duration, and ultimately to spawn spontaneous activity, I used the AMPAkine CX-546, which increases synaptic charge transfer by decreasing AMPAR desensitization (Nagarajan et al., 2001). In control networks that previously showed only a transient response to stimulation, 50-100 nM CX-546 was sufficient to convert this response into reverberation (Fig. 5.10a,b). However, further increasing this dose to 150-200 nM resulted in the emergence of spontaneous activity patterns (Fig. 5.10c,d). Importantly, this dose of CX-546 was not sufficient to produce spontaneous activity in an unstimulated network, but only did so in networks exhibiting reverberations, and only after they had occurred. Thus, increasing the efficacy of synapses is sufficient to enable the activity-dependent emergence of spontaneous activity.

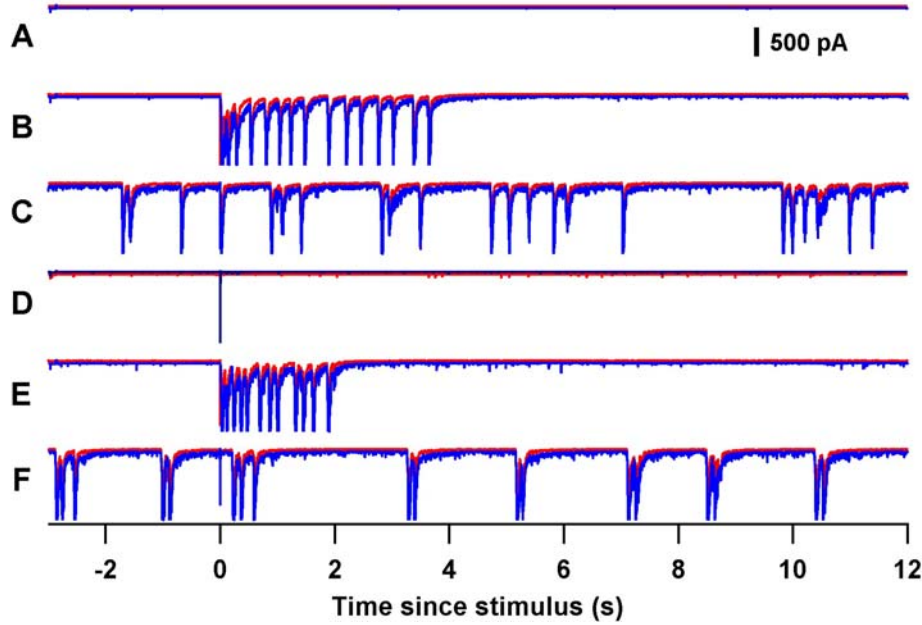


Figure 5.9: The transition to spontaneous activity can be reversed by temporary suspension of AMPAergic synaptic transmission. **A**, No synchronous network activity is present before stimulation. **B**, Reverberation can be evoked by stimulation. **C**, Spontaneous activity eventually replaces reverberation. **D**, Addition of 500 nM CNQX abolishes spontaneous activity and stimulus evoked reverberation. **E**, After washout of CNQX, reverberation can once again be evoked, and spontaneous synchronous network activity is absent. **F**, Spontaneous activity replaces reverberation, as in **C**. The recordings proceed chronologically from a single experiment from earliest to latest, and blue and red traces correspond to simultaneously recorded neurons.

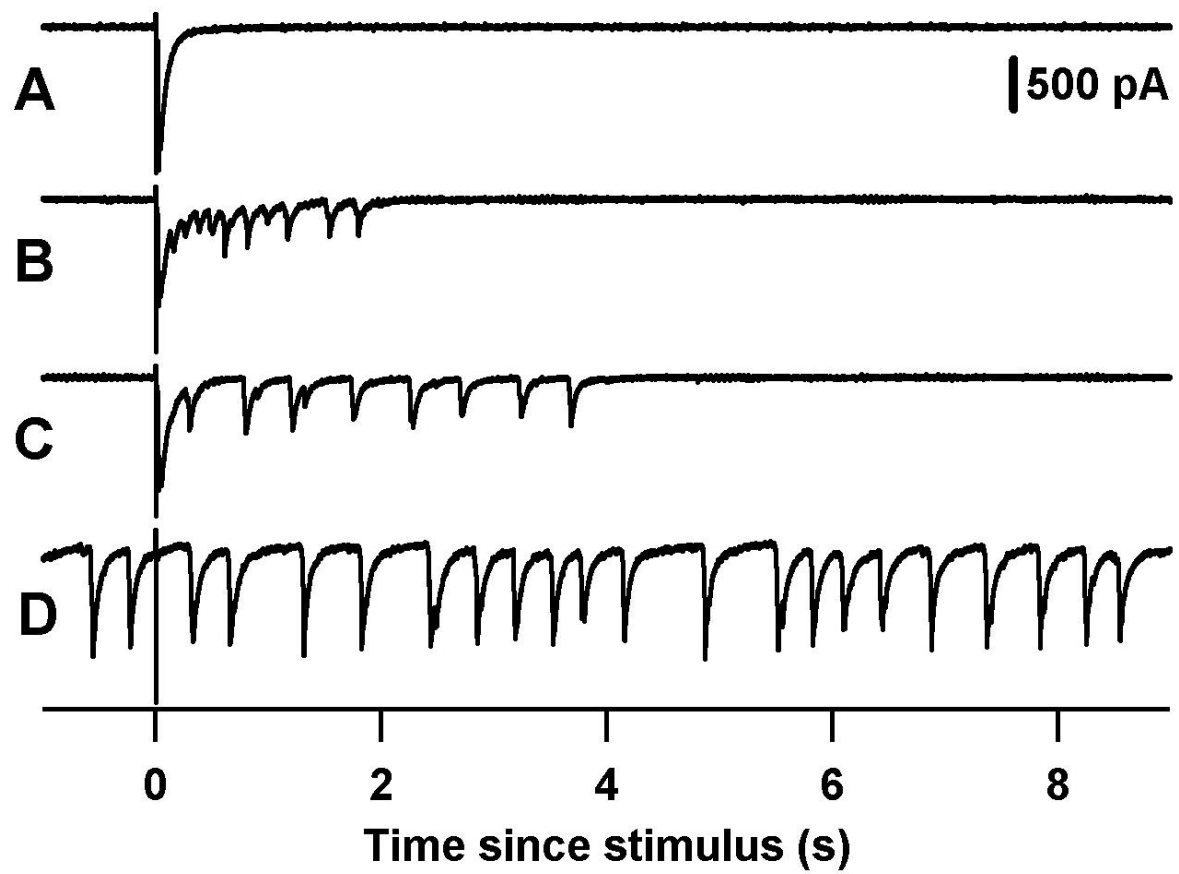


Figure 5.10: Pharmacological enhancement of synaptic efficacy results in the activity-dependent emergence of spontaneous activity. **A**, Example trace from a control network that did not exhibit reverberation. **B**, Addition of the AMPAkine CX-546 (100 μ M), increasing postsynaptic charge transfer, results in reverberation. **C**, Addition of 200 μ M CX-546 increases the duration of the reverberation. **D**, In the same concentration of CX-546, the reverberation ultimately gives way to spontaneous activity. The recordings proceed chronologically in a single experiment from earliest to latest.

5.4. DISCUSSION

Hebb predicted that activity-driven synaptic plasticity would consolidate reverberatory circuits, ensuring the stability of long-lasting memory traces (Hebb, 1949). However, the pathological hyper-activation of highly interconnected neuronal networks can reduce the capacity of those networks to encode and respond selectively to stimuli (Reid and Stewart, 1997; Leritz et al., 2006). It has been shown that synaptic scaling can act in a homeostatic fashion to counteract a challenge to neuronal activity levels ((Abbott and Nelson, 2000) and here, Fig. 5.2a). However, the consequences of this quiescent scaling on subsequent network output have not been clearly identified. We used reverberation, a model of persistent activity in small networks of cultured hippocampal neurons, to identify these consequences. Here we showed that scaling did not result in an immediate enhancement in either functional synaptic connectivity or reverberation. Instead, it predisposed neurons to a rapid increase in both synaptic connectivity and reverberation after the challenge was withdrawn.

Together with experiments showing the sensitivity of these persistent activity patterns to reductions in synaptic efficacy, and experiments illustrating the emergence of stimulus-independent activity patterns, our results imply that synaptic scaling mechanisms and the ongoing regulation of Hebbian plasticity drive spontaneously organizing cultured networks to a critical state in the synaptic configuration space. At this state, synapses are just strong enough to support stimulus-evoked reverberation, which can then be consolidated via limited synaptic potentiation. By blocking action potentials, a putative homeostatic control signal, these networks become primed for a rapid increase in synaptic connectivity. This favors reverberation, but gives way to stimulus-independent spontaneous activity facilitated by enhanced synaptic potentiation.

5.4.1. Quantal scaling vs. Functional scaling

Activity-dependent scaling of quantal amplitude, in which mEPSCs increase in amplitude (Turrigiano et al., 1998) and mIPSCs decrease in amplitude (Kilman et al., 2002) following chronic inactivation, is well established. However, the impact of this scaling on the likelihood and efficacy of functional synaptic connections between pairs of neurons has received little attention (Karmarkar and Buonomano, 2006). We found increases in the quantal amplitude of excitatory synaptic transmission, as measured by the recording of mEPSCs. However, the mean amplitude and numerical distribution of functional excitatory connections was not enhanced by TTX treatment, either immediately after the restoration of activity, or minutes later.

Given the apparent increase in quantal size as seen by measuring mEPSCs, it is not immediately apparent why the strengths of functional connections should not also be increased. Indeed, there is strong evidence that AMPAR accumulation at postsynaptic sites (Wierenga et al., 2005) and presynaptic release probability (Murthy et al., 2001) are both enhanced by inactivity. One possibility is that our observations stem from a parallel competition between Hebbian plasticity mechanisms in control cultures and enhanced synaptic scaling in TTX-treated cultures. The acceleration of homeostatic drive during incubation in TTX-treated cultures might produce the same distribution of synaptic efficacy among connected pairs as, for example, ongoing spike-timing-dependent plasticity during incubation in control cultures. Furthermore, whereas miniature synaptic current amplitudes are largely determined by the quantal size “ q ” of synaptic transmission, evoked current amplitudes are a product of “ q ”, the probability “ p ” of successful transmission, and the number of release sites “ n ” at a unitary synaptic connection. Differences in the distribution of any of these latter variables between control and TTX-treated cultures could account for the incongruity between miniature and evoked current amplitudes.

5.4.2. Reduction of inhibition by inactivity favors reverberation

Previous experiments have shown that inhibitory synapse density and quantal inhibitory transmission are reduced by chronic inactivity (Hartman et al., 2006). We have extended this finding to show that, in contrast to excitatory transmission, there is also a marked reduction in inhibitory synaptic connectivity between pairs of identified neurons. By blocking inhibitory transmission to control for differences in inhibitory connectivity between cultures, we showed that many of the differences in persistent activity patterns between control and TTX-treated networks were abolished. This suggests that inhibition is a "gatekeeper" that regulates the duration of these patterns. In the absence of inhibition, the duration may be determined by a combination of the strength of the excitatory subnetwork and the magnitude of the slowest timescale of synaptic depression (Volman et al., 2007), neither of which may be substantially altered by chronic inactivity.

5.4.3. Role of nonsynaptic changes

Despite the evidence for local, synaptic loci of the scaling response of inactivated neurons (Sutton et al., 2004; Sutton et al., 2006), we do not exclude the possibility of non-synaptic changes. For example, changes in intrinsic properties, by enhancing neuronal excitability (Marder and Goaillard, 2006), are likely to supplement positive synaptic scaling in the shift of network dynamics towards increased persistent activity. Such intrinsic changes may also favor spontaneous network oscillations (Trasande and Ramirez, 2007). In fact, we did observe increases in the excitability of TTX-treated neurons compared to controls. The current required

to elicit at least one action potential was slightly but significantly increased by chronic inactivation (Table 5.2: CTL: 104.1 ± 12.0 pA, n=27 cells; TTX: 67.7 ± 12.1 pA, n=25 cells; $p<0.005$ by Wilcoxon rank test).

The presence of hysteresis in the network response to experimentally-varied synaptic conductance (Fig. 5.9) argues that possible "online" changes in neuronal excitability are not sufficient to permanently enable the spontaneous activity state. In other words, alteration in intrinsic properties does not endow these neurons with a pacemaking capability sufficient to restore spontaneous activity when the pharmacological abolition of synaptic conductance is withdrawn. However, it remains possible that intrinsic excitability is continually and rapidly regulated during these alternating periods of activity and quiescence (van Welie et al., 2006).

5.4.4. Synaptic potentiation driven by reverberation

It has been shown previously that synchronous network activity can strengthen synaptic efficacy (Bains et al., 1999; Abegg et al., 2004; Debanne et al., 2006). However, here we show that the degree of this strengthening is enhanced in cultures pretreated with TTX. This form of metaplasticity (Abraham and Bear, 1996) could in principle be attributable to the addition of silent synapses after chronic inactivation (Nakayama et al., 2005). This would help to explain the similarity in the magnitude of detectable evoked monosynaptic currents across conditions (Figs. 5.2e, 5.5f), because the strengthening of existing connections could be quantitatively offset by the emergence of new, previously silent connections, preserving the mean current amplitude. It would also explain why an increase in pairwise connection probability in TTX-treated neurons (Figs. 5.2c, 5.5e) is seen only after the resumption of network activity.

Indeed, the unsilencing of these synapses is NMDAR-dependent, and AP5 reduced the reverberation-driven potentiation in TTX-treated cultures to control levels (Fig. 5.4d), and delayed the emergence of spontaneous activity (Fig. 5.8h). However, AP5 fully abolishes reverberation-driven synaptic potentiation of mEPSCs in control networks (Lau and Bi, 2008), whereas mGluRI antagonists abolish a fraction of synaptic potentiation in TTX-treated networks (Fig. 5.4d). This suggests that an additional, NMDAR-insensitive, mGluRI-sensitive form of potentiation may arise after chronic inactivity, as reported after experience *in vivo* (Clem and Barth, 2008).

5.4.5. Stable reverberation as a homeostatic target

Large networks of cultured hippocampal neurons, containing thousands of neurons, are used in a hippocampal culture model of epilepsy (Furshpan and Potter, 1989; Sombati and Delorenzo, 1995). In contrast to the spontaneous activity readily observed in large networks, the small networks studied here routinely exhibit reverberations without the emergence of spontaneous activity for the duration of recording (Fig. 5.7a,b). If spontaneous network activity is initiated by the spontaneous firing of at least one or a few well-connected neurons, it would not be surprising to see these patterns predominate in large networks, where the probability that one or a few cells could spontaneously discharge and trigger the activation of postsynaptic targets may be substantially increased. In small networks, synaptic scaling and Hebbian plasticity under control conditions may act to keep this probability low. However, in chronically inactivated networks both the size of spontaneous synaptic events and the probability of connections between neurons are ultimately enhanced, potentially favoring the emergence of spontaneous activity.

Does ongoing synaptic scaling, modulated by activity, drive synapses to a level appropriate for reverberatory behavior? This simple homeostatic interpretation is complicated by differences between recording conditions and culture incubation conditions (e.g. temperature) which are likely to affect the time constants of a number of processes. Thus, it would be surprising if synaptic scaling during incubation could target a set of synaptic parameters appropriate for recording conditions. Nonetheless, reverberation-induced synaptic potentiation is both weaker (Fig. 5.4d,e) and appears more rapidly saturable (Fig. 5.4b,c, note temporal extent of rising phase of red line) in control networks. This rapid saturability of synaptic potentiation is also observed in control networks where modifying stimulus design reveals reverberation in previously non-reverberatory networks (Lau and Bi, 2008). Thus, it is possible that control networks curb the degree of synaptic potentiation that occurs during correlated activity such that spontaneous activity patterns do not emerge. By contrast, TTX-treated networks may lack the ability to constrain synaptic potentiation (or alternatively, to exhibit synaptic depression), such that spontaneous activity commonly emerges. Such Hebbian synaptic potentiation may not be required for this emergence, as shown by the failure of putative blockers of such potentiation to prevent the eventual emergence of spontaneous activity (Fig. 5.8d). Nonetheless, it may nonetheless contribute to its genesis (Fig. 5.8c). Thus, metaplasticity, in addition to synaptic scaling, may enable control networks to tune their synapses to promote the stable exhibition of long-lasting stimulus-dependent activity traces.

5.4.6. Function of a “critical” level of persistent activity

To an ideal observer integrating activity over a limited temporal window, both a lack of reverberation or excessive spontaneous activity would make reconstruction of the timing of a sparse stimulus difficult. In control networks, each stimulus is typically preceded by silence and often followed by reverberation. Compared to chronically inactivated networks, this facilitates the identification of stimulus timing. Indeed, activity-dependent changes in the rules of synaptic plasticity were first posed as a mechanism to ensure the stimulus selectivity of neuronal responses (Bienenstock et al., 1982). Thus, persistent activity may act as a homeostatic control signal used to scale synaptic connectivity and restrict synaptic potentiability to levels that ultimately support stimulus-evoked reverberation, tuning a circuit to carry unambiguous information about stimulus timing.

The reverberatory capability of a network could in principle be turned on or off by modulatory inputs that alter the efficacy of synapses or the excitability of neurons. Because synaptic efficacy in control networks lies near the threshold for reverberation itself (Fig. 5.6b), the gain of such modulatory inputs in activating or inactivating reverberation is magnified. When this gain is large, even small modulatory inputs would be rapidly and reliably effective in tuning the circuit to support or oppose reverberation.

5.4.7. The origin of spontaneous activity

Spontaneous activity following chronic inactivity has been observed previously (Furshpan, 1991)(Trasande and Ramirez, 2007), but here we contrast three specific patterns of activity

(quiescence, stimulus-evoked reverberation, and stimulus-independent spontaneous activity), and evaluate the synaptic correlates of each. The emergence of spontaneous activity is correlated with treatment history and reverberation duration (Fig. 5.8b), as well as acute NMDAR activation (Fig. 5.8c), and depends on the accumulation of recent activity (Fig. 5.9). However, we were unable to identify an absolute synaptic requirement for the emergence of spontaneous activity (Fig. 5.8d). At the pharmacological level, such a requirement does not exist; alternatively, spontaneous activity may be a consequence of dynamical systems properties. For example, the increase in miniature synaptic current amplitude resulting from TTX treatment, while having little net impact on evoked currents dominated by synchronous release (Fig. 5.2), might have a greater impact on the asynchronous and spontaneous release that predominates in between network events (Lau and Bi, 2005).

5.4.8. Relevance to the brain

In neuronal networks *in vivo*, a single spike may be ineffective at producing synchronous network activity, in part because synaptic connectivity is far sparser than in cultured networks. However, the occurrence and timing of synchronous activity *in vivo* can still be determined by the activation of a restricted input (Anderson et al., 2000; MacLean et al., 2005). Thus, differences in connectivity across systems may simply demand a change in stimulation parameters to observe the relevant dynamics.

What is the relevance of reverberatory activity in cultured neurons to the brain *in vivo*?

In primary sensory or motor areas, stimulus/response coding may require networks to exhibit less synchrony and shorter “memory” than we observe for cultures. However, for areas whose

primary role is to span the gap between stimulus and response, i.e. those involved in memory, coding strategies are likely to be different. 4-10 Hz theta oscillations are a central feature of hippocampal activity during exploration, sleep, and wakeful resting (Buzsaki, 2002), and hippocampal beta-band oscillations may be involved in the encoding of novel contexts (Berke et al., 2008), indicating that population synchrony may have a role in memory.

The fundamental difference between these oscillations and reverberations is in the degree of participation of individual neurons. While only a small fraction of neurons may be recruited during each cycle of even the strongest oscillations *in vivo*, reverberations reflect the participation of nearly all neurons with each PSCC. Consequently, one could view reverberation as being a model system for a pathological condition such as epilepsy. Alternatively, one could consider each neuron in culture to be analogous to a large group of neurons *in vivo*. Such a view could harmonize disparities between neuron number, synaptic connectivity, and firing rates between the two systems.

Homeostatic plasticity occurs in the hippocampus *in vivo* (Echegoyen et al., 2007); however, it remains to be seen whether the characteristics of persistent activity patterns *in vivo* are modulated by synaptic scaling and metaplasticity in a fashion similar to those described here. If so, synaptic homeostasis, by changing the dynamics of the evocation and termination of persistent activity patterns, may be critical for ensuring that information is correctly processed in the brain.

6. ASYNCHRONOUS RELEASE DETERMINES NETWORK DYNAMICS IN CULTURED HIPPOCAMPAL NEURONS

6.1. INTRODUCTION

In order for neurons involved in a persistent activity pattern to be available for future computations, that activity pattern must eventually abate. Continuous, spontaneous activation of the same circuit may comprise a seizure, and may itself be epileptogenic (Morimoto et al., 2004; Sutula, 2004). Intuitively, for persistent activity to be both reliably evoked and terminated the statistics of neuronal excitability and synaptic connectivity should strongly favor recurrent activity at the onset, but eventually shift in favor of termination.

However, the cellular mechanisms that determine the dynamics of network activity are poorly understood. The timescales of both action potential refractoriness and fast synaptic transmission are not well-suited to sustain low-frequency rhythmic neuronal activity lasting for seconds. Nonetheless, brain rhythms with wavelengths ranging from hundreds of milliseconds to seconds are observed for a variety of behavioral states, ranging from exploration, to restful waking, to sleep (Steriade et al., 1993; Buzsaki, 2002).

A variety of processes with slow timescales have been invoked to explain these states, including NMDAR-dependent synaptic transmission (Wang, 1999), slow inhibition (Csicsvari et al., 1999), and slow membrane afterhyperpolarization (Fernandez de Sevilla et al., 2006). For

each of these cases, the individual ionic conductances are small, and the number of channels large; consequently, these processes may be nearly deterministic. By contrast, asynchronous synaptic transmission, the exocytosis of synaptic vesicles well after a presynaptic action potential, constitutes a comparatively infrequent process with a conductance of one quantum or more. As a highly stochastic process, it may be well-suited to explain coarsely-timed network output.

In small hippocampal cultures, stimulation of a single neuron can elicit network reverberations lasting for seconds; $[Ca^{2+}]$ -dependent asynchronous release is required for these reverberations, and is visibly elevated in between cycles of this oscillation (Lau and Bi, 2005). Here I show a linear mapping between the properties of reverberation and the values of synaptic parameters in a model incorporating asynchronous release and the dynamics of the synaptic vesicle cycle. This model explains the activity-dependent emergence of spontaneous activity in chronically inactivated neurons (Chapter 5). In explaining these phenomena, I argue that asynchronous release represents an underappreciated computational mechanism in the nervous system.

6.2. METHODS

6.2.1. The dynamics of presynaptic Ca^{2+}

In order to implement asynchronous release in a network model of spiking neurons, it was necessary to capture the dynamics of presynaptic Ca^{2+} . I assumed that Ca^{2+} influx with each

action potential is proportional to the driving force for calcium (according to the logic of the Nernst equation). I also assumed that presynaptic free calcium is buffered and extruded at a rate given by a Hill equation. This gives:

$$\frac{d[Ca^{2+}]}{dt} = -\frac{\beta_{on}(b-\Omega)[Ca^{2+}] - [Ca^{2+}_0]^n}{k_r^n + ([Ca^{2+}] - [Ca^{2+}_0])^n} + \beta_{off}\Omega + \gamma \log\left(\frac{[Ca^{2+}_e]}{[Ca^{2+}]}\right)\delta(t - t_{spike}) \quad \text{eq. 6.1}$$

$$\frac{d[\Omega]}{dt} = \frac{\beta_{on}(b-\Omega)[Ca^{2+}] - [Ca^{2+}_0]^n}{k_r^n + ([Ca^{2+}] - [Ca^{2+}_0])^n} - \beta_{off}\Omega - \varepsilon\Omega \quad \text{eq. 6.2}$$

In the above, γ is proportional to the conductance of the presynaptic Ca^{2+} channels, and was tuned to give $O(1 \mu M)$ per-spike increment in presynaptic $[Ca^{2+}]$ (Zucker, 1996), for extracellular Ca^{2+} concentration $[Ca^{2+}]_e$. β_{on} reflects the forward rate of Ca^{2+} extrusion and buffering, n is the cooperativity of these calcium clearance mechanisms, and k_r represents the value of $[Ca^{2+}]$ for which these clearance mechanisms operate at half of their maximum rate; the latter two were chosen to match experimental data (Carafoli, 2004). The total buffer concentration, b , is composed of the calcium-bound component, Ω , and free buffer, $(b - \Omega)$. β_{off} represents the reverse rate for the calcium clearance mechanism, which is a non-negligible reaction once Ω becomes large. A component of the calcium is cleared by irreversible extrusion mechanisms at rate ε . The relative contributions of buffering and extrusion are largely unknown empirically. In the limiting case of $b \gg \Omega$ and $\beta_{off} = 0$, the buffer has infinite capacity and no reverse reaction, and the presynaptic Ca^{2+} equations match a previously published model (Volman et al., 2007).

6.2.2. Residual Ca²⁺ and asynchronous release

Evidence suggests that the relationship between the rate of asynchronous release (η) and the calcium concentration obeys the Hill equation (Ravin et al., 1997; Kirischuk and Grantyn, 2003):

$$\eta = \eta_{\max} \frac{([Ca^{2+}])^m}{k_a^m + ([Ca^{2+}])^m} \quad \text{eq. 6.3}$$

Higher values of m make the [Ca²⁺]-dependence of asynchronous release steeper, and sharpen the distinction between the behavior associated with low and high calcium concentrations.

Experiments performed on single synapses (Ravin et al., 1997; Kirischuk and Grantyn, 2003) estimate $m \sim 4$. Much lower values of m are not compatible with our experimental data, as they produce either no reverberation, or indefinite activity, depending on the choice of other parameters. The threshold values of [Ca²⁺] needed to activate asynchronous release vary from $< 0.2 \mu M$ for chromaffin cells (Augustine and Neher, 1992) to $> 20 \mu M$ for retinal bipolar nerve terminals (Heidelberger et al., 1994). Guided by the reported importance of asynchronous transmitter release at hippocampal synapses (Hagler and Goda, 2001; Lau and Bi, 2005), and by the realization that the affinity for asynchronous release is evidently at least as high as the affinity for calcium clearance, I propose $k_a = 0.4 \mu M$ in the simulations.

6.2.3. Short-term synaptic dynamics

Short-term synaptic dynamics are based in part on the cycling of vesicles of neurotransmitter through various states. According to a tractable model of this cycle (Tsodyks et al., 2000), neurotransmitter leaves a readily releasable pool (state X) with each spike and enters a synaptic cleft pool (state Y) available to bind to postsynaptic receptors. Receptor unbinding and neurotransmitter transporter activity recover neurotransmitter (to state Z), and vesicle recycling within the presynaptic terminal (back to state X) completes the loop.

Because hippocampal synapses utilize multiple modes for vesicle recycling (Gandhi and Stevens, 2003), each marked by a different timescale, I proposed an additional state in the vesicle recycling pathway. This state (S) constitutes a parallel intermediate route for recovered neurotransmitter (Z) before it rejoins the readily releasable pool (X). If the $S \rightarrow X$ kinetics are slower than the $Z \rightarrow S$ kinetics, then the S state acts as a sink for synaptic resources during periods of elevated neuronal activity. This provides negative feedback by slowly reducing the neurotransmitter available in state X . Such a trafficking scheme, incorporating both synchronous and asynchronous release of neurotransmitter, is described by:

$$\frac{dX}{dt} = \frac{S}{\tau_s} + \frac{Z}{\tau_r} - X(\mu\delta(t - t_{sp}) + \eta) \quad \text{eq. 6.4}$$

$$\frac{dY}{dt} = -\frac{Y}{\tau_d} + X(\mu\delta(t - t_{sp}) + \eta) \quad \text{eq. 6.5}$$

$$\frac{dZ}{dt} = \frac{Y}{\tau_d} - \frac{Z}{\tau_r} - \frac{Z}{\tau_l} \quad \text{eq. 6.6}$$

$$\frac{dS}{dt} = \frac{Z}{\tau_l} - \frac{S}{\tau_s} \quad \text{eq. 6.7}$$

with $X + Y + Z + S = 1$ as a conservation criterion. The time-series t_{sp} indicate the arrival times of pre-synaptic action potentials (with a delay of 2 ms to conform to experiments), τ_d is the characteristic decay time of post-synaptic currents, and τ_r is the time constant of recovery from synaptic depression. The value of τ_d is chosen to reflect AMPAR current decay kinetics, since AMPARs, but not NMDARs, are critical for reverberations in hippocampal cultures (Lau and Bi, 2005). The variable μ describes the fraction of the readily releasable pool released by a presynaptic action potential. The parameters τ_l and τ_s determine the timescale of neurotransmitter accumulation into and release from the S state, respectively. This scheme is picturized in Figure 6.1.

If $\tau_s \gg \tau_l$, reverberations will be very brief, as neurotransmitter will rapidly accumulate in the S state and be unavailable for release. Reverberation duration will increase as $\tau_s/\tau_l \rightarrow 1$, and when $\tau_s < \tau_l$, reverberation can last indefinitely, as X will always be sufficiently large to sustain it. Reverberation terminates when state S becomes sufficiently occupied. However, if τ_s is sufficiently small, neurotransmitter will become available before presynaptic $[Ca^{2+}]$ has substantially decayed. Thus, asynchronous release may be sufficient to evoke a spontaneous network event, triggering another reverberation and possibly a transition to the spontaneous activity regime. In order to make neurotransmitter release a stochastic process, the release rate term $X(\mu\delta(t - t_{sp}) + \eta)$ in equations 6.4 and 6.5 (denoted r) was randomized about its mean at each time step according to $r = B(h,r)/h$, where $B(n,p)$ is a random number from the binomial distribution of n trials with probability p . Such randomization is motivated by the idea of h independent release sites at each connection determining the mean release rate r .

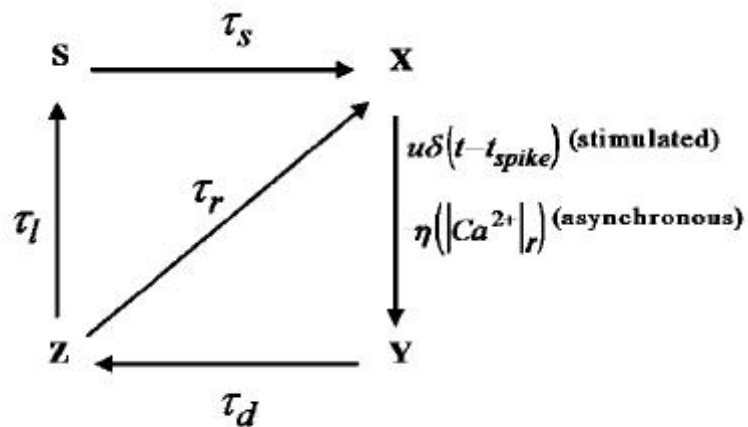


Figure 6.1: Short-term synaptic dynamics at synaptic connections in the reverberation model.

Neurotransmitter leaves a readily releasable pool (state X) with each spike or with $[Ca^{2+}]$ -dependent asynchronous release and enters a synaptic cleft pool (state Y) available to bind to postsynaptic receptors. Receptor unbinding and neurotransmitter transporter activity recover neurotransmitter (to state Z), and vesicle recycling within the presynaptic terminal (back to state X) completes the loop. Some neurotransmitter is recycled through state S , accounting for a slower time scale of synaptic depression and recovery.

6.2.4. Neuronal model and network connectivity

For simplicity, I used 64 quadratic integrate and fire neurons with threshold adaptation, simulated at 1 ms time steps, whose membrane potentials each evolved according to:

$$v' = a_0(v - v_L)(v - v_{\text{thresh}}) + I_{\text{syn}}/C \quad \text{eq. 6.8}$$

$$v_{\text{thresh}'} = a_1 \delta(t - t_{sp}) + (v_{\text{thresh}0} - v_{\text{thresh}})/\tau_{\text{thresh}} \quad \text{eq. 6.9}$$

v is reset to v_{reset} every time the membrane potential crosses v_{thresh} , and a spike is recorded.

Experimental observations (Lau and Bi, 2005) indicate that a single neuron fires 0-2 spikes during the PSC cluster. I tuned $v_{\text{thresh}0}$ so as to produce one post-synaptic spike upon activation.

Because only a small fraction of the neurons in cultured hippocampal networks are inhibitory, and reverberations are routinely recorded in the presence of BMI to block GABA_A receptors, I set all neurons to be excitatory to represent the subnetwork active in the presence of BMI. For each pair of model neurons, I establish unidirectional synaptic connections with probability ρ . After this random network topology was constructed (see (Volman et al., 2008) for topological considerations in reverberatory networks), I drew baseline synaptic efficacies, A_{ij} , between connected pairs from an exponential distribution with mean q . Note that q , although correlated with the experimental quantity quantal amplitude, is not identical. Instead, q corresponds to the conductance of the synaptic connection when all possible neurotransmitter is bound to postsynaptic receptors. Multiplying this conductance by the driving force at rest gives synaptic currents comparable to experimental values.

Synaptic currents are determined by short-term dynamics (the occupancy of state Y , reflecting the neurotransmitter in the synaptic cleft as a fraction of its maximum value), and baseline synaptic efficacies. Synaptic currents are given by:

$$I_{i,syn} = \sum_{j=1}^n A_{ji} Y_j (v_i - v_r) \quad \text{eq. 6.10}$$

where v_r is the reversal potential for these currents.

Table 6.1: Parameters for the reverberation model.

The values shown here are used throughout, unless indicated otherwise. Parameters have analogues in (Volman et al., 2007), except where marked with †.

Parameter	Value	Description	Comments and Source
a_0 (mV ⁻¹ ms ⁻¹)	0.01	Determines attraction rate for fixed points v_L and v_{thresh}	
v_L (mV)	-65	Leak current reversal ~ resting potential	
$v_{\text{thresh}0}$ (mV)	-45	Baseline action potential threshold	
v_r (mV)	0	Reversal potential for synaptic current	Free parameters to match membrane potential trajectories to experimental current clamp data. †
a_I (mV)	10	Threshold potential increment per action potential	
τ_{thresh} (ms)	200	Timescale for threshold potential decay to baseline	
C (pF)	0.05	Membrane capacitance for external currents	
q (nS)	10	Mean unitary synaptic conductance	$q(v_r-v)\mu = \text{Postsynaptic current per presynaptic spike at baseline} = 227.5 \text{ pA}; \text{ see Fig. 5.2}$
ρ	0.2	Probability of a unidirectional synaptic connection	Free parameter with experiments in 3.x as an upper bound due to experimental selection bias
μ	0.35	Fraction of available neurotransmitter released per A.P.	(Volman et al., 2007). Constant at excitatory synapses: (Tsodyks and Markram, 1997)
h	100	Number of vesicles per unitary connection	Used to discretize release. $h = \infty$ results in infinitesimally small quanta. See (Moulder and Mennerick, 2005)†
[Ca ²⁺ _e] (μM)	3000	External Ca ²⁺ concentration	Chosen experimentally (section 3.2.2)

$[Ca^{2+}_0]$ (μM)	0.05	Baseline internal Ca^{2+} concentration	(Yuste et al., 1999; Maravall et al., 2000)†
η_{max} (ms^{-1})	0.5	Maximum asynchronous release rate per connection	Free parameter used to match experimentally observed minimum and maximum release rates.
m	4	Hill exponent for asynchronous release	(Ravin et al., 1997; Kirischuk and Grantyn, 2003)
k_a (μM)	0.4	Hill coefficient for Ca^{2+} and asynchronous release	Bounded by (Augustine and Neher, 1992; Heidelberger et al., 1994)
γ ($\mu M/ms$)	0.125	Ca^{2+} accumulation per action potential	Tuned to match O(1 μM) Ca^{2+} transients in (Zucker, 1996).
n	2	Hill exponent for Ca^{2+} buffering/extrusion	(Carafoli, 2004)
k_r (μM)	0.4	Hill coefficient for Ca^{2+} buffering/extrusion	
β_{on} ($\mu M/ms$)	0.005	Buffering/extrusion rate for intracellular Ca^{2+}	Decay τ for $[Ca^{2+}]_i$ is ~ 200 ms (Majewska et al., 2000).
β_{off} (ms^{-1})	2.5×10^{-5}	Off-rate for buffering/extrusion of Ca^{2+}	Free parameters; for $b \rightarrow \infty$ and $\beta_{off} = 0$, ε is irrelevant and the model is comparable to (Volman et al., 2007); in this case, reverberations are similar to those reported here but spontaneous activity does not emerge. †
ε (ms^{-1})	5×10^{-5}	Rate for clearance of buffered/extruded Ca^{2+}	
b	100	Concentration of Ca^{2+} buffer	
τ_d (ms)	10	Decay τ for bound transmitter	Decay τ for synaptic current at excitatory hippocampal synapses \sim decay τ for AMPAR conductance.
τ_r (ms)	300	Recovery τ for released transmitter	Matches experimental data for single hippocampal synapses (Nauen and Bi, 2008).
τ_l (ms)	5000	τ for transmitter storage in inactive pool	(Volman et al., 2007)Free parameters; similar to time constants described in (Rosenmund and Stevens, 1996). $\tau_s > \tau_l$ is required for finite reverberation duration.
τ_s (ms)	10000	τ for transmitter release from inactive pool	

6.2.5. Identification and analysis of network activity

To identify and measure reverberations and spontaneous network events in both simulations and experiments, I used the techniques described in section 5.2.4. As in chapter 5, a polysynaptic current cluster (PSCC) is an epoch of inward current, as recorded in a single neuron, reflecting the contribution of many synaptic inputs in a short (<100 ms) time window. Each reverberation is composed of many such PSCCs.

6.2.6. Calculation of the probability of a polysynaptic current cluster (PSCC)

To provide a heuristic estimate of PSCC probability (Fig. 6.4), I considered that:

$$p(\text{PSCC}) = p(\text{spike}) * p(\text{PSCC} | \text{spike}) \quad \text{eq. 6.11}$$

where “spike” refers to an action potential which may or may not trigger a PSCC. If the timing of spontaneous synaptic input to a given neuron is random, and the rate of spontaneous inputs is sufficiently high, the synaptic current can be approximated as a normal distribution. For a simple neuronal integrator of this input, the membrane potential dynamics will then obey a random walk. The time to first passage (of firing threshold) for a random walk is given by an inverse Gaussian distribution (Chhikara and Folks, 1989), and it can be shown in simulation that the median, m , of this distribution and the expectation value of the smallest value, s , of a sample taken from this distribution are both inversely proportional to the variance of the driving source

(the synaptic current). In either case, this variance will in turn be proportional to the square of the frequency of the synaptic inputs, and to the square of the amplitude of those inputs.

The probability of spiking will be the inverse of the first passage time. This inverse will be $1/m$ or $1/s$, depending on whether I consider the spiking of a particular cell or of any cell, and is thus proportional to the square of the synaptic input frequency and the square of the synaptic input amplitude. The input frequency will be proportional to the connection probability ρ , and the rate of asynchronous release η , and the input amplitude will be proportional to q . Thus,

$$p(\text{first spike}) \propto (\rho q \eta)^2 \quad \text{eq. 6.12}$$

Given that one cell has spiked, the probability of recruiting the rest of the network to generate a PSC cluster is related to the number of neurons onto which the spiking cell makes synapses, and the instantaneous strength of those synapses, a function of short-term depression. To provide a lower bound for the difference in PSC cluster probability between strongly and weakly connected cultures, I assume that the spiking cell needs only to recruit one additional neuron to guarantee a PSC cluster; therefore, the probability of PSC cluster generation given one spike is proportional to the square of the expectation value of outgoing synaptic connection strengths:

$$p(\text{PSCC} | \text{first spike}) \propto (\rho X)^2 \quad \text{eq. 6.13}$$

where X is the size of the readily releasable pool. The results from chapter 5 (Fig. 5.2) indicate that the strength of functional connections may not be determined by q , and so q is excluded from the equation above. By equation 6.11:

$$p(\text{PSCC}) \propto (\rho q \eta)^2 (\rho X)^2 \quad \text{eq. 6.14}$$

6.3. RESULTS

6.3.1. Dependence of reverberatory output on synaptic parameters in a model with short-term synaptic dynamics

In chapter 5 I showed that some aspects of both reverberation and excitatory synaptic transmission are enhanced in TTX-treated cultures. To understand this result, I investigated the relationship between synaptic efficacy and the duration and probability of reverberation in a network model. Because the neuronal phenotypes, pairwise synaptic connectivity, neuronal firing dynamics, and short-term synaptic dynamics in small cultured hippocampal networks are well-understood, I constructed such a network model (adapted from (Volman et al., 2007)) and used these known parameters to make predictions about the effects of changes in synaptic efficacy on reverberation. To simplify the model, I ignored the effects of inhibition, which are not required to produce reverberation (Lau and Bi, 2005).

The probability of a unidirectional connection between neurons (maximal synaptic current > 0) we define as ρ , and it can be estimated from paired recordings. Because it is likely that paired recordings from neighboring neurons overestimate typical connection probabilities in a circuit (Pavlidis and Madison, 1999), I used lower values of ρ in the model than I obtained in experiments (Fig. 5.2). The maximal synaptic conductance, q , reflects the mean postsynaptic conductance of all such connections, in the extreme case that all available neurotransmitter is bound to postsynaptic receptors. The instantaneous synaptic conductance is equal to Xq , with X being the proportion of available neurotransmitter currently bound to postsynaptic receptors. While ρ differs in control and TTX-treated networks, while q appears to be similar (Fig. 5.2,

assuming that the evoked synaptic current is proportional to q). However, both values are likely to vary across networks, and thus I explored the effects of varying these parameters on the characteristics of reverberation.

For a single realization (simulation with a fixed pattern of existing connections) of a model network, there was a linear relationship between q and the duration of reverberations. Because the model was implemented with stochastic synaptic transmission (Methods, 6.2.3), both successes and failures of reverberation could be observed from trial to trial (Fig. 6.2a), as in experiments (Fig. 1.6). The probability of successful reverberation increased sublinearly and asymptotically towards 1 as the unitary conductance was increased (Fig. 6.2d). Across network realizations, similar results were observed (Fig. 6.2e,f), although the variability was slightly greater due to variations in network topology (Methods, 6.2.4). When ρ was varied, there was also a linear relationship with reverberation duration (Fig. 6.2g,h). However, there was a sharp threshold in ρ above which the reverberation probability increased sharply. Near the threshold, small increases in ρ caused large increases in the probability (p) of reverberation (Fig. 6.2h, $p=0.2$ to $p=0.8$ corresponds to a $\Delta \rho$ of 0.026).

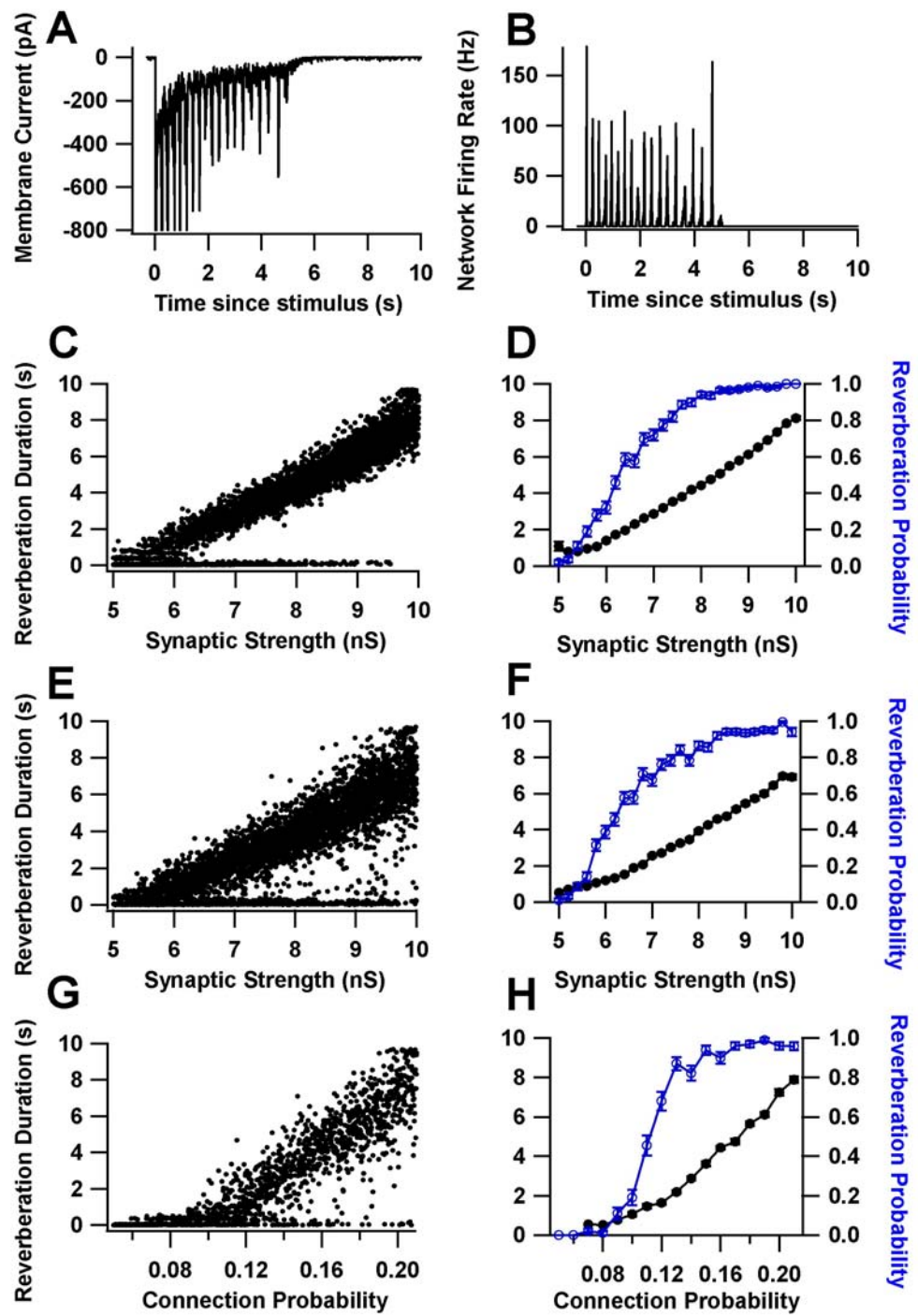


Figure 6.2: Effects of altered synaptic parameters on reverberation. **A**, An example reverberation generated from the model (Methods, 6.2.1-4). One model neuron is voltage clamped and the transmembrane current is measured, analogous to experiments. **B**, Average spike rate for all neurons in the network, from the reverberation in *A*. Notice that the spike rate is negligible in between synchronous network events and after the end of the reverberation. **C**, Duration of reverberation for a single instantiation of the model network, as a function of the mean peak synaptic conductance q . Each data point represents one simulation. **D**, Probability of reverberation, and duration of successful reverberations, for the values in *C*. **E**, Duration of reverberation, where each data point corresponds to an independently generated network, using the conductance q shown on the abscissa. Note that while the spread of the data is greater than in *C*, there is still a strong correlation between unitary synaptic conductance and reverberation duration and probability. **F**, Probability of reverberation, and duration of successful reverberations, for the values in *E*. **G**, Duration of reverberation, where each data point corresponds to an independently generated network, using synaptic connection probability ρ . **H**, Probability of reverberation, and duration of successful reverberations, for the values in *G*. Default values for all parameters are given in Table 6.1.

6.3.2. Critical threshold behavior in reverberatory networks

I reasoned that because most control networks do not exhibit reverberation (Fig. 5.2d), those that do are likely to have synapses just strong enough to support such activity patterns. Meanwhile, since most TTX-treated networks do exhibit reverberation, some of these networks likely have synaptic efficacies or connection probabilities that are well above the values necessary to observe reverberation. Earlier I showed that reverberatory activity in control networks were highly sensitive to small decrements in excitatory synaptic efficacy, while TTX-treated networks were less sensitive to such a decrement (Fig. 5.6). To determine if the model could also capture this behavior, I chose two levels of ρ , 0.125 and 0.25, to mimic control and TTX-treated cultures respectively. I then varied q in each network, a computational analogue of varying the CNQX concentration in experiments, and computed the mean reverberation duration, including failures. The results (Fig. 6.3) show that for the lower value of ρ , the sensitivity of reverberation to decreases in q is steep, reflecting threshold behavior for this level of recurrent connectivity. By contrast, for the higher value of ρ , a greater reduction in q is required to reduce or abolish reverberations. These results qualitatively matched those observed in the experimental data.

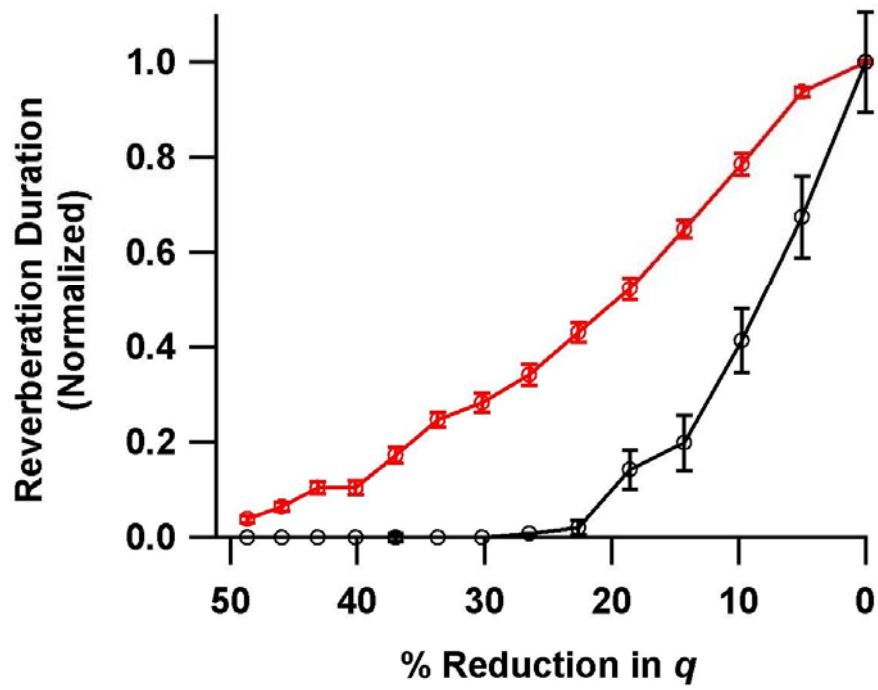


Figure 6.3: Critical threshold behavior in control networks. For connection probability $\rho=0.25$ (red) and $\rho=0.125$ (black), the synaptic conductance q was reduced from its default value, and mean reverberation duration in the model, including failures, was calculated. Networks with the lower connection probability experienced a much sharper drop in reverberation duration than networks with higher connection probability.

6.3.3. Intracellular calcium drives the regime of spontaneous activity

Hysteresis in the relationship between synaptic efficacy and network function (Fig. 5.9) provided evidence that the emergence of spontaneous activity may not require an online change in synaptic efficacy. Indeed, blockade of putative synaptic potentiation pathways delayed but did not prevent the arrival of a spontaneous activity regime (Fig. 5.8). Thus, the likelihood of transitions between reverberatory and spontaneous states may alternatively be governed by events that do not require long-lasting changes in cellular properties, and may be reflected in the recent history (seconds to minutes) of network activity. This history could in turn be determined in part by prior changes in synaptic efficacy.

If the activity-dependent emergence of spontaneous activity were driven by recent activity history on a time scale of seconds or minutes, I posited that a process with kinetics much slower than membrane or channel time constants must be responsible. Because, action potentials cause presynaptic Ca^{2+} accumulation, and because endogenous buffering and extrusion mechanisms do not instantaneously restore presynaptic $[\text{Ca}^{2+}]$ to baseline levels, neurotransmitter can be released asynchronously. Because the time constant for the decay of asynchronous release ($10^2\text{-}10^5$ ms, depending on the stimulus history) is orders of magnitude greater than that for synchronous release (~6 ms) (Goda and Stevens, 1994), I speculated that presynaptic Ca^{2+} accumulation and asynchronous release could be the slow process governing the transition to and sustenance of spontaneous activity.

To test the hypothesis that Ca^{2+} accumulation was necessary for the recurring spontaneous activity, I added the cell-permeable slow Ca^{2+} buffer EGTA-AM (30 μM) to the

bath after spontaneous activity had emerged. EGTA-AM substantially reduced spontaneous activity (Fig. 6.4a), indicating that intracellular Ca^{2+} is a requirement for the elevated spontaneous EPSC rate. This effect was duplicated with ryanodine (30 μM), which can block Ca^{2+} release from internal stores, and was reversible if washout was sufficiently rapid (Fig. 6.4b). If asynchronous EPSCs mediated the spontaneous activity, a reduction in their rate should be visible following a stimulus. Indeed, the rate of asynchronous EPSCs for several seconds following a stimulus was reduced after EGTA-AM wash-in (Fig. 6.4c,d).

When added to networks in the presence of TTX, prior to stimulation, EGTA-AM did not lower the rate of mEPSCs (Fig. 6.4f, n=6), even in networks where the baseline mEPSC rate well-exceeded typical post potentiation rates. This implies that resting $[\text{Ca}^{2+}]$ does not significantly contribute to spontaneous miniature neurotransmission. However, when EGTA-AM was applied after TTX wash-in following a period of reverberation, a period associated with a potentiation of the rate of mEPSCs (Fig. 5.4), the mEPSC rate was reduced (Fig. 6.4e,f, n=5, $p<0.005$), suggesting that the presynaptic $[\text{Ca}^{2+}]$ sensitivity of such transmission is enhanced, long after $[\text{Ca}^{2+}]$ has decayed to a steady-state value, and that this $[\text{Ca}^{2+}]$ -sensitive component underlies part of the potentiation of mEPSC frequency (Fig. 5.4a,e).

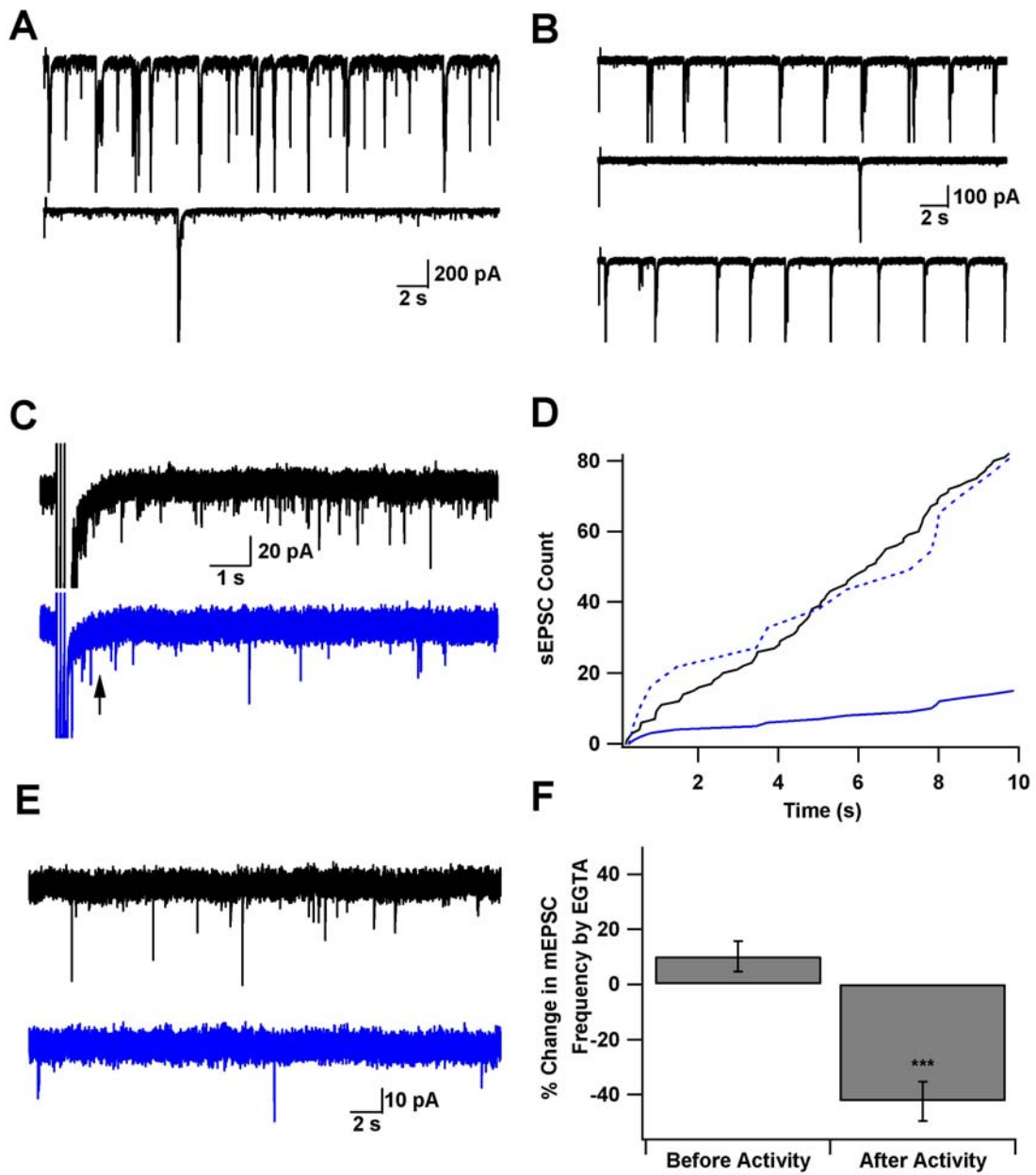


Figure 6.4: Intracellular $[Ca^{2+}]$ drives spontaneous activity, asynchronous release, and a component of reverberation-driven synaptic potentiation. **A**, The rate of spontaneous synchronous network events (top) is reduced by application of the cell permeable Ca^{2+} buffer EGTA-AM (30 μM , bottom). **B**, The same effect can be achieved with Ryanodine (30 μM), a reversible inhibitor of Ca^{2+} release from internal stores (middle). If there is sufficient remaining spontaneous activity, the spontaneous activity rate can be reversed upon washout (bottom). **C**, The rate of stimulation-dependent asynchronous EPSCs (black, top) is reduced after wash-in of EGTA-AM (blue, bottom). Stimulus responses of comparable magnitude were chosen to avoid a confounding effect of recent activity history. **D**, The timing of asynchronous EPSCs (counting begins at the arrow in C) is somewhat uniformly distributed in the control condition (black line), suggesting a random process. The solid blue line corresponds to the EGTA-AM condition, and the dashed blue line is the same data normalized to the number of EPSCs recorded in the control condition. **E**, mEPSCs recorded 30 minutes after the last reverberation before (top) and after (bottom) application of EGTA-AM. **F**, EGTA-AM has no effect on mEPSCs recorded prior to reverberation, but significantly reduces the frequency of mEPSCs recorded after reverberation, suggesting that a component of the reverberation-driven potentiation is dependent on changes in intracellular Ca^{2+} . *** indicates $p < 0.005$ vs. unity.

6.3.4. Presynaptic calcium dynamics can explain the activity-dependent emergence of spontaneous activity

To quantitatively describe the mechanism by which asynchronous release might serve this role, we considered the dynamics of the network model, originally designed (Volman et al., 2007) to explain the importance of asynchronous release in experimentally-observed reverberations (Lau and Bi, 2005). In this model, asynchronous release can maintain postsynaptic drive after a PSCC, thus sparking the emergence of the next PSCC after the recovery of synapses from synaptic depression. The model further proposes that reverberation ends when the readily available synaptic vesicle pool, depleted by activity (Methods, 6.2.3; growth of state S in eq. 6.7), is insufficient to produce the next PSCC.

Because presynaptic Ca^{2+} accumulates with each action potential, and the asynchronous release rate is a function of presynaptic $[\text{Ca}^{2+}]$, the asynchronous release rate rises significantly after a reverberation, before decaying to baseline levels over many seconds (Fig. 6.5a,b). If the rate of asynchronous release is sufficiently high, there exists a significant probability, $p(\text{spike}|\text{reverberation}, t)$, of some postsynaptic neuron exceeding its action potential threshold, a probability that is also dependent upon the quantal conductance of the asynchronous events. The probability that this action potential will produce a new PSCC, $p(\text{PSCC}|\text{spike})$, will be dependent upon the efficacy of evoked transmission, which is in turn dependent on the current state of synaptic depression. These probabilities can be multiplied to yield the probability of a subsequent PSCC, given a reverberation, $p(\text{psc}|\text{reverberation})$ (Methods, 6.2.6), which evolves in time along with the state variables governing synaptic transmission. The greater the connection probability between neurons, the longer the reverberation, the greater the accumulation of

presynaptic Ca^{2+} and asynchronous release, and the greater the probability of a PSCC during a period following the reverberation (Fig. 6.5c,d).

In TTX-treated cultures, increases in mEPSC size (Fig. 5.2a) may amplify the effect of high asynchronous release rates, accounting for a likelihood of emergence of spontaneous activity above that predicted from reverberation duration alone (Fig. 5.8b). Thus, networks with strong, abundant synapses are more likely to produce long reverberations, and these reverberations are more likely to trigger subsequent PSC clusters. Such a conclusion may seem obvious, but the steepness of the quantitative relationship between these variables, as evidenced from the simulations in Fig. 6.1h and the heuristic approximation in 6.5d, exceeds intuitive expectations.

One might argue that a PSCC observed during a reverberation and a PSC cluster observed after a reverberation has ended are in fact the same phenomenon. Accordingly, there would be no distinction between interminable spontaneous activity and an infinitely long reverberation. However, this conflates events obeying distinct temporal distributions. Figure 6.5e shows the probability of a subsequent PSC cluster drops sharply after a PSC cluster is observed, due to a sharp drop in the occupancy of state X , the readily available synaptic resource. This probability recovers towards a peak value as X is refilled on timescale τ_r . This peak value determines the most likely time of a PSC cluster in the midst of a reverberation (Fig. 6.5f). Because of the narrow width of this peak, the timing of the next PSC cluster within a reverberation can usually be predicted to within ~ 100 ms.

However, if a PSC cluster does not occur within several hundred milliseconds, the decline of presynaptic $[\text{Ca}^{2+}]$, and consequently of the asynchronous release rate, reduces the probability again. However, the recovery of neurotransmitter from pool S , on timescale τ_s , can

provide synapses with sufficient resources to sustain this probability at a non-negligible level for many seconds. The peak of this latter probability regime may be extremely broad, and thus the timing of PSC clusters during spontaneous activity can be highly variable (Fig. 5.7f).

Thus, there are two modes in the probability distribution for inter-PSC cluster intervals (Fig. 6.5e). The first mode, determined by the interplay between the short-term depression parameters μ and τ_r , reflects the interval between PSC clusters within a reverberation or spontaneous network event. The second mode, determined by τ_s and the dynamics of Ca^{2+} clearance and asynchronous release (eqs. 6.1-3), reflects the interval between spontaneous network events.

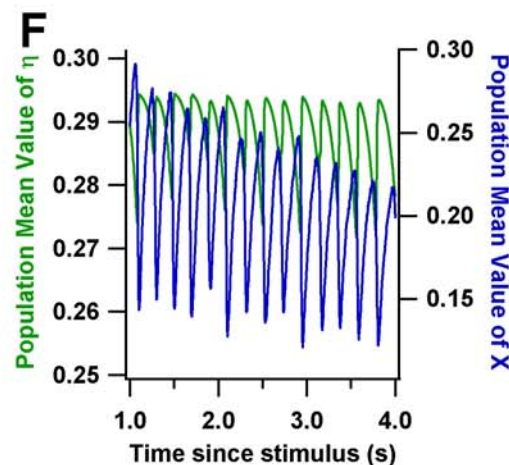
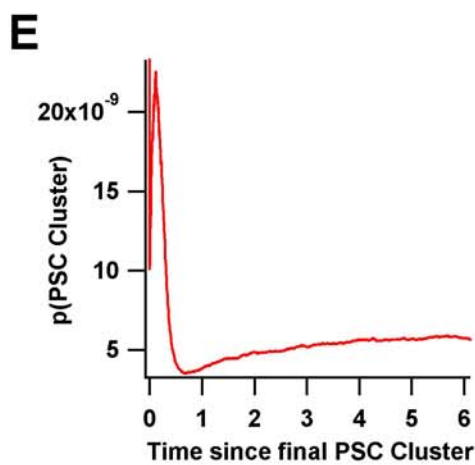
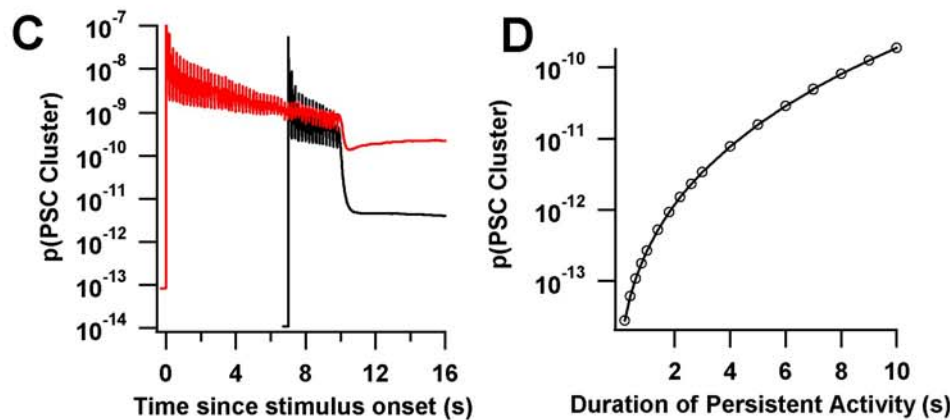
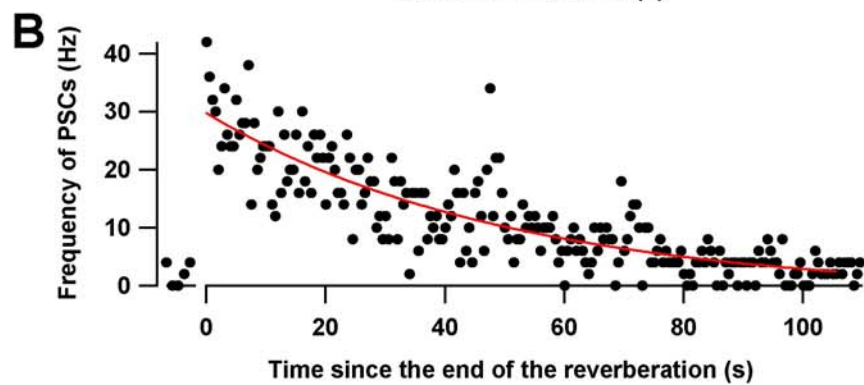
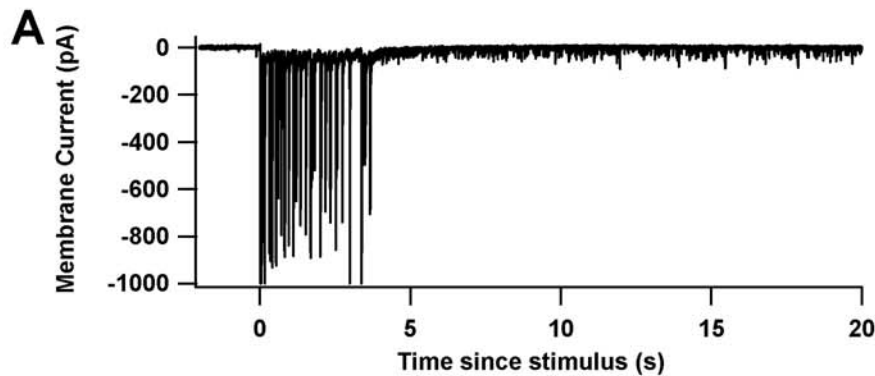


Figure 6.5: The probability of a subsequent, spontaneous synchronous network event increases with reverberation duration. **A**, Example of a reverberation, illustrating the elevation in the spontaneous EPSC after the reverberation has ended. **B**, Time course of spontaneous EPSC rate after the end of the reverberation. The red line is an exponential fit ($\tau = 51$ s). **C**, Two responses from a heuristic model (Methods, 6.2.3), in which postsynaptic responses are silenced, and every neuron is forced to spike at 5 Hz, to simplify conceptual illustration and enable calculation of a PSC cluster hazard probability function $p(\text{PSCC})$. This probability, heuristically computed according to section 6.2.6 (eq. 6.14, dropping a constant of proportionality), is orders of magnitude greater after the long spike train (red) than after the short spike train (black). **D**, Summary data for simulations like those shown in **C**, showing the steep increase in the probability of a spontaneous synchronous network event 5 seconds after the end of a period of persistent activity. **E**, Expansion of the region immediately following the final spike of the red trace in **C**, with the time axis normalized to the time of that spike. This illustrates the bimodal nature of the hazard probability function, with the first mode reflecting sharply timed PSC clusters within a reverberation, and the second mode coarsely times PSC clusters associated with spontaneous network events. **F**, In contrast to the spontaneous activity regime, the regular monotonically-increasing intervals of PSCC during a reverberation (Fig. 5.8a) is generated by the interplay between the recovery of the readily-releasable neurotransmitter pool (X , blue line), and the decay of the asynchronous release rate per releasable vesicle (η , green line). After each PSCC, these values approach 1 and ~ 0 , respectively, until a PSCC becomes exceedingly likely. The rundown of X over time is due to the accumulation of neurotransmitter in S (Fig. 6.1), and increases the time required for X to reach the level required for PSCC generation, accounting for the steady increase in inter-PSCC-intervals during a reverberation.

6.3.5. Synaptic states and the emergence of spontaneous activity

Motivated by the finding that persistent activity can increase the time constant for the decay of elevated $[Ca^{2+}]$ to baseline levels (Pal et al., 1999), I considered whether repetitive activation of neurons could saturate the Ca^{2+} -clearance machinery. To this end, I increased the realism of the model by making the Ca^{2+} buffering process both finite in capacity and reversible (Methods 6.2.1, eqs. 6.1-2). Doing so had negligible effects on single reverberations, because presynaptic Ca^{2+} accumulation during one reverberation was too limited to approach buffer saturation or for the unbinding of Ca^{2+} from buffer to contribute substantially to asynchronous release. I then simply increased the duration of the simulation to accommodate multiple stimulus-evoked reverberations, at 30 second intervals, without resetting variables. In some simulations, due to variability in the randomly generated network topology, this led to the emergence of spontaneous activity after a sufficient number of reverberations (Fig. 6.6a), culminating in continuous ~ 1 Hz network events (Fig. 6.6b). The spontaneous activity resulted from Ca^{2+} buffers slowly saturating and becoming unable to adequately regulate $[Ca^{2+}]$ (Fig. 6.6c), permitting asynchronous release to become dominant.

The evidence presented thus far is sufficient to propose an explanation for the emergence of spontaneous activity based upon the interaction between synaptic depression and asynchronous release. If synaptic efficacy is sufficiently low, reverberations will tend to be short, producing only low asynchronous release rates. These low rates combined with the small size of synaptic currents makes the likelihood of a spontaneous network event small, permitting synapses to recover from depression until the next stimulus. That stimulus, faced with a network recovered from synaptic depression, will produce a reverberation of similar length to the last (Fig. 5.7a,b).

However, if synaptic efficacy is sufficiently high, reverberations will tend to be long, producing high asynchronous release rates. These high rates combined with the larger size of synaptic currents are likely to cause a spontaneous network event. This event may in turn cause a reverberation, or, if the network has not sufficiently recovered from synaptic depression, may terminate after one or a few PSCCs. However, this event will, by further increasing presynaptic $[Ca^{2+}]$, boost the rate of asynchronous release. This will further increase the probability of a subsequent spontaneous network event. This positive feedback generation of network events can continue indefinitely, leading to interminable spontaneous activity (Fig. 6.6a,b).

Because spontaneous activity is a positive feedback process in this model, the hysteresis observed in the experimental data (Fig. 5.9) is readily observed (Fig. 6.6d). Escape from the spontaneous activity state cannot occur until the positive feedback loop is broken, which requires sufficiently low values of q to avoid the generation of spontaneous network events and to allow presynaptic $[Ca^{2+}]$ to return to baseline levels.

Since asynchronous release is stochastic, the positive feedback process can only be described probabilistically. However, because many of the steps in this transition are dependent upon ρ and q , the probability of the transition from stimulus-evoked reverberation to stimulus-independent spontaneous activity should exhibit a steep dependence on these quantities. Indeed, values of q associated with a very small probability of spontaneous activity emergence (Fig. 6.6e) are only $\sim 10\%$ lower than values likely to result spontaneous activity. This may explain the effectiveness of small doses of CNQX in preventing this activity from emerging in TTX-treated networks.

To explain the emergence of spontaneous activity in TTX-treated networks, which are associated with increases in ρ but not evoked synaptic amplitudes (Fig. 5.2c,e), I conducted

simulations for values of ρ between 0.15 and 0.2 (low ρ , by analogy to control networks) and between 0.2 and 0.25 (high ρ , by analogy to TTX-treated networks). The rates of spontaneous activity observed at the end of these simulations (Fig. 6.6f) compare favorably with experimental data from control and TTX-treated network (Fig. 5.8a). Thus, differences in both the probability of emergence and in the degree of spontaneous activity in these two kinds of networks can be explained by differences in ρ , which are observed experimentally. Lastly, I cast this ρ -dependence as a probability of transition from stimulus-evoked reverberation to totally spontaneous activity (Fig. 6.6g). Combining this relationship with the dependence of reverberation duration on ρ (Fig. 6.2h) reveals a narrow range of ρ (Fig. 6.6g, gray band) for which reverberation can be evoked, but is unlikely to generate interminable spontaneous activity.

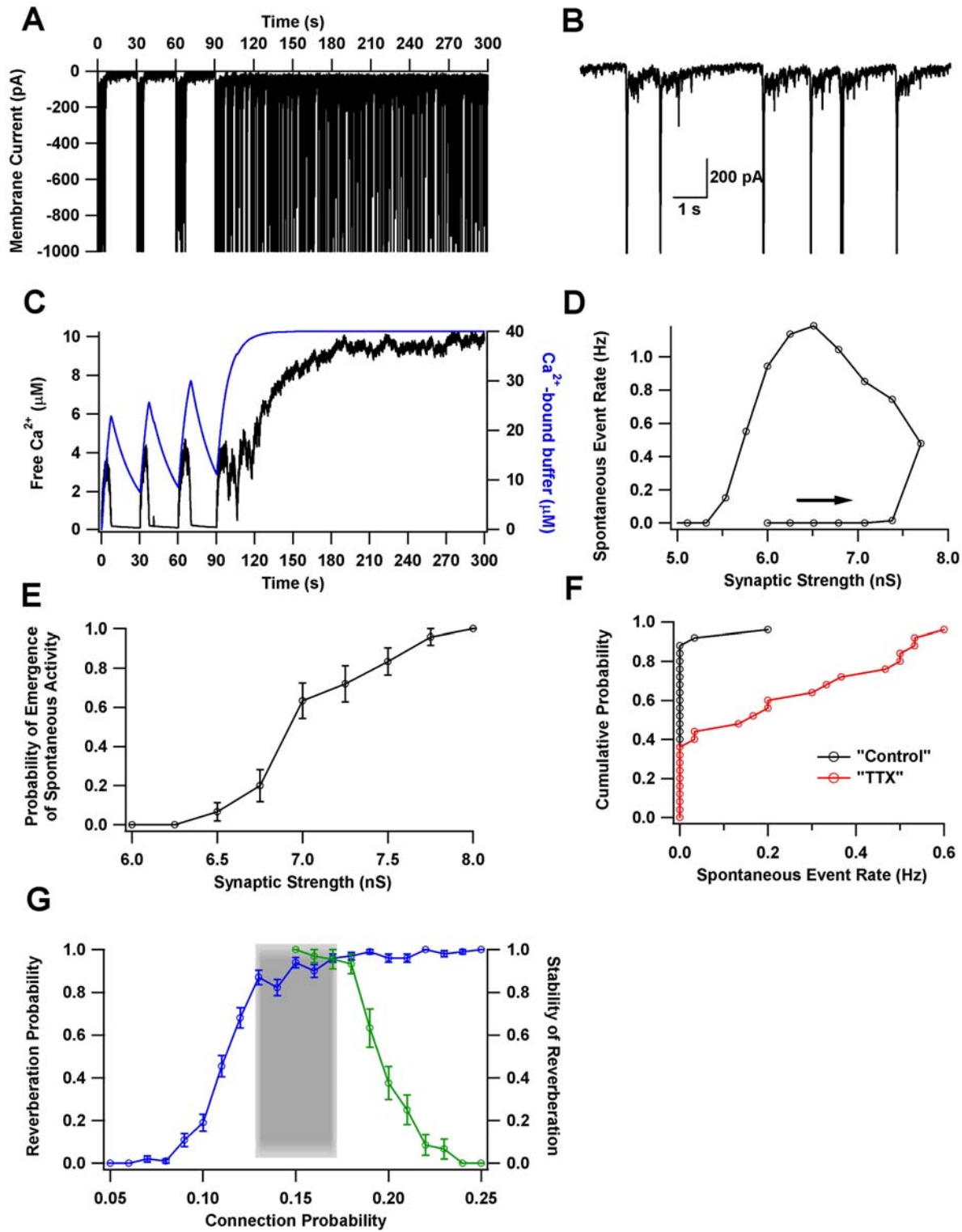


Figure 6.6: The activity-dependent emergence of spontaneous activity is dependent on synaptic connectivity, and leaves a limited connectivity regime for stable reverberation. **A**, In an example simulation, spontaneous activity emerges after the 4th stimulus-evoked reverberation and does not abate. **B**, Expansion of the temporal region indicated with a red line in *A*. **C**, Time course of average presynaptic $[Ca^{2+}]$ and concentration of calcium-bound buffer for the same simulation. This time course suggests two stable activity patterns, one for low $[Ca^{2+}]$ (quiescence), and one for high $[Ca^{2+}]$ (spontaneous activity). With each reverberation, there is a possibility of gravitating towards the second of these patterns, rather than returning to the first. **D**, Simulation performed by increasing q by 5% increments immediately before each stimulus. When spontaneous activity emerged, q was reduced by 5% with each stimulus. This shows hysteresis in the relationship between q and spontaneous activity, explaining the inability of small doses of CNQX to abolish spontaneous activity once it has emerged. **E**, Dependence of the emergence of spontaneous activity on the maximal unitary synaptic conductance q . Small reductions in the model parameter q , analogous to small doses of CNQX in experiments, can dramatically reduce the likelihood that spontaneous activity will emerge. Probability reflects the fraction of model network realizations for which spontaneous activity (spontaneous event rate > 0.1 Hz) had emerged after 300 seconds (10 stimuli) for a fixed value of q . For *D* and *E*, $\rho=0.2$. **F**, Emergent spontaneous event rates for a number of independent networks. The black line contains simulations done with synaptic connection probability $\rho=0.15-0.2$, and the red line contains simulations with $\rho=0.2-0.25$. **G**, Dependence of the emergence of spontaneous activity on the connection probability ρ , overlaid with the duration of reverberations from Fig. 6.2h. The gray zone indicates a region of stability, where networks can exhibit reverberations with a negligible

probability of the emergence of spontaneous activity. In *E*, *F*, and *G*, measurements of spontaneous activity were made following ten stimuli at 30 second intervals.

6.4. DISCUSSION

6.4.1. A critical level of synaptic connectivity supports stable reverberation

There is no *a priori* reason a level of recurrent connectivity strong enough to support reverberation, but weak enough to avoid the emergence of spontaneous activity must exist. In fact, in sufficiently large cultured hippocampal networks, such a level may not exist (Volman et al., 2008), which could explain why either quiescence or spontaneous activity, but not reverberation, is typically observed in confluent cultures of hippocampal neurons. In these larger networks, there is an increased probability that any one neuron will stochastically reach its firing threshold. Consequently, the level of connectivity below which spontaneous network events do not emerge could be less than that needed for the network to exhibit stimulus-evoked reverberation. Hence, the hippocampal culture model of epilepsy (Furshpan and Potter, 1989; Sombati and Delorenzo, 1995), which uses large cultured networks, may be a product of an incongruity between synaptic connectivity and network size.

However, for the island networks studied here, there apparently does exist such a level, because control networks routinely exhibit reverberations without the emergence of spontaneous activity for the duration of recording (Fig. 5.7a,b). This level could correspond to the range of values shown in the shaded area in Figure 6.6g, where such behavior is predicted to occur. Consequently, synaptic efficacy in reverberatory networks under control conditions may assume a value that is optimal for the reliable production of stimulus-evoked reverberations. By contrast, TTX-treated networks exhibit greater synaptic connectivity, corresponding to longer

reverberations, and a greater probability of spontaneous activity emergence. While such spontaneous activity after chronic inactivity is not a new observation (Furshpan, 1991), here I describe the activity-dependent dynamics leading to the expression of the spontaneous state.

6.4.2. Linearity of the mapping between synaptic parameters and network responses

The existence of a linear relationship between reverberation duration and both synaptic conductance (Fig. 6.2a,b) and connection probability (Fig. 6.2c,d) is an unexpected but intriguing result. Such a relationship could allow the duration of persistent activity to be precisely and predictably controlled by the synaptic architecture. This would also be true if the relationship were non-linear (but monotonic); however, linearity ensures that a plasticity event that, for example, increases q by a given amount will augment reverberation duration by the same amount regardless of the initial value of q . Consequently, a plasticity process would not need to retain information about the current state of the synaptic matrix before acting to effect precise changes in persistent activity patterns.

6.4.3. Online long-term synaptic plasticity

When I first implemented this model, I assumed that most of the differences between TTX-treated and control cultures strictly reflected synaptic scaling. However, upon further analysis most of the observed differences were due to metaplasticity; synaptic potentiability was augmented in TTX-treated cultures (Fig. 5.5). In principle, I could have implemented a synaptic

potentiation rule in the model, changing values of q or p in the midst of activity. However, there is substantial uncertainty as to what reflects an appropriate implementation of such plasticity. The only certainty in the field, that q or p (or both) change, is already captured in this analysis by varying the initial values of these parameters across simulations. Thus, analogies between highly connected model networks and TTX-treated cultures should apply most appropriately to those cultures in which activity has been restored and synaptic potentiation has already taken place. Changes in excitability or other intrinsic neuronal properties (Table 5.1) could also have been included. Not surprisingly, varying membrane parameters can also alter the duration and probability of model reverberations (data not shown). Further studies may explore the precise relationship between intrinsic excitability and reverberation properties.

6.4.4. Alternative implementations of synaptic transmission

The model assumes that $[Ca^{2+}]$ alone determines the fraction of available vesicles that are released asynchronously, while synchronous release is a constant fraction of available vesicles (μ) but independent of $[Ca^{2+}]$. Experimentally, it is difficult to test this assumption because it requires simultaneously determining the number of released vesicles and the instantaneous size of the available vesicle pool simultaneously. However, evidence from cortical neurons suggests that μ is indeed constant for a given connection (Tsodyks and Markram, 1997). One could imagine other implementations of the model in which synchronous release is also a function of $[Ca^{2+}]$ or history (Tsodyks et al., 2000). While there is no dispute that the synchronous release of vesicles is dependent on elevations in $[Ca^{2+}]$, whether the level of $[Ca^{2+}]$ immediately prior to the action potential determines the fraction of vesicles released is unknown.

I could also have constructed the model such that the rate asynchronous release exhibited less or no dependence on the instantaneous size of the available vesicle pool X . Such a change would be motivated by the observation that asynchronously released vesicles may only correspond to those docked at presynaptic active zones, whose population might remain somewhat invariant as X decreases. By analogy, the number of items currently at the top of a set of queues is invariant to the lengths of those queues. If this change were made, and asynchronous release were more invariant to decreases in X , the interval between PSC clusters within a reverberation would be reduced, because a lesser recovery of X would be required to observe the integration of asynchronous events into an action potential in a single neuron. Accommodating the experimentally observed intervals between PSC clusters would thus require a change in some other parameter, such as a decrease in the action potential threshold V_{thresh} .

6.4.5. Role of asynchronous release

Our definition of asynchronous release is somewhat broader than that used previously (Goda and Stevens, 1994). In particular, I have characterized spontaneous EPSCs occurring seconds after the cessation of spiking as the result of asynchronous release, whereas it could be argued that these events belong to a post-asynchronous regime of spontaneous release. However, I could not identify any obvious timescale on which asynchronous release gives way to another history-dependent form of release (e.g. Figure 6.5b). If all vesicular neurotransmitter release is simply a function of $[Ca^{2+}]$ in presynaptic terminals, there may not be a meaningful quantitative distinction between different phases of asynchronous release, despite the possibility of multiple, distinct, fusion-determining Ca^{2+} sensors in the presynaptic terminal (Nishiki and Augustine,

2004; Saraswati et al., 2007). Nonetheless, in more mature synapses asynchronous release is less prevalent than in juvenile synapses, which would have a substantial impact on the capacity of mature networks to produce either reverberatory behavior, or an activity-dependent transition to spontaneous activity.

Asynchronous release may be homeostatically regulated by activity history on longer timescales, such as those associated with chronic inactivation. By amplifying the “tail” of its own synaptic transmission, a neuron would give its postsynaptic partner a wider time window in which to integrate synaptic signals. This could be of use in a hyperpolarized environment where even a large conductance might be too brief to overcome the membrane time constant and evoke a postsynaptic action potential. However, measurement of changes in asynchronous release is a challenge because the population of asynchronous synaptic currents measured in a postsynaptic neuron are driven by many presynaptic partners. Comparing between control and TTX-treated networks would require enforcing identical activity levels on the two neuronal populations (controlling for the activity-dependence of asynchronous release), or reducing the presynaptic contribution to a single neuron. The first method is impractical, especially since it remains unclear exactly what kinds of similarities in network output should result in identical patterns of asynchronous release. The second would require pharmacologically abolishing all action potentials outside of the recorded neuronal pair, while leaving sufficient levels of asynchronous release between that pair to compute event statistics. I have been unable to devise an experimental protocol to satisfy these dual criteria. However, the activity-dependent emergence of EGTA-AM sensitivity in the spontaneous release of neurotransmitter (Fig. 6.4e,f) indicates the possibility of long-lasting changes in the properties of asynchronous release, at least in chronically inactivated neurons. These changes might be driven by long-term increases in

resting presynaptic $[Ca^{2+}]$, or by an increased sensitivity of the release machinery to calcium; in either case, asynchronous neurotransmission could be enhanced.

6.4.6. Future experimental investigation of presynaptic $[Ca^{2+}]$ as a determinant of network activity

While I have demonstrated computationally that asynchronous release and the finite, reversible nature of calcium buffers could explain the dynamics of the transition between reverberation and spontaneous activity, I have provided very little experimental evidence to support this explanation. Indeed, EGTA-AM reduces the rate of spontaneous events and of asynchronous release events, but any attempt to buffer intracellular calcium is certain to interfere with a whole host of cellular processes. Directly measuring presynaptic $[Ca^{2+}]$, perhaps with calcium-sensitive fluorophores, would provide a more direct test of the model. However, while such fluorophores typically bind to calcium slowly compared with the timescale of evoked, synchronous synaptic transmission (Sabatini and Regehr, 1998), asynchronous release may be nonetheless affected as even slow calcium buffers can reduce its magnitude (Cummings et al., 1996a). An ideal experiment might involve slow buffers that can be both photo-activated and photo-inactivated. After turning calcium buffers on, the model predicts that spontaneous activity should gradually terminate as asynchronous release fails to initiate further spontaneous network events. After turning them back off, it should be possible to evoke reverberation on a background of silence, until spontaneous activity emerges once again.

6.4.7. Asynchronous release interacts with synaptic depression on two timescales to determine network output

In our previous work (Volman et al., 2007), we showed that reverberation could be explained by the interplay between the decay of presynaptic Ca^{2+} concentrations (and the accompanying decay of the asynchronous release rate), and the recovery of synapses from fast synaptic depression, both processes with kinetics on the millisecond timescale. Here, I show that the emergence of spontaneous activity may be governed by a similar interaction between presynaptic Ca^{2+} and the recovery from a slower form of synaptic depression, with kinetics on the second timescale. Thus, the interaction of synaptic depression and presynaptic Ca^{2+} dynamics on two timescales may be essential to understanding the activity patterns of small cultured networks. Such a range of timescales is plausible because neither presynaptic Ca^{2+} clearance nor the synaptic vesicle cycle are governed by first-order kinetics, and are thus likely to have mechanisms spanning a wide range of time constants. Interestingly, there is evidence that changes in neuronal calcium homeostasis can underlie acquired epilepsy (Delorenzo et al., 2005). In our model, this could be achieved by reducing the concentrations, or increasing the off-rates, of calcium buffers. This which would result in high resting $[\text{Ca}^{2+}]$ and synapses for which asynchronous release rates did not sufficiently decay before a threshold of recovery from synaptic depression had been reached. Asynchronous release, previously held in check by depressed synapses, would promote positive feedback resulting in interminable, spontaneous, synchronous network activity.

7. GENERAL DISCUSSION

In the preceding chapters I have shown how postsynaptic Ca^{2+} , mediated by NMDAR subtypes, can implement a history-dependent spike-timing-dependent plasticity. These results inform the principles and mechanisms by which the timing of action potentials is translated into persistent synaptic modifications. I then examined the role of such synaptic modifications in determining the existence and stability of persistent activity patterns in small neuronal networks. In addition to those discussed in each chapter, several larger issues arise which concern the fundamental design, interpretation, and unification of these experiments and simulations, which I will address here.

7.1. GENERALIZATION OF STDP AS A UNIVERSAL RULE OF SYNAPTIC MODIFICATION

It has been shown that postsynaptic Ca^{2+} dynamics can explain first and second-order STDP rules in a variety of systems while simultaneously explaining the results of more conventional plasticity protocols (Shouval et al., 2002; Rubin et al., 2005). One is tempted to interpret this as evidence that plasticity induced by these conventional protocols is an artifactual consequence of such protocols utilizing intrinsic STDP “machinery”, and that STDP is the fundamental phenomenon of synaptic plasticity. But this over-reaching interpretation has been criticized

(Lisman and Spruston, 2005), in part because some less-appreciated forms of plasticity, such as those not requiring postsynaptic action potentials or involving timing-dependent synaptic integration within the dendritic tree, are not well explained by STDP or its underlying principles. Nonetheless, it seems plausible that multiple plasticity induction protocols (at least some of which are hoped to have relevance to ongoing synaptic plasticity *in vivo*) may harness the same molecular signaling networks, though perhaps in different ways.

7.2. SEPARATION OF THE STRUCTURAL AND SIGNALING ROLES OF A SINGLE MOLECULE

Unraveling the role of specific signals in bidirectional synaptic plasticity remains a controversial endeavor. This stems in part from an unwarranted assumption that the role of a synaptic protein in the induction of plasticity must parallel its role in the expression of plasticity. As clear counterexample, mutation of NR2B-NMDAR c-termini abolishes LTP expression in the rodent hippocampus (Barria and Malinow, 2005), but the activation of this NMDAR subtype is unnecessary for LTP induction in the same system (Liu et al., 2004). The possibility that a molecule could subserve distinct signaling and structural roles has only recently become appreciated (Sanhueza et al., 2007). This illustrates the dangers that can result from attempting to combine genetic and pharmacological data into a simplistic description of a biological process, when in fact multiple techniques may address multiple aspects of molecular function.

7.3. INTEGRATION OF NMDAR SUBTYPE SELECTIVITY INTO A REALISTIC DYNAMIC MODEL OF STDP

Since NMDAR subtypes are differentially responsible for spike-timing-dependent LTP and LTD, how might this influence the postsynaptic $[Ca^{2+}]$ detector model from chapter 2? That model preceded the NMDAR subtype results, and I elected to simplify it substantially to illustrate the implications of subtype selectivity in chapter 3. The primary change was to associate the potentiation module with NR2A-NRs and the depression module with NR2B-NRs. However, I did not specifically attribute this subtype specificity to differences in either spatial localization, signaling pathways, or receptor kinetics. All three of these could be implemented in the full $[Ca^{2+}]$ detector model by splitting $[Ca^{2+}]$ into two independent variables or implementing multiple NMDAR decay constants. Because the full model already uses kinetics (in part) to distinguish between potentiation and depression, implementing multiple NMDAR decay constants could further increase the robustness of the model.

7.4. COOPERATIVITY ACROSS SPIKE PAIRINGS CAN INFORM THE PARAMETER CHOICES IN THE DYNAMIC MODEL

The observation of cooperativity among spike pairings in the statistical model of chapter 4 could inform the choice of τ_w , the decay time of the final integrated plasticity output, in the calcium detector model of chapter 2. As indicated in discussion section 2.4, the biophysical determinants of τ_w could also dictate s_0 , the characteristic number of pairings required to approach p , the probability of synaptic potentiation in response to a single pairing. By combining the detector

model and the statistical model, and using the mean value of w in the interval between successive spike pairings to determine the instantaneous value of p , one could derive quantitative predictions of the potentiation resulting from arbitrary numbers of spike pairings, and how its magnitude might change with prior potentiation history. Furthermore, this method could be applied to arbitrary combinations of pre- and postsynaptic spikes, since the detector model putatively applies to these as well, provided that potentiation “wins” in response to these combinations. Addressing synaptic depression would require additional assumptions, as well as equations not formulated in the statistical model.

7.5. RECIPROCAL IMPACT OF STDP AND NETWORK ACTIVITY

The two major themes of my graduate research have been a) phenomena and mechanisms of STDP (chapter 2-4), and b) implications of synaptic plasticity on the behavior of neuronal networks (chapter 5-6). Integrating these, what are the implications of STDP on the behavior of such networks? Numerous modeling studies have sought to address this question, concluding that STDP shapes networks to support a wide variety of useful behaviors (see section 1.1.3). However, experimental support for the predictions generated by such models has been limited, and has typically addressed primarily feed-forward circuits (Yao and Dan, 2001; Meliza and Dan, 2006).

Here I had the opportunity to demonstrate the reciprocal impact of STDP on reverberations in hippocampal culture. However, I was limited by the absence of a decisive experimental manipulation that abolishes only STDP without interfering with other neuronal processes, including conventional forms of synaptic plasticity. Furthermore, I did not have

precise control of pre- and postsynaptic spike times in network experiments. Even when recording from two neurons, spiking activity is largely determined by synaptic input from a large number of uncontrolled afferents; furthermore, the heterosynaptic spread of STDP from other cells in the network could also interfere with measurements of synaptic modification in the recorded neurons (Tao et al., 2000).

Could chronic network inactivation modify the rules of STDP? In order to observe homeostatic responses in a system, it is necessary that the system be perturbed from its steady-state. Ongoing network activity in developing neurons in the absence of TTX is likely required for TTX to effect such a perturbation. In networks with sufficient neuronal density, such ongoing activity is typical (Chen et al., 2006). However, STDP experiments require identifying evoked monosynaptic currents uncontaminated by polysynaptic components, a condition that can only be readily obtained at low culture densities, where ongoing activity is less likely to exist. Thus, an incongruity in the culture density requirements for these two experimental preparations makes testing STDP in chronically inactivated cultures nearly impossible. I have been fortunate enough to obtain one data point for this condition. LTP of ~85% was obtained, far outstripping the mean value of ~20% obtained under control conditions. Ascertaining the robustness of this phenomenon for a significant sample size will be left to future researchers to discover, perhaps armed with a more accommodating preparation.

I elected not to incorporate any synaptic learning rules in the network model for reverberation. Given the findings in chapters 3 and 4, I could have implemented an STDP rule with an uncharacteristically high level of detail compared to existing network models. However, despite all that we have learned about the mechanics of STDP, my intuition is that our current models are still too crude to do justice to the complexity of the phenomenon, especially when

specific predictions about the structure of network activity on short timescales are to be made.

Again, I hope this bridge will one day be crossed.

7.6. LIMITATIONS OF USING TTX TO STUDY NETWORK HOMEOSTASIS

In chapter 5 and 6 I considered the impact of a saturating does of TTX on the potential homeostatic response of a neuronal network. Could TTX have other effects beyond the blockade of voltage-gated sodium channels? I know of no other reported effects of TTX at the concentration used here ($1 \mu\text{M}$). Furthermore, at this low concentration and for a low molecular weight protein (319.2), one might argue that off-target interactions are less likely than for more complex gene products with many potential binding sites, applied at higher concentrations.

However, it can be argued that any response observed in response to TTX application is not relevant to on-going homeostasis *in vivo*, because any compensatory changes in synaptic gain or intrinsic excitability still leave neurons unable to discharge action potentials. Without an achievable target, it cannot be argued that homeostasis has actually occurred in the presence of TTX. I concede that the response observed in the presence of TTX is not itself homeostasis. Rather, I hypothesize that homeostasis occurs under control conditions, and that the homeostatic feedback mechanism is mediated in some fashion by sodium action potentials. By adding TTX, I can provide evidence for this hypothesis by observing increases in synaptic efficacy, plasticity, and excitability in response to a decrease (in this case an abolition) of spiking activity. Thus, I have simply demonstrate that neurons can exhibit these responses. I then interpreted observations in control networks to be the product of neurons utilizing these responses to achieve homeostatic setpoints. By contrast to a genetic knockout or surgical ablation experiment, I am

not trying to deduce the function of that which was eliminated. For example, I do not maintain that the purpose of action potentials is to precisely regulate neuronal output. Rather, I am evaluating the response of other components of the system to the absence of action potentials, and I am inferring that action potentials carry information used to control the activity of these components.

Nonetheless, future experiments could involve the use of subsaturating doses of TTX in order to determine whether homeostatic setpoints can actually be achieved by the system in response to modest challenges. This would complement existing evidence that the statistical structure of network activity is such a setpoint, and that modest, experimentally imposed bidirectional changes in activity levels can be countered by neuronal networks to reestablish a target level (Beggs and Plenz, 2003).

7.7. RELEVANCE TO EPILEPSY *IN VIVO*

I have carefully avoided making an abundance of overt references to epilepsy in this work, out of respect for the vast literature showing that it is more than just a trivial consequence of recurrent excitation. Nonetheless, I hope the ideas presented here will be of interest to those searching for mechanistic understanding of seizure generation. Specifically, the roles of synaptic depression and asynchronous release, and their temporal interactions; synaptic scaling and metaplasticity; and calcium buffering capacity and kinetics, may all be viable candidates for further investigation.

7.8. EPILOGUE

I have provided evidence that synaptic efficacy is regulated by a variety of activity patterns on a variety of timescales. In principle, this “efficacy”, which I have assiduously avoided defining carefully, is governed by a master function $f(t, \text{history})$, determining the distributions from which individual values are randomly drawn. In practice, I report a sparse sampling of values from this multidimensional function. We are like the proverbial blind men of Indian folklore (Saxe, 1878), touching different parts of synaptic dynamics. By putting our disparate observations together, we hope to see that it is not simply a spear, a snake, or a wall, but an elephant.

8. GENERAL METHODS

8.1. CELL CULTURE

For all experiments, low-density cultures of dissociated embryonic rat hippocampal neurons were prepared as previously described (Wilcox et al., 1994; Wang et al., 2005). Hippocampi were removed from embryonic day 18–20 (E18–20) rats and treated with trypsin for 15 min at 37°C, followed by washing and gentle trituration. The dissociated cells were plated at densities of 20,000–80,000 cells/ml on poly-L-lysine-coated glass coverslips in 35 mm Petri dishes, and placed in an incubator at 37°C. The poly-L-lysine on the coverslips was applied in a hexagonal pattern of ~1 mm diameter circular spots using a custom made stamp, with ~1.5 mm between the centers of adjacent spots. The plating medium was DMEM (BioWhittaker, Walkersville, MD) supplemented with 10% heat-inactivated fetal bovine serum (Hyclone, Logan, UT), 10% Ham's F12 with glutamine (BioWhittaker), and 50 U/ml penicillin–streptomycin (Sigma, St. Louis, MO). For STDP experiments, 20,000 cells/ml was a typical density, whereas for network experiments, 60,000 cells/ml was used. Twenty-four hours after plating, 1/3 of the culture medium was replaced with the above medium, supplemented with 20 mM KCl. Both glial and neuronal cell types are present under these culture conditions.

8.2. ELECTROPHYSIOLOGY

At 10-15 DIV, pairs of potentially synaptically connected glutamatergic neurons were recorded using the perforated whole-cell patch-clamp technique at room temperature. The pipette solution contained (in mM): K-gluconate 136.5, KCl 17.5, NaCl 9, MgCl₂ 1, HEPES 10, EGTA 0.2, and 200 µg/ml amphotericin B (pH 7.2). The external bath solution contained (in mM): NaCl 150, KCl 3, CaCl₂ 3, MgCl₂ 2, HEPES 10, and glucose 5 (pH 7.4).

8.3. PHARMACOLOGY

Throughout the recordings, cultures were perfused with fresh HBS at a constant rate of ~1 ml/min. Stock solutions of all drugs were first prepared in water or DMSO and diluted (1:1000) in HBS when being used.

8.4. ANALYSIS AND STATISTICS

Data collection, analysis, and production of figures were done using Igor Pro (Wavemetrics). A bootstrap comparison of means was used for all statistical comparisons, unless otherwise indicated. A Bonferroni correction for multiple comparisons to the same control was made where applicable. Comparisons to unity (100%, no change in synaptic strength) remain uncorrected. Values are reported as mean ± SEM, and all error bars in graphs are SEM, unless indicated otherwise.

BIBLIOGRAPHY

- Abbott LF, Nelson SB (2000) Synaptic plasticity: taming the beast. *Nat Neurosci* 3 Suppl:1178-1183.
- Abbott LF, Varela JA, Sen K, Nelson SB (1997) Synaptic depression and cortical gain control. *Science* 275:220-224.
- Abenavoli A, Forti L, Bossi M, Bergamaschi A, Villa A, Malgaroli A (2002) Multimodal quantal release at individual hippocampal synapses: evidence for no lateral inhibition. *J Neurosci* 22:6336-6346.
- Abraham WC (2003) How long will long-term potentiation last? *Philos Trans R Soc Lond B Biol Sci* 358:735-744.
- Abraham WC, Bear MF (1996) Metaplasticity: the plasticity of synaptic plasticity. *Trends Neurosci* 19:126-130.
- Aitken PG, Breese GR, Dudek FF, Edwards F, Espanol MT, Larkman PM, Lipton P, Newman GC, Nowak TS, Jr., Panizzon KL, et al. (1995) Preparative methods for brain slices: a discussion. *J Neurosci Methods* 59:139-149.
- Akaike N, Harata N (1994) Nystatin perforated patch recording and its applications to analyses of intracellular mechanisms. *Jpn J Physiol* 44:433-473.
- Albensi BC, Oliver DR, Toupin J, Odero G (2007) Electrical stimulation protocols for hippocampal synaptic plasticity and neuronal hyper-excitability: are they effective or relevant? *Exp Neurol* 204:1-13.
- Altman J, Bayer SA (1990) Migration and distribution of two populations of hippocampal granule cell precursors during the perinatal and postnatal periods. *J Comp Neurol* 301:365-381.
- Amaral DG, Ishizuka N, Claiborne B (1990) Neurons, numbers and the hippocampal network. *Prog Brain Res* 83:1-11.
- Andrasfalvy BK, Magee JC (2001) Distance-dependent increase in AMPA receptor number in the dendrites of adult hippocampal CA1 pyramidal neurons. *J Neurosci* 21:9151-9159.

- Artola A, Singer W (1993) Long-term depression of excitatory synaptic transmission and its relationship to long-term potentiation. *Trends Neurosci* 16:480-487.
- Augustine GJ, Neher E (1992) Calcium requirements for secretion in bovine chromaffin cells. *J Physiol* 450:247-271.
- Bagal AA, Kao JP, Tang CM, Thompson SM (2005) Long-term potentiation of exogenous glutamate responses at single dendritic spines. *Proc Natl Acad Sci U S A* 102:14434-14439.
- Bains JS, Longacher JM, Staley KJ (1999) Reciprocal interactions between CA3 network activity and strength of recurrent collateral synapses. *Nat Neurosci* 2:720-726.
- Banker G, Goslin K (1998) *Culturing Nerve Cells*, Second Edition.
- Banker GA, Cowan WM (1977) Rat hippocampal neurons in dispersed cell culture. *Brain Res* 126:397-342.
- Barrett EF, Stevens CF (1972) The kinetics of transmitter release at the frog neuromuscular junction. *J Physiol* 227:691-708.
- Barria A, Malinow R (2005) NMDA Receptor Subunit Composition Controls Synaptic Plasticity by Regulating Binding to CaMKII. *Neuron* 48.
- Barth AL, Malenka RC (2001) NMDAR EPSC kinetics do not regulate the critical period for LTP at thalamocortical synapses. *Nat Neurosci* 4:235-236.
- Bartos M, Vida I, Jonas P (2007) Synaptic mechanisms of synchronized gamma oscillations in inhibitory interneuron networks. *Nat Rev Neurosci* 8:45-56.
- Bashir ZI (2003) On long-term depression induced by activation of G-protein coupled receptors. *Neurosci Res* 45:363-367.
- Bayer KU, De Koninck P, Leonard AS, Hell JW, Schulman H (2001) Interaction with the NMDA receptor locks CaMKII in an active conformation. *Nature* 411:801-805.
- Bear MF, Malenka RC (1994) Synaptic plasticity: LTP and LTD. *Curr Opin Neurobiol* 4:389-399.
- Bear MF, Cooper LN, Ebner FF (1987) A physiological basis for a theory of synapse modification. *Science* 237:42-48.
- Beggs JM, Plenz D (2003) Neuronal avalanches in neocortical circuits. *J Neurosci* 23:11167-11177.
- Bell CC, Han VZ, Sugawara Y, Grant K (1997) Synaptic plasticity in a cerebellum-like structure depends on temporal order. *Nature* 387:278-281.

- Bender VA, Bender KJ, Brasier DJ, Feldman DE (2006) Two coincidence detectors for spike timing-dependent plasticity in somatosensory cortex. *J Neurosci* 26:4166-4177.
- Bennett MR, Gibson WG, Robinson J (1994) Dynamics of the CA3 pyramidal neuron autoassociative memory network in the hippocampus. *Philos Trans R Soc Lond B Biol Sci* 343:167-187.
- Berberich S, Punnakkal P, Jensen V, Pawlak V, Seburg PH, Hvalby O, Kohr G (2005) Lack of NMDA receptor subtype selectivity for hippocampal long-term potentiation. *J Neurosci* 25:6907-6910.
- Berke JD, Hetrick V, Breck J, Greene RW (2008) Transient 23-30 Hz oscillations in mouse hippocampus during exploration of novel environments. *Hippocampus* 18:519-529.
- Bi GQ, Poo MM (1998) Synaptic modifications in cultured hippocampal neurons: dependence on spike timing, synaptic strength, and postsynaptic cell type. *J Neurosci* 18:10464-10472.
- Bi GQ, Rubin JE (2005) Timing in synaptic plasticity: from detection to integration. *Trends Neurosci* 28:222-228.
- Bienenstock EL, Cooper LN, Munro PW (1982) Theory for the development of neuron selectivity: orientation specificity and binocular interaction in visual cortex. *J Neurosci* 2:32-48.
- Blackstone C, Sheng M (2002) Postsynaptic calcium signaling microdomains in neurons. *Front Biosci* 7:d872-885.
- Bliss T, Schoepfer R (2004) Neuroscience. Controlling the ups and downs of synaptic strength. *Science* 304:973-974.
- Bliss TV, Lømo T (1973) Long-lasting potentiation of synaptic transmission in the dentate area of the anaesthetized rabbit following stimulation of the perforant path. *J Physiol (Lond)* 232:331-356.
- Blundon JA, Wright SN, Brodwick MS, Bittner GD (1993) Residual free calcium is not responsible for facilitation of neurotransmitter release. *Proc Natl Acad Sci U S A* 90:9388-9392.
- Bollmann JH, Sakmann B (2005) Control of synaptic strength and timing by the release-site Ca²⁺ signal. *Nat Neurosci* 8:426-434.
- Bolz J (1994) Cortical circuitry in a dish. *Curr Opin Neurobiol* 4:545-549.
- Bortolotto ZA, Fitzjohn SM, Collingridge GL (1999) Roles of metabotropic glutamate receptors in LTP and LTD in the hippocampus. *Curr Opin Neurobiol* 9:299-304.

- Bozdagi O, Shan W, Tanaka H, Benson DL, Huntley GW (2000) Increasing numbers of synaptic puncta during late-phase LTP: N-cadherin is synthesized, recruited to synaptic sites, and required for potentiation. *Neuron* 28:245-259.
- Bradshaw JM, Kubota Y, Meyer T, Schulman H (2003) An ultrasensitive Ca²⁺/calmodulin-dependent protein kinase II-protein phosphatase 1 switch facilitates specificity in postsynaptic calcium signaling. *Proc Natl Acad Sci U S A* 100:10512-10517.
- Brimecombe JC, Boeckman FA, Aizenman E (1997) Functional consequences of NR2 subunit composition in single recombinant N-methyl-D-aspartate receptors. *Proc Natl Acad Sci U S A* 94:11019-11024.
- Brody DL, Yue DT (2000) Release-independent short-term synaptic depression in cultured hippocampal neurons. *J Neurosci* 20:2480-2494.
- Burgess N, Maguire EA, O'Keefe J (2002) The human hippocampus and spatial and episodic memory. *Neuron* 35:625-641.
- Burnashev N, Rozov A (2005) Presynaptic Ca²⁺ dynamics, Ca²⁺ buffers and synaptic efficacy. *Cell Calcium* 37:489-495.
- Buzsaki G (1986) Hippocampal sharp waves: their origin and significance. *Brain Res* 398:242-252.
- Buzsaki G (2002) Theta oscillations in the hippocampus. *Neuron* 33:325-340.
- Buzsaki G, Chrobak JJ (2005) Synaptic plasticity and self-organization in the hippocampus. *Nat Neurosci* 8:1418-1420.
- Buzsaki G, Chen LS, Gage FH (1990) Spatial organization of physiological activity in the hippocampal region: relevance to memory formation. *Prog Brain Res* 83:257-268.
- Caeser M, Brown DA, Gahwiler BH, Knopfel T (1993) Characterization of a calcium-dependent current generating a slow afterdepolarization of CA3 pyramidal cells in rat hippocampal slice cultures. *Eur J Neurosci* 5:560-569.
- Cai Y, Gavornik JP, Cooper LN, Yeung LC, Shouval HZ (2007) Effect of stochastic synaptic and dendritic dynamics on synaptic plasticity in visual cortex and hippocampus. *J Neurophysiol* 97:375-386.
- Carafoli E (2004) Calcium signaling: a historical account. *Biol Res* 37:497-505.
- Carter C, Benavides J, Legendre P, Vincent JD, Noel F, Thuret F, Lloyd KG, Arbilla S, Zivkovic B, MacKenzie ET, et al. (1988) Ifenprodil and SL 82.0715 as cerebral anti-ischemic agents. II. Evidence for N-methyl-D-aspartate receptor antagonist properties. *J Pharmacol Exp Ther* 247:1222-1232.

- Chamberlin NL, Dingledine R (1989) Control of epileptiform burst rate by CA3 hippocampal cell afterhyperpolarizations in vitro. *Brain Res* 492:337-346.
- Chamberlin NL, Traub RD, Dingledine R (1990) Role of EPSPs in initiation of spontaneous synchronized burst firing in rat hippocampal neurons bathed in high potassium. *J Neurophysiol* 64:1000-1008.
- Charpak S, Gahwiler BH, Do KQ, Knopfel T (1990) Potassium conductances in hippocampal neurons blocked by excitatory amino-acid transmitters. *Nature* 347:765-767.
- Chen C, Thompson RF (1995) Temporal specificity of long-term depression in parallel fiber--Purkinje synapses in rat cerebellar slice. *Learn Mem* 2:185-198.
- Chen C, Chen L, Lin Y, Zeng S, Luo Q (2006) The origin of spontaneous synchronized burst in cultured neuronal networks based on multi-electrode arrays. *Biosystems* 85:137-143.
- Chen HX, Otmakhov N, Lisman J (1999a) Requirements for LTP induction by pairing in hippocampal CA1 pyramidal cells. *J Neurophysiol* 82:526-532.
- Chen LY, Rex CS, Casale MS, Gall CM, Lynch G (2007) Changes in synaptic morphology accompany actin signaling during LTP. *J Neurosci* 27:5363-5372.
- Chen N, Luo T, Raymond LA (1999b) Subtype-dependence of NMDA receptor channel open probability. *J Neurosci* 19:6844-6854.
- Chhikara R, Folks L (1989) The inverse gaussian distribution: theory, methodology, and applications. New York: Marcel Dekker.
- Christie BR, Magee JC, Johnston D (1996) Dendritic calcium channels and hippocampal long-term depression. *Hippocampus* 6:17-23.
- Clarke R, Johnson J (2005) Voltage-Dependent Gating of NMDA Receptors in the Presence and Absence of Magnesium. SFN Annual Meeting:721.726.
- Clem RL, Barth A (2006) Pathway-specific trafficking of native AMPARs by in vivo experience. *Neuron* 49:663-670.
- Clem RL, Barth AL (2008) Science In Press.
- Cohen IS, Van der Kloot W (1986) Facilitation and delayed release at single frog neuromuscular junctions. *J Neurosci* 6:2366-2370.
- Collingridge GL, Kehl SJ, McLennan H (1983) Excitatory amino acids in synaptic transmission in the Schaffer collateral-commissural pathway of the rat hippocampus. *J Physiol* 334:33-46.

- Cornelisse LN, van Elburg RA, Meredith RM, Yuste R, Mansvelder HD (2007) High speed two-photon imaging of calcium dynamics in dendritic spines: consequences for spine calcium kinetics and buffer capacity. PLoS ONE 2:e1073.
- Csicsvari J, Hirase H, Czurko A, Mamiya A, Buzsaki G (1999) Oscillatory coupling of hippocampal pyramidal cells and interneurons in the behaving Rat. J Neurosci 19:274-287.
- Cull-Candy S, Brickley S, Farrant M (2001) NMDA receptor subunits: diversity, development and disease. Curr Opin Neurobiol 11:327-335.
- Cull-Candy S, Kelly L, Farrant M (2006) Regulation of Ca²⁺-permeable AMPA receptors: synaptic plasticity and beyond. Curr Opin Neurobiol 16:288-297.
- Cull-Candy SG, Leszkiewicz DN (2004) Role of distinct NMDA receptor subtypes at central synapses. Sci STKE 2004:re16.
- Cummings DD, Wilcox KS, Dichter MA (1996a) Calcium-dependent paired-pulse facilitation of miniature EPSC frequency accompanies depression of EPSCs at hippocampal synapses in culture. J Neurosci 16:5312-5323.
- Cummings JA, Mulkey RM, Nicoll RA, Malenka RC (1996b) Ca²⁺ signaling requirements for long-term depression in the hippocampus. Neuron 16:825-833.
- Dan Y, Poo MM (1992) Hebbian depression of isolated neuromuscular synapses in vitro. Science 256:1570-1573.
- Debanne D, Gahwiler BH, Thompson SM (1998) Long-term synaptic plasticity between pairs of individual CA3 pyramidal cells in rat hippocampal slice cultures. J Physiol 507 (Pt 1):237-247.
- Del Castillo J, Katz B (1954) Statistical factors involved in neuromuscular facilitation and depression. J Physiol 124:574-585.
- Delorenzo RJ, Sun DA, Deshpande LS (2005) Cellular mechanisms underlying acquired epilepsy: the calcium hypothesis of the induction and maintainance of epilepsy. Pharmacol Ther 105:229-266.
- Desai NS, Cudmore RH, Nelson SB, Turrigiano GG (2002) Critical periods for experience-dependent synaptic scaling in visual cortex. Nat Neurosci 5:783-789.
- Dingledine R, Hynes MA, King GL (1986) Involvement of N-methyl-D-aspartate receptors in epileptiform bursting in the rat hippocampal slice. J Physiol 380:175-189.
- Douglas RM, Goddard GV (1975) Long-term potentiation of the perforant path-granule cell synapse in the rat hippocampus. Brain Res 86:205-215.

- Dragoi G, Harris KD, Buzsaki G (2003) Place representation within hippocampal networks is modified by long-term potentiation. *Neuron* 39:843-853.
- Dudek SM, Bear MF (1992) Homosynaptic long-term depression in area CA1 of hippocampus and effects of N-methyl-D-aspartate receptor blockade. *Proc Natl Acad Sci U S A* 89:4363-4367.
- Dudek SM, Bear MF (1993) Bidirectional long-term modification of synaptic effectiveness in the adult and immature hippocampus. *J Neurosci* 13:2910-2918.
- Duguid I, Sjostrom PJ (2006) Novel presynaptic mechanisms for coincidence detection in synaptic plasticity. *Curr Opin Neurobiol* 16:312-322.
- Eccles JC, O'Connor W J (1941) Abortive impulses at the neuro-muscular junction. *J Physiol* 100:318-328.
- Echegoyen J, Neu A, Gruber KD, Soltesz I (2007) Homeostatic plasticity studied using in vivo hippocampal activity-blockade: synaptic scaling, intrinsic plasticity and age-dependence. *PLoS ONE* 2:e700.
- Egger V, Feldmeyer D, Sakmann B (1999) Coincidence detection and changes of synaptic efficacy in spiny stellate neurons in rat barrel cortex. *Nat Neurosci* 2:1098-1105.
- Eichenbaum H (2001) The hippocampus and declarative memory: cognitive mechanisms and neural codes. *Behav Brain Res* 127:199-207.
- Ekstrom AD, Meltzer J, McNaughton BL, Barnes CA (2001) NMDA receptor antagonism blocks experience-dependent expansion of hippocampal "place fields". *Neuron* 31:631-638.
- El-Hassar L, Milh M, Wendling F, Ferrand N, Esclapez M, Bernard C (2007) Cell domain-dependent changes in the glutamatergic and GABAergic drives during epileptogenesis in the rat CA1 region. *J Physiol* 578:193-211.
- Erreger K, Dravid SM, Banke TG, Wyllie DJ, Traynelis SF (2005) Subunit-specific gating controls rat NR1/NR2A and NR1/NR2B NMDA channel kinetics and synaptic signalling profiles. *J Physiol* 563:345-358.
- Faber DS, Korn H (1991) Applicability of the coefficient of variation method for analyzing synaptic plasticity. *Biophys J* 60:1288-1294.
- Fagni L, Chavis P, Ango F, Bockaert J (2000) Complex interactions between mGluRs, intracellular Ca²⁺ stores and ion channels in neurons. *Trends Neurosci* 23:80-88.
- Fatt P, Katz B (1951) An analysis of the end-plate potential recorded with an intracellular electrode. *J Physiol* 115:320-370.

- Feinerman O, Segal M, Moses E (2005) Signal propagation along unidimensional neuronal networks. *J Neurophysiol* 94:3406-3416.
- Feldman DE (2000) Timing-based LTP and LTD at vertical inputs to layer II/III pyramidal cells in rat barrel cortex. *Neuron* 27:45-56.
- Feldman DE, Nicoll RA, Malenka RC (1999) Synaptic plasticity at thalamocortical synapses in developing rat somatosensory cortex: LTP, LTD, and silent synapses. *J Neurobiol* 41:92-101.
- Feng B, Tse HW, Skifter DA, Morley R, Jane DE, Monaghan DT (2004) Structure-activity analysis of a novel NR2C/NR2D-preferring NMDA receptor antagonist: 1-(phenanthrene-2-carbonyl) piperazine-2,3-dicarboxylic acid. *Br J Pharmacol* 141:508-516.
- Fernandez de Sevilla D, Garduno J, Galvan E, Buno W (2006) Calcium-activated afterhyperpolarizations regulate synchronization and timing of epileptiform bursts in hippocampal CA3 pyramidal neurons. *J Neurophysiol* 96:3028-3041.
- Fischer G, Mutel V, Trube G, Malherbe P, Kew JN, Mohacsi E, Heitz MP, Kemp JA (1997) Ro 25-6981, a highly potent and selective blocker of N-methyl-D-aspartate receptors containing the NR2B subunit. Characterization in vitro. *J Pharmacol Exp Ther* 283:1285-1292.
- Fitzjohn SM, Collingridge GL (2002) Calcium stores and synaptic plasticity. *Cell Calcium* 32:405-411.
- Florian RV (2007) Reinforcement learning through modulation of spike-timing-dependent synaptic plasticity. *Neural Comput* 19:1468-1502.
- Froemke RC, Dan Y (2002) Spike-timing-dependent synaptic modification induced by natural spike trains. *Nature* 416:433-438.
- Froemke RC, Poo MM, Dan Y (2005) Spike-timing-dependent synaptic plasticity depends on dendritic location. *Nature* 434:221-225.
- Froemke RC, Tsay IA, Raad M, Long JD, Dan Y (2006) Contribution of individual spikes in burst-induced long-term synaptic modification. *J Neurophysiol* 95:1620-1629.
- Fuenzalida M, Fernandez de Sevilla D, Buno W (2007) Changes of the EPSP waveform regulate the temporal window for spike-timing-dependent plasticity. *J Neurosci* 27:11940-11948.
- Fuhrmann G, Segev I, Markram H, Tsodyks M (2002) Coding of temporal information by activity-dependent synapses. *J Neurophysiol* 87:140-148.
- Furshpan EJ (1991) Seizure-like activity in cell culture. *Epilepsy Res* 10:24-32.

- Furshpan EJ, Potter DD (1989) Seizure-like activity and cellular damage in rat hippocampal neurons in cell culture. *Neuron* 3:199-207.
- Fusi S, Drew PJ, Abbott LF (2005) Cascade models of synaptically stored memories. *Neuron* 45:599-611.
- Fuster JM, Alexander GE (1971) Neuron activity related to short-term memory. *Science* 173:652-654.
- Gahwiler BH, Capogna M, Debanne D, McKinney RA, Thompson SM (1997) Organotypic slice cultures: a technique has come of age. *Trends Neurosci* 20:471-477.
- Gandhi SP, Stevens CF (2003) Three modes of synaptic vesicular recycling revealed by single-vesicle imaging. *Nature* 423:607-613.
- Gerkin RC, Lau PM, Nauen DW, Wang YT, Bi GQ (2007) Modular competition driven by NMDA receptor subtypes in spike-timing-dependent plasticity. *J Neurophysiol* 97:2851-2862.
- Giovagnoli AR, Avanzini G (1999) Learning and memory impairment in patients with temporal lobe epilepsy: relation to the presence, type, and location of brain lesion. *Epilepsia* 40:904-911.
- Goda Y, Stevens CF (1994) Two components of transmitter release at a central synapse. *Proc Natl Acad Sci U S A* 91:12942-12946.
- Goel A, Lee HK (2007) Persistence of experience-induced homeostatic synaptic plasticity through adulthood in superficial layers of mouse visual cortex. *J Neurosci* 27:6692-6700.
- Goldman-Rakic PS (1995) Cellular basis of working memory. *Neuron* 14:477-485.
- Gustafsson B, Wigstrom H, Abraham WC, Huang YY (1987) Long-term potentiation in the hippocampus using depolarizing current pulses as the conditioning stimulus to single volley synaptic potentials. *J Neurosci* 7:774-780.
- Haas HL, Jefferys JG (1984) Low-calcium field burst discharges of CA1 pyramidal neurones in rat hippocampal slices. *J Physiol* 354:185-201.
- Hablitz JJ (1984) Picrotoxin-induced epileptiform activity in hippocampus: role of endogenous versus synaptic factors. *J Neurophysiol* 51:1011-1027.
- Hablitz JJ, Langmoen IA (1986) N-methyl-D-aspartate receptor antagonists reduce synaptic excitation in the hippocampus. *J Neurosci* 6:102-106.
- Hagler DJ, Jr., Goda Y (2001) Properties of synchronous and asynchronous release during pulse train depression in cultured hippocampal neurons. *J Neurophysiol* 85:2324-2334.

- Hajos N, Ledent C, Freund TF (2001) Novel cannabinoid-sensitive receptor mediates inhibition of glutamatergic synaptic transmission in the hippocampus. *Neuroscience* 106:1-4.
- Harris KM, Teyler TJ (1984) Developmental onset of long-term potentiation in area CA1 of the rat hippocampus. *J Physiol* 346:27-48.
- Harris KM, Fiala JC, Ostroff L (2003) Structural changes at dendritic spine synapses during long-term potentiation. *Philos Trans R Soc Lond B Biol Sci* 358:745-748.
- Hartman KN, Pal SK, Burrone J, Murthy VN (2006) Activity-dependent regulation of inhibitory synaptic transmission in hippocampal neurons. *Nat Neurosci* 9:642-649.
- Harvey CD, Svoboda K (2007) Locally dynamic synaptic learning rules in pyramidal neuron dendrites. *Nature* 450:1195-1200.
- Hatton CJ, Paoletti P (2005) Modulation of triheteromeric NMDA receptors by N-terminal domain ligands. *Neuron* 46:261-274.
- Hayashi Y, Shi SH, Esteban JA, Piccini A, Poncer JC, Malinow R (2000) Driving AMPA receptors into synapses by LTP and CaMKII: requirement for GluR1 and PDZ domain interaction. *Science* 287:2262-2267.
- Hebb D (1931) Conditioned and Unconditioned Reflexes and Inhibition. Master's Thesis, McGill University.
- Hebb DO (1949) The Organization of Behavior. New York: Wiley.
- Heidelberger R, Heinemann C, Neher E, Matthews G (1994) Calcium dependence of the rate of exocytosis in a synaptic terminal. *Nature* 371:513-515.
- Hellier JL, Grosshans DR, Coultrap SJ, Jones JP, Dobelis P, Browning MD, Staley KJ (2007) Nmda Receptor Trafficking at Recurrent Synapses Stabilizes the State of the Ca3 Network. *J Neurophysiol*.
- Helmchen F, Borst JG, Sakmann B (1997) Calcium dynamics associated with a single action potential in a CNS presynaptic terminal. *Biophys J* 72:1458-1471.
- Hermans E, Challiss RA (2001) Structural, signalling and regulatory properties of the group I metabotropic glutamate receptors: prototypic family C G-protein-coupled receptors. *Biochem J* 359:465-484.
- Hoffman AF, Macgill AM, Smith D, Oz M, Lupica CR (2005) Species and strain differences in the expression of a novel glutamate-modulating cannabinoid receptor in the rodent hippocampus. *Eur J Neurosci* 22:2387-2391.
- Holmes WR (2000) Models of calmodulin trapping and CaM kinase II activation in a dendritic spine. *J Comput Neurosci* 8:65-85.

- Huerta PT, Lisman JE (1995) Bidirectional synaptic plasticity induced by a single burst during cholinergic theta oscillation in CA1 in vitro. *Neuron* 15:1053-1063.
- Isaac J, Nicoll R, Malenka R (1995) Evidence for silent synapses: implications for the expression of LTP. *Neuron* 15:427-434.
- Isaac JT, Ashby M, McBain CJ (2007) The role of the GluR2 subunit in AMPA receptor function and synaptic plasticity. *Neuron* 54:859-871.
- Ismailov I, Kalikulov D, Inoue T, Friedlander MJ (2004) The kinetic profile of intracellular calcium predicts long-term potentiation and long-term depression. *J Neurosci* 24:9847-9861.
- Izhikevich EM (2006) Polychronization: computation with spikes. *Neural Comput* 18:245-282.
- Izhikevich EM, Desai NS (2003) Relating STDP to BCM. *Neural Comput* 15:1511-1523.
- Jahr CE, Stevens CF (1990a) Voltage dependence of NMDA-activated macroscopic conductances predicted by single-channel kinetics. *J Neurosci* 10:3178-3182.
- Jahr CE, Stevens CF (1990b) A quantitative description of NMDA receptor-channel kinetic behavior. *J Neurosci* 10:1830-1837.
- Jahr CE, Stevens CF (1993) Calcium permeability of the N-methyl-D-aspartate receptor channel in hippocampal neurons in culture. *Proc Natl Acad Sci U S A* 90:11573-11577.
- Janssens N, Lesage AS (2001) Glutamate receptor subunit expression in primary neuronal and secondary glial cultures. *J Neurochem* 77:1457-1474.
- Jiang B, Trevino M, Kirkwood A (2007) Sequential development of long-term potentiation and depression in different layers of the mouse visual cortex. *J Neurosci* 27:9648-9652.
- Kaech S, Banker G (2006) Culturing hippocampal neurons. *Nat Protoc* 1:2406-2415.
- Kampa BM, Letzkus JJ, Stuart GJ (2006) Requirement of dendritic calcium spikes for induction of spike-timing-dependent synaptic plasticity. *J Physiol* 574:283-290.
- Kampa BM, Letzkus JJ, Stuart GJ (2007) Dendritic mechanisms controlling spike-timing-dependent synaptic plasticity. *Trends Neurosci* 30:456-463.
- Kampa BM, Clements J, Jonas P, Stuart GJ (2004) Kinetics of Mg²⁺ unblock of NMDA receptors: implications for spike-timing dependent synaptic plasticity. *J Physiol* 556:337-345.
- Karmarkar UR, Buonomano DV (2002) A model of spike-timing dependent plasticity: one or two coincidence detectors? *J Neurophysiol* 88:507-513.
- Karmarkar UR, Buonomano DV (2006) Different forms of homeostatic plasticity are engaged with distinct temporal profiles. *Eur J Neurosci* 23:1575-1584.

- Katz B, Miledi R (1968) The role of calcium in neuromuscular facilitation. *J Physiol* 195:481-492.
- Kempter R, Gerstner W, van Hemmen JL (2001) Intrinsic stabilization of output rates by spike-based Hebbian learning. *Neural Comput* 13:2709-2741.
- Kennedy MB, Beale HC, Carlisle HJ, Washburn LR (2005) Integration of biochemical signalling in spines. *Nat Rev Neurosci* 6:423-434.
- Kerr JN, Greenberg D, Helmchen F (2005) Imaging input and output of neocortical networks in vivo. *Proc Natl Acad Sci U S A* 102:14063-14068.
- Kew JN, Richards JG, Mutel V, Kemp JA (1998) Developmental changes in NMDA receptor glycine affinity and ifenprodil sensitivity reveal three distinct populations of NMDA receptors in individual rat cortical neurons. *J Neurosci* 18:1935-1943.
- Kilman V, van Rossum MC, Turrigiano GG (2002) Activity deprivation reduces miniature IPSC amplitude by decreasing the number of postsynaptic GABA(A) receptors clustered at neocortical synapses. *J Neurosci* 22:1328-1337.
- Kim MJ, Dunah AW, Wang YT, Sheng M (2005) Differential Roles of NR2A- and NR2B-Containing NMDA Receptors in Ras-ERK Signaling and AMPA Receptor Trafficking. *Neuron* 46:745-760.
- Kirischuk S, Grantyn R (2003) Intraterminal Ca²⁺ concentration and asynchronous transmitter release at single GABAergic boutons in rat collicular cultures. *J Physiol* 548:753-764.
- Kirkwood A, Rioult MC, Bear MF (1996) Experience-dependent modification of synaptic plasticity in visual cortex. *Nature* 381:526-528.
- Kistler WM, van Hemmen JL (2000) Modeling synaptic plasticity in conjunction with the timing of pre- and postsynaptic action potentials. *Neural Comput* 12:385-405.
- Koester HJ, Sakmann B (1998) Calcium dynamics in single spines during coincident pre- and postsynaptic activity depend on relative timing of back-propagating action potentials and subthreshold excitatory postsynaptic potentials. *Proc Natl Acad Sci U S A* 95:9596-9601.
- Korn SJ, Giacchino JL, Chamberlin NL, Dingledine R (1987) Epileptiform burst activity induced by potassium in the hippocampus and its regulation by GABA-mediated inhibition. *J Neurophysiol* 57:325-340.
- Kuner T, Schoepfer R (1996) Multiple structural elements determine subunit specificity of Mg²⁺ block in NMDA receptor channels. *J Neurosci* 16:3549-3558.
- Kutsuwada T, Kashiwabuchi N, Mori H, Sakimura K, Kushiya E, Araki K, Meguro H, Masaki H, Kumanishi T, Arakawa M, et al. (1992) Molecular diversity of the NMDA receptor channel. *Nature* 358:36-41.

- Lau P, Bi G (2008) In Preparation.
- Lau PM, Bi GQ (2005) Synaptic mechanisms of persistent reverberatory activity in neuronal networks. *Proc Natl Acad Sci U S A* 102:10333-10338.
- Law AJ, Weickert CS, Webster MJ, Herman MM, Kleinman JE, Harrison PJ (2003) Expression of NMDA receptor NR1, NR2A and NR2B subunit mRNAs during development of the human hippocampal formation. *Eur J Neurosci* 18:1197-1205.
- Lazebnik Y (2002) Can a biologist fix a radio?--Or, what I learned while studying apoptosis. *Cancer Cell* 2:179-182.
- Le Ray D, Fernandez De Sevilla D, Belen Porto A, Fuenzalida M, Buno W (2004) Heterosynaptic metaplastic regulation of synaptic efficacy in CA1 pyramidal neurons of rat hippocampus. *Hippocampus* 14:1011-1025.
- Lengyel M, Kwag J, Paulsen O, Dayan P (2005) Matching storage and recall: hippocampal spike timing-dependent plasticity and phase response curves. *Nat Neurosci* 8:1677-1683.
- Leritz EC, Grande LJ, Bauer RM (2006) Temporal lobe epilepsy as a model to understand human memory: the distinction between explicit and implicit memory. *Epilepsy Behav* 9:1-13.
- Lester RA, Quarum ML, Parker JD, Weber E, Jahr CE (1989) Interaction of 6-cyano-7-nitroquinoxaline-2,3-dione with the N-methyl-D-aspartate receptor-associated glycine binding site. *Mol Pharmacol* 35:565-570.
- Letzkus JJ, Kampa BM, Stuart GJ (2006) Learning rules for spike timing-dependent plasticity depend on dendritic synapse location. *J Neurosci* 26:10420-10429.
- Letzkus JJ, Kampa BM, Stuart GJ (2007) Does spike timing-dependent synaptic plasticity underlie memory formation? *Clin Exp Pharmacol Physiol* 34:1070-1076.
- Leutgeb S, Leutgeb JK (2007) Pattern separation, pattern completion, and new neuronal codes within a continuous CA3 map. *Learn Mem* 14:745-757.
- Leutgeb S, Leutgeb JK, Moser MB, Moser EI (2005) Place cells, spatial maps and the population code for memory. *Curr Opin Neurobiol* 15:738-746.
- Levy WB, Steward O (1983) Temporal contiguity requirements for long-term associative potentiation/depression in the hippocampus. *Neuroscience* 8:791-797.
- Li S, Tian X, Hartley D, Feig L (2006) Distinct Roles for Ras-Guanine Nucleotide-Releasing Factor 1 (Ras-GRF1) and Ras-GRF2 in the Induction of Long-Term Potentiation and Long-Term Depression. *J Neurosci* 26:1721-1729.
- Liao D, Hessler N, Malinow R (1995) Activation of postsynaptically silent synapses during pairing-induced LTP in CA1 region of hippocampal slice. *Nature* 375:400-404.

- Lin JW, Fu Q, Allana T (2005) Probing the endogenous Ca²⁺ buffers at the presynaptic terminals of the crayfish neuromuscular junction. *J Neurophysiol* 94:377-386.
- Lisman J (1989) A mechanism for the Hebb and the anti-Hebb processes underlying learning and memory. *Proc Natl Acad Sci U S A* 86:9574-9578.
- Lisman J, Spruston N (2005) Postsynaptic depolarization requirements for LTP and LTD: a critique of spike timing-dependent plasticity. *Nat Neurosci* 8:839-841.
- Lisman J, Schulman H, Cline H (2002) The molecular basis of CaMKII function in synaptic and behavioural memory. *Nat Rev Neurosci* 3:175-190.
- Lisman JE (2001) Three Ca²⁺ levels affect plasticity differently: the LTP zone, the LTD zone and no man's land. *J Physiol* 532:285.
- Lisman JE, Zhabotinsky AM (2001) A model of synaptic memory: a CaMKII/PP1 switch that potentiates transmission by organizing an AMPA receptor anchoring assembly. *Neuron* 31:191-201.
- Lisman JE, McIntyre CC (2001) Synaptic plasticity: a molecular memory switch. *Curr Biol* 11:R788-791.
- Liu G, Tsien RW (1995) Properties of synaptic transmission at single hippocampal synaptic boutons. *Nature* 375:404-408.
- Liu L, Wong TP, Pozza MF, Lingenhoehl K, Wang Y, Sheng M, Auberson YP, Wang YT (2004) Role of NMDA receptor subtypes in governing the direction of hippocampal synaptic plasticity. *Science* 304:1021-1024.
- Lorente De No R (1933) Vestibulo-ocular reflex arc. *Arch Neurol Psych* 30:245–291.
- Lorente De No R (1934) Studies on the structure of the cerebral cortex. II. Continuation of the study of ammonic system. *J Psych Neurol* 46:113–177.
- Louvel J, Avoli M, Kurcewicz I, Pumain R (1994) Extracellular free potassium during synchronous activity induced by 4-aminopyridine in the juvenile rat hippocampus. *Neurosci Lett* 167:97-100.
- Lu HC, Gonzalez E, Crair MC (2001) Barrel cortex critical period plasticity is independent of changes in NMDA receptor subunit composition. *Neuron* 32:619-634.
- Lu JT, Li CY, Zhao JP, Poo MM, Zhang XH (2007) Spike-timing-dependent plasticity of neocortical excitatory synapses on inhibitory interneurons depends on target cell type. *J Neurosci* 27:9711-9720.
- Lynch G, Larson J, Kelso S, Barrio G, Schottler F (1983) Intracellular injections of EGTA block induction of hippocampal long-term potentiation. *Nature* 305:719-721.

- MacVicar BA, Tse FW (1989) Local neuronal circuitry underlying cholinergic rhythmical slow activity in CA3 area of rat hippocampal slices. *J Physiol* 417:197-212.
- Magee JC, Johnston D (1997) A synaptically controlled, associative signal for Hebbian plasticity in hippocampal neurons. *Science* 275:209-213.
- Majewska A, Brown E, Ross J, Yuste R (2000) Mechanisms of calcium decay kinetics in hippocampal spines: role of spine calcium pumps and calcium diffusion through the spine neck in biochemical compartmentalization. *J Neurosci* 20:1722-1734.
- Malenka RC, Nicoll RA (1999) Long-term potentiation -- a decade of progress. *Science* 285:1870-1874.
- Malenka RC, Bear MF (2004) LTP and LTD: an embarrassment of riches. *Neuron* 44:5-21.
- Malenka RC, Kauer JA, Zucker RS, Nicoll RA (1988) Postsynaptic calcium is sufficient for potentiation of hippocampal synaptic transmission. *Science* 242:81-84.
- Mallon AP, Auberson YP, Stone TW (2004) Selective subunit antagonists suggest an inhibitory relationship between NR2B and NR2A-subunit containing N-methyl-D- α -aspartate receptors in hippocampal slices. *Exp Brain Res*.
- Mann EO, Paulsen O (2007) Role of GABAergic inhibition in hippocampal network oscillations. *Trends Neurosci* 30:343-349.
- Maravall M, Mainen ZF, Sabatini BL, Svoboda K (2000) Estimating intracellular calcium concentrations and buffering without wavelength ratioing. *Biophys J* 78:2655-2667.
- Markram H, Lubke J, Frotscher M, Sakmann B (1997) Regulation of synaptic efficacy by coincidence of postsynaptic APs and EPSPs. *Science* 275:213-215.
- Marr D (1971) Simple memory: a theory for archicortex. *Philos Trans R Soc Lond B Biol Sci* 262:23-81.
- Martin KC, Kosik KS (2002) Synaptic tagging -- who's it? *Nat Rev Neurosci* 3:813-820.
- Massey PV, Johnson BE, Moult PR, Auberson YP, Brown MW, Molnar E, Collingridge GL, Bashir ZI (2004) Differential roles of NR2A and NR2B-containing NMDA receptors in cortical long-term potentiation and long-term depression. *J Neurosci* 24:7821-7828.
- Mayer ML, Westbrook GL, Guthrie PB (1984) Voltage-dependent block by Mg²⁺ of NMDA responses in spinal cord neurones. *Nature* 309:261-263.
- McBain CJ, Traynelis SF (2006) Malevolent lurkers no more: NMDA receptors come of age. *J Physiol* 575:317-318.
- McCormick DA, Contreras D (2001) On the cellular and network bases of epileptic seizures. *Annu Rev Physiol* 63:815-846.

- McNaughton N, Morris RG (1987) Chlordiazepoxide, an anxiolytic benzodiazepine, impairs place navigation in rats. *Behav Brain Res* 24:39-46.
- Mehta MR, Barnes CA, McNaughton BL (1997) Experience-dependent, asymmetric expansion of hippocampal place fields. *Proc Natl Acad Sci U S A* 94:8918-8921.
- Mehta MR, Quirk MC, Wilson MA (2000) Experience-dependent asymmetric shape of hippocampal receptive fields. *Neuron* 25:707-715.
- Meliza CD, Dan Y (2006) Receptive-field modification in rat visual cortex induced by paired visual stimulation and single-cell spiking. *Neuron* 49:183-189.
- Meredith RM, Floyer-Lea AM, Paulsen O (2003) Maturation of long-term potentiation induction rules in rodent hippocampus: role of GABAergic inhibition. *J Neurosci* 23:11142-11146.
- Miledi R, Thies R (1971) Tetanic and post-tetanic rise in frequency of miniature end-plate potentials in low-calcium solutions. *J Physiol* 212:245-257.
- Miles R, Wong RK (1986) Excitatory synaptic interactions between CA3 neurones in the guinea-pig hippocampus. *J Physiol* 373:397-418.
- Miles R, Wong RK (1987) Inhibitory control of local excitatory circuits in the guinea-pig hippocampus. *J Physiol* 388:611-629.
- Miles R, Wong RK, Traub RD (1984) Synchronized afterdischarges in the hippocampus: contribution of local synaptic interactions. *Neuroscience* 12:1179-1189.
- Miles R, Traub RD, Wong RK (1988) Spread of synchronous firing in longitudinal slices from the CA3 region of the hippocampus. *J Neurophysiol* 60:1481-1496.
- Miller EK, Erickson CA, Desimone R (1996) Neural mechanisms of visual working memory in prefrontal cortex of the macaque. *J Neurosci* 16:5154-5167.
- Milner B, Penfield W (1955) The effect of hippocampal lesions on recent memory. *Trans Am Neurol Assoc*:42-48.
- Miyashiro K, Dichter M, Eberwine J (1994) On the nature and differential distribution of mRNAs in hippocampal neurites: implications for neuronal functioning. *Proc Natl Acad Sci U S A* 91:10800-10804.
- Miyashita Y (1988) Neuronal correlate of visual associative long-term memory in the primate temporal cortex. *Nature* 335:817-820.
- Mizuno T, Kanazawa I, Sakurai M (2001) Differential induction of LTP and LTD is not determined solely by instantaneous calcium concentration: an essential involvement of a temporal factor. *Eur J Neurosci* 14:701-708.

- Montgomery JM, Madison DV (2002) State-dependent heterogeneity in synaptic depression between pyramidal cell pairs. *Neuron* 33:765-777.
- Monyer H, Burnashev N, Laurie DJ, Sakmann B, Seeburg PH (1994) Developmental and regional expression in the rat brain and functional properties of four NMDA receptors. *Neuron* 12:529-540.
- Monyer H, Sprengel R, Schoepfer R, Herb A, Higuchi M, Lomeli H, Burnashev N, Sakmann B, Seeburg PH (1992) Heteromeric NMDA receptors: molecular and functional distinction of subtypes. *Science* 256:1217-1221.
- Morimoto K, Fahnestock M, Racine RJ (2004) Kindling and status epilepticus models of epilepsy: rewiring the brain. *Prog Neurobiol* 73:1-60.
- Morin F, Beaulieu C, Lacaille JC (1998) Selective loss of GABA neurons in area CA1 of the rat hippocampus after intraventricular kainate. *Epilepsy Res* 32:363-369.
- Morishita W, Lu W, Smith GB, Nicoll RA, Bear MF, Malenka RC (2006) Activation of NR2B-containing NMDA receptors is not required for NMDA receptor-dependent long-term depression. *Neuropharmacology*.
- Morris RG, Garrud P, Rawlins JN, O'Keefe J (1982) Place navigation impaired in rats with hippocampal lesions. *Nature* 297:681-683.
- Moulder KL, Mennerick S (2005) Reluctant vesicles contribute to the total readily releasable pool in glutamatergic hippocampal neurons. *J Neurosci* 25:3842-3850.
- Mueller AL, Dunwiddie TV (1983) Anticonvulsant and proconvulsant actions of alpha- and beta-noradrenergic agonists on epileptiform activity in rat hippocampus in vitro. *Epilepsia* 24:57-64.
- Mulkey RM, Malenka RC (1992) Mechanisms underlying induction of homosynaptic long-term depression in area CA1 of the hippocampus. *Neuron* 9:967-975.
- Murthy VN, Sejnowski TJ, Stevens CF (1997) Heterogeneous release properties of visualized individual hippocampal synapses. *Neuron* 18:599-612.
- Murthy VN, Sejnowski TJ, Stevens CF (2000) Dynamics of dendritic calcium transients evoked by quantal release at excitatory hippocampal synapses. *Proc Natl Acad Sci U S A* 97:901-906.
- Murthy VN, Schikorski T, Stevens CF, Zhu Y (2001) Inactivity produces increases in neurotransmitter release and synapse size. *Neuron* 32:673-682.
- Nagarajan N, Quast C, Boxall AR, Shahid M, Rosenmund C (2001) Mechanism and impact of allosteric AMPA receptor modulation by the ampakine CX546. *Neuropharmacology* 41:650-663.

- Nakazawa K, McHugh TJ, Wilson MA, Tonegawa S (2004) NMDA receptors, place cells and hippocampal spatial memory. *Nat Rev Neurosci* 5:361-372.
- Nakazawa K, Quirk MC, Chitwood RA, Watanabe M, Yeckel MF, Sun LD, Kato A, Carr CA, Johnston D, Wilson MA, Tonegawa S (2002) Requirement for hippocampal CA3 NMDA receptors in associative memory recall. *Science* 297:211-218.
- Nauen D, Bi G (2008) Single synapses in hippocampal culture. In Preparation.
- Nevian T, Sakmann B (2004) Single spine Ca²⁺ signals evoked by coincident EPSPs and backpropagating action potentials in spiny stellate cells of layer 4 in the juvenile rat somatosensory barrel cortex. *J Neurosci* 24:1689-1699.
- Nevian T, Sakmann B (2006) Spine Ca²⁺ signaling in spike-timing-dependent plasticity. *J Neurosci* 26:11001-11013.
- Neyton J, Paoletti P (2006) Relating NMDA Receptor Function to Receptor Subunit Composition: Limitations of the Pharmacological Approach. *J Neurosci* 26:1331-1333.
- Nishiki T, Augustine GJ (2004) Synaptotagmin I synchronizes transmitter release in mouse hippocampal neurons. *J Neurosci* 24:6127-6132.
- Nishiyama M, Hong K, Mikoshiba K, Poo MM, Kato K (2000) Calcium stores regulate the polarity and input specificity of synaptic modification. *Nature* 408:584-588.
- Noceti F, Baldelli P, Wei X, Qin N, Toro L, Birnbaumer L, Stefani E (1996) Effective gating charges per channel in voltage-dependent K⁺ and Ca²⁺ channels. *J Gen Physiol* 108:143-155.
- Nowak L, Bregestovski P, Ascher P, Herbet A, Prochiantz A (1984) Magnesium gates glutamate-activated channels in mouse central neurones. *Nature* 307:462-465.
- Nowotny T, Zhigulin VP, Selverston AI, Abarbanel HD, Rabinovich MI (2003) Enhancement of synchronization in a hybrid neural circuit by spike-timing dependent plasticity. *J Neurosci* 23:9776-9785.
- O'Brien RJ, Kamboj S, Ehlers MD, Rosen KR, Fischbach GD, Huganir RL (1998) Activity-dependent modulation of synaptic AMPA receptor accumulation. *Neuron* 21:1067-1078.
- O'Connor DH, Wittenberg GM, Wang SS (2005a) Graded bidirectional synaptic plasticity is composed of switch-like unitary events. *Proc Natl Acad Sci U S A* 102:9679-9684.
- O'Connor DH, Wittenberg GM, Wang SS (2005b) Dissection of bidirectional synaptic plasticity into saturable unidirectional processes. *J Neurophysiol* 94:1565-1573.
- O'Keefe J, Recce ML (1993) Phase relationship between hippocampal place units and the EEG theta rhythm. *Hippocampus* 3:317-330.

- Obenaus A, Esclapez M, Houser CR (1993) Loss of glutamate decarboxylase mRNA-containing neurons in the rat dentate gyrus following pilocarpine-induced seizures. *J Neurosci* 13:4470-4485.
- Oertner TG, Sabatini BL, Nimchinsky EA, Svoboda K (2002) Facilitation at single synapses probed with optical quantal analysis. *Nat Neurosci* 5:657-664.
- Okabe S, Collin C, Auerbach JM, Meiri N, Bengzon J, Kennedy MB, Segal M, McKay RD (1998) Hippocampal synaptic plasticity in mice overexpressing an embryonic subunit of the NMDA receptor. *J Neurosci* 18:4177-4188.
- Okada M, Corfas G (2004) Neuregulin1 downregulates postsynaptic GABA_A receptors at the hippocampal inhibitory synapse. *Hippocampus* 14:337-344.
- Pal S, Sombati S, Limbrick DD, Jr., DeLorenzo RJ (1999) In vitro status epilepticus causes sustained elevation of intracellular calcium levels in hippocampal neurons. *Brain Res* 851:20-31.
- Palmer MJ, Isaac JT, Collingridge GL (2004) Multiple, developmentally regulated expression mechanisms of long-term potentiation at CA1 synapses. *J Neurosci* 24:4903-4911.
- Paoletti P, Neyton J (2007) NMDA receptor subunits: function and pharmacology. *Curr Opin Pharmacol* 7:39-47.
- Pavlidis P, Madison DV (1999) Synaptic transmission in pair recordings from CA3 pyramidal cells in organotypic culture. *J Neurophysiol* 81:2787-2797.
- Penfield W, Milner B (1958) Memory deficit produced by bilateral lesions in the hippocampal zone. *AMA Arch Neurol Psychiatry* 79:475-497.
- Perouansky M, Yaari Y (1993) Kinetic properties of NMDA receptor-mediated synaptic currents in rat hippocampal pyramidal cells versus interneurons. *J Physiol* 465:223-244.
- Petersen CC, Malenka RC, Nicoll RA, Hopfield JJ (1998) All-or-none potentiation at CA3-CA1 synapses. *Proc Natl Acad Sci U S A* 95:4732-4737.
- Philpot BD, Espinosa JS, Bear MF (2003) Evidence for altered NMDA receptor function as a basis for metaplasticity in visual cortex. *J Neurosci* 23:5583-5588.
- Pike FG, Meredith RM, Olding AW, Paulsen O (1999) Rapid report: postsynaptic bursting is essential for 'Hebbian' induction of associative long-term potentiation at excitatory synapses in rat hippocampus. *J Physiol* 518 (Pt 2):571-576.
- Poirazi P, Brannon T, Mel BW (2003a) Arithmetic of subthreshold synaptic summation in a model CA1 pyramidal cell. *Neuron* 37:977-987.
- Poirazi P, Brannon T, Mel BW (2003b) Pyramidal neuron as two-layer neural network. *Neuron* 37:989-999.

- Potter SM, DeMarse TB (2001) A new approach to neural cell culture for long-term studies. *J Neurosci Methods* 110:17-24.
- Pozzo-Miller LD, Pivovarova NB, Connor JA, Reese TS, Andrews SB (1999) Correlated measurements of free and total intracellular calcium concentration in central nervous system neurons. *Microsc Res Tech* 46:370-379.
- Prince DA (1968) The depolarization shift in "epileptic" neurons. *Exp Neurol* 21:467-485.
- Rae J, Cooper K, Gates P, Watsky M (1991) Low access resistance perforated patch recordings using amphotericin B. *J Neurosci Methods* 37:15-26.
- Rao RP, Sejnowski TJ (2001) Spike-timing-dependent Hebbian plasticity as temporal difference learning. *Neural Comput* 13:2221-2237.
- Ravin R, Spira ME, Parnas H, Parnas I (1997) Simultaneous measurement of intracellular Ca²⁺ and asynchronous transmitter release from the same crayfish bouton. *J Physiol* 501 (Pt 2):251-262.
- Reid IC, Stewart CA (1997) Seizures, memory and synaptic plasticity. *Seizure* 6:351-359.
- Remy S, Spruston N (2007) Dendritic spikes induce single-burst long-term potentiation. *Proc Natl Acad Sci U S A* 104:17192-17197.
- Rioult-Pedotti MS, Friedman D, Donoghue JP (2000) Learning-induced LTP in neocortex. *Science* 290:533-536.
- Roberts P (2005) Recurrent neural network generates a basis for sensory image cancellation. *Neurocomputing* 65-66:237-242.
- Rosenmund C, Westbrook GL (1993) Rundown of N-methyl-D-aspartate channels during whole-cell recording in rat hippocampal neurons: role of Ca²⁺ and ATP. *J Physiol* 470:705-729.
- Rosenmund C, Stevens CF (1996) Definition of the readily releasable pool of vesicles at hippocampal synapses. *Neuron* 16:1197-1207.
- Rosenzweig ES, Barnes CA (2003) Impact of aging on hippocampal function: plasticity, network dynamics, and cognition. *Prog Neurobiol* 69:143-179.
- Rubin JE (2001) Steady states in an iterative model for multiplicative spike-timing-dependent plasticity. *Network* 12:131-140.
- Rubin JE, Gerkin RC, Bi GQ, Chow CC (2005) Calcium time course as a signal for spike-timing-dependent plasticity. *J Neurophysiol* 93:2600-2613.
- Rutecki PA, Lebeda FJ, Johnston D (1985) Epileptiform activity induced by changes in extracellular potassium in hippocampus. *J Neurophysiol* 54:1363-1374.

- Sabatini BL, Regehr WG (1998) Optical measurement of presynaptic calcium currents. *Biophys J* 74:1549-1563.
- Sabatini BL, Oertner TG, Svoboda K (2002) The life cycle of Ca(2+) ions in dendritic spines. *Neuron* 33:439-452.
- Sanhueza M, McIntyre CC, Lisman JE (2007) Reversal of synaptic memory by Ca2+/calmodulin-dependent protein kinase II inhibitor. *J Neurosci* 27:5190-5199.
- Sano K (1997) Hippocampus and Epilepsy Surgery. *Epilepsia* 38:4-10.
- Saraswati S, Adolfsen B, Littleton JT (2007) Characterization of the role of the Synaptotagmin family as calcium sensors in facilitation and asynchronous neurotransmitter release. *Proc Natl Acad Sci U S A* 104:14122-14127.
- Sato N, Yamaguchi Y (2003) Memory encoding by theta phase precession in the hippocampal network. *Neural Comput* 15:2379-2397.
- Saviane C, Silver RA (2006) Errors in the estimation of the variance: implications for multiple-probability fluctuation analysis. *J Neurosci Methods* 153:250-260.
- Saxe J (1878) The Blind Men and the Elephant. In: Poetry of America, pp 150-151. London: William Clowes and Sons.
- Schneggenburger R, Neher E (2000) Intracellular calcium dependence of transmitter release rates at a fast central synapse. *Nature* 406:889-893.
- Schneggenburger R, Neher E (2005) Presynaptic calcium and control of vesicle fusion. *Curr Opin Neurobiol* 15:266-274.
- Schneggenburger R, Sakaba T, Neher E (2002) Vesicle pools and short-term synaptic depression: lessons from a large synapse. *Trends Neurosci* 25:206-212.
- Schwartzkroin PA, Prince DA (1977) Penicillin-induced epileptiform activity in the hippocampal in vitro preparation. *Ann Neurol* 1:463-469.
- Schwartzkroin PA, Prince DA (1978) Cellular and field potential properties of epileptogenic hippocampal slices. *Brain Res* 147:117-130.
- Schwartzkroin PA, Stafstrom CE (1980) Effects of EGTA on the calcium-activated afterhyperpolarization in hippocampal CA3 pyramidal cells. *Science* 210:1125-1126.
- Seung HS (2000) Half a century of Hebb. *Nat Neurosci* 3 Suppl:1166.
- Sheng M, Cummings J, Roldan LA, Jan YN, Jan LY (1994) Changing subunit composition of heteromeric NMDA receptors during development of rat cortex. *Nature* 368:144-147.
- Shi S, Hayashi Y, Esteban JA, Malinow R (2001) Subunit-specific rules governing AMPA receptor trafficking to synapses in hippocampal pyramidal neurons. *Cell* 105:331-343.

- Shouval HZ, Kalantzis G (2005) Stochastic properties of synaptic transmission affect the shape of spike time-dependent plasticity curves. *J Neurophysiol* 93:1069-1073.
- Shouval HZ, Bear MF, Cooper LN (2002) A unified model of NMDA receptor-dependent bidirectional synaptic plasticity. *Proc Natl Acad Sci U S A* 99:10831-10836.
- Silver RA (2003) Estimation of nonuniform quantal parameters with multiple-probability fluctuation analysis: theory, application and limitations. *J Neurosci Methods* 130:127-141.
- Sinha SR, Wu LG, Saggau P (1997) Presynaptic calcium dynamics and transmitter release evoked by single action potentials at mammalian central synapses. *Biophys J* 72:637-651.
- Sjostrom PJ, Nelson SB (2002) Spike timing, calcium signals and synaptic plasticity. *Curr Opin Neurobiol* 12:305-314.
- Sjostrom PJ, Turrigiano GG, Nelson SB (2001) Rate, timing, and cooperativity jointly determine cortical synaptic plasticity. *Neuron* 32:1149-1164.
- Sjostrom PJ, Turrigiano GG, Nelson SB (2003) Neocortical LTD via coincident activation of presynaptic NMDA and cannabinoid receptors. *Neuron* 39:641-654.
- Sombati S, Delorenzo RJ (1995) Recurrent spontaneous seizure activity in hippocampal neuronal networks in culture. *J Neurophysiol* 73:1706-1711.
- Sombati S, Coulter DA, DeLorenzo RJ (1991) Neurotoxic activation of glutamate receptors induces an extended neuronal depolarization in cultured hippocampal neurons. *Brain Res* 566:316-319.
- Song S, Miller KD, Abbott LF (2000) Competitive Hebbian learning through spike-timing-dependent synaptic plasticity. *Nat Neurosci* 3:919-926.
- Staley KJ, Longacher M, Bains JS, Yee A (1998) Presynaptic modulation of CA3 network activity. *Nat Neurosci* 1:201-209.
- Staley KJ, Bains JS, Yee A, Hellier J, Longacher JM (2001) Statistical model relating CA3 burst probability to recovery from burst-induced depression at recurrent collateral synapses. *J Neurophysiol* 86:2736-2747.
- Stemmer PM, Klee CB (1994) Dual calcium ion regulation of calcineurin by calmodulin and calcineurin B. *Biochemistry* 33:6859-6866.
- Steriade M, McCormick DA, Sejnowski TJ (1993) Thalamocortical oscillations in the sleeping and aroused brain. *Science* 262:679-685.
- Stevens CF (1996) Strengths and weaknesses in memory. *Nature* 381:471-472.
- Stevens CF (1998) A million dollar question: does LTP = memory? *Neuron* 20:1-2.

- Stevens CF, Wesseling JF (1998) Activity-dependent modulation of the rate at which synaptic vesicles become available to undergo exocytosis. *Neuron* 21:415-424.
- Strata F (1998) Intrinsic oscillations in CA3 hippocampal pyramids: physiological relevance to theta rhythm generation. *Hippocampus* 8:666-679.
- Sudhof TC (2004) The synaptic vesicle cycle. *Annu Rev Neurosci* 27:509-547.
- Sullivan JM (2007) A simple depletion model of the readily releasable pool of synaptic vesicles cannot account for paired-pulse depression. *J Neurophysiol* 97:948-950.
- Sun J, Pang ZP, Qin D, Fahim AT, Adachi R, Sudhof TC (2007) A dual-Ca²⁺-sensor model for neurotransmitter release in a central synapse. *Nature* 450:676-682.
- Sutherland GR, McNaughton B (2000) Memory trace reactivation in hippocampal and neocortical neuronal ensembles. *Curr Opin Neurobiol* 10:180-186.
- Sutula TP (2004) Mechanisms of epilepsy progression: current theories and perspectives from neuroplasticity in adulthood and development. *Epilepsy Res* 60:161-171.
- Swann JW, Smith KL, Brady RJ (1991) Age-dependent alterations in the operations of hippocampal neural networks. *Ann N Y Acad Sci* 627:264-276.
- Tang YP, Shimizu E, Dube GR, Rampon C, Kerchner GA, Zhuo M, Liu G, Tsien JZ (1999) Genetic enhancement of learning and memory in mice. *Nature* 401:63-69.
- Tao H, Zhang LI, Bi G, Poo M (2000) Selective presynaptic propagation of long-term potentiation in defined neural networks. *J Neurosci* 20:3233-3243.
- Tigaret CM, Thalhammer A, Rast GF, Specht CG, Auberson YP, Stewart MG, Schoepfer R (2006) Subunit dependencies of N-methyl-D-aspartate (NMDA) receptor-induced alpha-amino-3-hydroxy-5-methyl-4-isoxazolepropionic acid (AMPA) receptor internalization. *Mol Pharmacol* 69:1251-1259.
- Tovar KR, Westbrook GL (1999) The incorporation of NMDA receptors with a distinct subunit composition at nascent hippocampal synapses in vitro. *J Neurosci* 19:4180-4188.
- Trasande CA, Ramirez JM (2007) Activity deprivation leads to seizures in hippocampal slice cultures: is epilepsy the consequence of homeostatic plasticity? *J Clin Neurophysiol* 24:154-164.
- Traub R, Miles R (1991) Neural Networks of the Hippocampus. New York: Cambridge University Press.
- Traub RD, Wong RK (1982) Cellular mechanism of neuronal synchronization in epilepsy. *Science* 216:745-747.

- Traub RD, Miles R, Wong RK (1989) Model of the origin of rhythmic population oscillations in the hippocampal slice. *Science* 243:1319-1325.
- Traub RD, Jefferys JG, Miles R (1993) Analysis of the propagation of disinhibition-induced after-discharges along the guinea-pig hippocampal slice in vitro. *J Physiol* 472:267-287.
- Traub RD, Jefferys JG, Whittington MA (1994a) Enhanced NMDA conductance can account for epileptiform activity induced by low Mg²⁺ in the rat hippocampal slice. *J Physiol* 478 Pt 3:379-393.
- Traub RD, Wong RK, Miles R, Michelson H (1991) A model of a CA3 hippocampal pyramidal neuron incorporating voltage-clamp data on intrinsic conductances. *J Neurophysiol* 66:635-650.
- Traub RD, Borck C, Colling SB, Jefferys JG (1996) On the structure of ictal events in vitro. *Epilepsia* 37:879-891.
- Traub RD, Jefferys JG, Miles R, Whittington MA, Toth K (1994b) A branching dendritic model of a rodent CA3 pyramidal neurone. *J Physiol* 481 (Pt 1):79-95.
- Tsodyks M, Uziel A, Markram H (2000) Synchrony generation in recurrent networks with frequency-dependent synapses. *J Neurosci* 20:RC50.
- Tsodyks MV, Markram H (1997) The neural code between neocortical pyramidal neurons depends on neurotransmitter release probability. *Proc Natl Acad Sci U S A* 94:719-723.
- Tsvetkov E, Carlezon WA, Benes FM, Kandel ER, Bolshakov VY (2002) Fear conditioning occludes LTP-induced presynaptic enhancement of synaptic transmission in the cortical pathway to the lateral amygdala. *Neuron* 34:289-300.
- Turrigiano GG, Leslie KR, Desai NS, Rutherford LC, Nelson SB (1998) Activity-dependent scaling of quantal amplitude in neocortical neurons. *Nature* 391:892-896.
- Tzounopoulos T, Kim Y, Oertel D, Trussell LO (2004) Cell-specific, spike timing-dependent plasticities in the dorsal cochlear nucleus. *Nat Neurosci* 7:719-725.
- Tzounopoulos T, Rubio ME, Keen JE, Trussell LO (2007) Coactivation of pre- and postsynaptic signaling mechanisms determines cell-specific spike-timing-dependent plasticity. *Neuron* 54:291-301.
- van Welie I, van Hooft JA, Wadman WJ (2006) Background activity regulates excitability of rat hippocampal CA1 pyramidal neurons by adaptation of a K⁺ conductance. *J Neurophysiol* 95:2007-2012.
- Vicini S, Wang JF, Li JH, Zhu WJ, Wang YH, Luo JH, Wolfe BB, Grayson DR (1998) Functional and pharmacological differences between recombinant N-methyl-D-aspartate receptors. *J Neurophysiol* 79:555-566.

- Volman V, Gerkin R, Bi G (2008) The role of network topology on persistent activity patterns in a model of hippocampal cultured networks. In preparation.
- Volman V, Gerkin RC, Lau PM, Ben-Jacob E, Bi GQ (2007) Calcium and synaptic dynamics underlying reverberatory activity in neuronal networks. *Phys Biol* 4:91-103.
- Wang HX, Gerkin RC, Nauen DW, Bi GQ (2005) Coactivation and timing-dependent integration of synaptic potentiation and depression. *Nat Neurosci* 8:187-193.
- Wang XJ (1999) Synaptic basis of cortical persistent activity: the importance of NMDA receptors to working memory. *J Neurosci* 19:9587-9603.
- Watt AJ, Sjostrom PJ, Haussler M, Nelson SB, Turrigiano GG (2004) A proportional but slower NMDA potentiation follows AMPA potentiation in LTP. *Nat Neurosci* 7:518-524.
- Weitlauf C, Honse Y, Auberson YP, Mishina M, Lovinger DM, Winder DG (2005) Activation of NR2A-containing NMDA receptors is not obligatory for NMDA receptor-dependent long-term potentiation. *J Neurosci* 25:8386-8390.
- Whitlock JR, Heynen AJ, Shuler MG, Bear MF (2006) Learning induces long-term potentiation in the hippocampus. *Science* 313:1093-1097.
- Whittington MA, Traub RD, Kopell N, Ermentrout B, Buhl EH (2000) Inhibition-based rhythms: experimental and mathematical observations on network dynamics. *Int J Psychophysiol* 38:315-336.
- Wierenga CJ, Ibata K, Turrigiano GG (2005) Postsynaptic expression of homeostatic plasticity at neocortical synapses. *J Neurosci* 25:2895-2905.
- Wilcox KS, Buchhalter J, Dichter MA (1994) Properties of inhibitory and excitatory synapses between hippocampal neurons in very low density cultures. *Synapse* 18:128-151.
- Williams K (1993) Ifenprodil discriminates subtypes of the N-methyl-D-aspartate receptor: selectivity and mechanisms at recombinant heteromeric receptors. *Mol Pharmacol* 44:851-859.
- Wittenberg GM, Wang SS (2006) Malleability of spike-timing-dependent plasticity at the CA3-CA1 synapse. *J Neurosci* 26:6610-6617.
- Wyart C, Ybert C, Bourdieu L, Herr C, Prinz C, Chatenay D (2002) Constrained synaptic connectivity in functional mammalian neuronal networks grown on patterned surfaces. *J Neurosci Methods* 117:123-131.
- Xu J, He L, Wu LG (2007) Role of Ca(2+) channels in short-term synaptic plasticity. *Curr Opin Neurobiol* 17:352-359.
- Yang SN, Tang YG, Zucker RS (1999) Selective induction of LTP and LTD by postsynaptic [Ca2+], elevation. *J Neurophysiol* 81:781-787.

- Yang Y, Ge W, Chen Y, Zhang Z, Shen W, Wu C, Poo M, Duan S (2003) Contribution of astrocytes to hippocampal long-term potentiation through release of D-serine. *Proc Natl Acad Sci U S A* 100:15194-15199.
- Yao H, Dan Y (2001) Stimulus timing-dependent plasticity in cortical processing of orientation. *Neuron* 32:315-323.
- Yao H, Shen Y, Dan Y (2004) Intracortical mechanism of stimulus-timing-dependent plasticity in visual cortical orientation tuning. *Proc Natl Acad Sci U S A* 101:5081-5086.
- Yuste R, Majewska A, Cash SS, Denk W (1999) Mechanisms of calcium influx into hippocampal spines: heterogeneity among spines, coincidence detection by NMDA receptors, and optical quantal analysis. *J Neurosci* 19:1976-1987.
- Zhabotinsky AM (2000) Bistability in the Ca(2+)/calmodulin-dependent protein kinase-phosphatase system. *Biophys J* 79:2211-2221.
- Zhang J, Bi G (2007) Sensitization of spike-timing dependent plasticity in hippocampal neurons by dopamine via D1 receptors. In Preparation.
- Zhang L, Kirschstein T, Sommersberg B, Merkens M, Manahan-Vaughan D, Elgersma Y, Beck H (2005) Hippocampal synaptic metaplasticity requires inhibitory autophosphorylation of Ca2+/calmodulin-dependent kinase II. *J Neurosci* 25:7697-7707.
- Zhang LI, Tao HW, Holt CE, Harris WA, Poo M (1998) A critical window for cooperation and competition among developing retinotectal synapses. *Nature* 395:37-44.
- Zhao JP, Phillips MA, Constantine-Paton M (2006) Long-term potentiation in the juvenile superior colliculus requires simultaneous activation of NMDA receptors and L-type Ca2+ channels and reflects addition of newly functional synapses. *J Neurosci* 26:12647-12655.
- Zhao MG, Toyoda H, Lee YS, Wu LJ, Ko SW, Zhang XH, Jia Y, Shum F, Xu H, Li BM, Kaang BK, Zhuo M (2005) Roles of NMDA NR2B subtype receptor in prefrontal long-term potentiation and contextual fear memory. *Neuron* 47:859-872.
- Zhou YD, Acker CD, Netoff TI, Sen K, White JA (2005) Increasing Ca2+ transients by broadening postsynaptic action potentials enhances timing-dependent synaptic depression. *Proc Natl Acad Sci U S A*.
- Zucker RS (1993) Calcium and transmitter release. *J Physiol Paris* 87:25-36.
- Zucker RS (1996) Exocytosis: a molecular and physiological perspective. *Neuron* 17:1049-1055.
- Zucker RS (1999) Calcium- and activity-dependent synaptic plasticity. *Curr Opin Neurobiol* 9:305-313.
- Zucker RS, Regehr WG (2002) Short-term synaptic plasticity. *Annu Rev Physiol* 64:355-405.